REPORT DOCUMENTATION PAGE

Form Approved OMB No. 0704-0188

1. REPORT DATE *(DD-MM-YYYY)*	2. REPORT TYPE	3. DATES COVERED *(From – To)*
04-08-2005	Final Report	30 May 2003 - 27-Mar-06

4. TITLE AND SUBTITLE

Ignition and Supersonic Burning of Air - Fuel Mixtures Initiated by Electrical Discharges

5a. CONTRACT NUMBER
FA8655-03-D-0001, Delivery Order 0007

5b. GRANT NUMBER

5c. PROGRAM ELEMENT NUMBER

6. AUTHOR(S)

Professor Vladimir A Levin

5d. PROJECT NUMBER

5d. TASK NUMBER

5e. WORK UNIT NUMBER

7. PERFORMING ORGANIZATION NAME(S) AND ADDRESS(ES)

Moscow State University
1 Mitchurinsky Prospekt
Moscow 119192
Russia

8. PERFORMING ORGANIZATION REPORT NUMBER

N/A

9. SPONSORING/MONITORING AGENCY NAME(S) AND ADDRESS(ES)

EOARD
PSC 802 BOX 14
FPO 09499-0014

10. SPONSOR/MONITOR'S ACRONYM(S)

11. SPONSOR/MONITOR'S REPORT NUMBER(S)
EOARD Task 03-9001

12. DISTRIBUTION/AVAILABILITY STATEMENT

Approved for public release; distribution is unlimited.

13. SUPPLEMENTARY NOTES

14. ABSTRACT

This report results from a contract tasking Moscow State University as follows: The contractor will investigate the use of pulsed plasma jets and transversal pulsed-periodic discharges to ignite and efficiently combust hydrocarbon fuel/air mixtures in supersonic flows. Effects of pulse duration, pulse power, electrode material, and operating frequency will be determined for both propane/air and kerosene/air mixtures over equivalence rations from 0.3 to 1.0 at Mach 1.5, 2.0 and 3.0. Diagnostics will be used to determine the radiation spectra for the different discharges in the supersonic flow. Measurements of chemical radical and electron concentrations will also be made. Corresponding numerical simulations will be compared to the experimental data.

15. SUBJECT TERMS
EOARD, ignition, Supersonic Combustion, Combustion

16. SECURITY CLASSIFICATION OF:			17. LIMITATION OF ABSTRACT	18, NUMBER OF PAGES	19a. NAME OF RESPONSIBLE PERSON
a. REPORT	b. ABSTRACT	c. THIS PAGE			SURYA SURAMPUDI
UNCLAS	UNCLAS	UNCLAS	UL	138	19b. TELEPHONE NUMBER *(Include area code)* +44 (0)20 7514 4299

U.S. CIVILIAN RESEARCH AND DEVELOPMENT FOUNDATION FOR THE INDEPENDENT STATES OF THE FORMER SOVIET UNION

GRANT ASSISTANCE PROGRAM

FINAL TECHNICAL REPORT

Project Title: "Ignition and Supersonic Burning of Air Fuel Mixture Initiated by Electrical Discharges"

CRDF Project #: RC0-1383-MO- 03

Principal Organization: Research Institute of Mechanics, MSU

Project Director: Vladimir Alexseevich Levin

Reporting Period: May 30, 2003 – May 30, 2005

Summary

Experimental investigations of ignition in air-propane supersonic flow.

The test bed for experimental researches of an ignition and burning stabilization of fuel/air mixture supersonic flows by electrical discharge has been designed, manufactured and approved. The developed facility involves air and fuel supply systems, test channel with installed plasma generators, measurement system of gasdynamic and electrical parameters, and system of visual observation and video taping of flow visualization. The test channel consists of supersonic nozzle, insulator and combustor. Outlet nozzle airflow Mach number is M=2, total pressure is P_{tot} = 2-6 bar and total temperature is T_{tot} =300-900 K. Insulator and combustor have constant cross sections. Between lower surfaces of insulator and combustor is backward step so cross section of combustor is greater in 1.6 times than one for insulator. Propane is delivered to channel from injectors placed at the begin and end of insulator, and on the step surface.

Longitudinally-transversal constant current discharge of power 1.5 -2.0 kW, magneto-plasma compressor (MPC), microwave torch discharge of power 0.8-0.9kW and spark plugs generated in the flow region behind the step were used in experiments.

Undertaken experiments showed that constant current electrode discharge and MPC – discharge can be used for ignition of the fuel mixture practically in the whole volume of supersonic airflow. At the same time the plasma MW torch and plasma discharge of aviation plug can be applied for the fuel mixture ignition in the stagnant zone and on the flow boundary. It is necessary to emphasize that constant current discharge duration can be varied in rather wide limits: from 1 ms to some seconds, but MPC discharge duration is limited by storing condenser capacity and is 50 – 150 μs.

The main results have been obtained for longitudinally-transversal discharges. Electric characteristics of this discharge type in supersonic airflow were studied in details. High-speed photo discharge data were obtained and partially represented in reports for cases of motionless air, supersonic air flow, and supersonic propane/air mixture flow. Exposure time of one frame in represented photos is 20 μs and time interval between the neighboring frames is 50 ms. These data allow to trace development of discharge in the channel for different conditions.

Set of experiments was performed at variation of mass coefficient α that is the ratio of propane and air masses delivered to the channel. It is observed that the discharge picture in the case of the ignition is essentially different from photos obtained at the discharge in airflow and from the picture of the discharge in the fuel gas without ignition. This observation allows to conclude that ignition of propane-air mixture takes place during some definite moments of the discharge process. However process of ignition has relatively spontaneous character: frames with weakly represented combustion effect follow the frames with detected fuel mixture combustion, then again the ignition of the mixture is seen.

On basis of statistical treatment of the frames set a dependence of the ignition probability in the supersonic flow with respect to the value of the mass coefficient α was found. Built dependence shows that there is a large scattering of the probability value at close values of α, that is explained by chaotic ignition character of the fuel mixture. Greatest values of the ignition probability are concentrated in the area of α variation from 0.06 to 0.1.

An attempt of partial limiting of the flow in the channel was made in order to gain more stable ignition of the fuel mixture in the discharge. For this purpose additional wedges of different orientation were installed in the discharge area. The obtained photos shown that fuel ignition probability rises at existence of partial flow limiting in the discharge area. However there is also no stable mixture ignition in this case. The most values of the ignition probability are for downstream wedge orientation.

Optical diagnostics of all considered discharge types has been performed. Spectroscopic measurements validated observed propane-air mixture inflammation and its combustion in the discharge region with temperature level T=2400-2800 ^{0}K.

Numerical modeling of fuel/air ignition in the test channel by electrical discharge

New numerical models and codes were developed to provide fulfillment the Project Task 4. In these models gas is considered as an ideal one-temperature reacting mixture of perfect gases. For description of turbulent flows Favre averaged Navier-Stokes equations and known $k-\omega$ turbulence model is used. Global, quasi-global and detailed chemical mechanisms are employed for simulation of chemical processes in gas mixture On the first stage of investigations the heat source model of gas discharge was employed for description of discharge effect on gas flow. Thermochemical models including local databases on thermodynamic, kinetic and transport properties of individual gases for fuel mixture hydrogen/air, propane/air and kerosene/air were developed to provide researches under Project.

The main attention was given to numerical researches of propane/air mixture ignition and combustion stabilization in supersonic channel by electrical discharge for experiments condition.
Two chemical models were used for calculation. Simplified model involves 12 species, one global reaction and 20 elementary reactions. Full model involves 28 species and 70 elementary chemical reactions. For estimate of gas heating rate calculations for non-reacting gas model were performed also.

Planar model of the channel including nozzle, insulator and combustor sections was used in calculations. Between lower surfaces of insulator and combustor is backward step. Propane is injected to air supersonic flow in normal direction from injector placed on the lower surface of first section of the channel (insulator) at the origin of this duct. Two schemes of heat supply in the channel were considered. In the first scheme heat is supplied into near wall region of specified location and configuration placed at the end of insulator (before step). In the second scheme heat is supplied into rectangular region placed after step into separated area.

Parametric calculations of steady state propane/air mixture flow in the channel were performed for each from schemes. Propane mixture ignition and combustion stabilization by the heat supply is demonstrated. Effects of chemical model, and heat source power, configurations and location on ignition and burning processes in channel were analyzed.

It is shown that for first scheme of the heat deposition when heat source is located before step the ignition occurs for heating power $P_d \geq$ 4 kW/cm. Combustion completeness C_B on the channel outlet for this scheme reaches of 0.43. For heat deposition after step the ignition occurs already at power P_d =0.5 kW/cm. Value of C_B in considered cases reaches of 0.2 for this scheme. There is essential difference of results obtained for scheme 1 using reduced and detailed chemical mechanisms. Predicted by reduced model value of combustion completeness is near 0.01.

Unsteady processes at the heat deposition turning on and turning of were studied. It was shown that after heating shuts down the combustion in channel is finished. Estimates of inductive and relaxation time were obtained.

Similar investigations of the steady state flows for gaseous kerosene injection in supersonic channel were performed also. One-formula kerosene model $C_{12}H_{24}$ and quasi-global chemical model including 11 species, 2 global and 12 elementary reactions was employed in computations.

The parametric calculations of the channel flow were performed for the same mass injection rate as for propane case. Effects of the heat source power and location on the kerosene/air mixture ignition and burning effectiveness are analyzed. It is shown that for heat deposition before step with power P_d =3.5 kW/cm and higher the mixture is ignited. For heat deposition after step the ignition occurs already for power P_d =0.5 kW/cm. Value of burning completeness in considered cases does not exceed of 0.045 for first scheme and 0.016 for second scheme heat deposition.

Introduction

There is a wide interest in aviation applications of different electric discharge plasmas for improvement of ignition and stabilization of combustion of hydrogen and hydrocarbon fuels. Some of these gas-discharge devices were successfully applied in experimental investigations on the ignition of air-fuel mixtures in supersonic flows that were carried out in MSU. Promising prospects of discharge devices application as ignition systems has been shown. Some basic results of these researches were discussed during Workshops on Weakly Ionized Gases.

Basic problems appearing at creation of a supersonic combustor of perspective propulsion system and at organization of external burning on surfaces of supersonic vehicles are: mixing of submitted fuel with a supersonic airflow, reliable ignition of intermixed air–fuel mixtures and organization of burning effective process. During these processes a gas flow can be both laminar and turbulent. The design-theoretical and experimental researches carried out earlier have shown that the organization of effective fuel combustion in supersonic airflows is difficult. The application of electric gas discharges is one of other ways of reliable ignition organization of air-fuel mixtures and intensification of burning process. As it was shown by preliminary experiments in case of electrical discharges (transversal gas discharges, plasma jets) a delay time of an ignition can be essentially reduced in comparison with that of self-ignition process. Realization of both design-theoretical and experimental researches is necessary for revealing and detection of primary laws of the ignition and burning of various fuels in supersonic airflows.

Analysis of typical conditions (P=0.3-0.8 bar and T=400-600 K) for initiation and stabilization of combustion, which are in high velocity air flows, showed that the ignition delay of air/hydrocarbon mixtures (methane, propane and more over kerosene) is one – two orders of magnitude larger of residence time for this mixture in considered reactor (channel) of 1 meter length. It should be to distinguish cases of premixed flow (homogeneous mixture) and real existed flows of non-uniform air-fuel distribution with diffusion type combustion, for example, in air breathing engines. In the last case the acceptable conditions from the mixture composition point of view (corresponding to fuel/air equivalence ratio β) must be provided in region, where ignition and combustion stabilization are proposed.

In frame of requirements posed by the Project it was proposed to research influence of plasma formations caused by different types electrical discharge on initiation and combustion stabilization in initially (before the combustion) supersonic flow of air/gaseous hydrocarbon fuel mixture and effect of flow parameters: pressure *P*, temperature *T*, velocity *V* and mixture composition (β) on its, influence of discharge on flow excitation, and also to define possibility of ignition and combustion stabilization under simulating flow parameters. In accordance with the Project the researches were proposed to be conducted at M=2 flow.

Next types of plasma generators were proposed to use for study:

1. Plasma jet generator of τ =1 sec time operation duration, installing in flow separation region just behind the reverse step;
2. Plasmadynamic generator of $\tau \approx 0.1$ ms and frequency *f* up to 1 kHz;
3. Generator of surface and volumetric discharges initiated by electrodes installing at the end of insulator section or in base region behind the reverse step on the low wall;
4. Microwave torch generator of 1 kW power and λ=12 cm in the base region installed and forming the active volume of flux wave length radius and 1 Hz to 1 kHz frequencies of energy impulses and impulse duration from 500 ms down to 1μs.

In the present Report we describe our experimental investigations in developed, manufactured and mounted supersonic stand in MSU laboratory at total pressure P_{tot}=0.07-0.3 MPa and T_{tot}= 290 K (M=2±.0.02). Intermediate results of researches contain in quarterly reports [1-7].

Experimental investigations of plasma generators are made in above represented conditions at their location in the widening part of the combustion chamber behind the step. In particular we undertook investigations with the following plasma generators: longitudinally-transversal constant current discharge of power 1.5 -2.0 kW, magneto-plasma generator, microwave torch discharge of power 0.8-0.9kW and spark plugs.

Spectroscopic measurements validated observed propane-air mixture inflammation in the supersonic flow and its combustion in the discharge region with temperature level T=2400-2800 K.

Analysis of all obtained results show necessity of continuation of investigations on initiation and stabilization of hydrocarbon-air mixtures with a help of plasma generators with prior application of preliminary air and fuel heating up to temperatures T=800-900 ^{0} K.

The developed in the Research Institute of Mechanics MSU effective numerical technique of high-temperature gas flow modeling have been modified to study ignition and burning of turbulent supersonic air-fuel mixtures by electrical discharges. The developed technique is based on software package including solvers of governing equations for various classes of gas-phase models and databases on thermodynamic, kinetic and transport properties of gases. On the first stage of investigations the heat source model of gas discharge was employed for description of discharge effect on gas flow. Developed numerical technique have been employed to research steady state and unsteady propane/air and kerosene/air mixture heating and ignition in a planar model of test channel with back step on lower surface for two schemes of fuel injection and heat deposition. Considered schemes simulate ignition of fuel/air mixture by the surface or volumetric gas discharges.

In frames of item 4.2 of the Project Task 4 calculations of hydrogen/air and propane/air turbulent supersonic flow over flat plate in the presence of surface discharge modeling by heat source were performed also [2]. Calculations were carried out for conditions of flow parameters in the first section of facility created under the Project. Steady and impulse heat sources were considered. Results of investigations are presented in the quarterly report [2]

The main attention was given to numerical researches of propane/air mixture ignition and combustion stabilization in supersonic channel by electrical discharge for experiments condition. Two chemical models were used for calculation. Simplified model involves 12 species, one global reaction and 20 elementary reactions. Full model involves 28 species and 70 elementary chemical reactions. For estimate of gas heating rate calculations for non-reacting gas model were performed also.

Parametric calculations of steady state flow in channel were performed for each from schemes. Fuel mixture ignition and combustion stabilization by the heat supply is demonstrated. Effect of chemical model, and heat source power, configurations and location on ignition and burning processes in channel were analyzed.

Unsteady processes at the heat deposition turning on and turning of were studied. It was shown that after heating shut down combustion in channel is finished. Estimates of inductive and relaxation time were obtained. Results of the propane/air flow calculations are presented in quarterly report [5] and in the present report.

Similar investigations of the steady state flows for gaseous kerosene injection in supersonic channel were performed also. One-formula kerosene model $C_{12}H_{24}$ and quasi-global chemical model including 11 species, 2 global and 12 elementary reactions was employed in computations. Effects of the heat source power and location on the fuel mixture ignition and burning effectiveness is researched. Results of investigations are presented in quarterly report [6] and in the present report.

References to Introductions

1. Quarterly Technical Report under CRDF Project # RC0-1383-MO- 03 for Period May 30, 2003 – August 30, 2003, Moscow
2. Quarterly Technical Report under CRDF Project # RC0-1383-MO- 03 for Period August 31 – November 30, 2003, Moscow
3. Quarterly Technical Report under CRDF Project # RC0-1383-MO- 03 for Period December 01, 2003 – February 28, 2004, Moscow
4. Quarterly Technical Report under CRDF Project # RC0-1383-MO- 03 for Period March 01, 2004 – May 30, 2004, Moscow
5. Quarterly Technical Report under CRDF Project # RC0-1383-MO- 03 for Period June 01, 2004 – August 31, 2004, Moscow
6. Quarterly Technical Report under CRDF Project # RC0-1383-MO- 03 for Period September 01 2004 – November 30, 2004, Moscow
7. Quarterly Technical Report under CRDF Project # RC0-1383-MO- 03 for Period December 01, 2004 – February 28, 2005, Moscow

Technical description

1. Experimental investigations of ignition in air-propane supersonic flow.

1.1. Goal of experimental works

Main results of experimental investigations are represented in this paper. These results were carried out in accordance with Technical task and planned schedule.

The goal of these work consisted in:

- Development and creation of experimental stand for undertaking of experiments in supersonic airflow and fuel mixture and determination of supersonic channel main parameters.
- Creation of diagnostic complex for undertaking of electrical, optical and photometric measurements and also for determination of parameters of supersonic flow.
- Investigation of different plasma generators applicability in this experimental stand and determination of their main characteristics. Perspective estimate of definite plasma generator for ignition of supersonic flow of the fuel mixture.
- Undertaking of experimental measurements on investigation of air-propane fuel mixture ignition possibility in the supersonic flow.
- Formulation of recommendations for further works in this experimental stand basing on results of undertaken investigations.

1.2. Supersonic channel

1.2.1. Scheme of the test bed. General realistic scheme of the experimental bed is represented in Fig.1.1. The principle of the bed functioning is the follows: a compressor (2) pumped air over the pipeline воздух (4) through the collector (5) to the balloon ramp (6). At that the total volume of the high pressure receiver (the receiver of the compressor with the balloon ramp) is 0.5 m^3. Working pressure in the receiver is controlled by manometers (7), it can reach 16 atm. Air compressed in the receiver up to required value goes through the operating pneumatic valve (8) to the ohmic heater (9), there its temperature can rise up the value ≤ 800 K, then it goes to the supersonic channel (11) through the shaped nozzle. Main characteristics of the channel are the following: Mach number M = 2, static pressure P = 0.25 - 0.6 atm., a pressure in the compressor receiver P_{tot} = 2 - 6 atm.; time of the combustor stationary mode of functioning no less than 4 seconds for possible ranges of total pressure and fuel mass rates in the channel; propane and kerosene are assumed fuels.

The supersonic channel is supplied with the system of pressure sensors (12) (sensors number is about 20 pieces) and the system of a fuel supply (17). A fuel comes to the channel through the fuel distributing flanges (15) both to the supersonic tract directly and to the region behind the step of channel. Air-fuel mixture is ignited by the wall electrical discharges or (and) plasma igniter located in the region behind the reverse step of the channel. Plasma generator is brought into the combustor through lower flange (16). The diagnostics of the source plasma and of the flame plasma is undertaken by the spectroscopy methods in the first section of the combustor (directly behind the step) and in the diagnostic chamber (13). For this purpose the diagnostic chamber and the supersonic channel are equipped by the illuminators (14). Air-fuel mixture rejection takes place in the vacuum chamber (1).

Works on assembling of supersonic channel of experimental bed have been carried out in accordance with Technical task and planned schedule. General appearance of the assembled supersonic channel is represented in photos (Fig. 1.2, 1.3).

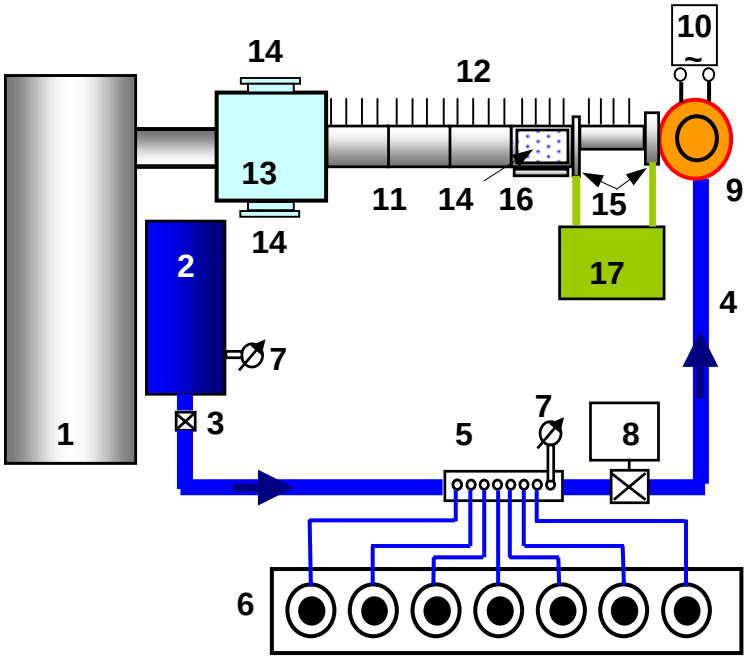

Fig. 1.1. Schematics of MSU test facility

1 – vacuum chamber, 2 – air compressor, 3 – tap, 4 - air manifolds, 5 – air collector, 6 – vessels, 7 – pressure manometers, 8 – control valve, 9 – electric storage heater, 10 – power unit, 11 – supersonic channel, 12 - pressure gauges, 13 – diagnostic chamber, 14 – optical windows,15 – fuel collectors, 16 – plasma generator installation unit, 17 – fuel supply system

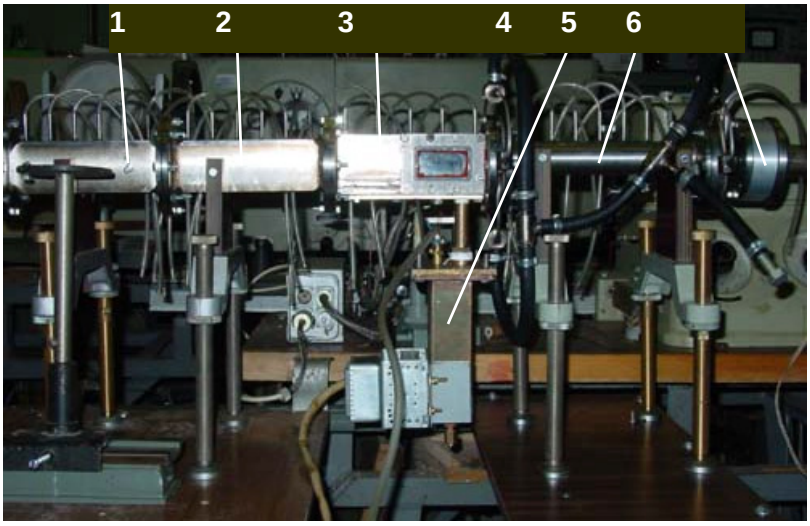

Fig. 1.2. Input discharge energy (single pulse)

$$W = \int_0^{\tau} IUd\tau \ =0.5 \text{ J}$$

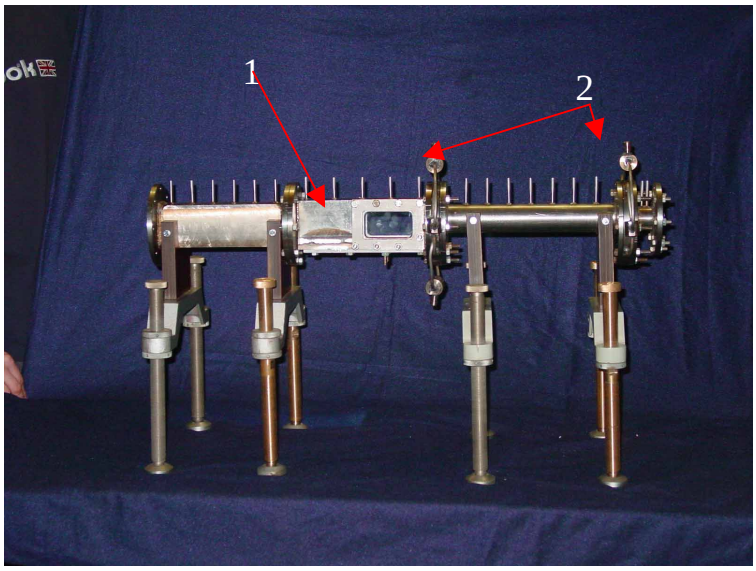

(a)

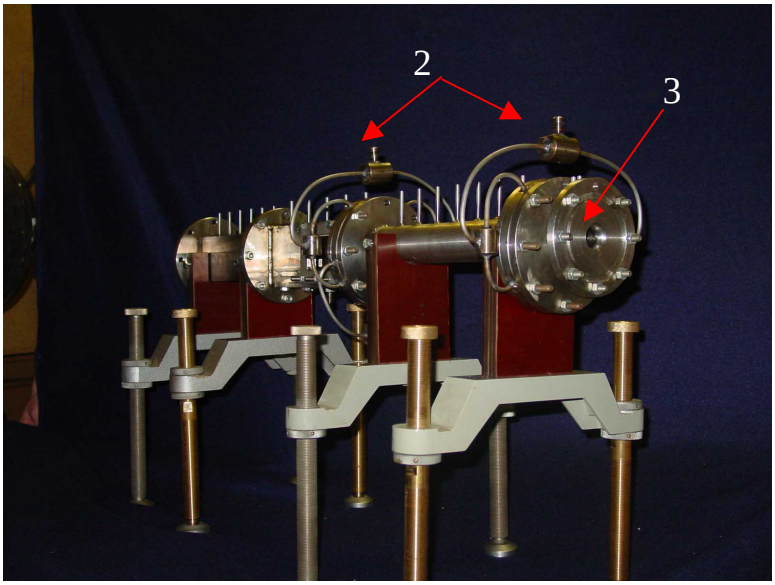

(b)

Fig. 1.3. General appearance of the supersonic channel.
1 – diagnostic section, 2 – fuel distribution collectors, 3 – supersonic profiled nozzle

1.2.2 Supersonic nozzle and test channel. Fig. 1.4 shows scheme of the test gasdynamic tract involving supersonic nozzle and supersonic channel. Shaped supersonic nozzles resulting in M=2 airflow of total air parameters P_{tot}=2-6 bar and T_{tot}=300-800 K were designed and manufactured both for axisymmetrical and two-dimensional channel configurations. Nozzle exit dimensions are equal to ∅25mm and 25×25mm^2 correspondingly.

Supersonic channel consists of two main parts – insulator channel of constant cross section and 250mm length, which should to prevent spreading of pressure increase resulted in combustion upstream to the nozzle and combustor section in which is proposed to organize intensive burning of air/fuel mixtures. Insulator channel has been designed and manufactured in axisymmetrical and

two-dimensional variants. Combustor section has been designed and manufactured as two-dimensional one with flame holder on the bottom wall.

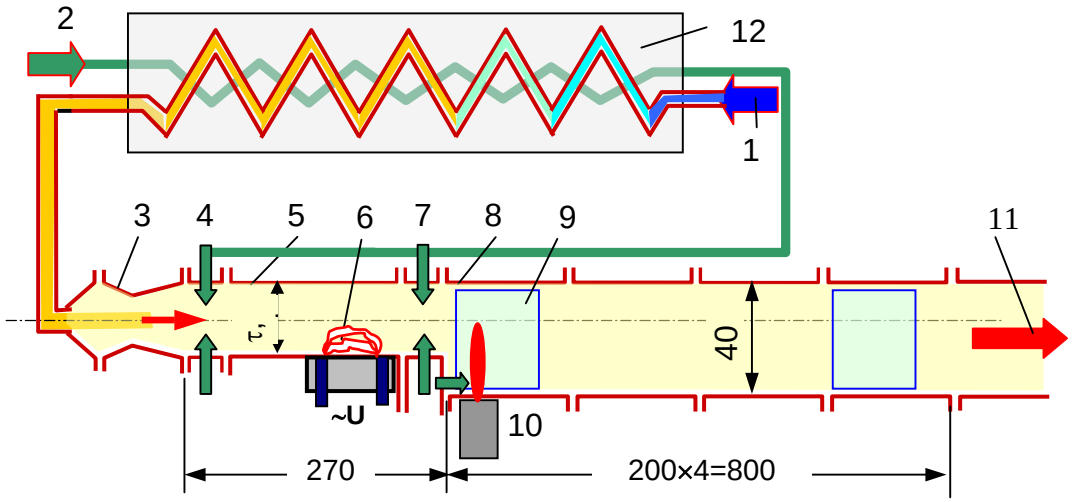

Fig. 1.4. Schematics of test channel (all dimensions in mm).

1 – air intake to storage heater, 2 – fuel intake, 3 – supersonic M=2 nozzle, 4 – collectors of preliminary fuel injection, 5 – insulator, 6 – surface discharge generator, 7 - fuel collector of normal and tangential injection, 8 – channel section (4 sections), 9 – quarts optical window, 10 – torch igniter, 11 – to vacuum chamber, 12 – storage (electric) heater

Combustor channel (CC) consists of two main parts – insulator channel of constant cross section and 250 mm length and combustor section, in which is proposed to organize intensive burning of air/fuel mixtures. The channel width along the whole combustor is constant and equal to 20 mm. Two fuel collectors with four fuel normal injectors in each one are installed just behind the nozzle (Fig 1.5a) and at the end of the insulator section (1.5b) to provide different fuel distributions between the injector sets (preliminary and main ones). Besides, two orifices of 1 mm diameter were done on the fuel collector rear side wall formed the reverse step to inject some fuel (3-7% of total fuel rate) directly into the separation zone behind the reverse step (Fig 1.5b) and to provide required fuel concentration in a stabilization zone for enhancing of combustion initiation and stabilization. Also, the first section is arranged by radio-transparent window for placement of plasma generators or electrodes for initiation of transversal or surface MW discharges.

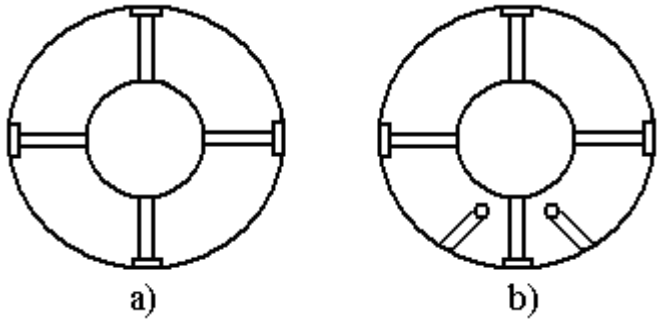

Fig.1.5

In the given configuration the step of 15 mm height on low channel side is proposed to act as a flame holder for the burning fuel jets and creates separation zone, which is favorable for plasma discharges existence.

Combustor main section of 25mm ×40mm constant rectangular cross area along the length includes some (from 2 up to 4) subsections of 200 mm length each one. Cross section area of CC is larger by magnitude of 1.6 in comparison with the insulator duct area. This section is equipped by

the quartz side windows for video taping and photo registration of the flow field, an ignition and combustion processes and the hatches for installation of different plasma generators on low channel wall. Static pressure and wall temperature are measured along the combustor duct. During the calibration tests Pitot and static pressures at the exit of the nozzle were measured and average Mach number was defined as M=1.96±0.04 for incoming airflow parameters P_{tot}=0.2-0.4 MPa and T_{tot}=300-450K.

The storage heater is warmed by the 0.25 MW electric heater, which operates before the runs. Intake fuel and airflow parameters are the following: fuel/air equivalence ratios β =0.- 1.0, fuel temperature T_{fuel}=550-880K, M=2, $P_{tot,air}$=0.2-0.6 MPa, $T_{tot,air}$=650-900K. Control of the test rig components during each run is realized in computerized mode according to the sequence diagram. According to the typical run diagram the tested igniters can operate during 1-2 seconds. Constant rate fuel is supplied during 2-3 seconds. Total duration of run is 2-4 seconds. It is possible to conduct researches with different liquid and gaseous fuels.

Plasma jet and near wall electrical discharges will be used for ignition and stabilization of air-fuel mixture (Fig. 1.6). Plasma jet is supposed to inject into stagnation range of flow in combustor after reverse step. Near wall discharges are planed to place on the bottom surface of insulator (in the end of one) or on the bottom surface of combustor (just after step).

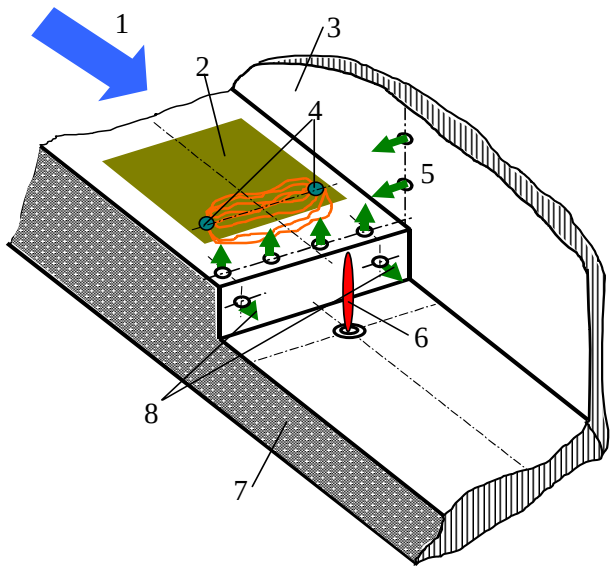

Fig. 1.6. Schematics of plasma generators placement in rectangular cross section channel (upper and side walls were removed)
1 – incoming airflow, 2 – insulator insert, 3 – side wall, 4 - sliding discharge generator, 5 – wall fuel injection (second fuel injector set), 6 – plasma jet from plasma torch generator, 7 – bottom wall, 8 – fuel supply into the flame holder zones

1.3. Diagnostic complex.

Main experimental methods of plasma discharges diagnostics are described in this section. They are connected with diagnostics in motionless air, supersonic airflow and in supersonic fuel air-propane mixture.

1.3.1. Determination of electrical discharge parameters. Voltage dividers, shunts and Rogovskyi belts were used for determination of electrical parameters. Voltage dividers used for measuring of the voltage drop on a discharge were assembled of small induction resistances with division coefficient 1000 – 10000 and were switched parallel to the discharge circuit. Discharge current value was measured with a help of shunts. They represented small induction resistances of 0,3 – 0,02 Ohms. They were included series with discharge gap. Rogovskyi belts were used for the same target, i.e. for determination of the discharge current. Pulse signals from voltage dividers and shunts were delivered to the inlet of two-beam storage oscilloscope Tektronics – 210.

Digital camera and high-speed video were used for determination of discharge appearance and its temporary variation. Integral discharge photography was made during photo camera exposure time. High-speed video worked on a base of CCD-ruler with electronic shutter. It allowed to get series of frames in the mode of several photo frames and in the mode of video recording. Discharge image was delivered from the camera to PC, see Fig. 1.7. Modes of internal and external synchronization were foreseen in CCD, there were also possibilities of single frame exposure time control. The exposure time in frame-by-frame mode was changed from 3 ms до 1 s, and starting from 60 μs to some seconds in video recording mode.

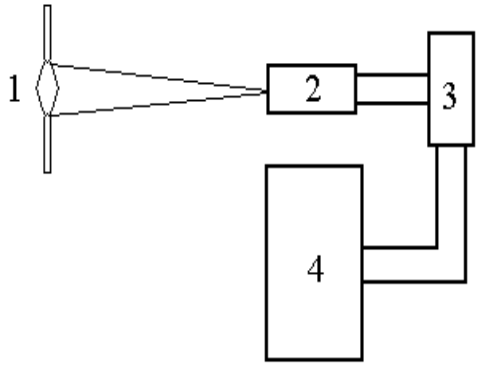

Fig. 1.7.
1- discharge, 2-CCD-camera, 3-interface plate, 4- PC.

Time interval between frames was 50 μs in the first case, and 20 ms in the second case. Most of experiments were made with resolution of 20 μs. This insured satisfactory time resolution from one hand normal discharge image brightness from another hand.

1.3.2. The automatic system of radiation spectra detection. This system has been developed and manufactured during this works. It is aimed for the optical diagnostics of different type discharges and of combustion spectra of fuel/air mixtures in the stabilization region of the combustion chamber in the last section of the supersonic channel.

The spectra measurement system is schematically represented in Fig.1.8. It consists of two subsystems. The first subsystem consists of the small sized high-aperture monochromator MDR–41 type (4), the control block insuring the scanning with the given speed and the control of the current wavelength (6), the photomultiplier (PM) (5), the PM power supply block, ADC- 1250 plate placed in the computer and the software. The working range of the wavelengths is limited by the sensitivity region of the PM and is 200 – 830 nm.

The second subsystem consists of the diffraction spectrograph DFS- -452 type (or ISP-30) and of the multichannel optic spectra analyzer (MOSA-2), which includes two photoheads with the photo diode CCD toolbars Toshiba TDS1250A type and the interface plate, inserted to one of the serial computer ports. The photoheads are fixed to a plate, which is located in the focal plate on the place of the spectrograph cassette. The photoheads are connected with the interface head through the cable. A special program is used for the work with the system (MOSA-2).

There are about of 3700 sensitive elements 8 μm length and 200 μm height (the total toolbar length is 30 mm). The spectral sensitivity range is 180 ÷1000 nm. The time of the signal storing is given by the toolbars inquiry period and can varied in the range 80 ÷ 20000 ms. Since 12 digits analogue-digital converter is included to the composition of each photo head then only digital signal are transmitted to the computer over the interface cable. This insures rather high noise protection of the system.

The spectrograph DFS-452 allows to work in the whole range of the toolbars sensitivity. The reverse linear dispersion is 1.6 nm/mm or 0.013 nm per the element of the toolbar at the work with the grating 600 lines/mm. The reverse linear dispersion is 0.8 nm/mm and 0.0065 nm per the element of the toolbar at the work with the grating 1200 lines/mm. One of the bars is placed along the dispersion direction of the spectrograph and is used for the spectrum detection, and the other one is directed perpendicular. It is aimed for measurements of the intensity distribution over the slit height at the given wavelength.

The program for the work with the system (MOSA-2) allows to realize the inquiry of any of the photodiode bars, or of both simultaneously, with arbitrary time of storing, cyclically and once. It

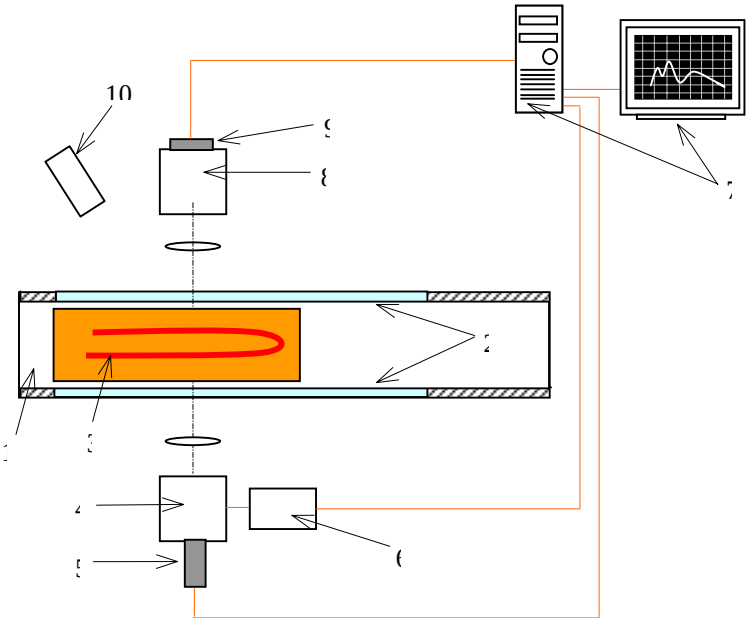

Fig.1.8. Optical measurements system.

1 - the first section of the supersonic channel combustion chamber; 2 - the quartz illuminators; 3 – the discharge plasma and the ignition region; 4 – the monochromator MDR -41; 5 – the photomultiplier; 6 – the monochromator control block; 7 –PC-AT with the interface and ADC plates; 8 – the spectrograph; 9 - photoheads with CCD toolbars; 10 - CCD-camera.

also allows to put to the screen the signal from any bar or two signals from two bars simultaneously. The automatic registration (extraction) of the dark signal is possible and the summation over several consequent inquiry of the bars. The program allows to make simple arithmetic operations with the detected spectra and keep them on a disc in the file form or in the special format, or ASCII codes.

The discharge image or of some definite combustion plasma volume is projected to the spectrographs inletting slit with a help of the quartz condenser with the focus distance about of 240 mm. For the absolute measurements of the intensities it is important that the solid angle (from which the radiation is collected) has to be the same obtained at the plasma detection and from the standard source. So the location of the diaphragm is supposed before a condenser in a form of the vertical slit $\approx$ 5 mm width, which limits the solid angle of the radiation collection. The typical values of the spectrograph inletting slit size will be 10÷50 μm with respect to the source radiation intensity.

The time of the signal storing was changed from 100 to 1000 ms with respect to the signal value. Storing time and cycling time at obtaining of one required spectrum was determined on a base of the signal amplitude realized on PC monitor and convenient for following processing and determination of discharge parameters.

Besides, two-channel fiber-optic spectroscope AvaSpec – 2048-2 of Avantes. Company was used for detection of discharges spectra. One channel of this spectrograph with working range from 200

to 1000 nm but with small dispersion was used for getting of panoramic spectrum in the whole area of detection. Another channel of the spectroscope with working range from 350 to 450 nm, but with large resolution (large dispersion), was used for getting of rather well resolved molecular spectra in indicated range of wavelengths. This spectroscope worked together with PC. The corresponding computer code allowed to totally control the spectrograph working mode: exposure time and storing time at processing of the spectrum, synchronization modes at work with external radiation source, spectroscope work in frame-by-frame mode or in video mode, etc. Besides, this computer code allowed to make automatic processing and analysis of obtained spectra

Standard sources were used for preliminary and working calibration of obtained spectra. Their working principle was based on constant current electric discharge in vapors of copper, mercury, zinc etc. Neon was used as a buffer gas in these sources.

1.3.3. Synchronizing system. Special synchronizing scheme was developed and created for controlling of normal work of the whole set up, it is represented in Fig. 1.9.

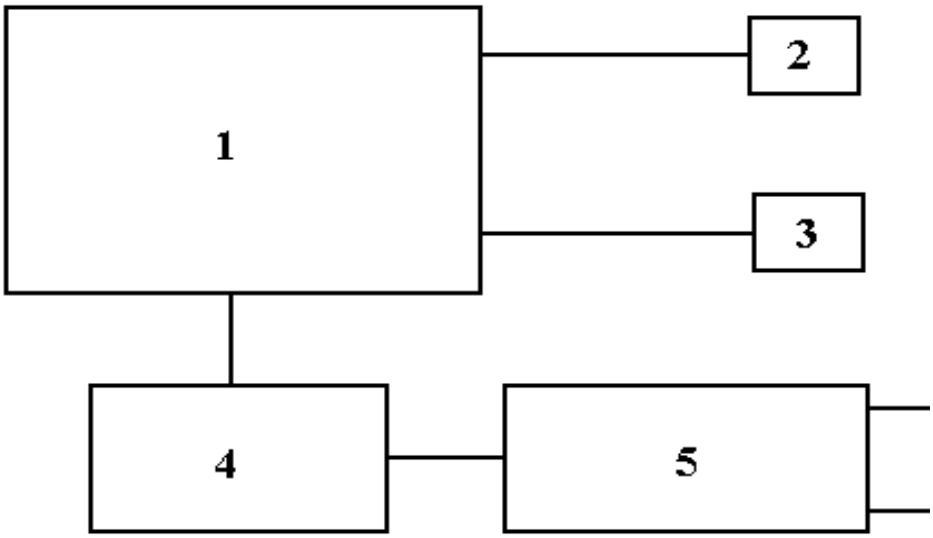

Fig. 1.9. System of sinchronization

Controlled block (1) is main part of this system, it produces signals for following work of main elements of the set up. The block generates the feeding source pulse of electromagnetic valve of air delivery system (2) and valve of gas delivery to the supersonic channel (3). This block realizes the synchronic pulse for starting of intermediate generator (4), which controls the work of constant voltage source (5), the pulse is delivered to electrodes (6).

Let us consider the principle of synchronization scheme work using, for example, temporary diagrams represented in Fig.1.10. Feeding voltage is realized to air system valve after the start pulse delivery to the control block. This valve is of double operation, so, because of large inertia, it is opened with some delay time τ = 0,3 – 0,4 ms. Duration of air valve (T_1) open state can be regulated in the range from 100 μs to 10 s with spacing of 0,1 s. Feeding voltage is realized to the valve of gas delivery system to the channel with delay Δt_{12} with respect to the starting pulse. The delay time Δt_{12} is varied in limits 0,1 ms – 1 s with spacing of 0,1 s, and duration of the feeding pulse of the channel (T_2) can be in the range from 0,1 ms to 10 s spacing of 0,1 s. The synchronizing pulse for starting of the generator is realized in the control block simultaneously with the starting pulse. The generator controls the pulse duration of the high voltage constant current source, i.e. it determines duration and delay of the discharge pulse with respect to the start.

Discharge delay time Δt_{13} is varied in the range from 100 μs to 10 s with spacing of 0,1 s, and discharge pulse (T_3) - is varied in the range from 100 μs to 10 s with spacing of 0,1 s.

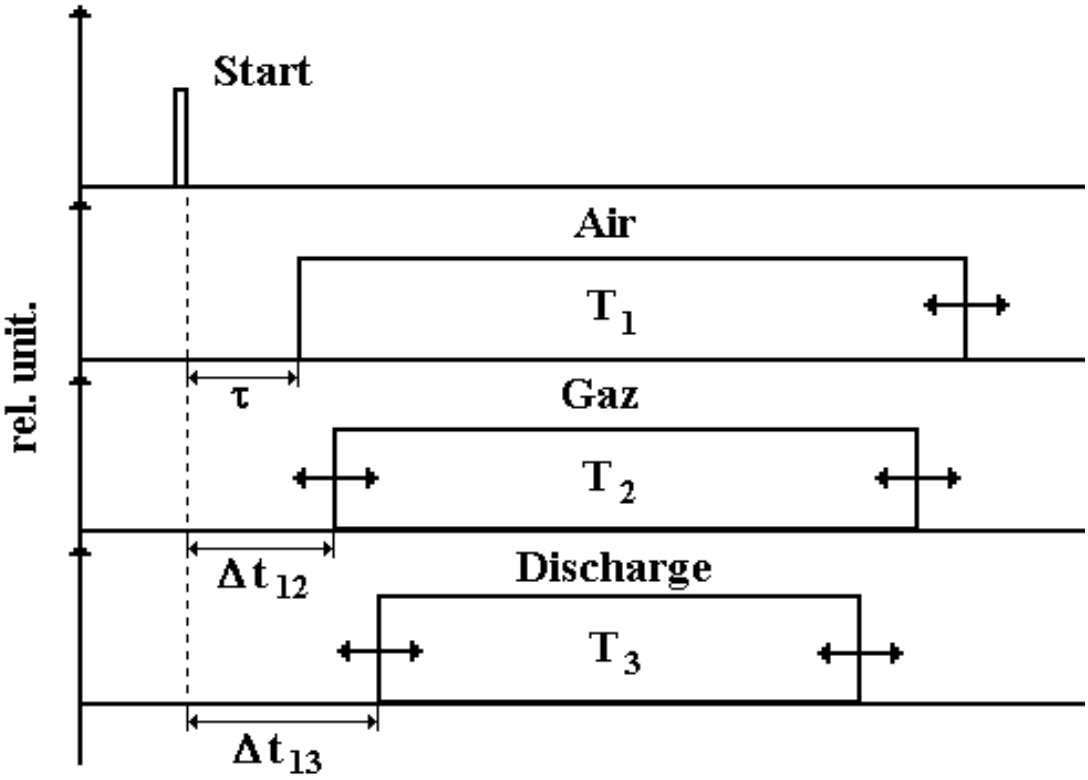

Fig. 1.10. Temporary diagrams

1.4. Supersonic flow parameters controlling system

Model combustion chamber (CC) as it was noted earlier was designed in correspondence with results of investigations [1,2], there methane combustion was investigated in CC in sizes analogous to this chamber. However we have to emphasize the following features of combustion process in the channel in the present investigation, see Fig.1.11.

1. Supersonic (SS) flow of M=2 was created by the axisymmetrical nozzle with outlet diameter of ∅25 mm in the channel of the isolator, at the same time cannel section were of rectangular cross section 25×40 mm^2 behind the reverse step;
2. Airflow temperature was approximately constant T=290K in the channel receiver, and the gas pressure was varied in the range Pt=0.7-2 atm;
3. Pressure in the outlet collector was set by the pressure in the vacuum chamber P_{VC}, and main part of tests was carried out at initial value of P_{VC} =20-30 Torr;
4. Propane was delivered to CC by two means: 1 – through the preliminary and main collectors over 4 holes of ∅1.5 mm diameter in each normally to airflow direction, and 2 – only through the main collector. Propane in both cases was additionally delivered through 2 holes of ∅1 mm diameter located on the step wall. Mass flow rate though delivery sections was distributed proportionally to areas and rates coefficients of the holes;
5. The channel of constant cross section (behind the reverse step) was equipped by quartz optical windows for video taping and includes three sections.

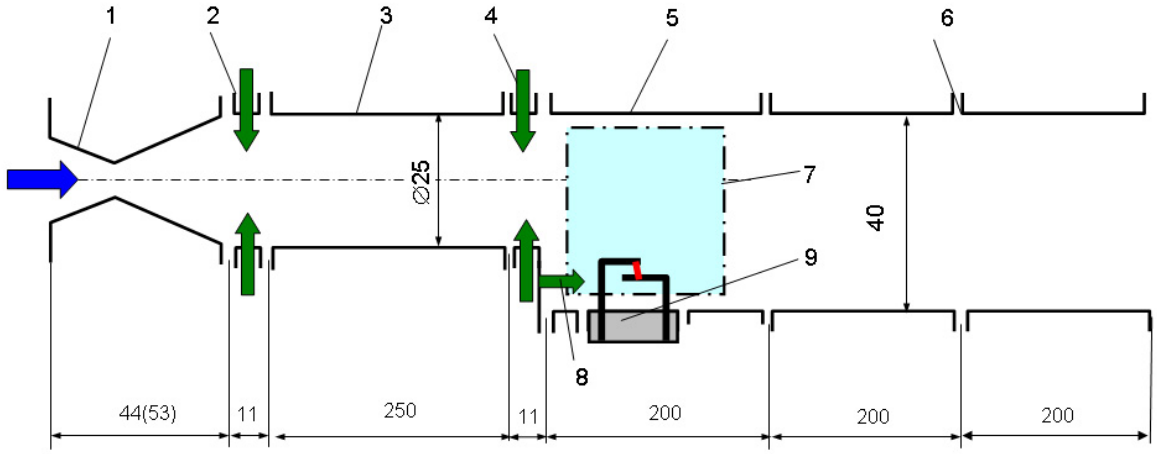

Fig.1.11. Schematics of test channel (sections “5” and “6” are fabricated twice)

1 – nozzle, 2 – collector of preliminary fuel injection, 3 – insulator, 4 - collectors of main fuel injection (second injector set), 5 – 1st section of combustor, 6 – 2nd section of combustor, 7 – quartz window1 – supersonic M=2 nozzle, 2 – collectors of preliminary fuel injection (first injector set), 3 – insulator channel, 8 – third fuel injector set, 9 – plasma jet generator (linear dimensions of test sections are the same both for axisymmetrical and two-dimensional channel configurations except for the nozzle section “1”,

1.4.1. Pressure sensor system and their calibration. Pressure sensors, see Fig. 1.12. are a base of main SS flow main parameters controlling system. They are connected with pressure receivers located on all sections of the working channel. Thin wall tubes have external diameter of 4 mm and internal diameter of 2 mm, they are used for pressure delivery. These tubes are soldered to the upper walls of channel sections and are connected directly with pressure sensors with a help of thin flexible hoses of 0.2-0.3m length.

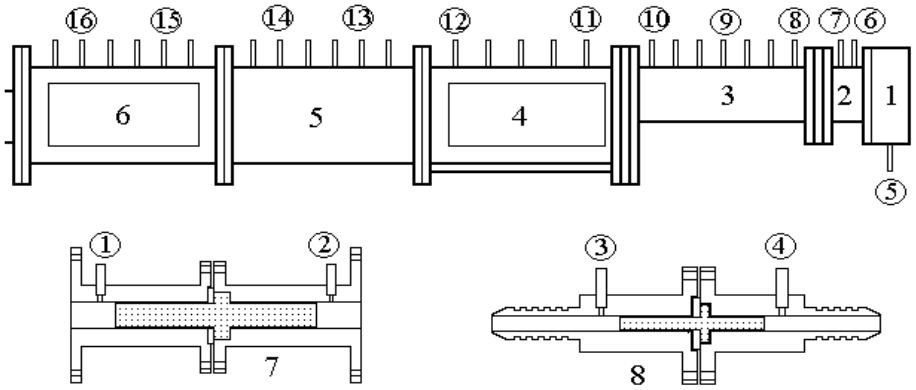

Fig. 1.12. Pressure sensor system

1- flange for fixing of thermocouple and pressure sensor, 2-nozzle, 3- forming channel, 4-working section, 5,6-measuring sections, 7- airflow meter, 8- gas flow meter, in circles 1-16 – pressure sensors in the channel.

There are also 2 pressure receivers (numbers in the circles 6 and 7) placed in the nozzle section, 7 receivers (numbers in the circles from 8 to 10) are in the isolating section, 5 receivers (numbers in the circles 11 and 12) are in the working section, 6 receivers are placed in each measuring section (numbers in the circles from 13 to 16). All measurements are used for determination of flow

parameters distribution over the channel length and energy release influence on a flow in the duct of model CC.

A block consisting of the thermocouple and one more sensor (number in the circle 5) is located at the inlet to the supersonic nozzle. Sensors allow to determine the flow pressure and temperature at the outlet from the thermostat. Besides, there are two pressure sensors are located in the gas-mains before and after air measuring nozzles (position 7 numbers in the circles 1 and 2) and of the fuel (position 8 numbers in the circles 3 and 4).

Ten more sensors are used for pressure distribution measurements over the channel cross section, see Fig. 1.13. Analogous thin tubes are used for pressure delivery to them. These tubes are placed on a special platform, which is located in the lower hatch of the working section so that the open tube ends are directed towards the flow at its exit from the forming section, and are placed along the radius.

Sensors from 6 to 16 have the working range from 0. to 3. atm over pressure, and sensors from 0 to 5 have the working range from 0. to 5. atm.

In the present work we used absolute pressure sensors of tenzometric type. This sensor principle of work consists in the following: a plate located inside the sensor is bended proportionally to the pressure applied to the sensor. Four tenzo resistors are integrated to the plate, they change their resistance with respect to deformation.

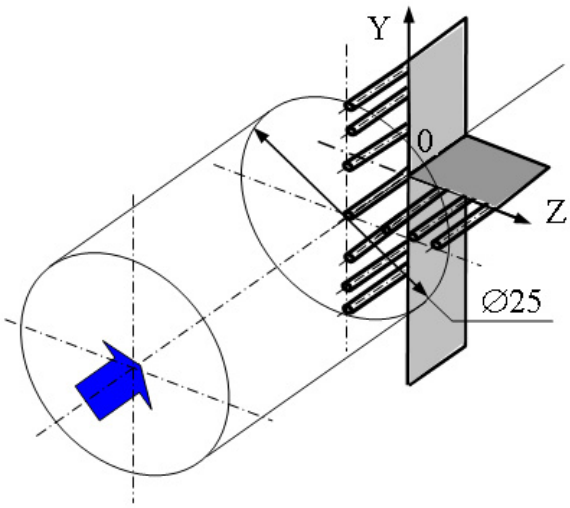

Fig. 1.13. Pitot tube rake at the insulator exit installed

Tenzoresistors are connected by the bridge scheme so that deregulation takes place at the plate bending (i.e. at delivery of pressure to the sensor), and some voltage corresponding to this deregulation is realized at the outlet of the sensor. The outlet voltage is delivered from the sensor to the differential amplifier united with the reference voltage stabilizer necessary for the sensor work. Both these elements are placed directly near each sensor. Mutual feeding of chips is realized from the matching plate, and then to automatic digital transformer (ADT) plate with USB-port and interface, which is connected with USB-port of PC. PC has software allowing to control this ADT plate. So signals from each sensor are delivered to PC monitor screen.

ADT plate used in this work allowed to deliver either 16 channels with differential output or 32 channels with unidirectional output. Clear detection of signals from the sensors was realized in the mode of the differential output because of measuring conditions. So in was possible to detect by PC only 16 signals from the sensors. Choice of sensors, from which signal detection was realized was changed with respect to conditions of definite experiment carrying out.

In Fig. 1.14 one can see typical signals from the sensors placed along the supersonic pressure. These signals were obtained when air under the pressure of 2 atm was delivered to air system and gas letting system, initial pressure in the channel was 0,14 atm at that.

In Figures 1.15-1.18 are separately represented signals from the flow meters, see Fig. 1.15, at the inlet to the channel and in the supersonic nozzle, see Fig. 1.16, in the forming channel (isolator), see Fig.1.17, and in working sections, see Fig.1.18. Numbers near each signal correspond to the sensor numbers represented in Fig.1.12.

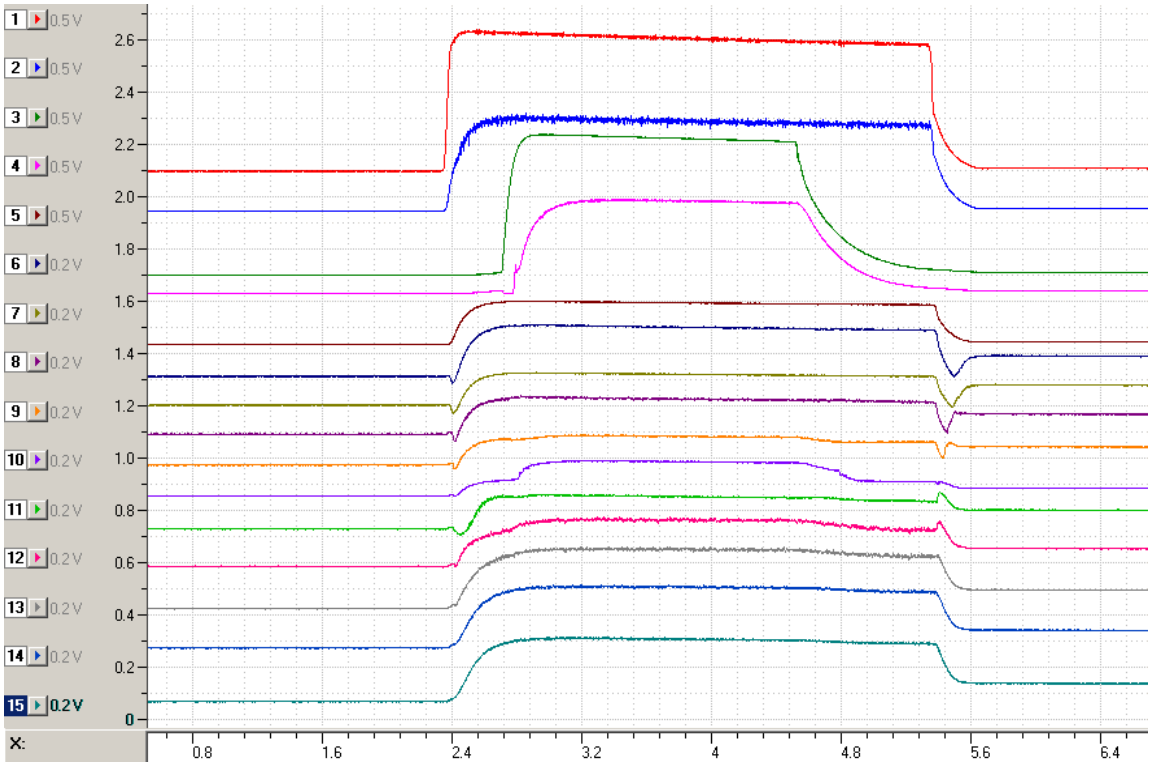

Fig. 1.14. Typical signals from the pressure sensors

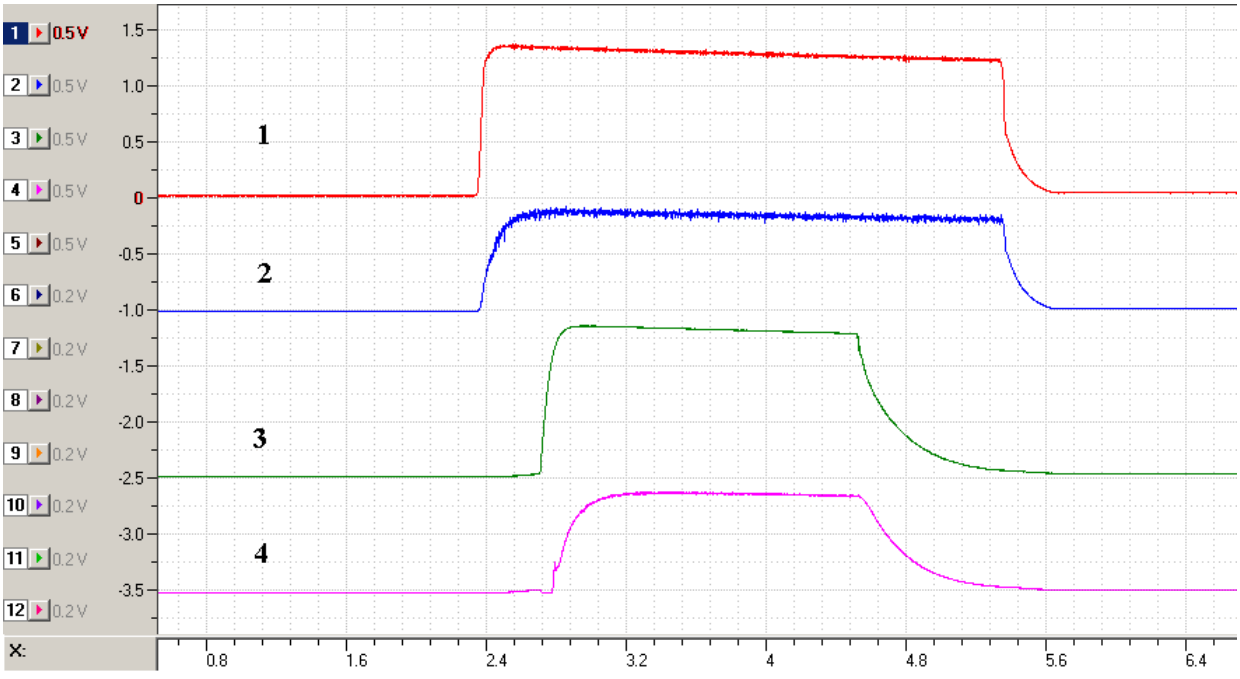

Fig. 1.15. Signals from the pressure sensors numbers 1 – 4.

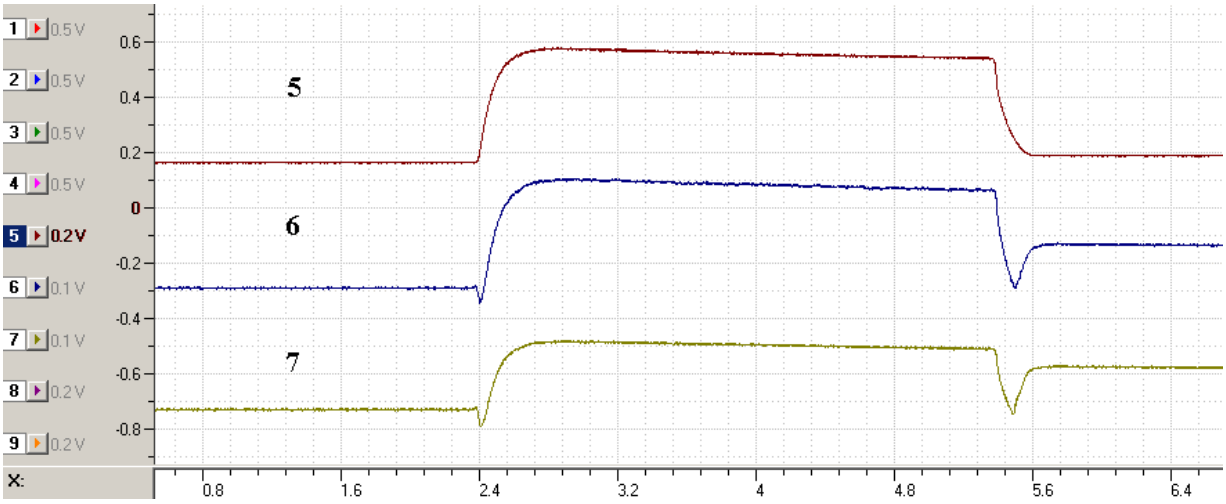

Fig. 1.16. Signals from the pressure sensors numbers 5 – 6.

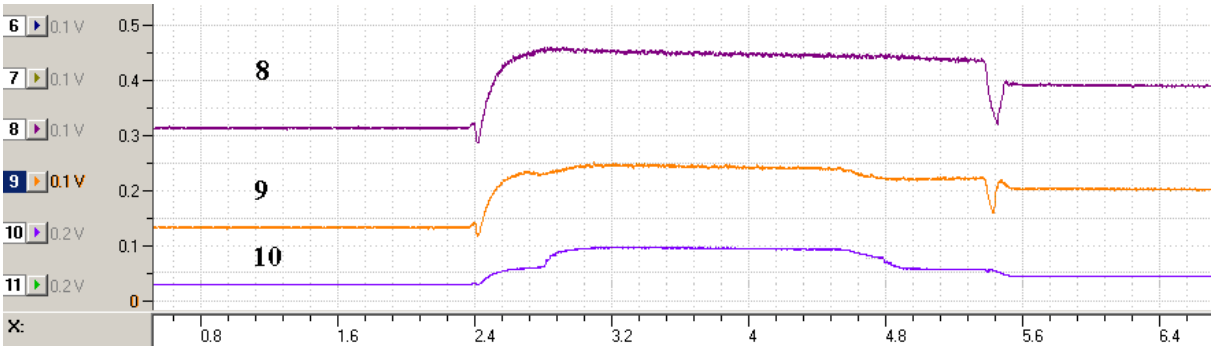

Fig. 1.17. Signals from the pressure sensors numbers 8 – 10.

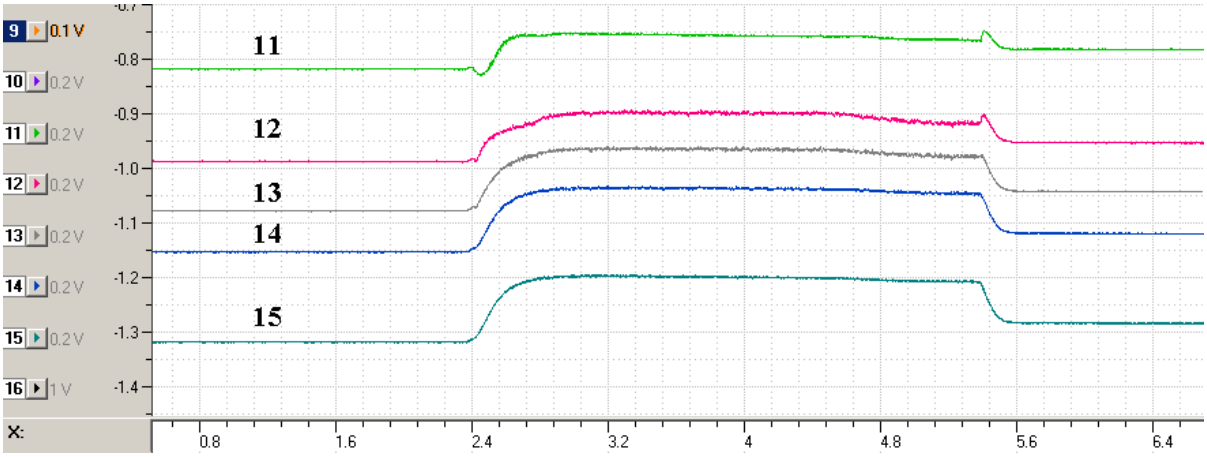

Fig. 1.18. Signals from the pressure sensors numbers 11 – 15.

For calculation of true pressure in the channel it is necessary to make a calibration characteristic in a form of the signal value dependence (in V) on pressure (in atm). The calibrating characteristics were obtained at slow pressure variation in the channel in the result of air letting from the atmosphere after preliminary pumping out down to 15 Torr. By this way we calibrated sensors working at the pressure below the atmospheric one. We made

additional calibrating for sensors measuring the pressure above the atmospheric one at air pumping to the channel up to the pressure of 3 atm.

Examples of these calibrating characteristics for two sensors are represented in Fig. 1.19 (a and b). One can see that sensor signal values are practically linearly rise with pressure increase.

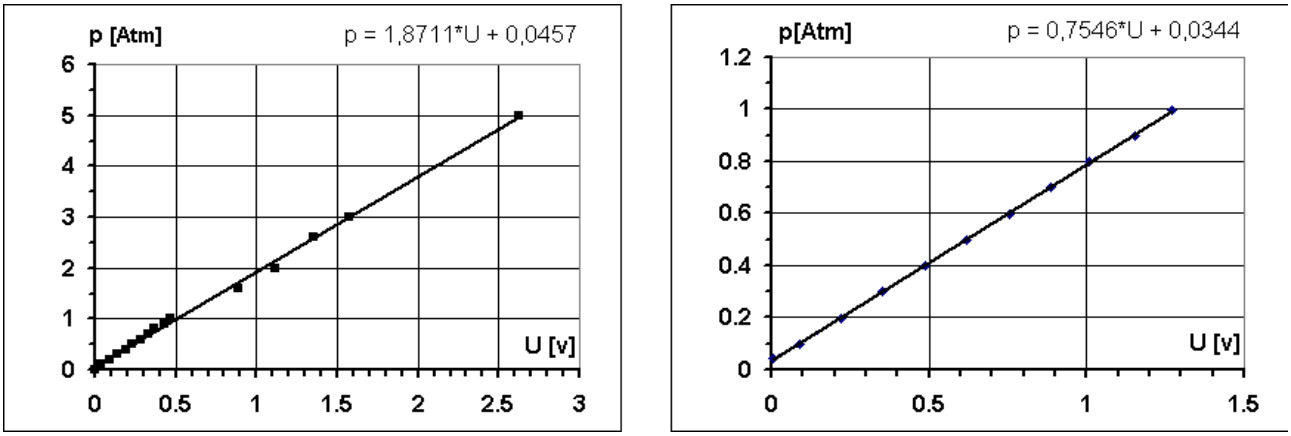

a) b)

Fig. 1.19. Calibrating characteristics for two pressure sensors

The dependence represented in Fig. 1.19a corresponds to the sensor with working pressure up to 5 atm, and with working up to 3 atm in Fig. 1.19b.

The full cycle of the sensor signal analysis consisted in the following. Firstly digitized signals recorded by the computer were translated into text files with a help of the special code. At that we obtained too large data massive summed over all sensors. So the next operation consisted in obtaining of the massive of some definite data lines: for example, each 50-th or each 100-th line. This operation allowed to diminish the initial massive by 5 – 10 times. Then we made absorption of points that did not carry the information: beginning and end of the signal recording. Final text file obtained by this way was put to the Excel code. There the following mathematical analysis of the data was made (transition from the sensor voltage signal value temporary dependence to the pressure in the channel temporary dependence in the place of the sensor location) with accounting of calibrating curves for each the sensor. In the result there was created the data massive characterizing the pressure temporary dependence in the channel in the points of sensor locations. One can see an example of these dependencies in Fig. 1.20 (a and b). Numbers corresponding to the color of the curve equals to the channel numbers from the sensors.

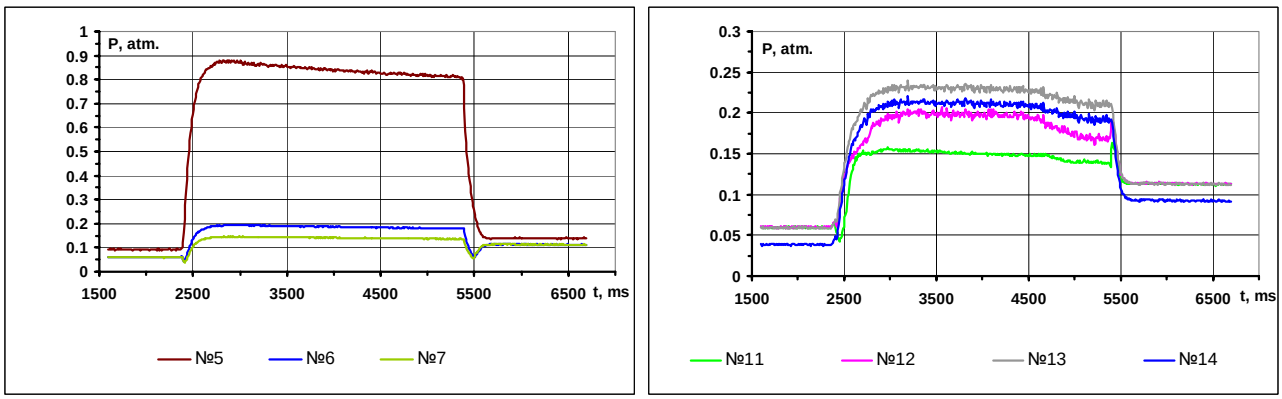

a) b)

Fig. 1.20. Pressure temporary dependence

1.4.2. Flow rate measuring. Airflow and propane flow rates were measured by the measuring nozzles, which geometrical sizes were chosen with a help of conventional ratios of Venturi nozzles. Flow rate values were calculated with a help of the pressure measured before the measuring nozzle P_i and the area of the critical cross section $F_{c,i}$ according to the ratio:

$$G_i = m \times P_i \times q(\lambda) \times F_{c,i} / \mathrm{sqrt}(T_i),$$

here $m=0.396$, $q(\lambda)=F/F_c=1$ – is gasdynamic function.

Summed fuel excess coefficient ϕ_Σ was calculated with a help of equation

$$\phi_\Sigma = (G_{fuel} / G_{air}) \times L_0 = (P_3/P_1) \times F_{c,\,fuel} / F_{c,\,air} \times L_0,$$

here P_i and T_i – are the pressure and temperature of the i-th component at the inlet to the measuring nozzle, L_0 – is stoichiometric coefficient approximately equal to $L_0 = 14{,}5$. One can transform the equation above accounting the sizes of measuring nozzles to the following:

$$\phi_\Sigma = P_3/P_1 \times 0.639.$$

Typical pressure variation diagrams in the system of air and fuel delivery (over the inletting time) are represented in Fig.1.21.

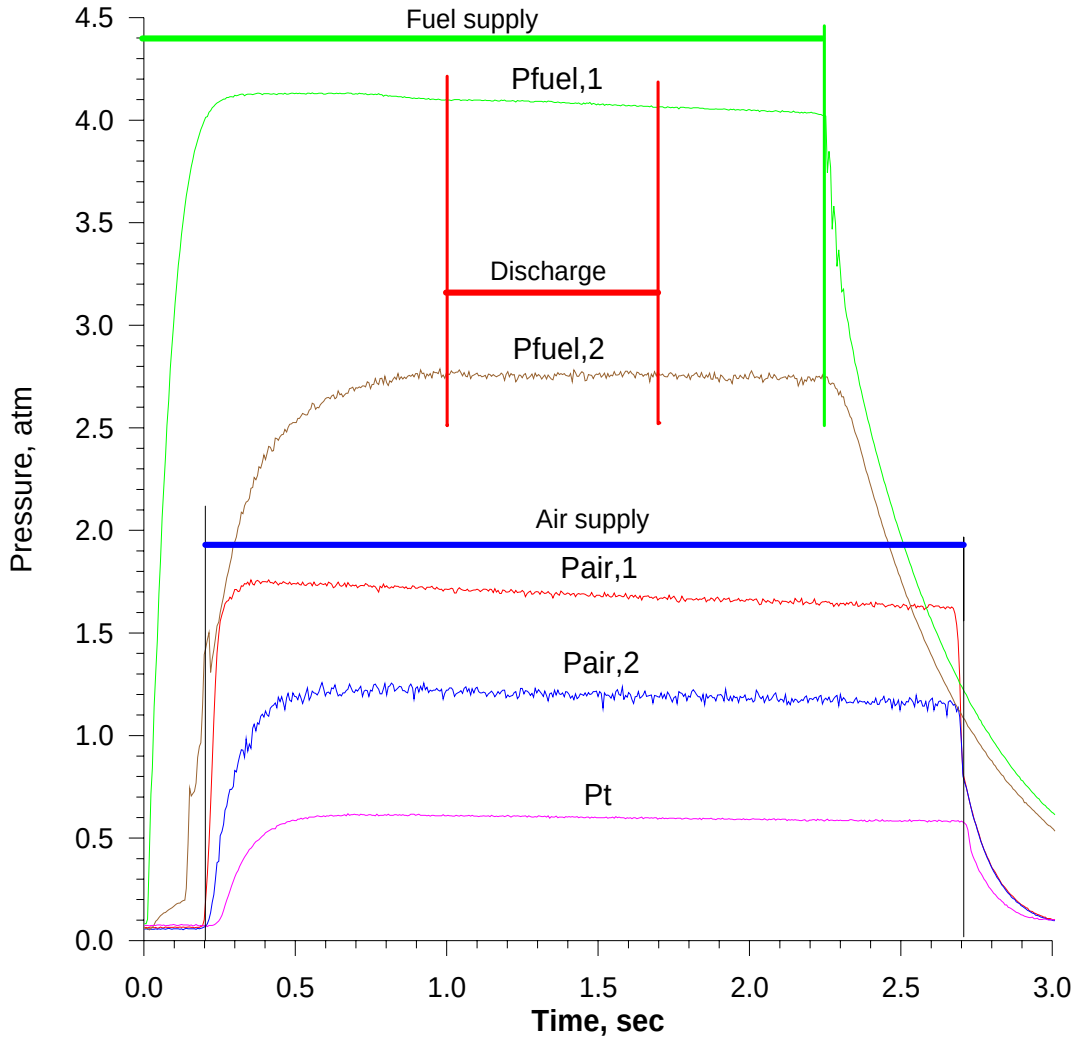

Fig. 1.21. Time histories of pressures before and after metering nozzles in air manifolds - $P_{air,1}$ and $P_{air,2}$ and in fuel manifolds – $P_{fuel,1}$ and $P_{fuel,2}$ and in receiver pressure - P_t

We have to note that quasi stationary mode in the fuel line is established approximately after 1 s , and after about 0.6s in the air line due to delay of air and fuel valves opening. The average rate of air pressure drop is (0.5-1)10-2 atm/s during the startup, i.e. one can say that there is quasi stationary gasdynamic process in the channel at the discharge absence. Required duration of the quasi-stationary process realization of 2-3 s is reached even at low pressures P_t=0.5-1atm in the channel receiver. So in main part of startups the command of plasma generator work start was given with the delay time of 1 s. Tests were carried out without air heating but Cowper heater was included to air line of the stand. In the result considerable pressure losses were observed see Fig.1.22.

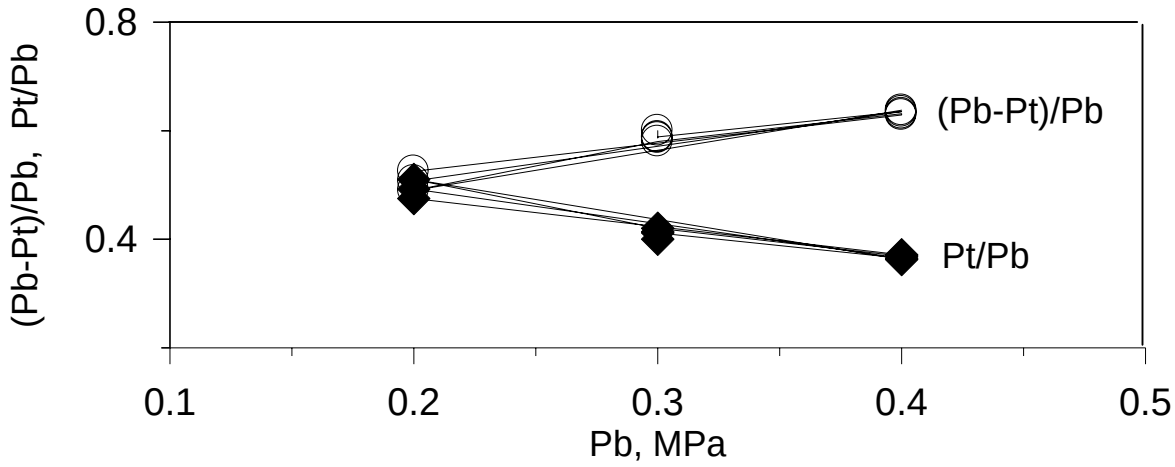

Fig.1.22. Pressure losses in manifolds of air supply system

The comb of 10 full pressure nozzles was placed in the outlet cross section of the isolator for determination of the flow parameters in the channel, see Fig.1.13. Examples of measured pressure waveforms for flow modes without of the discharge are represented in Fig.1.23 and Fig.1.24.

Mach number values in vertical and horizontal directions of the outlet isolator cross section are represented in Fig.1.25, they were determined with a help of full pressure measurements. Dimensionless static pressure distribution over the channel length including the nozzle, the isolator and the first channel section with plasma generator is represented in Fig.1.26.

Represented results show that pressure variation P_t in the receiver in the range P_t=0.05-0.2 MPa practically does not influence the flow in the channel. Increase of pressure both at the isolator section and in the channel behind the step is observed in test with propane, see Fig.1.26, it is caused by mass delivery and local flow separations before jets. Propane mass flow rate was changed in the range from 5 to 15% of the air mass flow rate, this corresponded to the fuel excess coefficient value ϕ=0.8-2.0

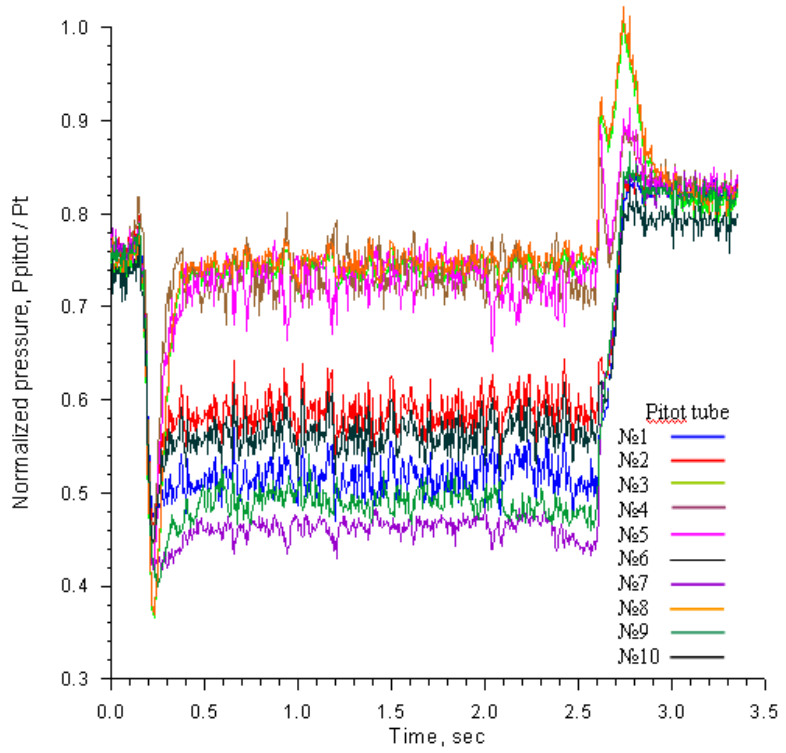

Fig.1.23. Histories of normalized Pitot pressure (without discharge), P_{tot}=0.2 MPa

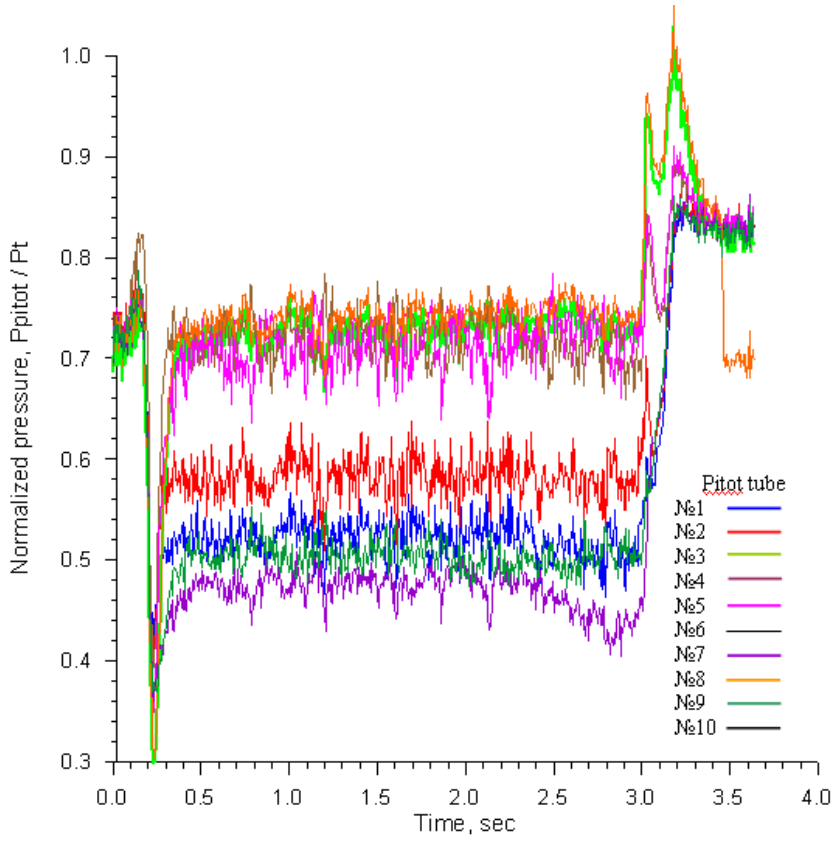

Fig.1.24. Time histories of normalized Pitot pressure (without discharge), P_{tot}=0.07MPa

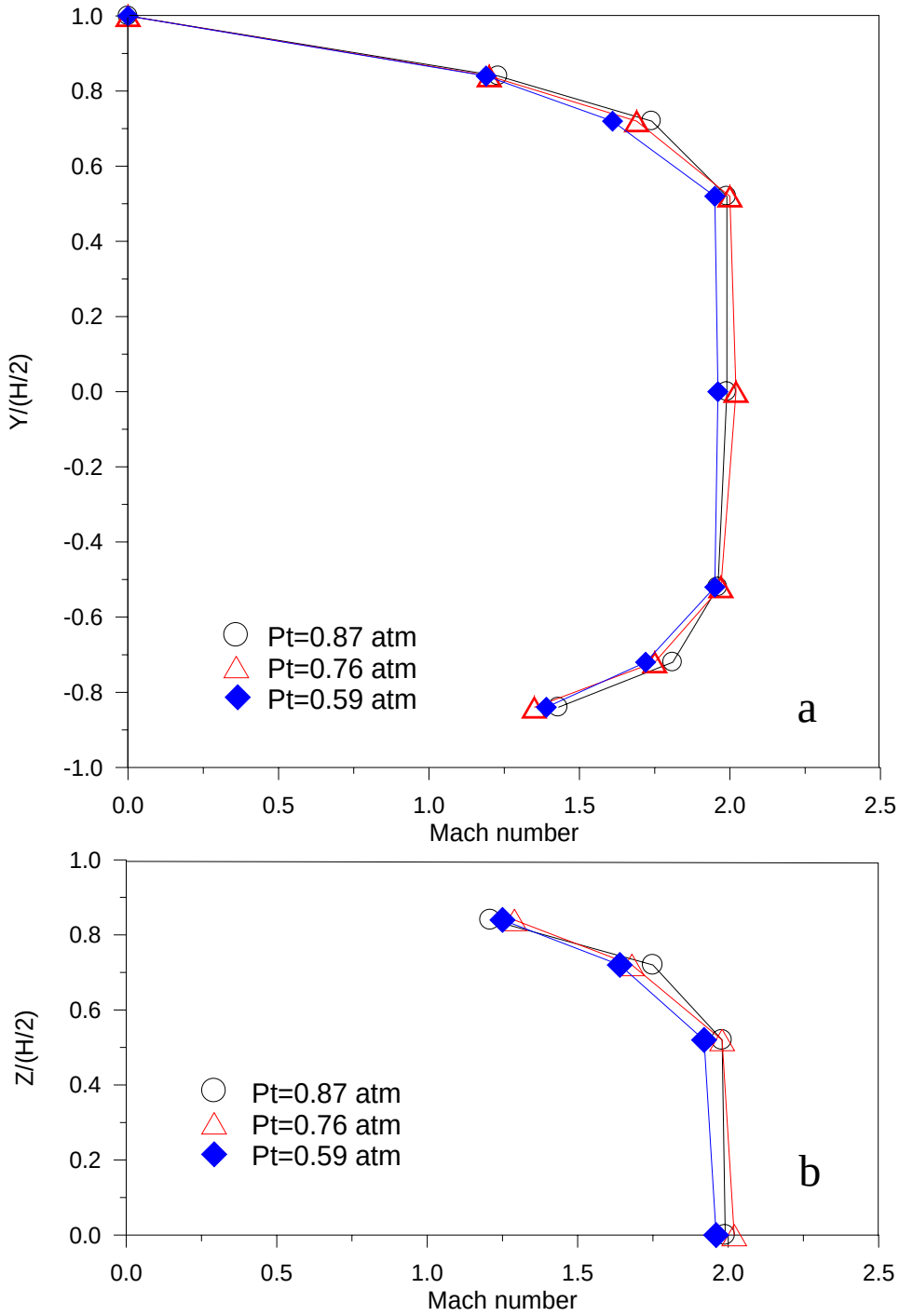

Fig. 1.25. Mach number profiles on Pitot pressure measurements calculated a – along Y axis, b – along Z axis

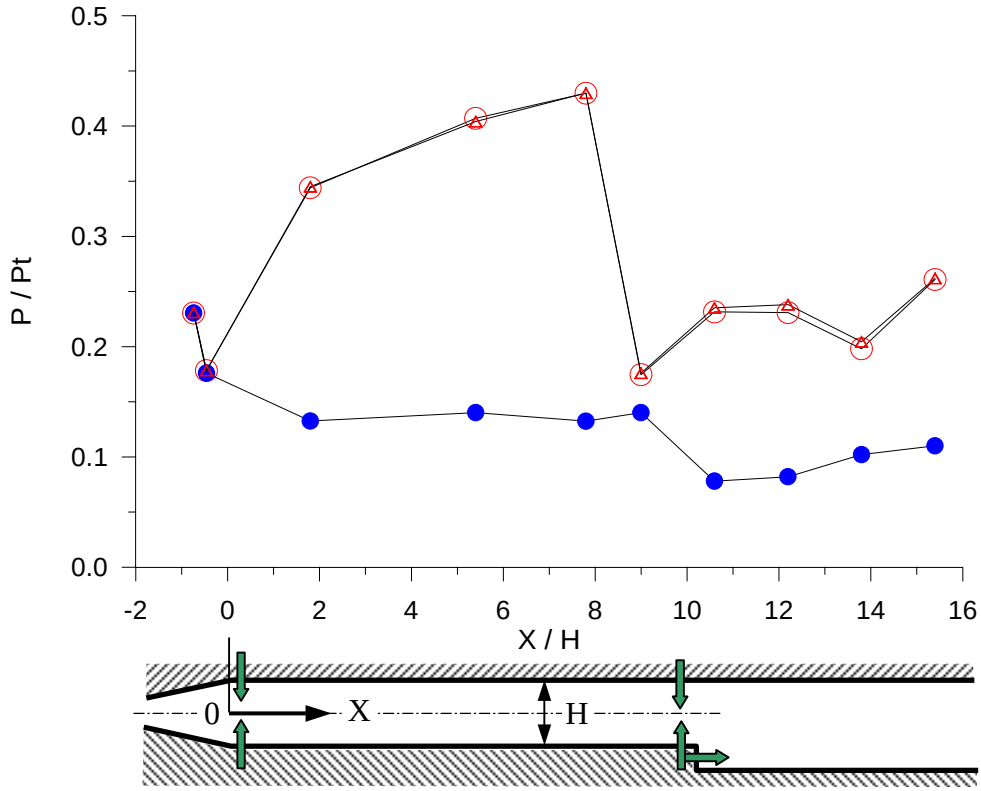

Fig. 1.26. Pressure distribution P/P_{tot} along combustor channel with transversal-longitudinal discharge and propane injection, ϕ_{Σ} = 1.6, Pt=0,84 atm
● - without propane injection,
○ - with fuel injection and without discharge,
△ - with fuel injection and discharge

1.5. Plasma generators

1.5.1. Spark plug. For study and comparative analysis of different plasma discharge generators preliminary performance of standard spark plug, used for ignition of kerosene/air mixtures in ground power plants, were defined (Fig. 1.27-1.28). The spark plug realizes the pulse-periodical spark discharge of f=30-50Hz frequency and pulse W .0.5J energy during a single pulse of .6mks duration. Reserved initial energy was equal to 1.2J at U=1.2kV voltage.

One can see from represented photos that the discharge creating the plasma is realized not over the whole surface of the plug face (what is typical for end face MPC), but only in the narrow sector. This is connected with the fact that values of currents and voltages are rather small in the discharge, so the power put to the discharge is also small. This leads to the result that magneto dynamic effects typical for classical MPC are not realized.

Temporary resolved shadow photos of the process were made for determination of dynamic characteristics (motion of the plasma and shock wave (SW)) of this discharge. Typical shadow pictures are represented in Fig. 1.28. In the photos one can distinctly see disturbance front (SW) motion with respect to the end face of the plug.

Fig. 1.27. Spark plug (front view)

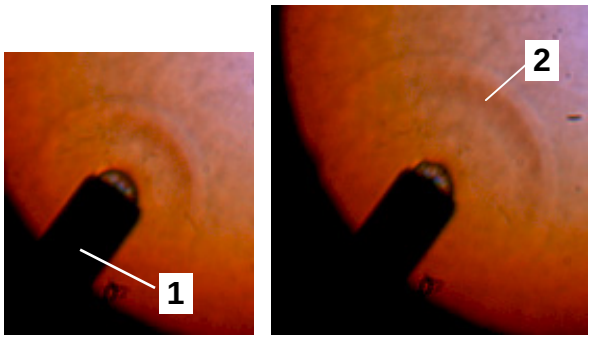

τ=30 mks τ=50 mks

Fig.1.28. Pictures of spark discharge vs time (time of exposition - 2 mks)
1 – spark plug, 2 – shock wave

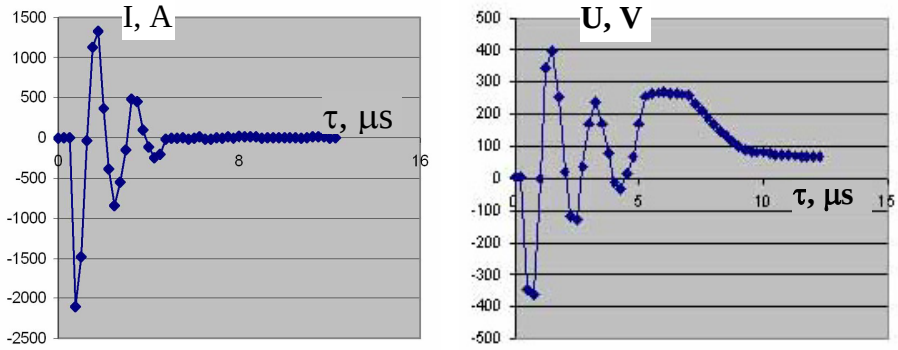

Fig. 1.29. Processed time histories of current and voltage vs time (single pulse), I_{max}= 2 kA, U_{max}~ 400 V, τ_{pulse} ~ 6 μs.

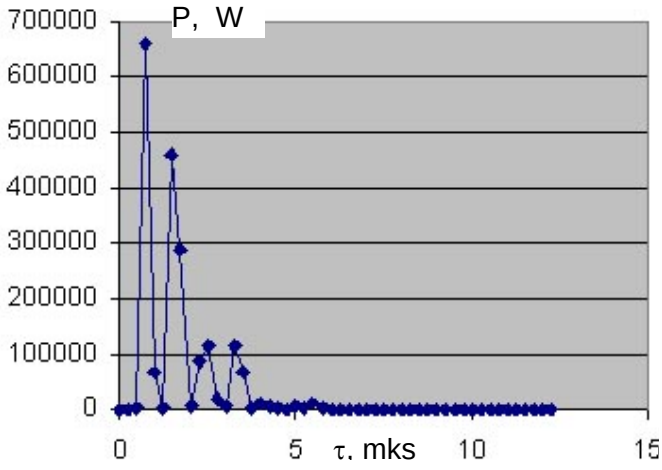

Fig. 1.30. Input discharge power $P(\tau) = I(\tau)U(\tau)$.

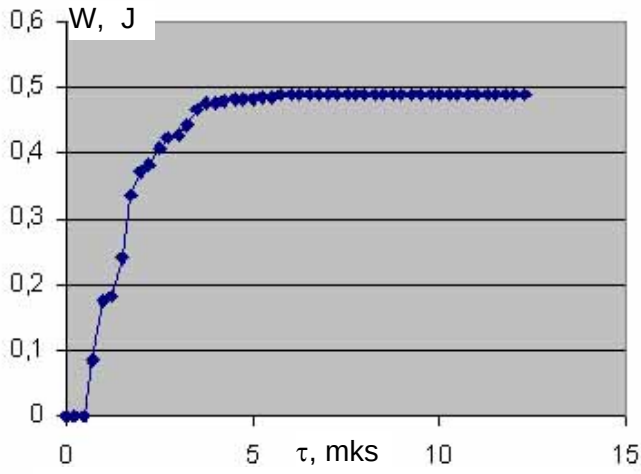

Fig. 1.31. Input discharge energy (single pulse)

$$W = \int_{0}^{\tau} IUd\tau = 0{,}5 \text{ J}$$

Analysis of the series of analogous photos obtained in different time moments allowed to determine the propagation velocity of this disturbance. In Fig. 1.32 one can see results of this analysis in a form of the distance via time covered by SW from the end face of the plasma generator. It can be seen from this figure that the distance covered by SW is practically linearly rises in time with constant current close to the sound velocity (v~300 m/s). Unfortunately time resolution of the high-speed camera (about 3 μs) did not allow to get shadow pictures in the beginning of the discharge (which time is about 4 μs as it was noted earlier) when the main energy put takes place. However, existing data allows to suppose that SW velocity reaches ~ (1 – 1,5) km/s at initial discharge stages, this is comparable and even greater than supersonic flow velocity. Initial temperature of the gas heating of ~ 1000 ^{0}K corresponds to this SW velocity.

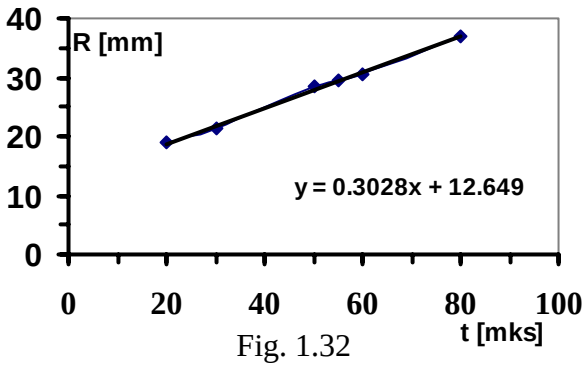

Fig. 1.32

It follows from the waveforms represented in Fig.1.29 that both the current pulse and the voltage pulse are the relaxation oscillations with mutual duration of about 10 μs and quasi period of ~ 4 μs. At that the maximum amplitude of the discharge current reaches the value of about 2 κA, and of the voltage– 400 V.

Analysis of analogous waveforms allows to determine power and energy variation that are released in the discharge plasma in time. In Fig. 1.30 one can see typical temporary dependence of released power. It is possible to calculate energy released in plasma temporary dependence making numerical integration. Typical example of such a calculation is represented in Fig. 1.31.

From represented dependences one can see that the time of main energy release practically coincides with the first quasi period of the discharge, i.e. approximately it is equal 4 μs. Power maximum value reaches the value of about 700 kW and the discharge energy – 0,5 J. This figure confirms the fact that the discharge of the plug essentially differs from the discharge of MPC, for which typical power values are about of tens of MW, and energy stored in the discharge is of hundred of joules and even kJ.

1.5.2. Transversal-longitudinal discharge. As distinct from early studied the transversal and longitudinal discharges [1-4] a new scheme of the electrodes placement is considered, Fig.1.33. which provides combined (transversal-longitudinal) discharge. Copper electrodes of 3mm diameter are placed relatively to each other fixed as shown in Fig. 1.33. The tests of this type plasma generator in channel installed were conducted at the motionless and at the supersonic M=2 airflow conditions for two positions of the electrode unit relatively the low channel wall, that is, in the first case the low electrode was placed on the low wall, Fig. 1.34 and in the second case the distance between the wall and low electrode was 5.5mm, Fig. 1.35. The electrode unit was situated in the test channel behind the reverse step. The parameters of the incoming airflow were the following as: nominal Mach number – M=2, total pressure and temperature p_t=(0.2-0.4)×10 ^{5} Pa and T t= 300K correspondingly. For initiation of discharge constant voltage of 4 κV was provided and during the discharge process the current I was equal to 2A. Photos of discharge with and without airflow are presented in Fig. 1.33-1.35. Neutral light filter was used to weaken an intensity of lighting. All represented discharge photos in the flow were obtained at initial pressure 100 Torr in the channel and 3 atm pressure in the receiver. All experiments were undertaken at feeding source voltage of U

= 5 kV and discharge current value of I = 2A, this was achieved at series including of the ballast resistance of 2,5 kOhms.

In case of tests with airflow and low position of the electrode unit, Fig.1.33, the realized discharge is situated in separation zone behind the step and so its image looks like one in a motionless space. In case of tests with high speed M=2 airflow and upper position of the electrode unit the discharge is situated mostly outside the separation zone in transonic air flow by the electrodes disturbed. One can see the discharge is under the strong influence of external flow and is pulled down by the airflow and looks like a torch discharge [5]. Average gas temperature in discharge volume according to Ref. 3, 4 data is equal to T_{gas}=2000-2500K.

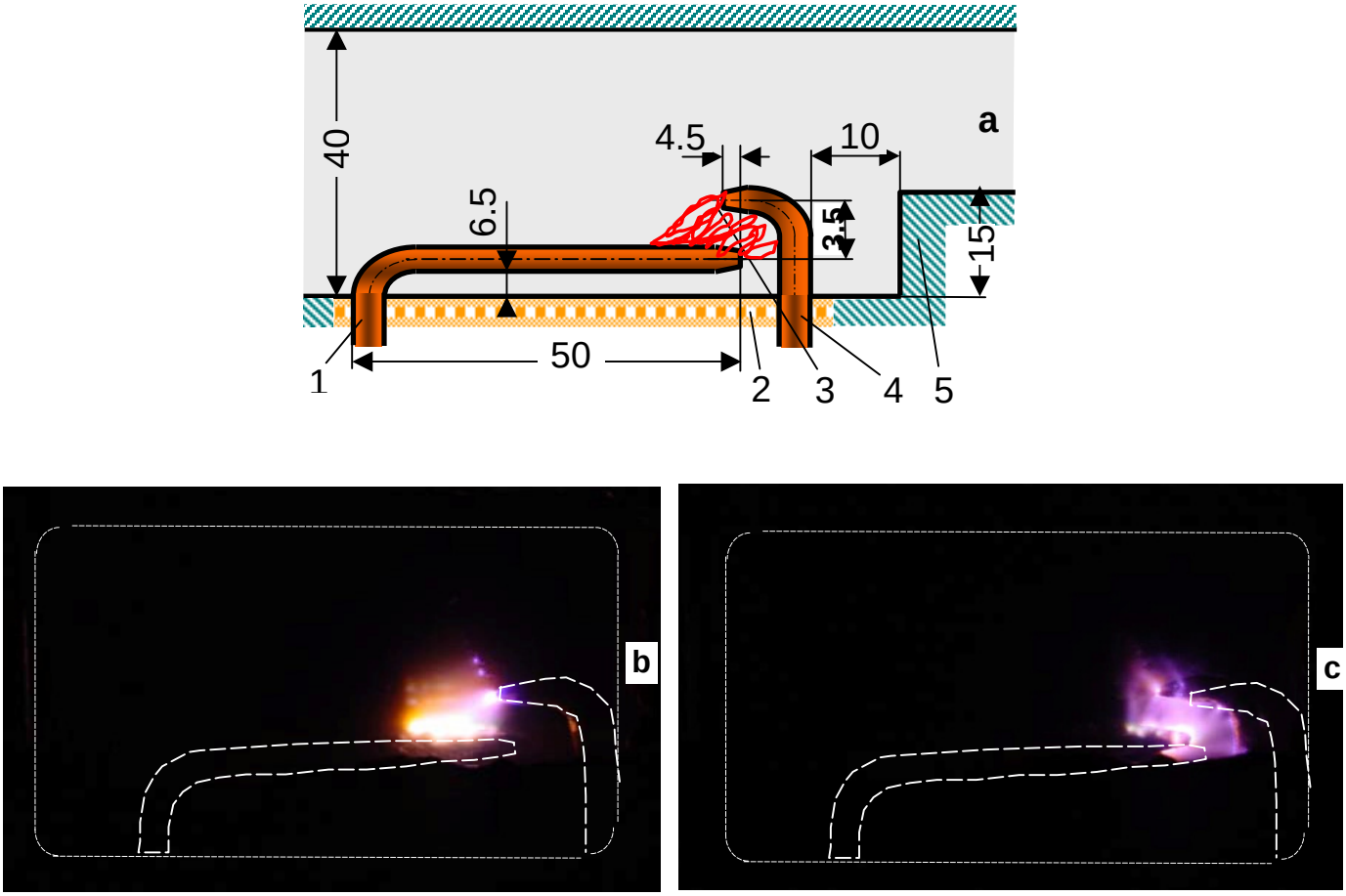

Fig. 1.33. Photos of two electrodes discharge in a channel at zero airflow velocity and exposition time of τ= 1/100s. a – scheme of electrodes placement in channel: 1 – anode, 2 – isolator, 3 – discharge, 4 – cathode, 5 – reverse step – flameholder; b – P = 10^5 Pa, c – P = 10^4 Pa

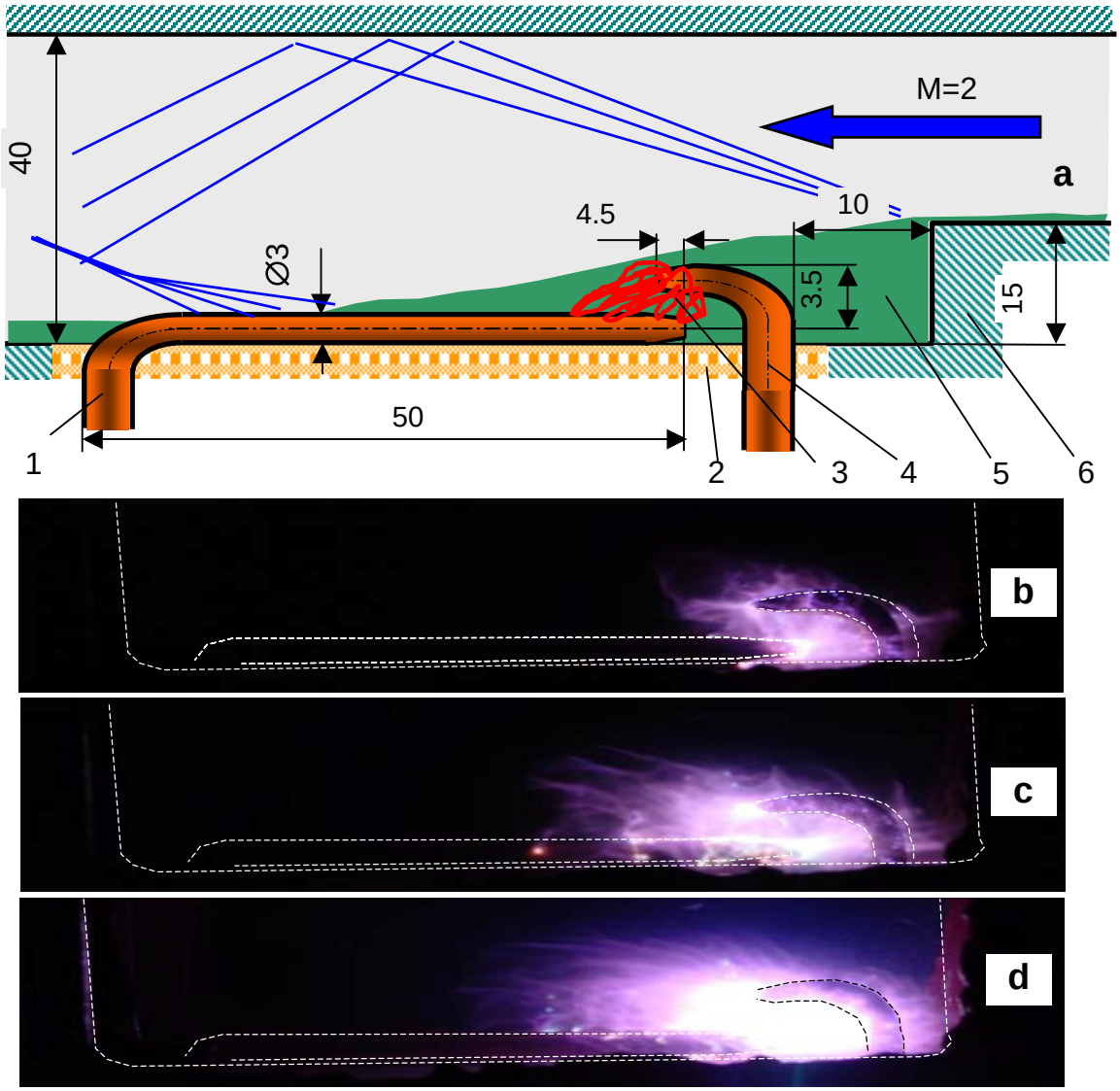

Fig. 1.34. Photos of two electrodes discharge in a M=2 airflow at low position of electrodes
a - scheme of discharge in channel
1– anode, 2– isolator, 3– discharge, 4– cathode, 5 – separation zone, 6 – reverse step,
b– exposition time τ=0.01s, c- τ=0.025s, d-τ=0.1s

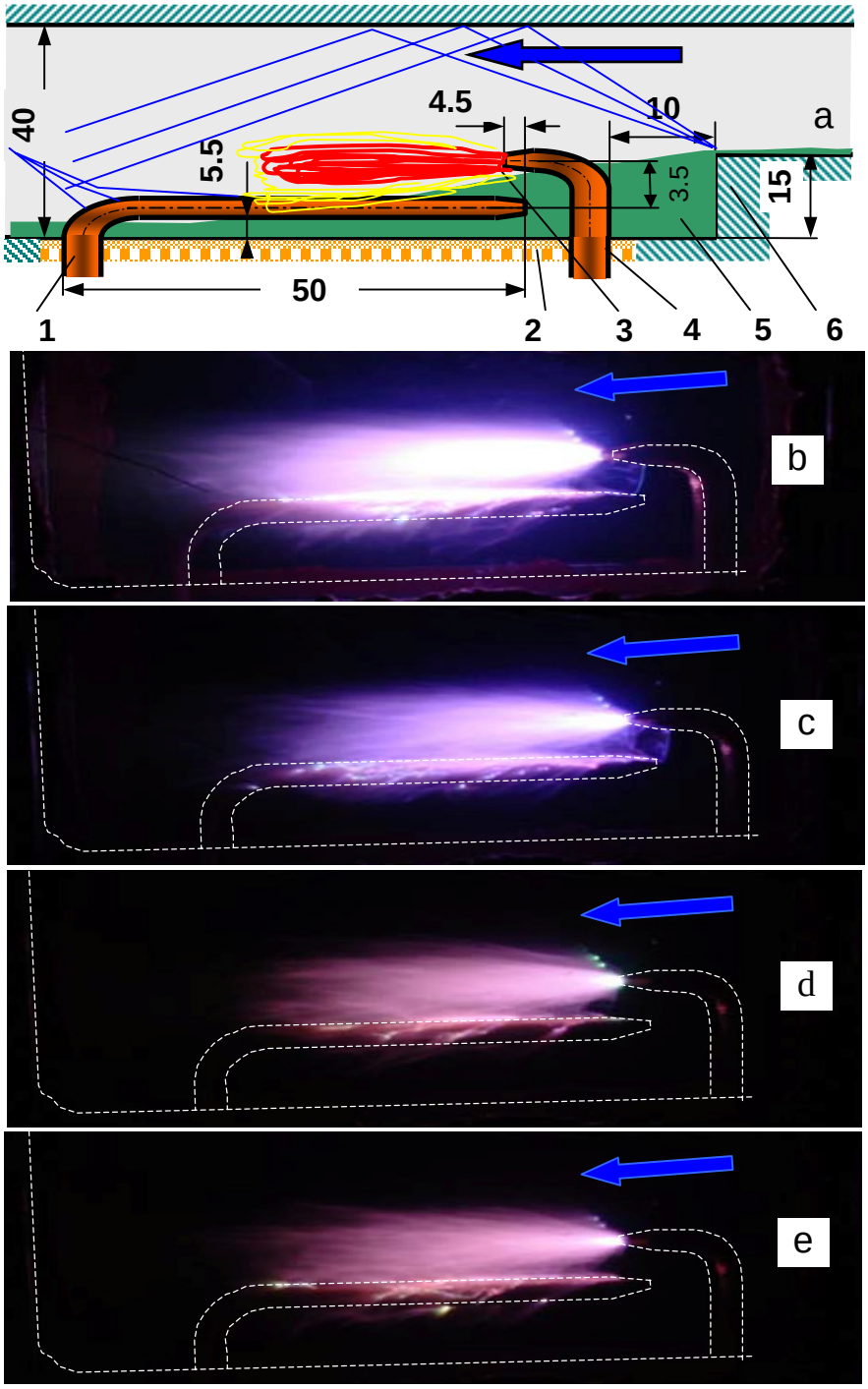

Fig. 1.35. Photos of discharge in a channel
M=2 flow at upper position of electrodes
a – scheme of electrodes placement
in channel: 1 – anode, 2 – isolator,
3 – discharge, 4 – cathode,
5 – separation zone, 6 – reverse step,
b –exposition time τ=0.1s, c - τ=0.01s,
d - τ=0.005s at P_t=3x10^{5}Pa,
e - τ=0.005s at P_t=2x10^{5}Pa

Undertaken experiments show that change of initial pressures in the supersonic channel do not lead to substantial differences between discharge development processes. Note that typical jet plasma flows over the supersonic flow and along the lower electrode are observed in all the discharge in the flow photos.

1.5.3. Magneto-Plasma Compressor (MPC). Scheme of plasma generator is shown in Fig. 1.36. This MPC was specially designed to study interaction of supersonic airflow and plasma formations. According to Ref.6, 7 data an initial velocity of plasma formation reaches 2 km/s and plasma parameters in a cumulating zone are the following as: temperature T =(18-20)×10^3 K.and electron concentration n=5 ×10^{16} -10^{17} cm $^{-3}$. Parameters of power source were the next: charge capacity - 50 μF, voltage – 3 kV and it corresponds to 225J of stored energy. Duration of the first discharge current semi period was 20 μs (first quasi period of discharge current is approximately 50 μs). Scheme of MPC installation in channel is shown in Fig. 1.37,a and direction of MPC axis was chosen basing on arguments of maximal plasma penetration depth into the airflow and to obtain long-lived plasma formations [7]. Photos of discharges with and without airflow demonstrate the same pictures of airflow/plasma interaction and argue that the penetration of plasma formations does not depend on airflow velocity at these test conditions.

Main near axis part of the plasma – its core conserves the angle of propagation both without the flow and with it. The flow influence is revealed only at the jet periphery, transversal sizes of which become much smaller in the result of the flow influence.

One can see from the photos obtained at different pressures in the receiver that jet core direction of propagation is practically constant, at the same time the transversal sizes of the periphery area are decreased, and the greater is the pressure in the receiver the more they are decreased. Besides, the longitudinal sizes of the plasma jet decrease with increase of pressure.

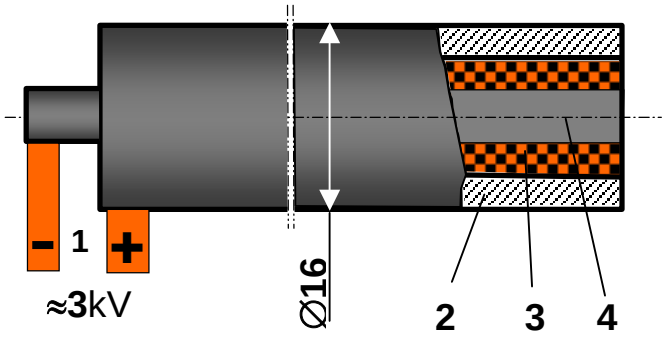

Fig. 1.36. Schematics of pulse plasma generator
1 – input energy 200-250J, τ≈50mks,
2 – anode, 3 – isolator, 4 - cathode

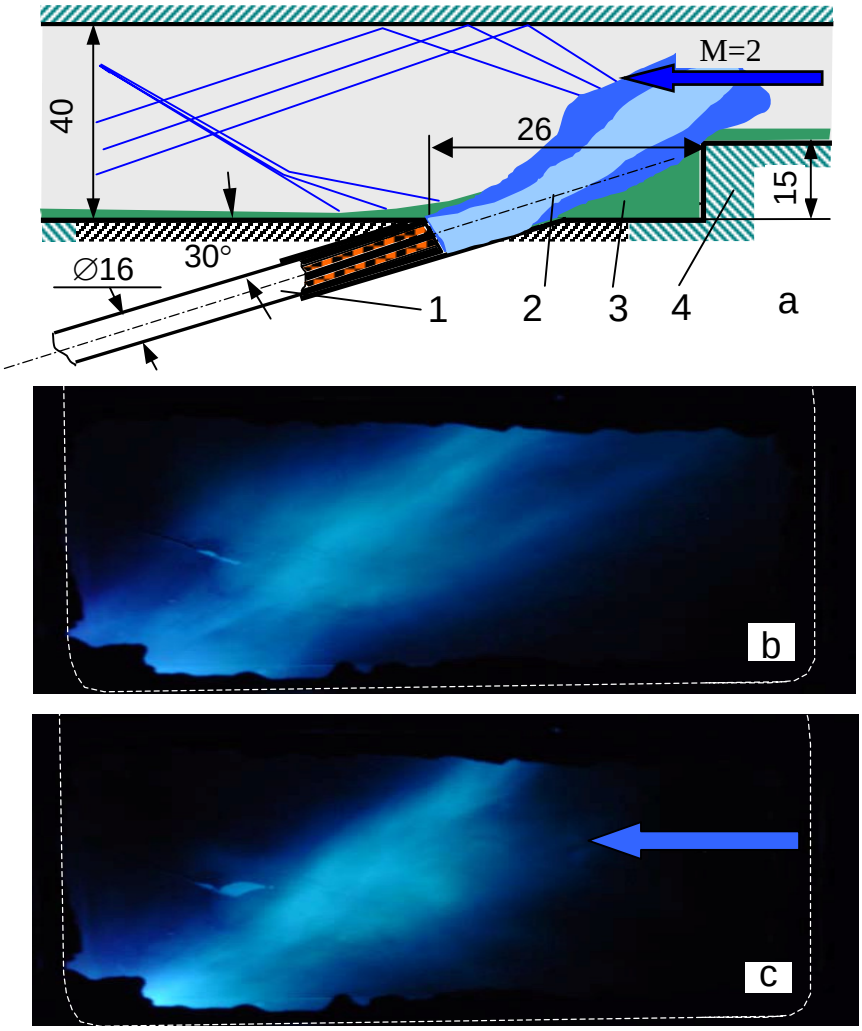

Fig. 1.37. PG installation and photos of the plasma jet (E=200-250J) in a channel
a – schematics of flowfield
1 – pulse plasma generator, 2 – plasma jet, 3 – separation zone, 4 – reverse step,
b – plasma jet in motionless air,
c – jet in a M=2 air flow (P_t=0.3MPa)

1.5.4. MW plasma torch generator. This type of generator was chosen because of small required power (less 1kW) for operation and possibility to operate with small rates (0.5-5.0 g/s) of different working gases flowing through the central electrode: argon, air, hydrogen, propane and others in the range of outer pressure P=(0.01-0.1)x10 ^{5} Pa. This high frequency MW discharge is characterized by the wave length of λ=12.2 cm, duration of MW impulse – 8 μs and time interval between the pulses – 12 μs. Preliminary diagnostic measurements of plasma jet give values of temperature decreased from (4-5)x10^{3}^{3}K in kernel zone down to 2500-3000K in.peripheral plasma jet regions [8]. As a source of MW flux a common magnetron used in the oven was applied.

The placement of the MW torch in channel is shown in Fig. 1.38 and the photos of discharge with and without airflow are presented here. The difference in pictures of MW plasma torch/airflow interaction points on strong influence of airflow dynamic pressure on depth of penetration into the airflow, but at total pressures P_{tot}=(0.2-0.4)x10^5 Pa an operation of generator was stable.

It is proposed to continue researches of surface MW discharge generator in combustion stabilization zone installed. Discharge will be initiated by the small metal particles distributed along the isolator surface and irradiated by the MW flux [9,10].

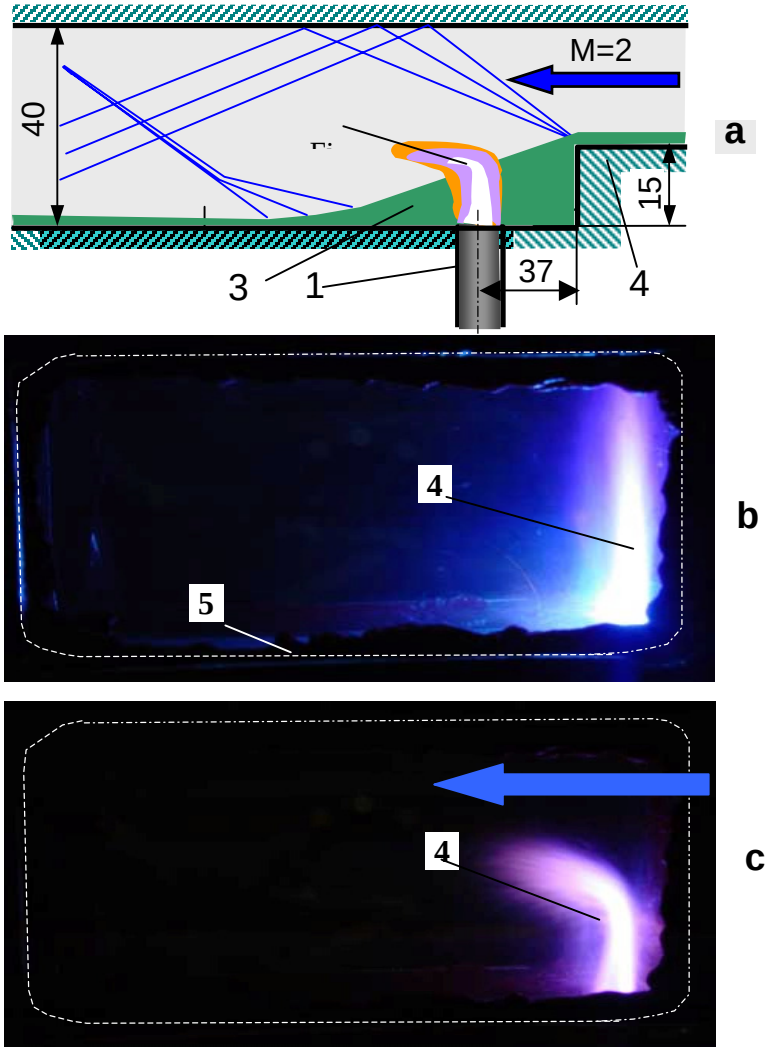

Fig. 1.38. Photos of the plasma jet initiated by the MW generator in channel installed
a – schematics of the flowfield in a channel
1 –MW generator, 2 – plasma jet, 3 – separation zone, 4 – reverse step, b – plasma jet in motionless air, c – plasma jet in a M=2 airflow and $P_t=3\times10^5$Pa , 4 - plasma jet, 5 - optical window

Undertaken experiments showed that constant current electrode discharge and MPC – discharge can be used for ignition of the fuel mixture practically in the whole volume of supersonic airflow. At the same time the plasma MW torch and plasma discharge of aviation plug can be applied for the fuel mixture ignition in the stagnant zone and on the flow boundary. It is necessary to emphasize that constant current discharge duration can be varied in rather wide limits: from 1 ms to some seconds, but MPC discharge duration is limited by storing condenser capacity and is 50 – 150 μs.

So further experiments on ignition possibility of supersonic fuel mixture were undertaken mainly with constant current longitudinally-transversal discharge application, this allowed to vary experimental conditions in wide ranges.

1.6. Electrical characteristics of longitudinally-transversal discharge in supersonic flow.

Experiments on ignition possibility of supersonic fuel mixture investigations were undertaken mainly with constant current longitudinally-transversal discharge as it was noted above. So this section is devoted to description of main electric characteristics of current longitudinally-transversal discharge in supersonic airflow.

Feeding source with outlet voltage up to 5 kV and maximum current up to 10 A was used for creation of the discharge at constant current. The current value was controlled by the ballast resistances included in series with the discharge gap. Location scheme and electrode forms are represented in Fig.1.39.

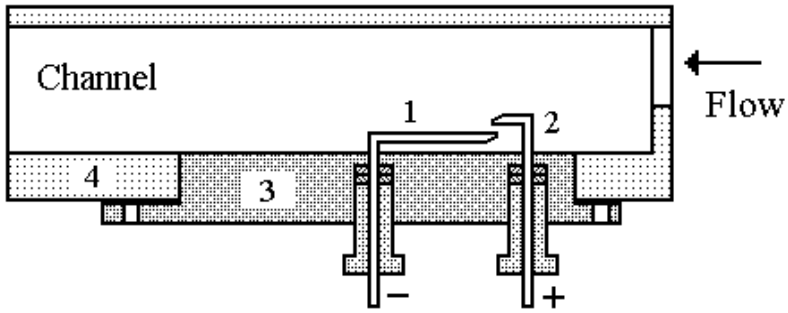

Fig.1.39

Electrodes (see Fig.1.39, positions # 1 and #2) were vacuum-type fixed to the dielectric plate (3), which was placed in the hatch of the working section of the supersonic channel (4). Electrodes were made of brass wire of 3 mm diameter. Length of horizontal part of positive electrode (2) was 10 mm, and 40 mm of negative electrode (1). Electrodes were placed coaxially along the flow, construction of their fixing at that allowed to change the electrode position with respect to height and relative distance between them.

Experiments have been executed at two positions of electrodes with respect to flow boundary: in lower positions when two electrodes were located in ‘stagnation zone”, and in upper position, when electrodes were located at the flow boundary. All measurements were carried out at feeding source voltage U = 5 kV, and at four values of discharge current, this was achieved at series switching on of different ballast resistances at voltage pulse duration variation from 0,1 to 1 second.

Fast-speed recording of the discharge picture was made with a help of super high speed CCD camera, which frame duration could be varied from the minimal equal to 3 μs to maximal of about 1 s. CCD camera was working in mode of movie recording, it allowed to get up to 100 separate frames during the whole discharge process.

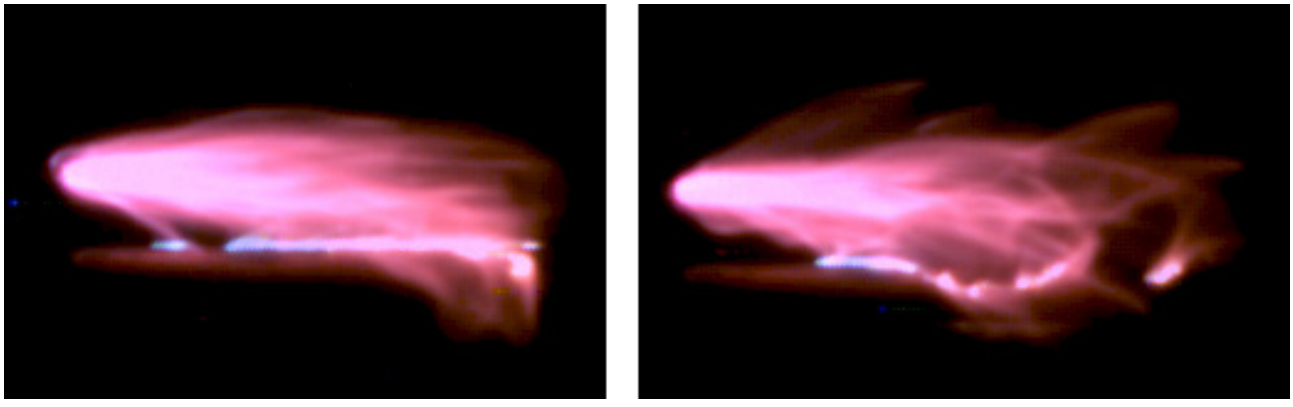

Fig. 1.40. Two typical fragments of fast recording of the discharge

In Fig.1.40 one can see two typical fragments of fast recording of the discharge, which were obtained at frame duration of 1 ms (frames were obtained at pressure of 0.28 atm in the working

channel, and 2 atm in receiver, duration of the voltage pulse was 1 s). It can be seen that at this exposure one obtains integral picture of the discharge.

In Fig.1.41 one can see also two fragments obtained at the frame duration of 60 μs (frames were obtained at pressure of 0.14 atm in the working channel, and 3 atm in the receiver, voltage pulse duration was 1 s). In this case it becomes possible to resolve discharge temporary evolution. One can see that the discharge propagates along the flow in a form of separate channels. Analysis of large number of analogous frames has shown that their sizes and spatial structure have absolutely chaotic character. Unfortunately the CCD camera optical efficiency did not allow to obtain large temporary resolution during present experiments.

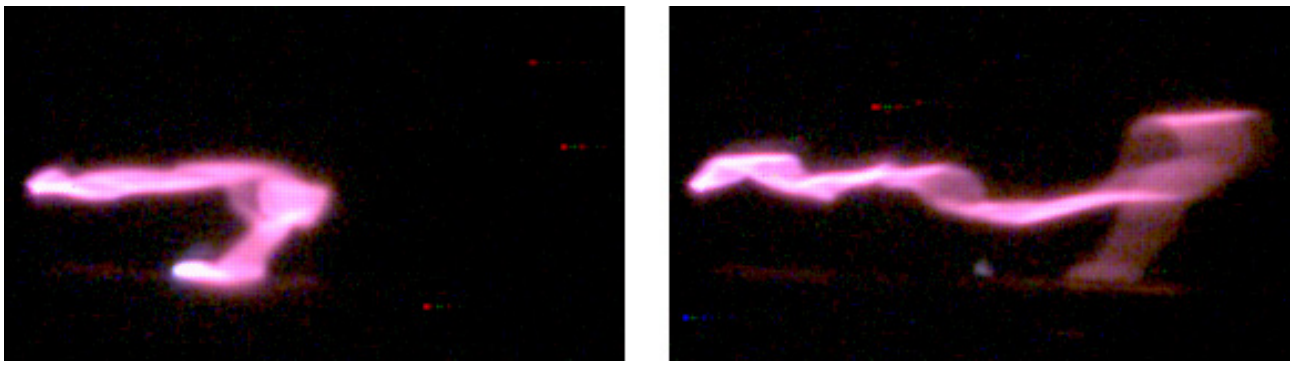

Fig. 1.41.

On a basis of analysis of large number of frames we determined dependencies of average length of plasma channel on initial conditions, namely on pressures in the supersonic channel and in the receiver, on voltage pulse duration and discharge current value. At that the maximum discharge length was measured in each frame, then the average value over all frames obtained at the same external parameters was determined. Typical results of such analysis are represented in Fig.1.42 and Fig. 1.43.

In Fig.1.42 one can see dependence of average length of the discharge on initial pressure in the working section: the upper curve corresponds to pressure of 3 atm in the receiver, and the lower 2 atm. In Fig.1.43 one can see dependence of average length of the discharge on initial pressure in the receiver: the upper curve corresponds to pressure of 0,14 atm, and the lower – 0,28 atm. It can be seen that these dependencies are rather weak (the discharge length changes for 2-3 mm, it practically coincides with accuracy of measurements), however there is definite tendency to decrease of the plasma length in the supersonic flow with increase of initial pressure in the working section and vice versa to its growth at increase of pressure in the receiver.

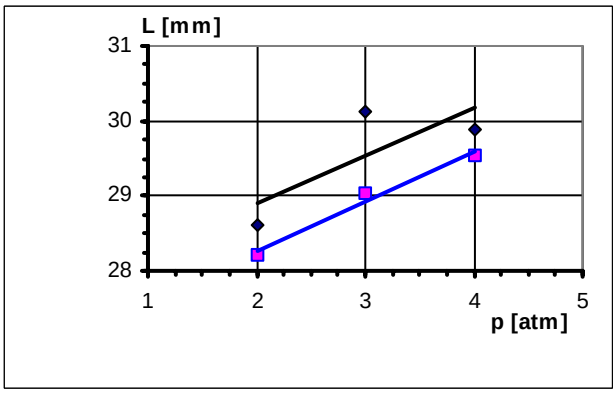

Fig. 1.42.

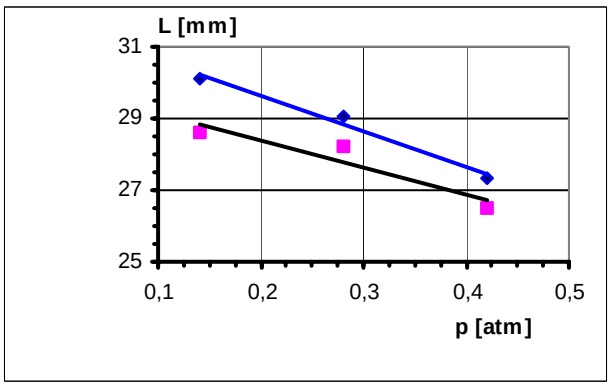

Fig. 1.43.

Electrical plasma parameters were measured with a help of ohmic voltage divider (voltage drop at the discharge) with the coefficient of division 9300, it is switched on parallel to inter electrode gap, and of shunt (value of the discharge current) with resistance of R = 0,31 Ohm switched on in series to the discharge. Signals from the voltage divider and from the shunt were detected with a help of two-beam storage oscilloscope «Tektroniks – 210» type. In Fig. 1.44 (a and b) typical waveforms of current and voltage at the discharge without flow (see Fig.1.44a) and with flow (see Fig.1.44b) are represented.

Upper waveforms in this figure correspond to voltage at the discharge (sensitivity 50 mV per point) and lower correspond to discharge current (sensitivity 500 mV per point). Temporary scan out was 500 ms per point, the whole voltage pulse duration was 1 s, initial pressures in the channel and in the receiver were 0,14 atm. and 3 atm., respectively.

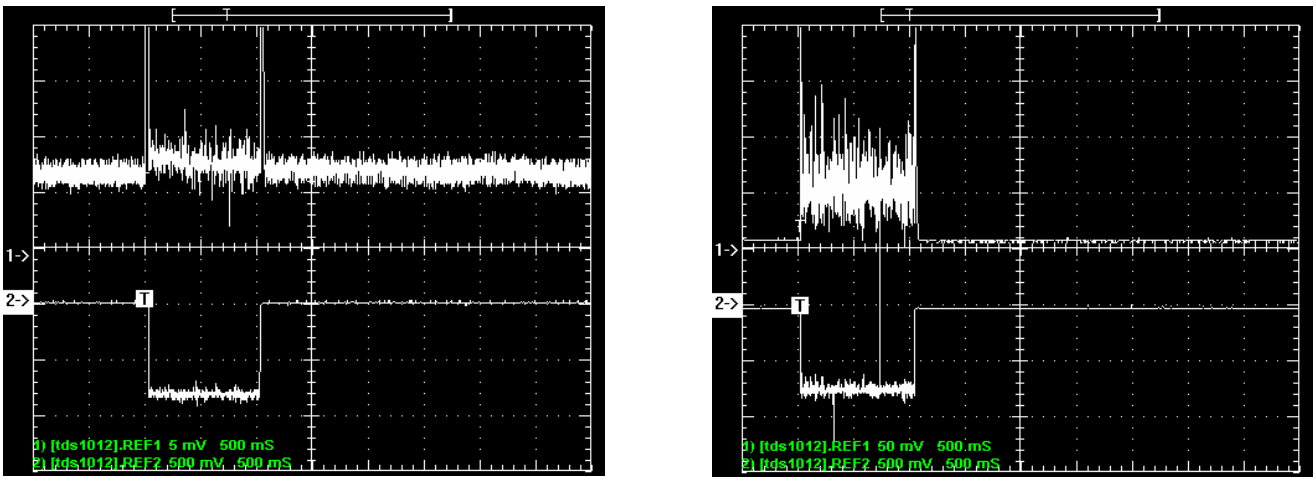

a) b)

Fig.1.44. Typical waveforms of current and voltage at the discharge without flow

One can see from the waveforms that discharge current value in both cases stays practically constant, at the same time significant voltage oscillations at the discharge in the flow are observed. Such voltage oscillations evidently correspond to secondary breakdowns in the discharge, which in this case have non periodic but practically chaotic character. At the same time visible current vibrations are absent. This is connected with the fact that the current is determined mainly by the ballast resistance, which is much greater than plasma resistance, and the voltage is directly proportional to the plasma resistance, which changes in time proportionally to the length of the plasma channel in the flow. This fact is confirmed by the data of the discharge photos obtained at small exposure (60 μs).

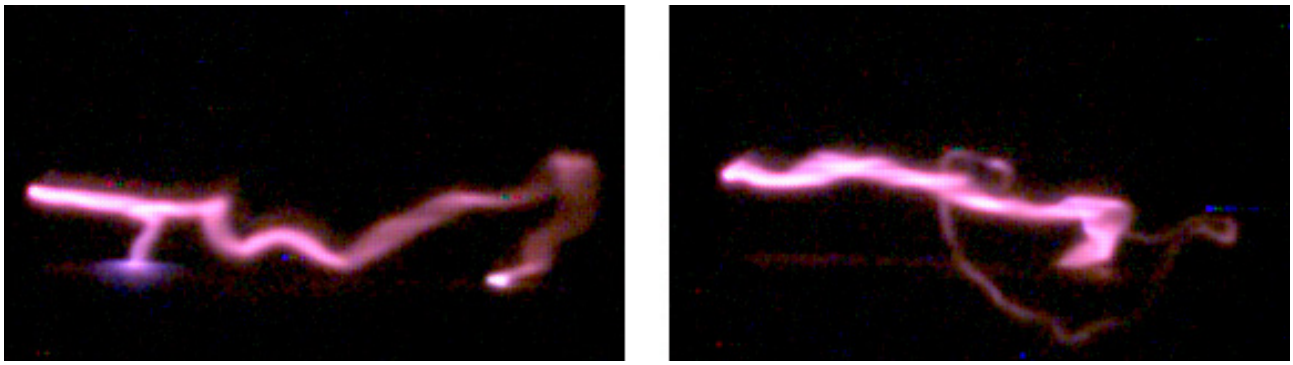

a) b)

Fig. 1.45. Fragments of high-speed video recording of discharge

In Fig. 1.45 (a and b) are represented fragments of high-speed video recording, one can see in them that the length of plasma formation changes constantly, and hence plasma resistance and voltage drop at the discharge change. In these frames besides one can distinctly see secondary breakdowns of inter-electrode gap and traces of the plasma, which cools after the secondary breakdown.

Photos in Fig.1.45 have been obtained at pressure of 0.14 atm. in the working channel and of 3 atm. in the receiver, voltage pulse duration was 1s. Note that such current and voltage oscillations were observed also in previous experiments on investigation of interaction of the discharge with supersonic flow created between electrodes placed perpendicular to the flow [1]. However such oscillations in these experiments had periodic character. But in the case of the longitudinally transversal character voltage value vibrations take place absolutely arbitrarily, i.e. chaotically. This difference can be explained by the following. Secondary breakdowns causing oscillations of the current and voltage at strictly transversal discharge take place in the fixed discharge place, and namely, in the area of the first Mach jewel (disc) created by wave structure of the flow, its position stays practically constant during the discharge. Secondary breakdowns in the case of longitudinally-transversal discharge can take place in any place of the negative electrode (we remind that its length is 40 mm). This fact determines accidental changes of plasma channel length and hence its resistance, which changes in their turn determine chaotic voltage vibrations at the discharge.

On a basis of analysis of the set of analogous waveforms we obtained Ampere-Volt characteristics of the discharge at different pressures in the channel $p_{к,}$), in the receiver ($p_р$), and at variation of voltage pulse duration. In Fig.1.46 (a and b) one can see Ampere-Volt characteristic of the discharge without air flow (see Fig.1.46a) and in the flow (see Fig.1.46b). Corresponding points in Fig.1.46b were obtained by averaging of numerical data obtained from the voltage waveforms because voltage drop waveforms at the discharge (as it was already noted) have strongly oscillating character. The upper curve in Fig. 1.46a corresponds to initial pressure 0,14 atm in the working section, and the lower curve to 0,28 atm. All curves in Fig.46b were obtained at pressure 0,14 atm in the working section, the upper curve corresponds to initial pressure 4 atm in the receiver, the middle curve to 3 atm., and the lower to 2 atm.

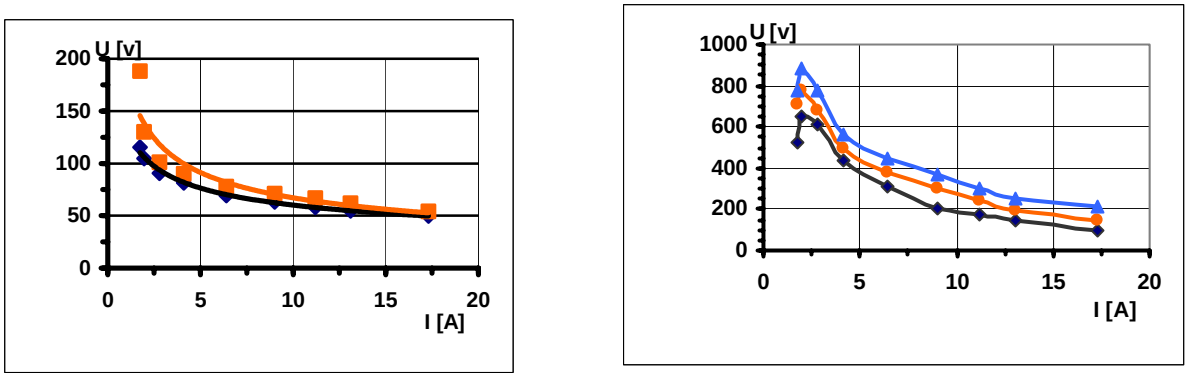

a)

Fig. 1.46. Ampere-Volt characteristics of the discharge at different pressures in the channel

From represented AVC one can see that the voltage at the discharge drops with rise of the discharge current both in the flow and without the flow. Such dependence takes place in arc discharges, so one can conclude that the discharge has the arc character. Note existence of maximum on AVC in supersonic flow, which is observed on all curves at initial pressure of 0.14 atm in the working section. Such AVC behavior testifies the transition to the arc discharge mode. One can see that maximum is already absent at initial pressure p_C = 0,28 atm. (see Fig. 1.47a), i.e. the discharge is the arc type starting from the minimum current.

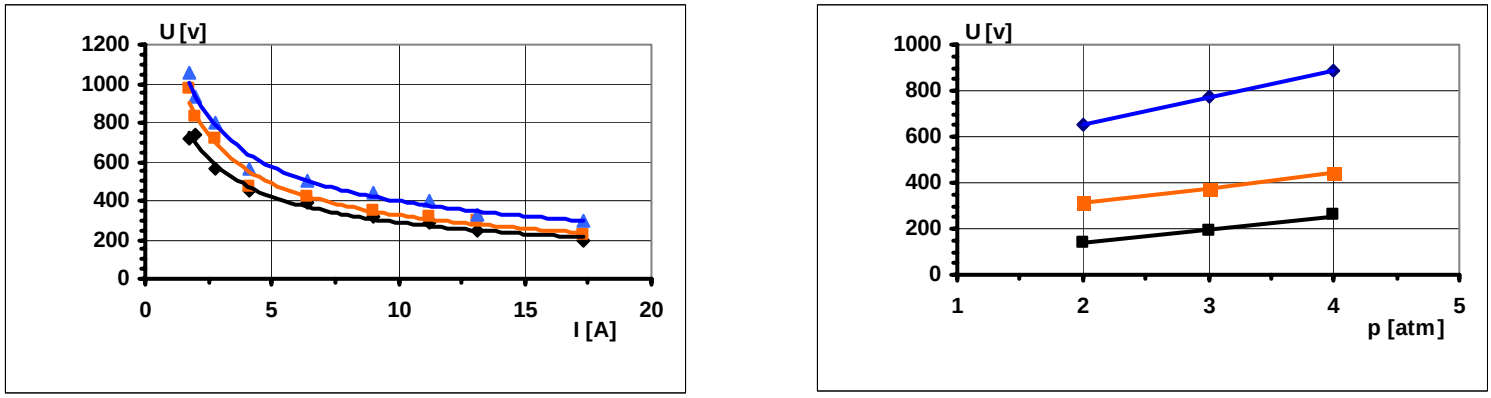

a) b)

Fig. 1.47. Dependence of the voltage drop on the discharge in the flow via the pressure

Dependences represented in Fig.1.47a were obtained at the following initial parameters: the upper curve corresponds to initial pressure of 4 atm in the receiver, the middle to 3 atm., and the lower to 2 atm.

In Fig. 1.47b one can see the dependence of the voltage drop on the discharge in the flow via the pressure in the receiver. It was obtained at initial pressure of 0,14 in the channel and the following currents: 2 A for the upper dependence, 6.4 A – for the middle dependence and 13 A – for the lower.

From the figure one can see that the voltage drop at the discharge rises with rise of pressure in the receiver at the same current. Such voltage rise evidently can be explained by growth of length of the discharge channel, and respectively, by growth of its resistance. It finally leads to growth of the voltage drop at the discharge.

It is possible to determine the average power released in the discharge using measured data of Ampere-Volt characteristic. It follows from Fig1.46 and Fig.1.47 that the value of this power varies from 1,6 kW to 3.5 kW.

We have to emphasize one typical feature connected with longitudinally transversal discharge. Namely, it was possible to stably observe the breakdown of the inter electrode gap (at the distance of 3 mm between electrodes) in motionless air at voltate of 5 kV of the feeding source only at initial pressure in the channel not exceeding 0,36 atm. At the same time the stable breakdown between electrodes with following creation of the plasma channel was observed at initial pressures higher than 0.42 atm in the working section. So one can conclude that presence of supersonic air flow facilitates breakdown conditions of inter-electrode gap.

1.7. Experimental investigation of propane-air fuel mixture ignition at application of longitudinally – transversal discharge.

In the present part of Report we represent main results on experimental investigation of propane-air mixture ignition in supersonic flow. Experiments were carried out with application of longitudinally-transversal constant current discharge. Electrodes at that were located both in the lower position (near the stagnant zone) and in the upper position (at the height of approximately 15 mm from the lower wall). Application of this discharge allowed to change comparably easy different initial conditions at execution of experiments (i.e. feeding voltage pulse duration, its temporary position with respect to start up, etc.).This allowed to reveal main characteristics of the fuel mixture ignition and inflammation processes in the supersonic flow in more details.

1.7.1. High-speed photo discharge data. It was possible to get photos of different discharge development phases changing relative positions of voltage pulse delivery times to electrodes and times of air and gas systems opening with a help of the synchronization system. So in Fig. 1.48 one can see typical photos of the discharge process when electrodes were located in the upper position.

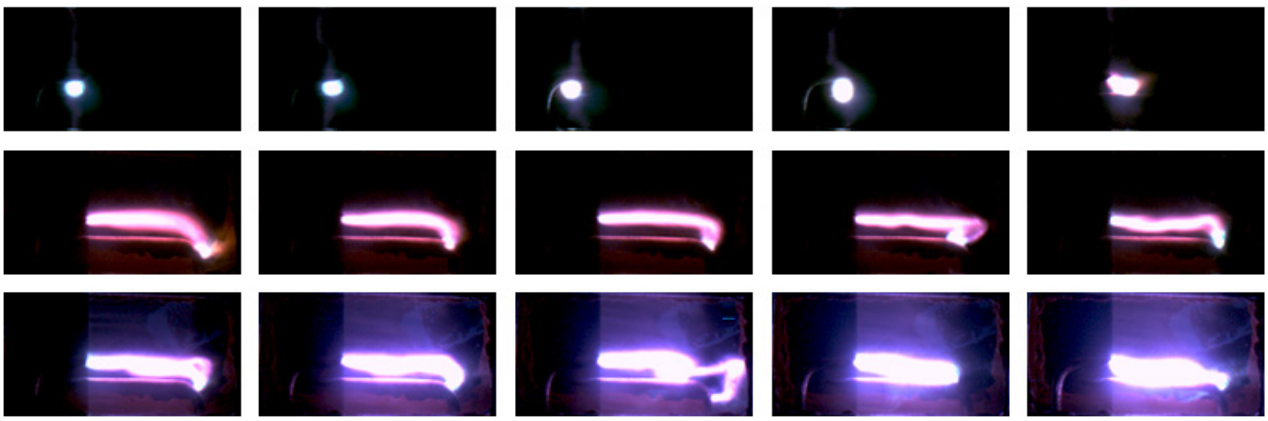

Fig. 1.48. Photos of the discharge process for electrodes located in the upper` position

The first frame row corresponds to the discharge development without supersonic the flow and gas delivery. The second row corresponds to the discharge in the supersonic flow but without fuel gas delivery. The third frame row demonstrates the discharge character in propane-air mixture flow. These photos were obtained at initial air pressure 1.6 atm and 4 atm of the gas in the system and 30 Torr in the channel. Discharge current value was 11 A. Each frame in Fig. 1.48 corresponds to the time exposure of 20 μs, and intervals between frames in all the rows are 50 ms.

One can see from the photos that the discharge develops exceptionally in the electrode area at the discharge absence as it was expected. Then at flow starting the discharge propagates along the flow, this was also noted earlier. Qualitative discharge appearance change takes place at propane presence in the flow: the plasma still propagates along the flow but the intensity of the glow considerably increases, the discharge becomes more volumetric (it develops in the direction perpendicular to the flow). However in this example there is still no gas ignition in the flow. It would be more exact to speak about the electrical discharge with air containing fuel gas addition, or simply about the discharge in the gas without the combustion.

For following description of flammable mixture ignition in the supersonic flow let us introduce the mass coefficient α is the ratio of propane and air masses delivered to the channel. Conventional value of fuel excess coefficient ϕ is calculated by multiplying of the mass coefficient α by the value of the stoichiometric coefficient Lo =14.5. By the definition: $\alpha = m_2/m_1$, where m_1 and m_2 are respectively masses of air and the gas delivered to the channel. Air and gas masses in each time moment are determined (as it was described above) with a help of pressure sensors records before and after the measuring nozzles basing on the following equations:

$$m_1 = 0{,}396\frac{P_1}{\sqrt{T_1}} \times S_1 \qquad \text{and} \qquad m_2 = 0{,}396\frac{P_2}{\sqrt{T_2}} \times S_2 ,$$

here P_1 and P_2 are pressures at the inlets of air and gas flow meters, respectively, S_1 and S_2 are the critical through cross sections of air and gas flow meters, T_1 and T_2 are air and gas temperatures at the inlets of the flow meters, respectively. In this case one obtains the following formulae for α calculation at the condition of air and gas temperatures equality at the inlet to the channel:

$$\alpha = \frac{P_2}{P_1} \times \frac{S_2}{S_1} = \frac{P_2}{P_1} \times \left(\frac{d_2}{d_1}\right)^2 ,$$

here d_1 and d_2 are diameters of the through cross sections of air and gas flow meters, respectively.

On Figures 1.49 -1.55 one can see photos of the constant current longitudinal discharge in the fuel mixture supersonic flow at the upper position of electrodes. All the photos are obtained at initial pressure of 25 Torr in the channel and at constant discharge current value of 18 A. Initial propane pressure in the balloon was constant and it was equal to 6 atm. The difference in initial conditions of represented processes in the figures consists only in variation of the pressure in the receiver, i.e. of initial air pressure at the inlet to the channel. By changing of pressure in the system of air delivery we could vary the mass ratio propane-air or the value of the coefficient α.

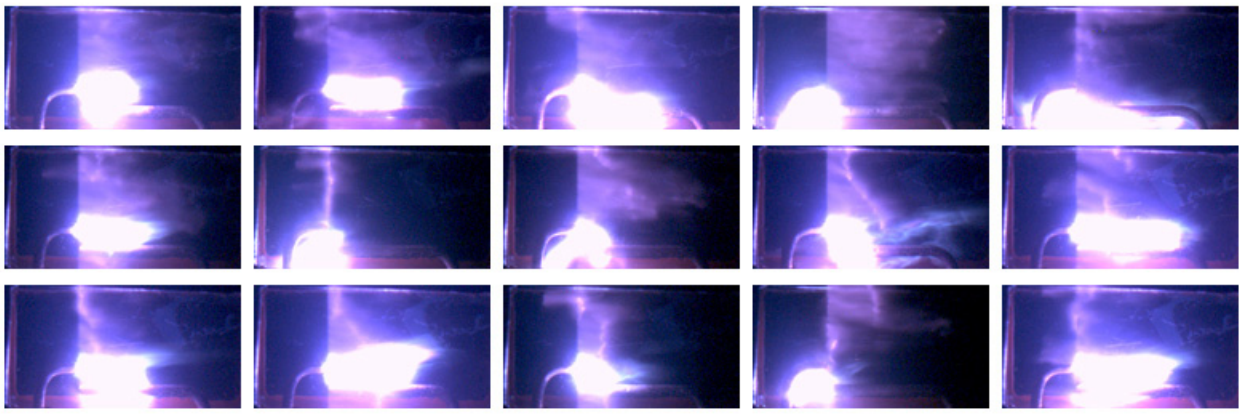

Fig. 1.49, α = 0,069.

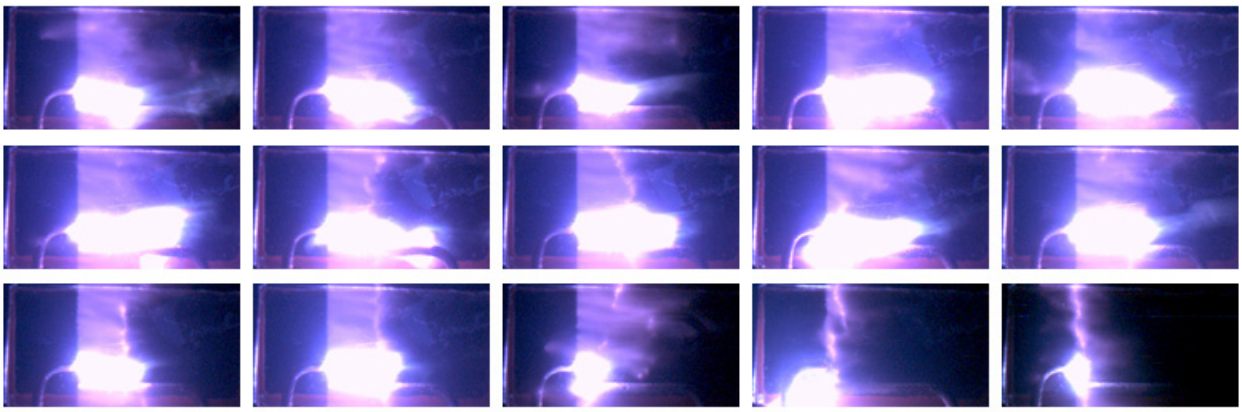

Fig. 1.50, α = 0,081.

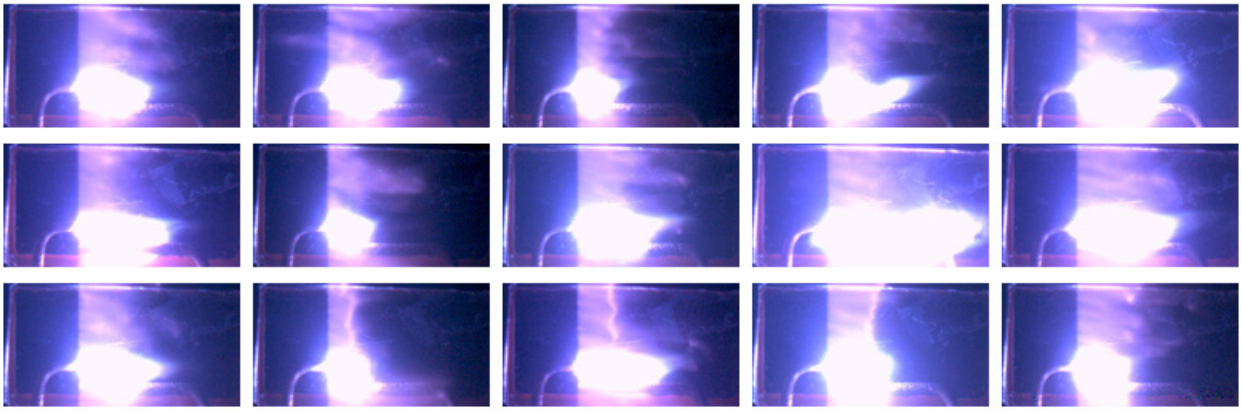

Fig. 1.51, α = 0,082.

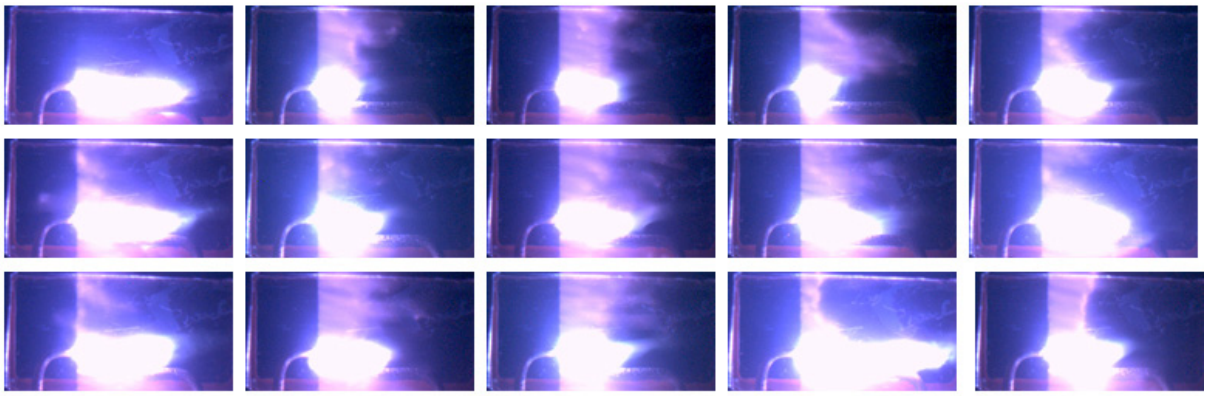

Fig. 1.52, α = 0,087.

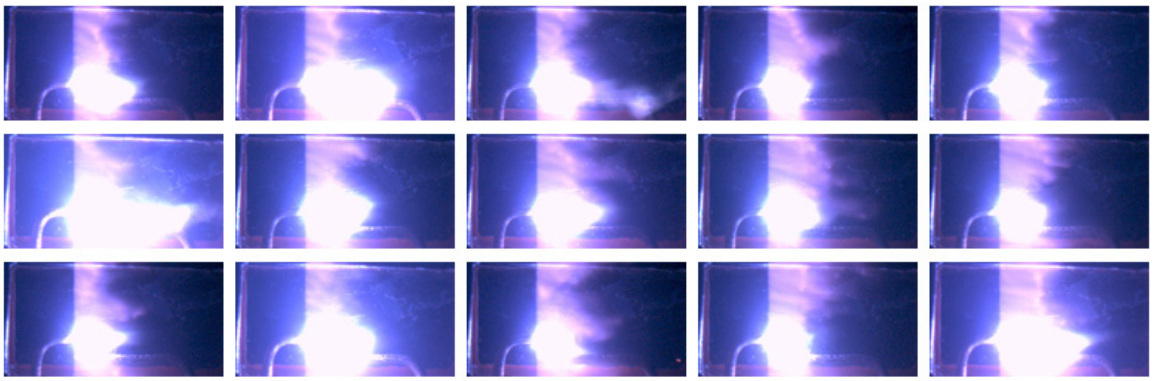

Fig. 1.53, α = 0,101.

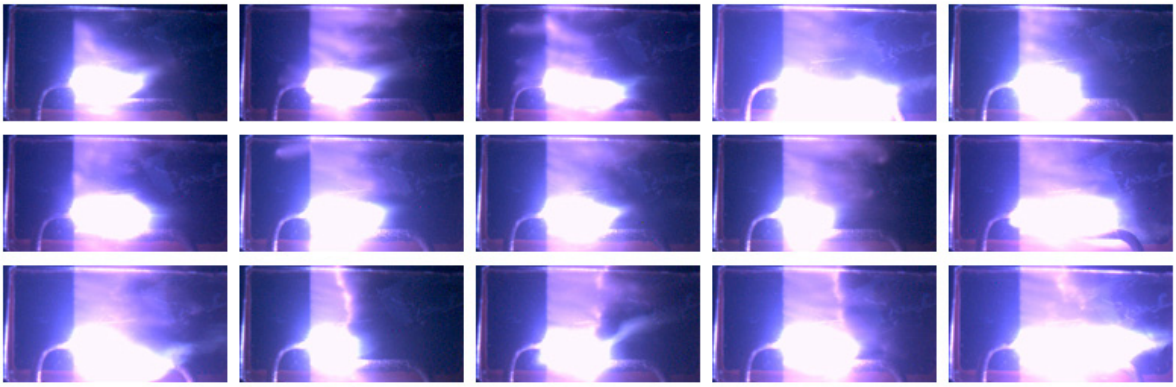

Fig. 1.54, α = 0,103.

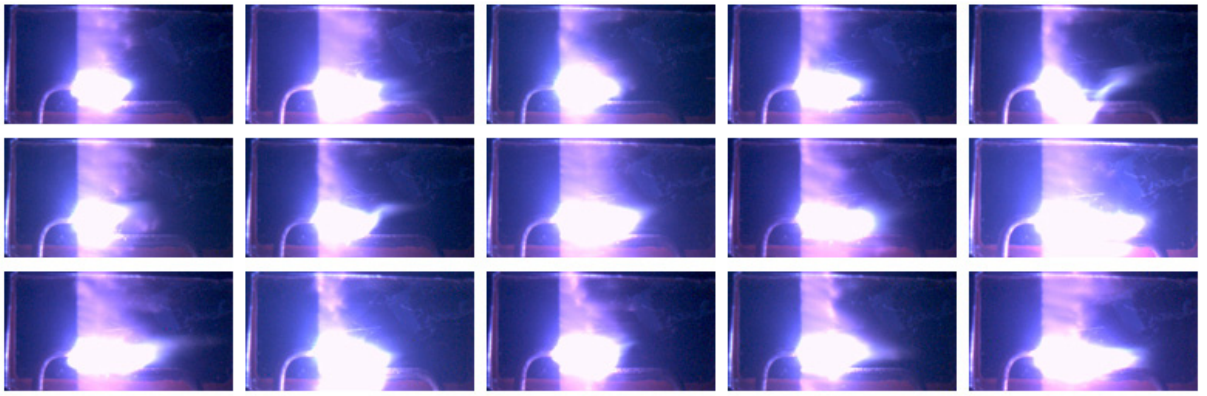

Fig. 1.55, α = 0,127.

One can see from the represented photos that the discharge picture in the case of the ignition is essentially different from photos obtained at the discharge in airflow and from the picture of the discharge in the fuel gas. This allows to conclude that ignition of propane-air mixture takes place during some definite moments of the discharge process. However we have to note that this process of ignition has relatively spontaneous character: frames with weakly represented combustion effect follow the frames with detected fuel mixture combustion, then we again see the ignition of the mixture. At the same time at variation of α we observe some definite tendency to some stabilization of the ignition process. Analogous results were obtained also for lower electrode position. In Fig.1.56 – 1.59 one can see discharge photos for this case.

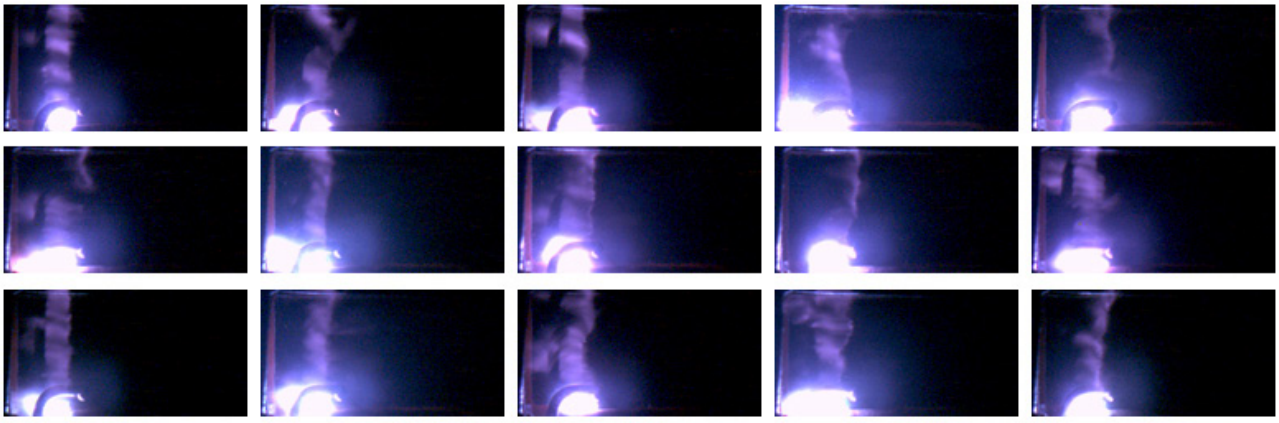

Fig. 1.56. α = 0,072.

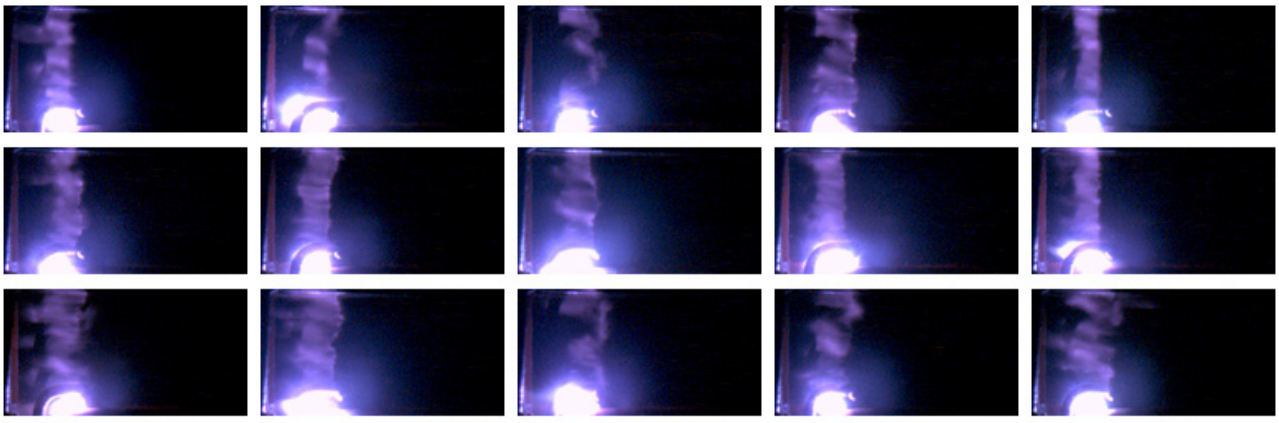

Fig. 1.57. α = 0,080

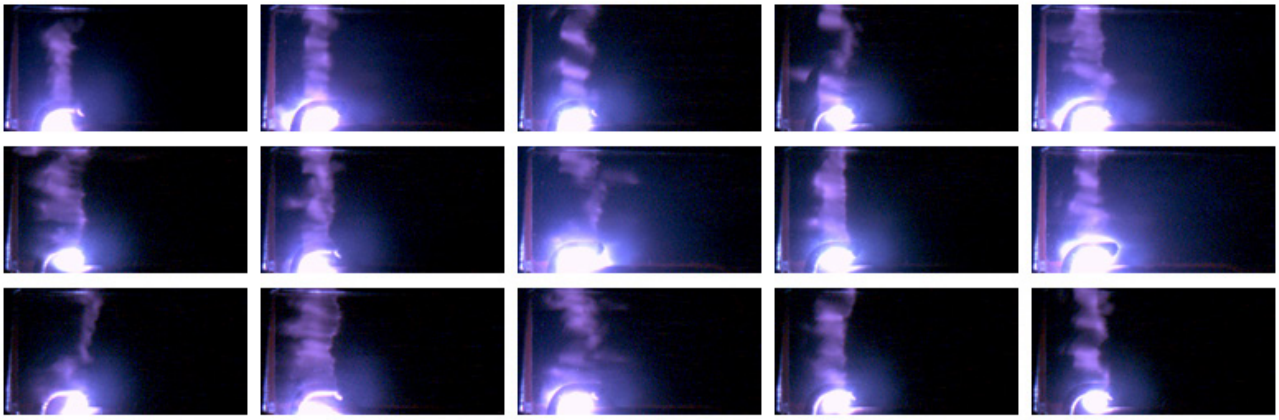

Fig. 1.58. α = 0,095.

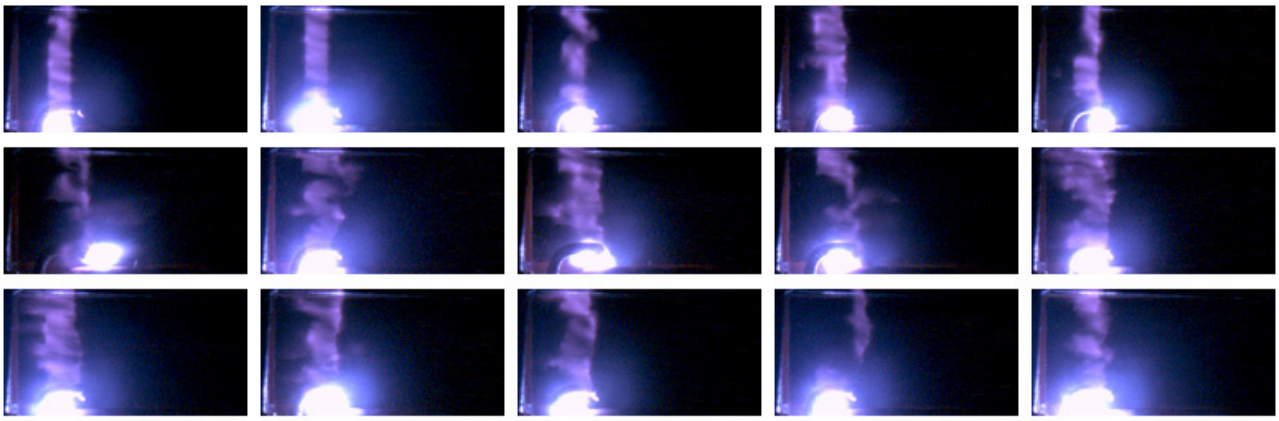

Fig. 1.59. α = 0,110.

Obtained results show that ignition of the fuel mixture at the discharge in the lower position (i .e. in the stagnant zone) takes place less intense than in the upper position. The mass coefficient influence is revealed weaker in this case. In separate frames, see Fig.1.56 and Fig.1.59 one can see the combustion propagation towards the supersonic flow. Flammable mixture ignition in the discharge has, in general, pure spontaneous character also as in the case of upper electrode position. наблюдается распространение горения навстречу сверхзвуковому потоку. One can say that better ignition of the fuel mixture takes place at the mass coefficient value α = 0,072 , see Fig. 1.56, than at other values of α.

Let us note again that all the photos were made at initial pressure of 25 Torr in the channel and constant discharge current value of 18 A. Initial propane value was also constant and it was equal to 6 atm. The mass coefficient variation was achieved by changing of initial pressure in the receiver of air system. Besides, the exposure time of one frame in represented photos was, to be exact, 20 μs and time interval between the neighboring frames was 50 ms.

Let us try to describe presented above results in the graphic form. For this purpose let us introduce the notion of gas ignition probability in the supersonic flow by the following way. Let W

equal to a probability of the gas ignition, and N_i – is a number of frames in the photo consisting of the frame series, which was obtained in definite conditions when this ignition was detected, N_0 – is the full frames number in the considered photo. Then the searched probability we define as the ratio of N_i and N_0:

$$W = N_i / N_0 .$$

In Fig.1.60 we represent dependencies of the introduced above fuel gas ignition probability in the supersonic flow with respect to the value of the mass coefficient α. Fig.1.60a is obtained only for the upper electrode position, and at Fig. 1.60b one can see results of all cases of the gas ignition both in the upper and the lower positions of electrodes.

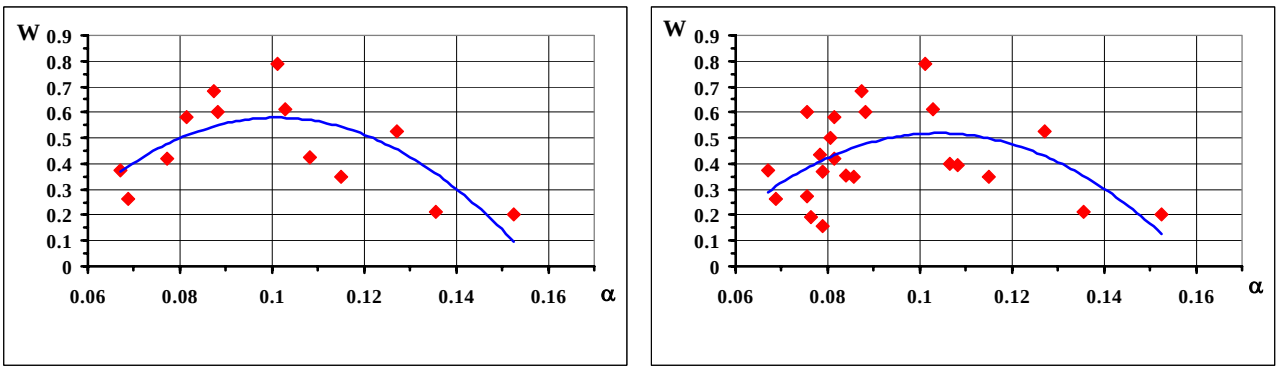

a) b)

Fig. 1.60. Ignition probability

One can see in represented graphs that there is a large scattering of the probability value at close values of α, that is evidently explained by chaotic ignition character of the fuel mixture. Nevertheless one can make two conclusions on a base of obtained results. The first one is the following: both dependencies in Fig. 1.60a and b have explicit maximum at α = 0.1. And the second one is: greatest values of the ignition probability are concentrated in the area of α variation from 0.06 to 0.1. This result allowed to undertake the follows experiments namely in this variation area of the mass coefficient.

An attempt of partial limiting of the flow in the channel was made in order to gain more stable ignition of the fuel mixture in the discharge. For this purpose we located additional wedge in the discharge area. Its height was 12 mm, its base was 36 mm, and the angle at the top was 18^0. The wedge width was equal to the channel width, see Fig. 1.61. The wedge was located with its sharp angle towards the flow in the first series of experiments. The electrodes in this case were in the upper position. Photos obtained in this case for different values of α are represented in Fig.1.62 and Fig.1.63.

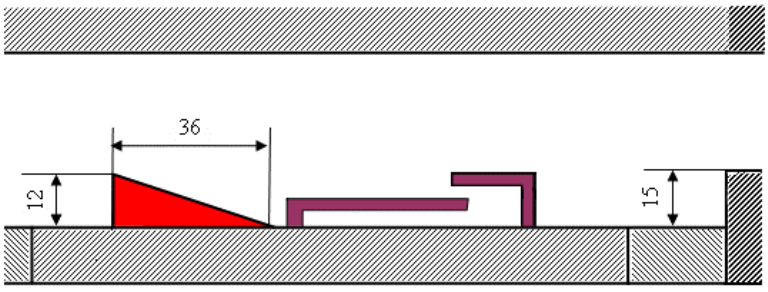

Fig.1.61

The given photos show that fuel ignition probability defined above rises at existence of partial flow limiting in the discharge area. However there is also no stable mixture ignition in this case.

The wedge was located with its vertical plane towards the flow in the next series of experiments. Discharge photos corresponding to this case are represented in Fig.1.64.

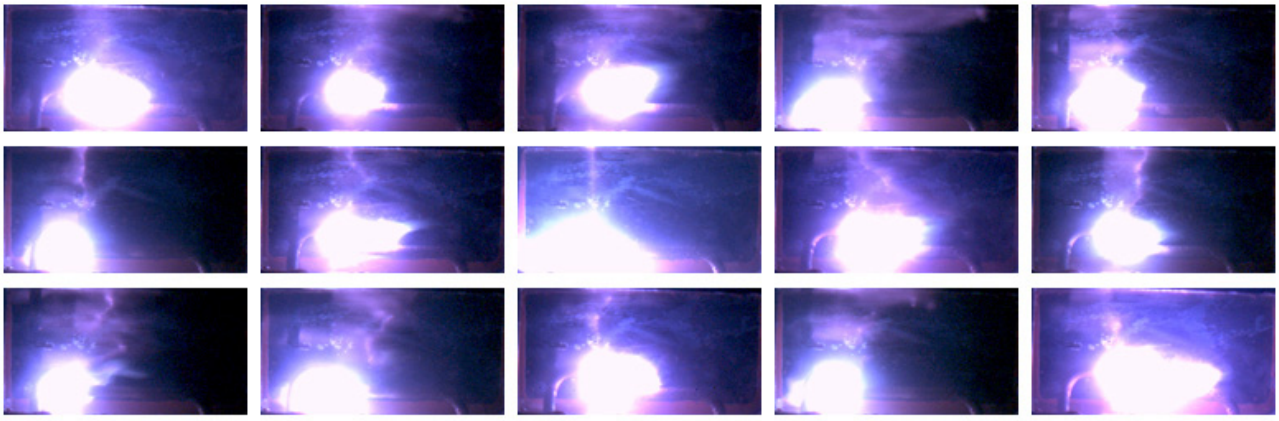

Fig.1.62. α = 0,071

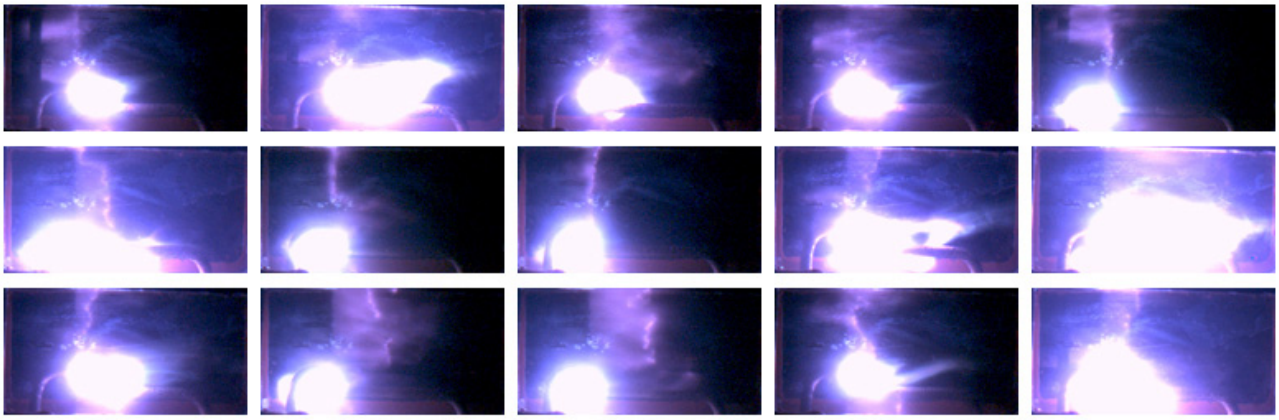

Fig.1.63. α = 0,086

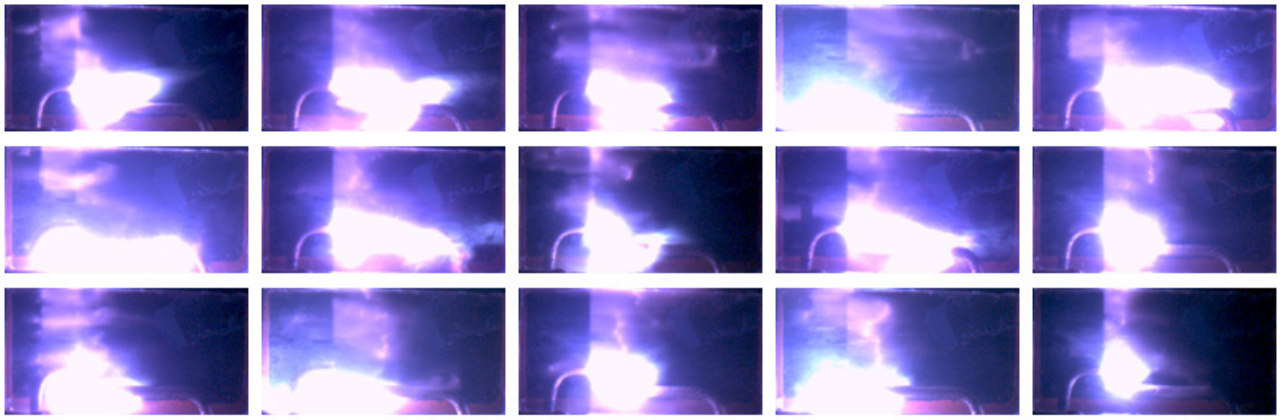

Fig.1.64. α = 0,071

One can see from this photo that the fuel ignition probability raised more in this case, i.e. the fuel mixture ignition process is observed practically in each frame of the photo.

In Figs.1.65 and 1.66 are represented the discharge photos obtained at low electrodes position. The wedge was placed with its vertical plane towards the flow, as in the previous case.

All the photos represented in Fig. 1.62 – 1.66 were obtained at initial pressure of 25 Torr in the channel and constant discharge current value of 18 A. Initial propane pressure was also constant and it was equal to 6 atm. Temporary intervals between frames and exposure times were the same.

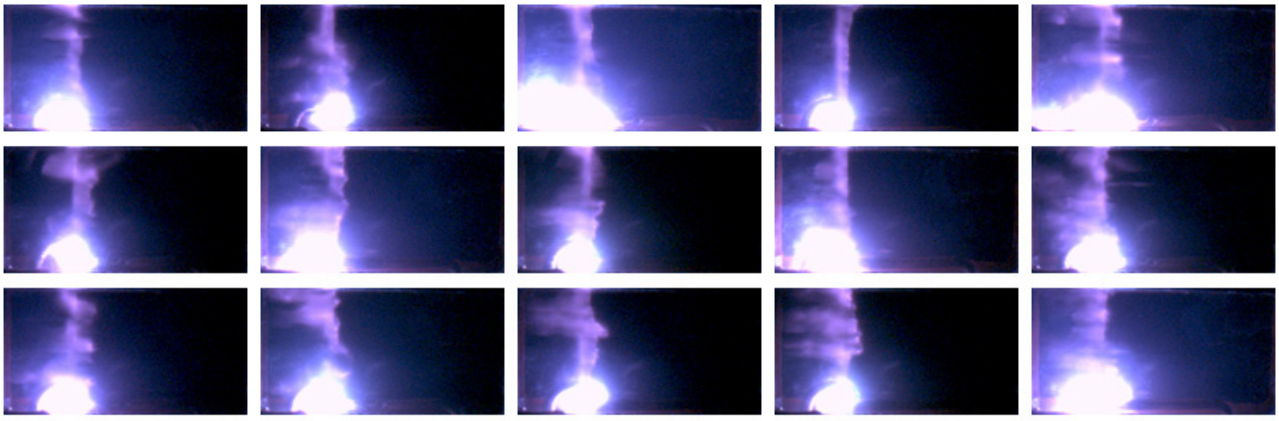

Fig.1.65. α = 0,075

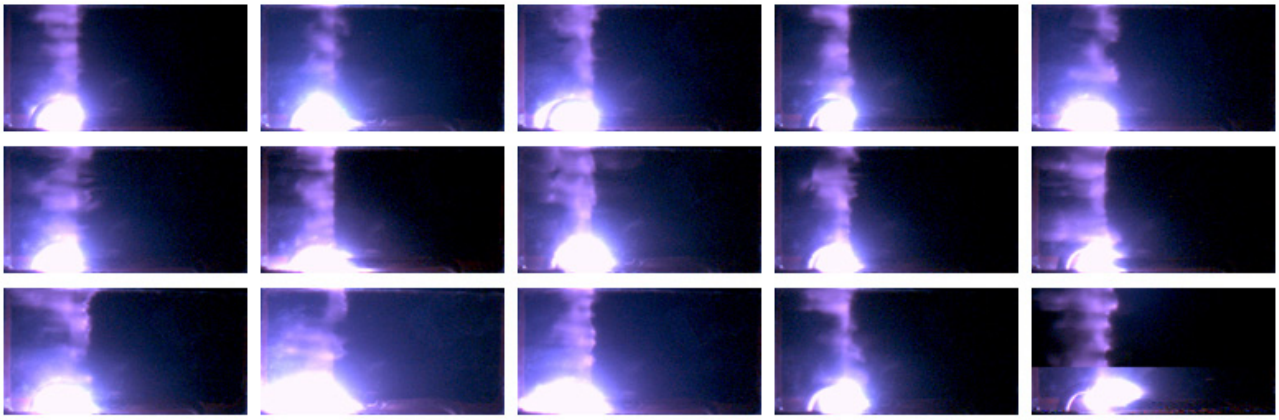

Fig.1.66. α = 0,084

One can see from these photos that mixture ignition probability somehow rises at lower electrodes position with partial flow limiting in comparison with infinite flow also as in the previous case. However, also in this case we were unable to organize stable ignition of the fuel mixture in the supersonic flow.

1.7.2. Results of analysis of signal from the pressure sensors. Analysis of the pressure sensor signals shows that plasma discharge presence in the supersonic channel practically does not influence the discharge distribution in the channel independently on partial ignition of propane –air mixture in the discharge or not. However, some change of the signal from the sensor located directly over the discharge area was detected in separate case. Examples of this disturbance are represented in Figs. 1.67 and 1.68. Note that five pressure sensors were located in the measuring section at undertaking of these examples series, and only at one of them we managed to detect the indicated disturbance. Signals in Fig.1.67 were obtained at the discharge in the upper position of the electrodes at discharge current of 18 A, pressure of 6 atm in gas delivery system, voltage pulse duration of 1.0 s and α = 0,082. Given conditions correspond to the discharge photo represented in Fig. 1.51. Signals in Fig. 1.68 were obtained at the same initial conditions but with insertion of the wedge when its vertical plane was directed towards the flow. These signals were obtained simultaneously with the corresponding photo represented in Fig.1.64 at α = 0,071.

Comparison of represented photos shows that the disturbance connected with the fuel mixture ignition is revealed more clearly at partial locking of the channel by the wedge and corresponds to the higher value of the ignition probability.

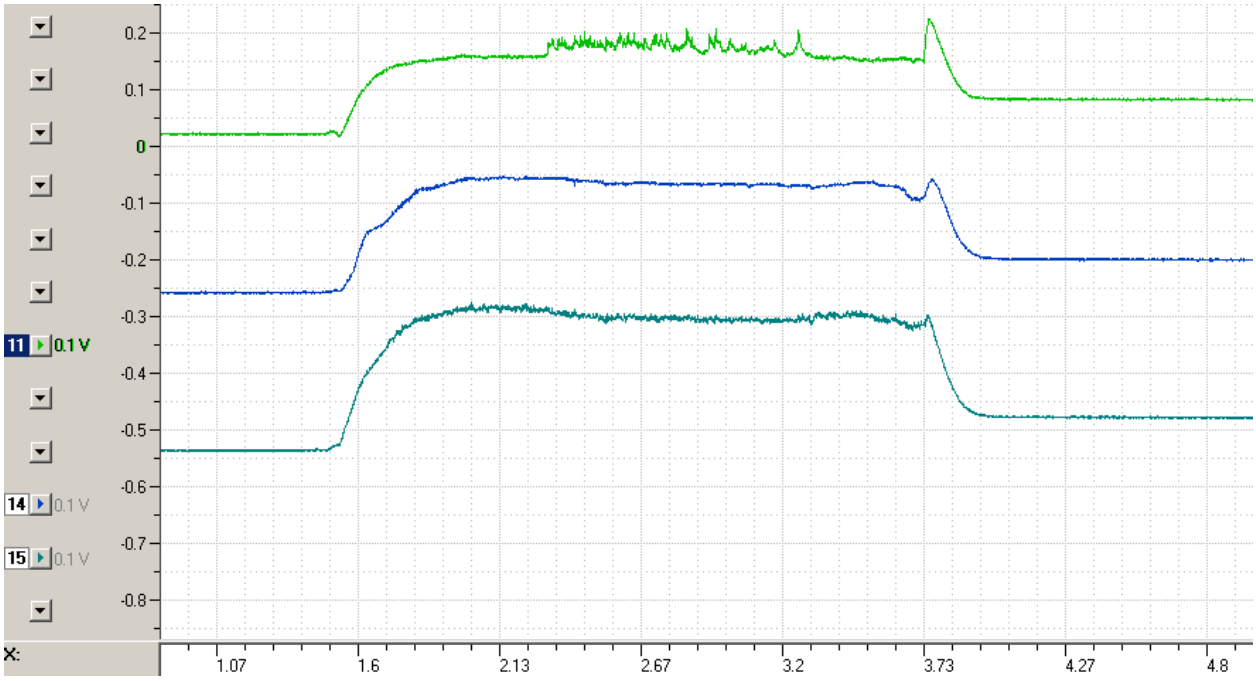

Fig. 1.67. Pressure sensor signals

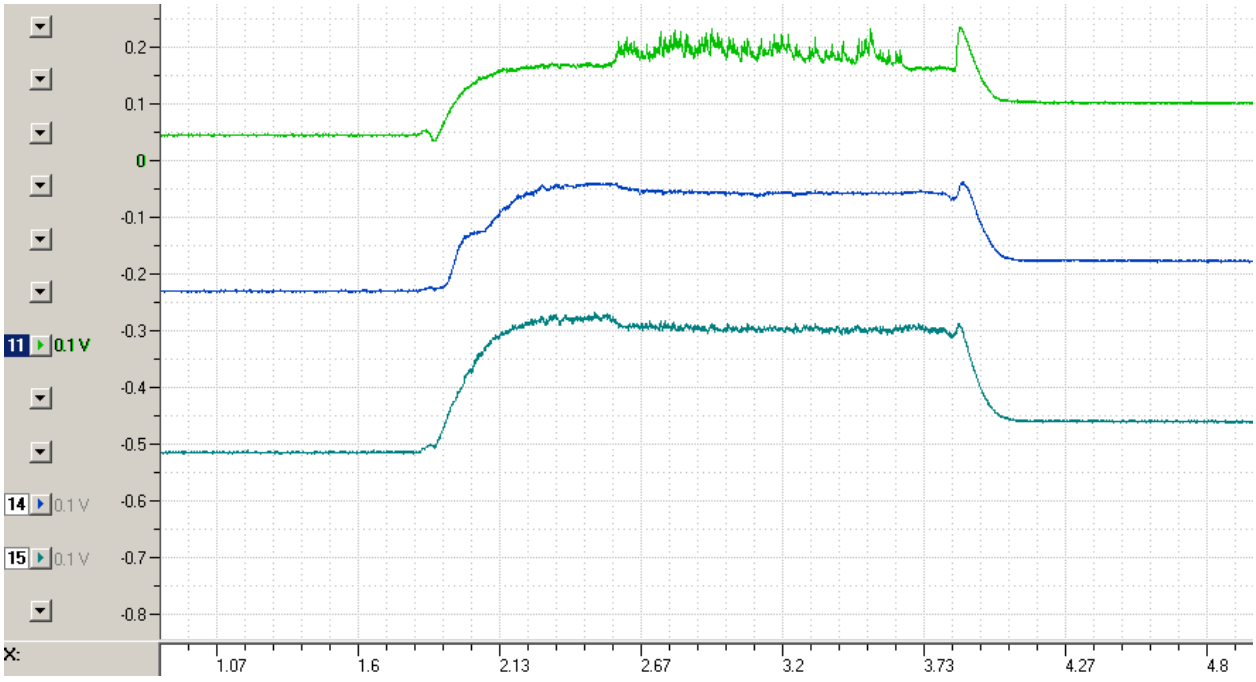

Fig. 1.68. Pressure sensor signals

Undertaken experiments allow to make the following comments:

1. Plasma generators located in the section behind the step in the condition of breakdown absence to the channel walls does not completely correspond to required effect from the point of view of ignition and combustion stabilization in the separation zone, i.e. realization first of all of the residual flames mode [14]. Combustion is observed directly in the separation zone side with electrodes of the plasma generator, this is well seen in photos of the flow. One can see the combustion in the near wall area, it propagates in the step direction. The glow becomes more intense with the increase of the distance between electrodes and the lower wall, it is caused by the interaction with the flown flow, it was earlier discussed in the work [14]. Propane-air mixture combustion is observed only in the zone side with electrodes. However, the heat delivery level is small, and its influence on the flow is practically absent, i.e. the pressure in the channel stays at the same level. Naturally, the combustion in the near wall area stops with the discharge switching off. It is expedient to move electrodes up the flow to the step wall in order to improve the stabilization characteristics of longitudinally- transversal discharge and probable flow erosive impact on electrodes.

2. Flow static parameters are very low in the zone behind the step and even more in the main flow, so it is problematic to expect the combustion stabilization. [1,2]. Estimates of stabilization possibility with respect to the flow parameters and the step size made on a basis of the criteria process model represented in the work [15] also show that the mode of residual flames is impossible. So the following tests in the channel of the chosen configuration are to be continued with air and propane heating.

1.8. Results obtained with application of magneto-plasma compressor (MPC) and plasma generators on a basis of MW radiation.

In the present Report section we will be described main results of experiments on investigation of plasma interaction with the supersonic flow of the fuel mixture. This plasma was created with a help of plasma generators made on a basis of MPC and MW sources.

1.8.1. MPC plasma generator design and its positioning in the working section of the supersonic channel were described in details in the paragraph 1.4 of the present report so we restrict to only experimental data consideration.

In Fig.1.69 one can see typical integral photos of the plasma jet created by MPC in: motionless air, see Fig.1.69a, in supersonic flow, see Fig.1.69b and in fuel mixture flow, see Fig. 1.69c.

a) b) c)

Fig. 1.69. Flow propagates from left to right.

These photos are obtained at the frame exposure time 20 μs (besides we used neutral filters weakening plasma glow intensity by 1,5 times) at initial pressure 25 Torr in the channel, at 2,4 atm in the air inletting system, and 6 atm of the gas. This corresponded to the mass coefficient value $\alpha = 0{,}08$. Parameters of power source were the next: charge capacity - 50 μF, voltage – 3 kV and it corresponds to 225 J of the stored energy.

One can see from the represented photos that the axis of plasma jet propagation stays constant and does not depend on existence of the supersonic flow in the channel or not. However one can see some change of the jet form, in particular in the periphery area. The periphery plasma area transversal sizes decrease in the supersonic flow, see Fig.1.69b, especially from the flow side, see Fig.1.69b. This decrease of the transversal sizes is more noticeable in the case of the discharge in propane-air mixture, see Fig.1.69c. The cover area practically disappears around the discharge core. Note that sharp blow sound is distinctly detected at the discharge of MPC in the fuel mixture, it is typical for sudden increase of the pressure.

Data obtained from the pressure sensors clearly witnesses about sharp rise of the pressure in the channel during the MPC discharge pulse in the fuel mixture. In Fig.1.70 one can see the signal diagram from the sensors in the case of MPC discharge in supersonic airflow without the fuel gas (the shown signals are from 7-th to 15-th sensors) and in Fig.1.71 (signals from 7-th to 10-th sensors) and in Fig.1.72 (from 11-th to 15-th sensors) there are shown separate signal fragments from the sensors. These results were obtained at working conditions indicated above at zero pressure in the gas inletting system. Sensors were located along the channel length according with the scheme represented in Fig.1.12. One can see that relatively weak signal disturbance is detected during MPC discharge pulse. This disturbance is maximal in the area of the plasma creation, i.e. in the region of 10 –th and 11–th sensor. Then it is decreased both in the direction of the supersonic nozzle and in the opposite side, at that decrease of the disturbance amplitude is more sharp in the direction of the nozzle, because the disturbance amplitude detected by the 9-th sensor placed at the distance of 7 cm from the discharge area is approximately equal to the signal amplitude from the 15-th sensor, which distance from the center of the discharge area is 42 cm.

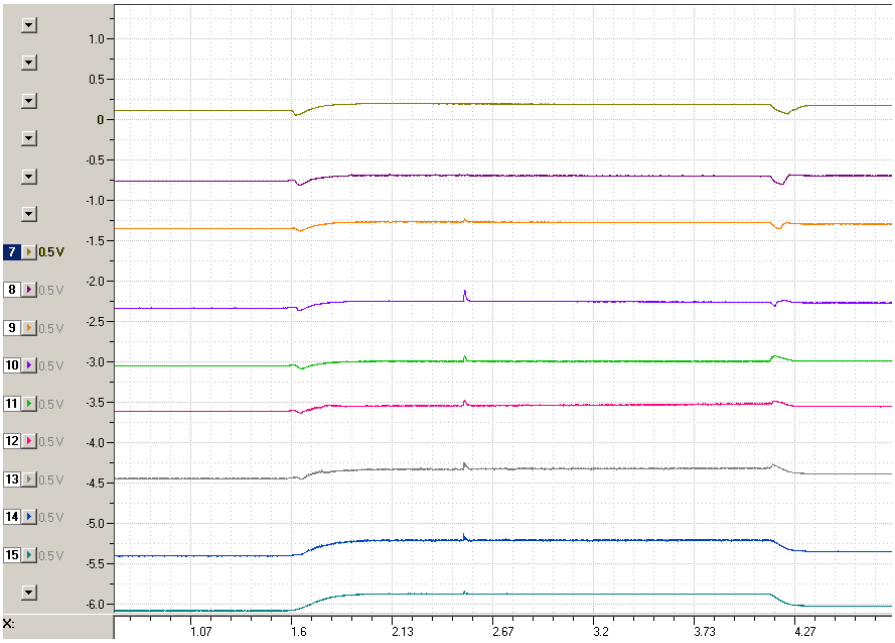

Fig. 1.70. Signals from 7 to15-th sensor

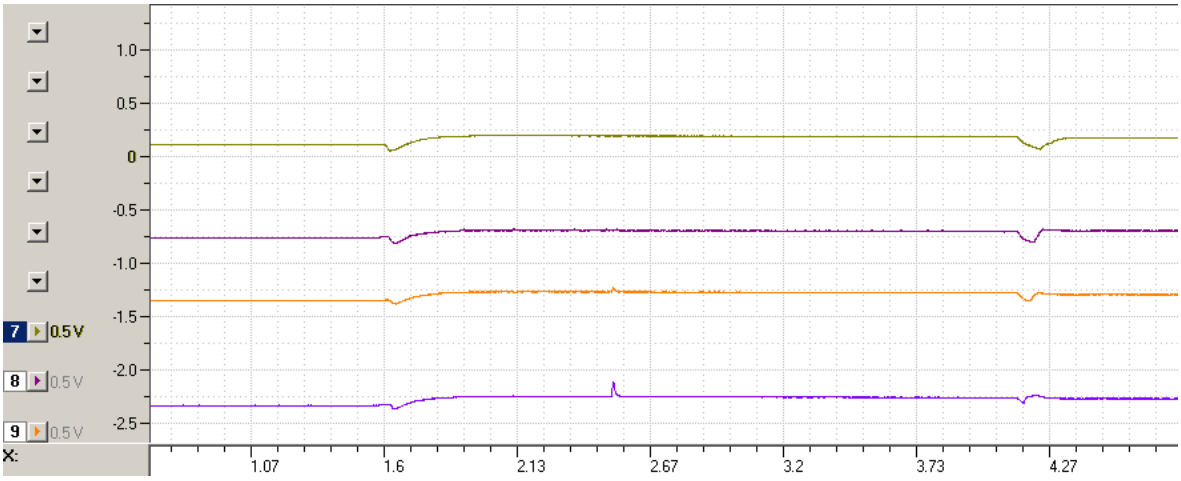

Fig. 1.71. Signals from 7 to 10- th sensor

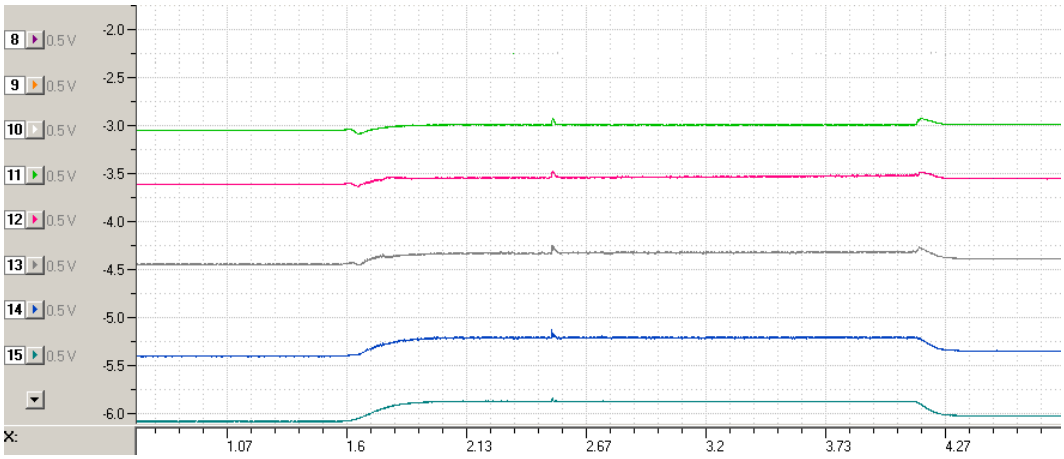

Fig. 1.72. Signals from 11-th to 15-th sensor.

The situation is sharply changed at MPC discharge realization in the supersonic flow of the fuel mixture. In Fig.1.73 (review diagram), Fig.1.74 and Fig.1.75 (fragments from separate sensors) one can see signals from the same sensors obtained at the same initial conditions but at fuel gas in the flow. The review diagram corresponds to the sensors from 7 to 15-th, as in previous case; In Fig. 1.74 one can see signals from 7 to10 sensors, and in Fig. 1.75 – from 11 –th to 15-th sensors.

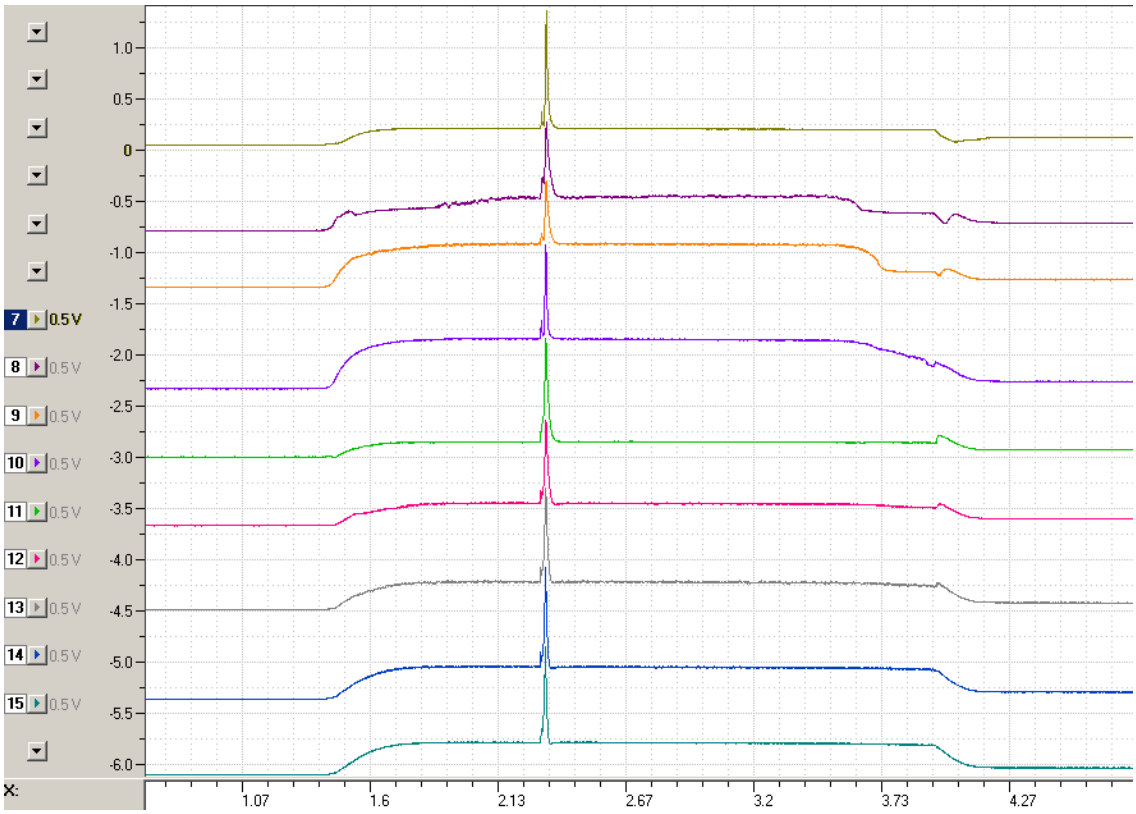

Fig. 1.73. Signals from 7 to 15-th sensors.

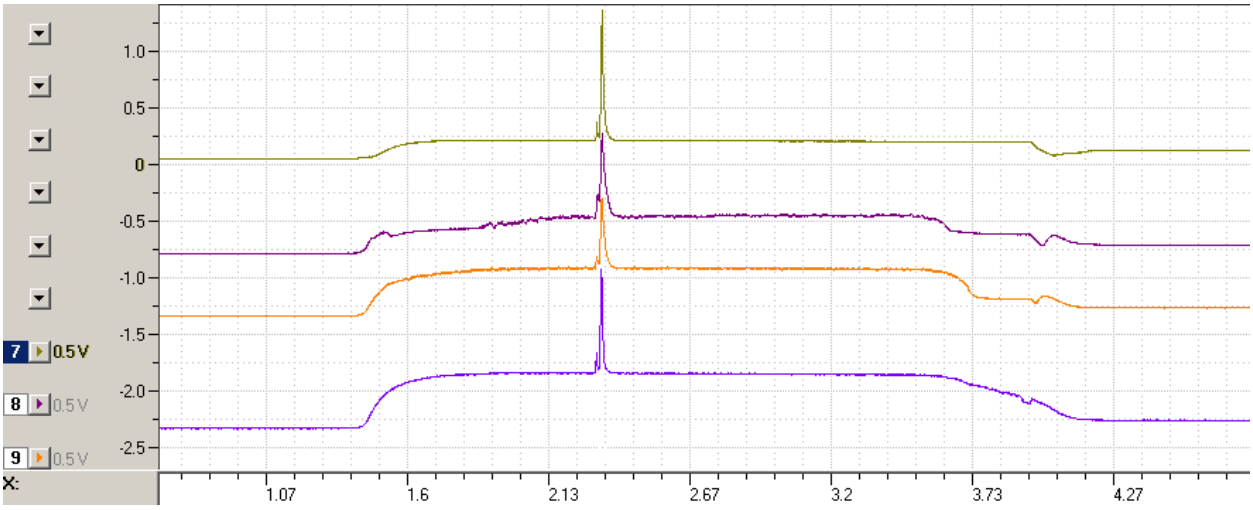

Fig. 1.74. Signals from 7 to 10-th sensors.

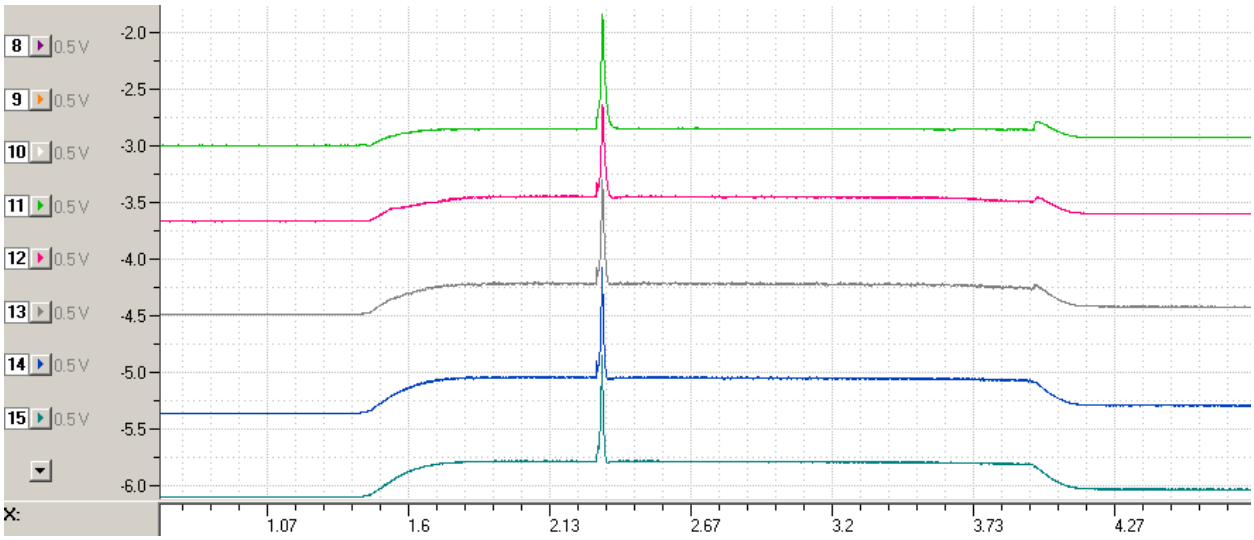

Fig. 1.75. Signals from 11 –th to 15 –th sensors.

All the signals in Fig.1.73 – 1.75 are represented in the same scale as in Fig.1.70 –1.72.

One can see from the comparison of represented results that sharp (by several times) pressure increase is detected in the channel at MPC discharge in the fuel, At that this strong disturbance of the pressure propagates approximately with constant amplitude to both sides from the place of the discharge origin. However, there is no observed pressure rise in the supersonic nozzle and behind it. Unfortunately temporary resolution of signal detection from the sensors system did not allow to exactly determine a velocity of this disturbance propagation along the channel, but rough estimates give a value of this velocity of about 100 – 300 m/s.

Obtained results allow to conclude that apparently the fuel ignition takes place in the whole discharge area at MPC discharge in supersonic flow of air-propane mixture, and there is realized the process of detonation combustion type, which propagates in both sides from the source. This leads

to practically complete fuel burning out over the whole channel length and to partial (or complete) short time chocking of the flow. Evidently by this process is possible to explain some stabilization of the discharge form that is observed in Fig.1.69c.

1.8.2. Experiments on investigation of the fuel mixture ignition possibility by MW torch. These experiments were undertaken at the same initial conditions, i.e. at initial pressure 25 Torr in the channel, pressure of 2,4 atm in the air inletting system, and 6 atm of the gas, $\alpha = 0{,}08$. Description of MW generation location in the channel scheme is represented in the paragraph 1.4. The generator continuous power was about 800 W. In Fig. 1.76 one can see photos of MW discharge obtained with time resolution of 30 ms. Upper photos row in this picture corresponds to MW torch working mode without fuel gas delivery and without a flow (the last frame in this photos row was obtained at the beginning of the flow motion). The next photos row shows MW discharge in the flow but without fuel gas delivery and finally the lower row was obtained in the case of fuel mixture presence in the flow. The supersonic flow propagates from left to right. Note that all these photos were obtained during the same flow startup.

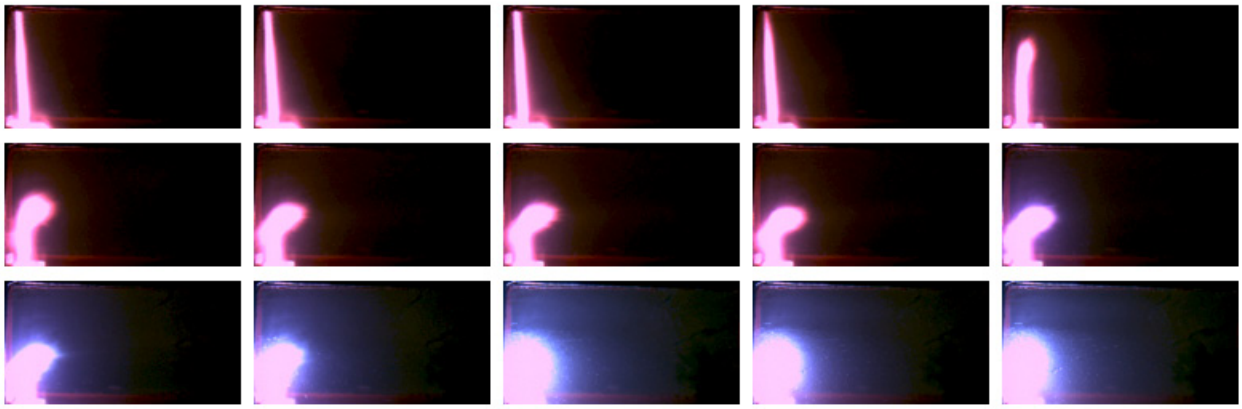

Fig. 1.76. MW torch in the flow.

One can see from the represented photos that partial ignition of the fuel mixture takes place in the case of MW torch in the discharge area and in the stagnant zone, this is practically analogous to constant current transversal-longitudinal discharge. But fuel stable burning there was not observed.

The next experimental series was devoted to investigation of ignition possibility with a help of the surface discharge initiated by MW radiation. MW generator location scheme for this case is represented in Fig. 1.77.

Surface initiated MW discharge creation principle consists in the following. Microwave radiation from the magnetron (see paragraph 1.4) comes to the transition waveguide (3) through the intermediate waveguide (4). The transition waveguide is used for matching of intermediate waveguide sizes with a hole in the working section of the channel. So the intermediate waveguide is directly fixed in the setting hatch of the working section (1). Thing quartz plate (2) is fixed at the outlet of the intermediate waveguide at the level of the lower wall of the channel. Small needles in the form of metallic chips are glued to upper plane of the plate. These non uniformities cover the whole external surface of the plate. The surface discharge appears on these non uniformities at MW power delivery, the discharge is initiated by MW radiation.

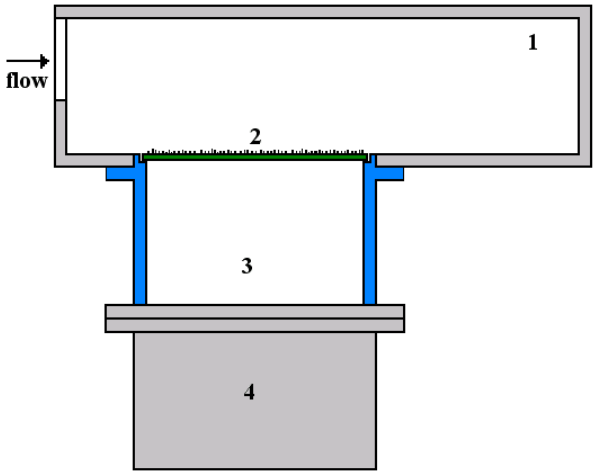

Fig.1.77. Surface MW discharge location in the channel scheme

In Fig. 1.78 one can see photos of this discharge: without a flow – see the upper frames row, with the flow but without fuel gas- see the middle row, and with the flow and fuel gas delivery – see the lower row. The flow propagates from left to right. Initial conditions of experiments undertaking were the same.

Represented photos show that there is partial ignition of the supersonic mixture, at that its combustion takes place more stable than in all previous experiments. The combustion area even propagates towards the flow to the stagnant zone. However, there is no ignition of the whole flow area with respect to its cross section. Note that pressure sensors do not detect any disturbances during the discharge at startups with the surface discharge.

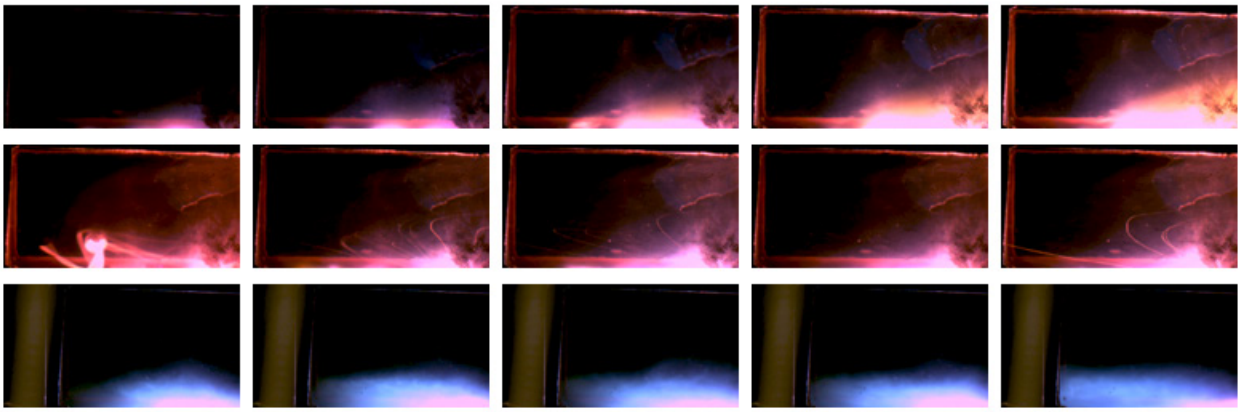

Fig. 1.78.

1.9. Spectral investigations of propane-air flow ignition

Different gas discharges and plasma jets were applied for propane-air mixture flow ignition, they were: longitudinally- transversal constant current (electrode) discharge, surface quasi-stationary MW discharge, MW torch and magneto plasma compressor. For spectra recording we used two-channel spectrograph of "Avantes" company. First channel allowed to record the review spectrum in 250-800 nm wave range. With a help of the second channel we recorded with good resolution the discharge plasma radiation spectrum in 350-450 nm wave range.

1.9.1. Longitudinally- transversal constant current (electrode) discharge. In Fig. 1.79 one can see the spectrum in 350-450 nm wave range of plasma radiation created by longitudinally-transversal constant current discharge in air flow in the stagnant area of the channel. The review spectrum in the wave range 250-800 nm is represented in Fig. 1.80. One can see that radiation of molecular nitrogen first and second positive system bands are observed in the spectrum, also there are weakly evident Cyan (CN) radiation bands.

For measuring of the gas temperature we used the band (0,2) λ=380.5 nm of second positive nitrogen system. For example, there is a spectrogram of this band in Fig.1.81. It was obtained In conditions of longitudinally- transversal constant current discharge in air. In Fig. 1.82 one can see gas temperature dependence in the longitudinally- transversal constant current discharge in airflow via static pressure in the pressure chamber. The static pressure was changed from 100 to 300 Torr. It can be seen that the gas temperature increases somehow with increase of pressure, at that it stays in the range 2200-2800 K.

Detecting spectrum was substantially changed in the case of discharge creation in propane-air mixture flow. In Figs. 1.83-1.84 one can see recorded plasma radiation spectra in the wave range 350-450 nm and 250-800 nm, respectively. The plasma was created with a help of longitudinally-transversal constant current discharge in the stagnant zone of the aerodynamic channel in propane-air mixture flow. One can see that radiation intensity of Cyan bands sharply rises (more than for an order of magnitude), at that the bands of second positive nitrogen system are not practically recorded. Swan bands of molecular carbon, weak bands of CH and atomic lines of hydrogen and electrode erosion products are also observed.

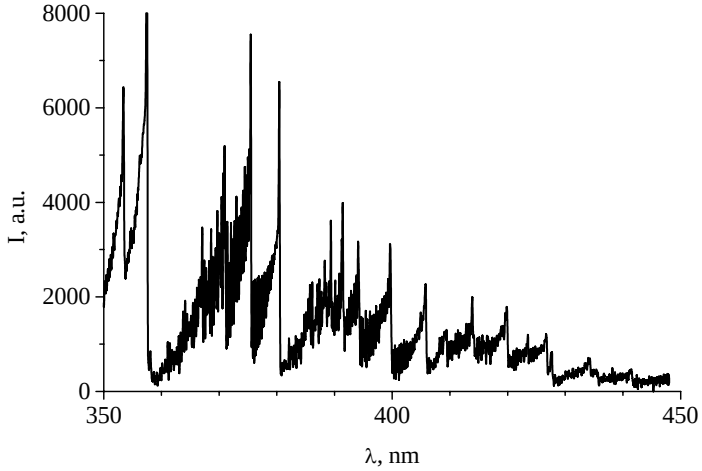

Fig. 1.79. The plasma radiation spectrum in the wave range 350-450 nm. The plasma is created with a help of longitudinally- transversal constant current discharge in the stagnant zone of the aerodynamic channel in airflow. Air pressure in the high pressure receiver is p_{air}=2 atm, static pressure in the pressure chamber is p_0=100 Torr, discharge current is i=2.0 A, discharge current pulse duration is t=800 ms.

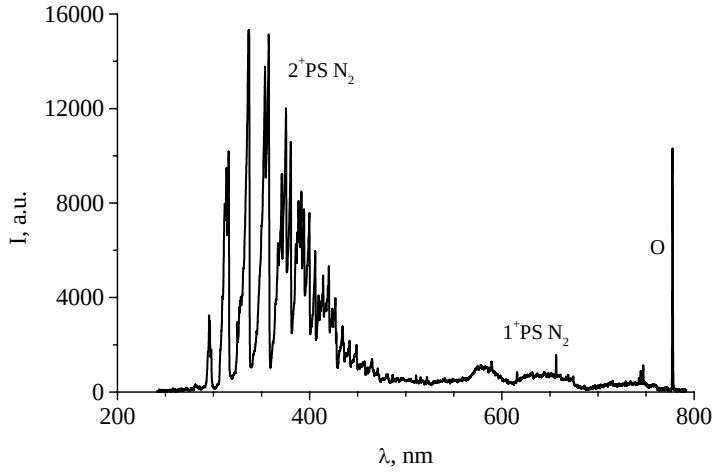

Fig. 1.80. The reviw spectrum in the wave range 200-800 nm. The plasma is created with a help of longitudinally- transversal constant current discharge in the stagnant zone of the aerodynamic channel in airflow. Air pressure in the high pressure receiver is p_{air}=2 atm, static pressure in the pressure chamber is p_0=100 Torr, discharge current is i=2 A, discharge current pulse duration is t=800 ms.

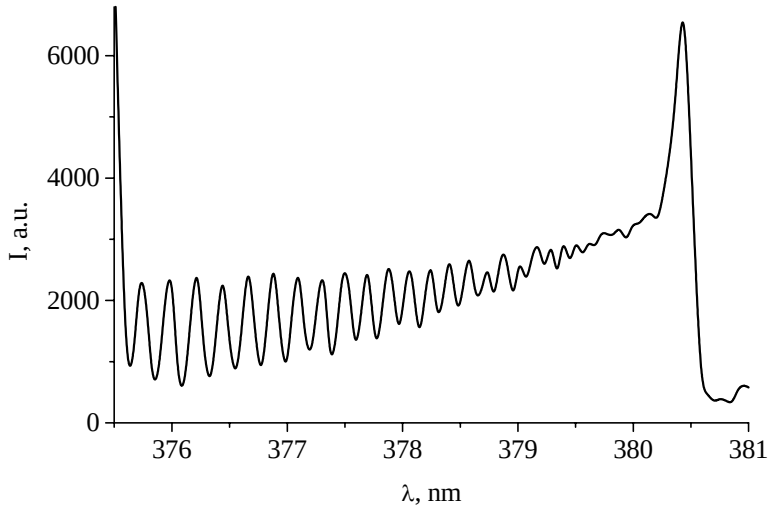

Fig. 1.81. The spectrogram of the band (0,2) λ=380.5 nm of nitrogen second positive system, in conditions of longitudinally- transversal constant current discharge in ai. Air pressure in the high pressure receiver is p_{air}=2 atm, static pressure in the pressure chamber is p_0=100 Torr, discharge current is i=2 A, discharge current pulse duration is t=800 ms.

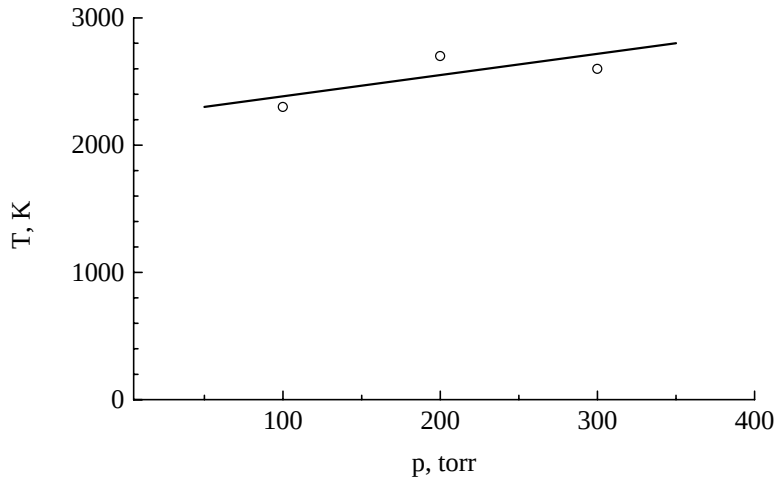

Fig. 1.82. Temperature gas dependence via static pressure in the pressure chamber in conditions of longitudinally- transversal constant current discharge in ai. Air pressure in the high pressure receiver is p_{air}=2 atm, static pressure in the pressure chamber is p_0=100 Torr, discharge current is i=2 A, discharge current pulse duration is t=800 ms.

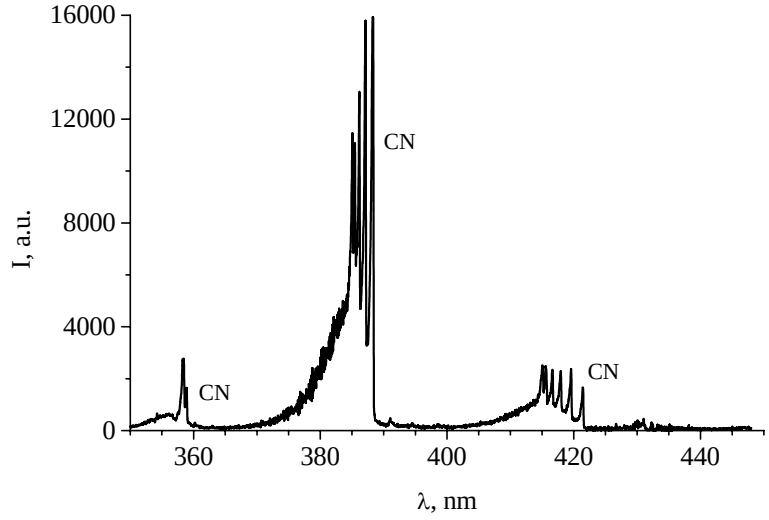

Fig. 1.83. Plasma radiation spectrum in wavelength range 350-450 nm. The plasma is created with a help of longitudinally- transversal constant current discharge in the stagnant zone of the aerodynamic channel in propane-air mixture flow. Air pressure in the high pressure receiver is p_{air}=2 atm, static pressure in the pressure chamber is p_0=100 Torr, discharge current is i=2 A, discharge current pulse duration is t=800 ms. Propane pressure in the high pressure receiver is p_p=4 atm.

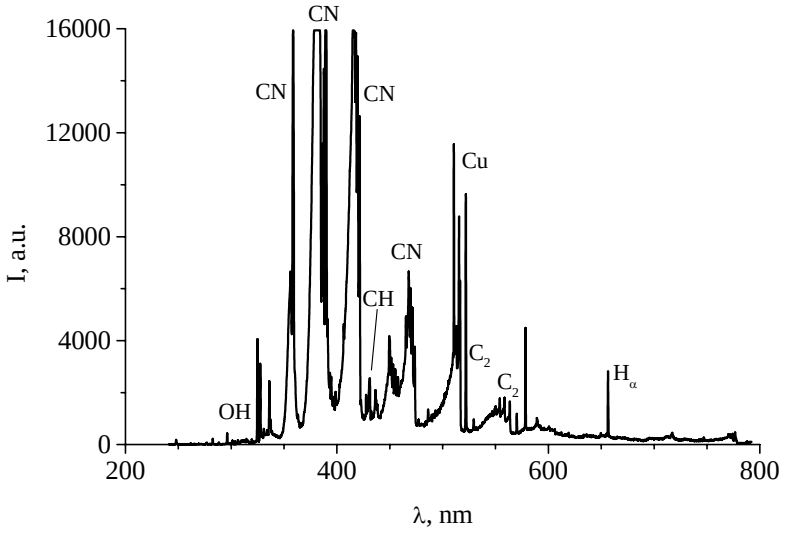

Fig. 1.84. Plasma radiation review spectrum in the wavelength range 250-800 nm. The plasma is created with a help of longitudinally- transversal constant current discharge in the stagnant zone of the aerodynamic channel in propane-air mixture flow. Air pressure in the high pressure receiver is p_{air}=2 atm, static pressure in the pressure chamber is p_0=100 Torr, discharge current is i=2 A, discharge current pulse duration is t=800 ms. Propane pressure in the high pressure receiver is p_p=4 atm.

Temporary variation of CN bands 388.3 nm, 387.1 nm, 386.1 nm spectrograms in course of propane-air mixture flow inflammation with a help of longitudinally- transversal constant current discharge in the stagnant zone behind the step of the aerodynamic channel is represented in Fig. 1.85. One can see from these data that combustion process in the discharge area is unstable during the discharge existence.

In Fig. 1.86 one can see plasma temperature variation of longitudinally- transversal constant current discharge in propane-air flow measured with a help of ratio of bands intensity I(1,1)/I(0,0) with cyan lengths of quanta $\lambda_{(1,1)}$=387,1 nm and $\lambda_{(0,0)}$=388,3 nm. It can be seen that plasma temperature somehow rises during discharge current pulse. Temperature also rises with increase of the discharge current.

Presence of atomic copper lines in the plasma radiation spectrum allowed us to also determine the distribution temperature of copper atoms over excited states. One can suppose that this temperature was close to electron temperature in conditions of experiments. In Fig. 1.87 is represented temporary way of temperature distribution over excited states of copper atoms measured by ratio of Cu lines with wavelengths λ_1=510.54 nm and λ_2=521.82 nm. One can see that measured temperature decreases in conditions of experiments during discharge current pulse, staying at the level 0.8-0.9 eV.

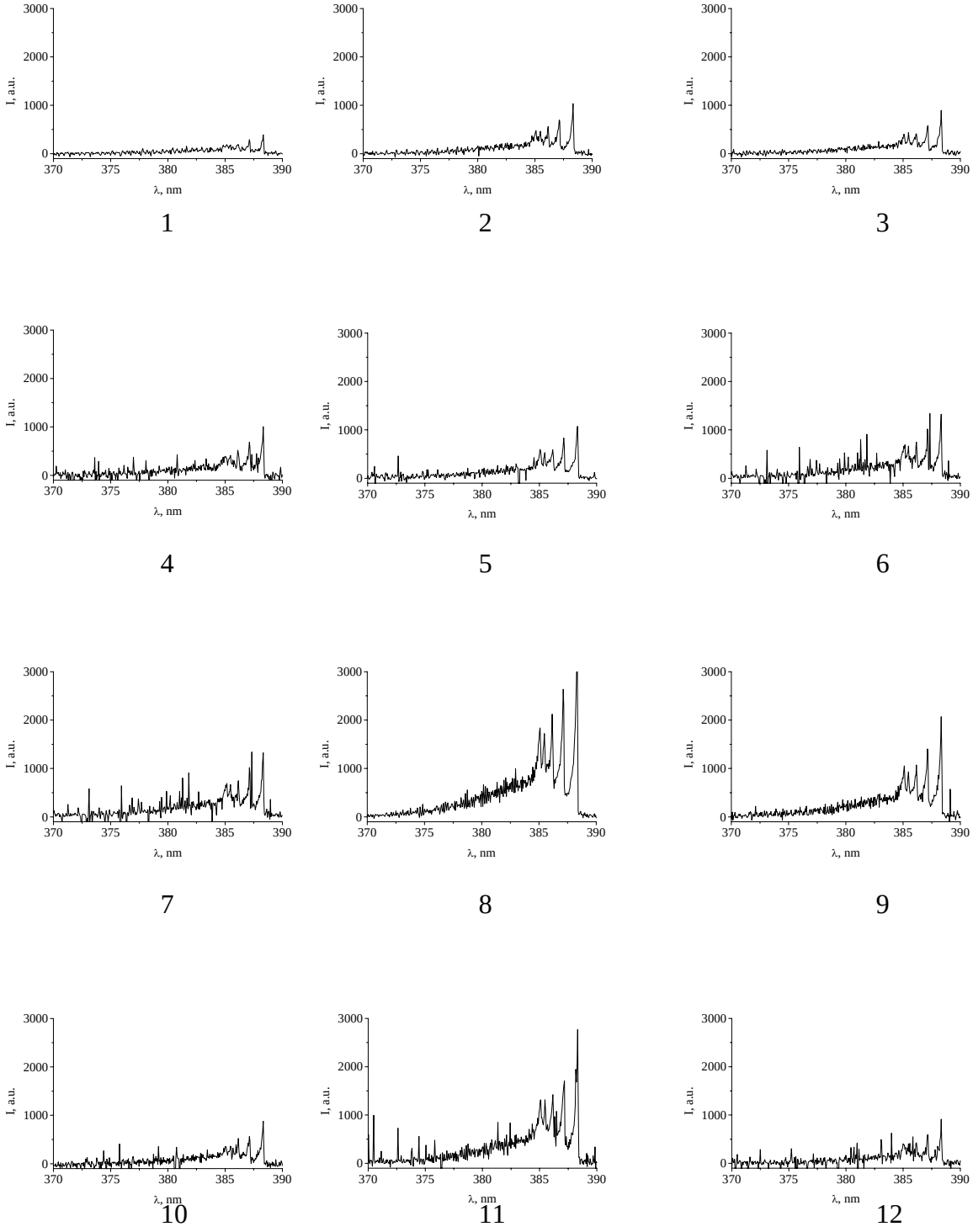

Fig. 1.85. CN bands 388.3 nm, 387.1 nm, 386.1 nm spectrogram temporary variation in inflammation process of propane-air mixture flow created with a help of longitudinally- transversal constant current discharge in the stagnant zone behind the step of aerodynamic channel. Time of signal accumulation 20 ms, time interval between frames 100 ms, discharge current is i=12 A.

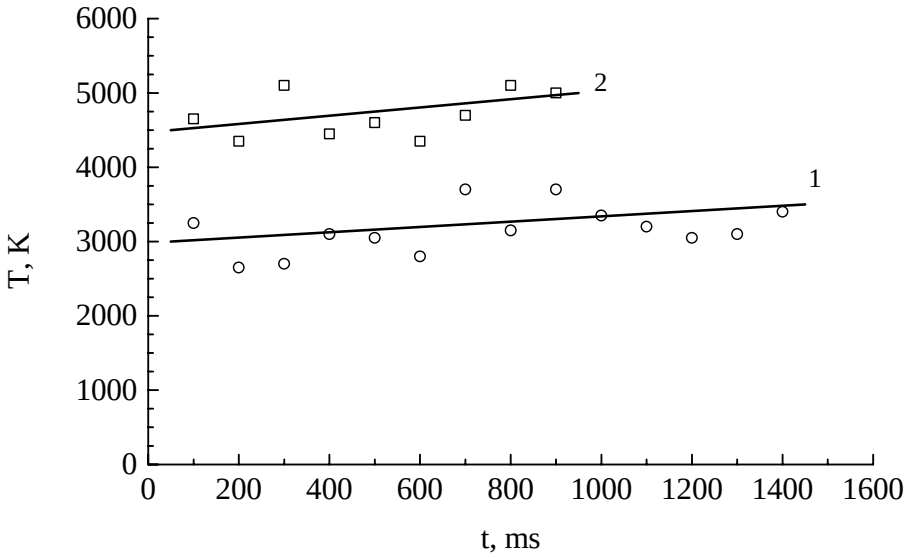

Fig. 1.86. Temperature variation of longitudinally- transversal constant current discharge in propane-air flow measured with a help of ratio of bands intensity I(1,1)/I(0,0) with cyan lengths of quanta $\lambda_{(1,1)}$=387,1 nm and $\lambda_{(0,0)}$=388,3 nm. At p_{air}=2 atm, p_p=5 atm, p_0=100 Torr, and discharge current i: 1 – 12 A; 2 – 18 A.

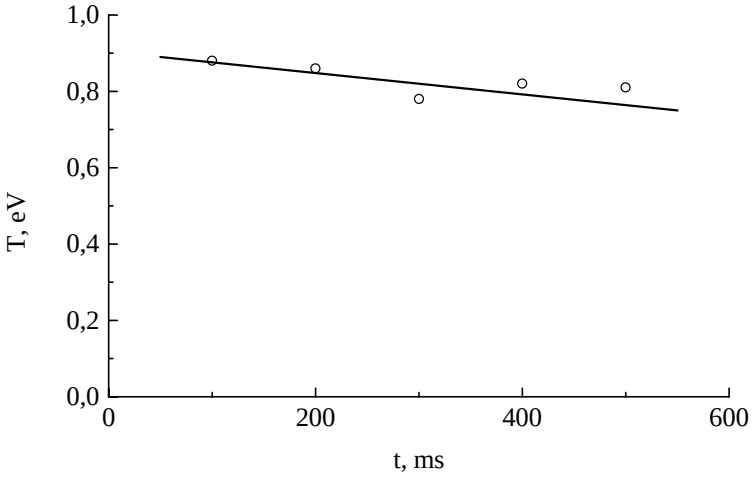

Fig. 1.87. Temporary way of temperature distribution over excited states of copper atoms measured by ratio of Cu lines with wavelengths λ_1=510.54 nm and λ_2=521.82 nm. Longitudinally- transversal constant current discharge in airflow, p_{air}=2 atm, p_0=100 torr, i=12 A.

1.9.2. Magneto plasma compressor (MPC). Radiation spectrum was recorded from the area of plasma jet in the case of application of MPC for propane-air mixture flow. The jet area was located at the distance of about 5 cm from MPC end face. In Fig.1.88 one can see plasma jet review spectrum when the plasma was created with a help of MPC in airflow. In Fig.1.89 the plasma was created with a help of MPC in –. It can be seen that radiation spectrum is more intense at plasma jet injection to airflow in comparison with its injection to propane-air mixture flow. Obtained spectra pictures show that spectral lines are strongly broadened. This is connected with high electron concentration in the plasma jet. Temperature of the distribution over excited states of copper atoms measured by ratio of Cu lines with wavelengths λ_1=510.54 nm and λ_2=521.82 nm has a value of 1.2-1.4 eV, which is possible to equate with electron temperature in conditions of strongly ionized plasma jet.

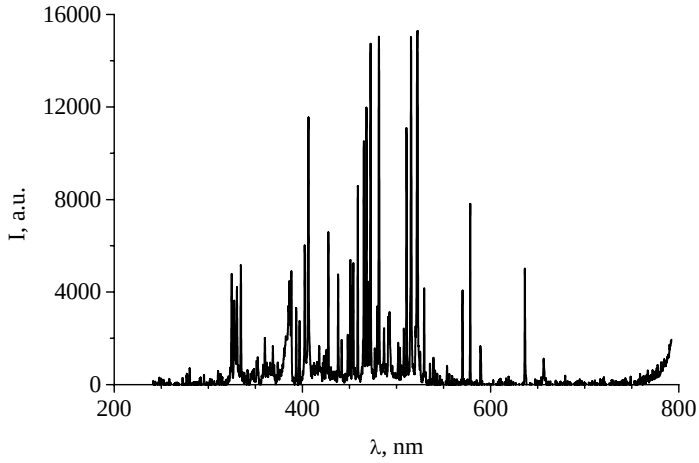

Fig. 1.88. Plasma jet review spectrum when the plasma was created with a help of MPC in airflow. Atomic lines of erosion products.

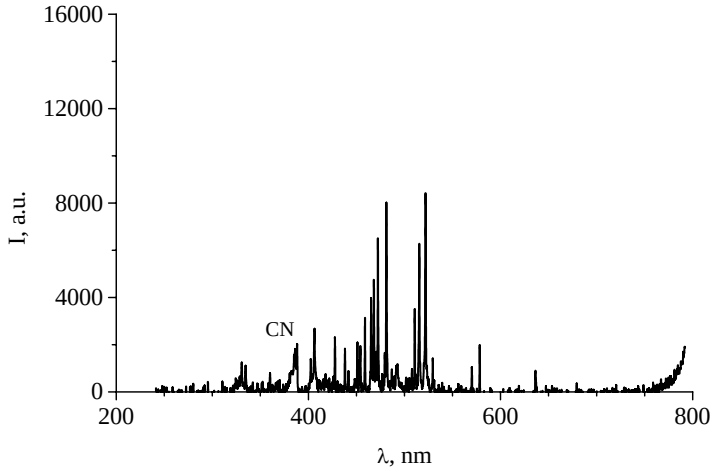

Рис. 1.89. Plasma jet review spectrum when the plasma was created with a help of MPC in propane-air mixture flow.

1.9.3. MW torch. MW torch plasma review spectrum in airflow created in the stagnant zone of the aerodynamic channel is represented in Fig.1.90. There are molecular bands of nitrogen second positive system, band of OH hydroxyl and weal Cyan bands in the spectrum. In the case of MW torch discharge creation in propane-air mixture flow, see Fig.1.91, one can observe different systems of CN bands, Swan bands of molecular carbon, molecular bands of CH and OH, and also hydrogen atomic line H_α. Gas temperature in the torch discharge of airflow equals to 750 K. Gas temperature rises up to 2900 K in propane-air mixture flow. Inflammation is observed only in nearest vicinity of torch MW discharge.

1.9.4. Surface quasi-stationary MW discharge Quasi-stationary surface MW discharge was initially excited in motionless air with a help of metallic- dielectric target placed in the stagnant zone. Then air flow was started with time delay t_{air}=1-2 s, after that propane was injected to the aerodynamic channel with time delay t_p=1 s. Plasma radiation was investigated in this series of experiments from large area of the target surface occupied by MW discharge without spatial resolution. The discharge radiation for this purpose came to the spectrograph inlet through the light guide located near the discharge without application of the focusing lens. Accumulation time of the light flux was enlarged up to 1 s for reliable detection of weak bands in the spectrum of MW discharge radiation.

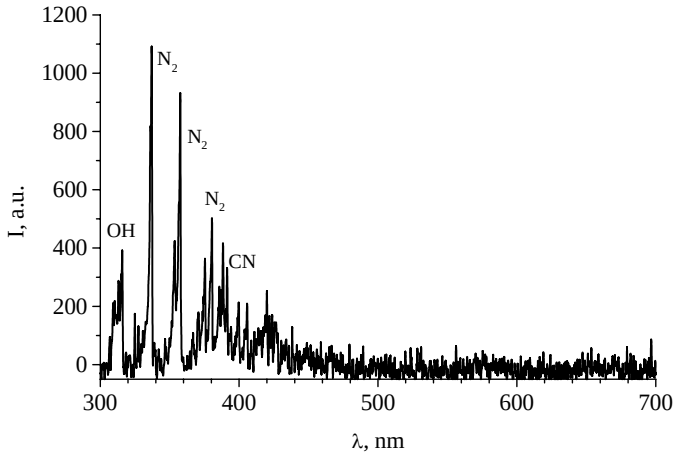

Fig. 1.90. Plasma radiation review spectrum of MW torch in airflow.

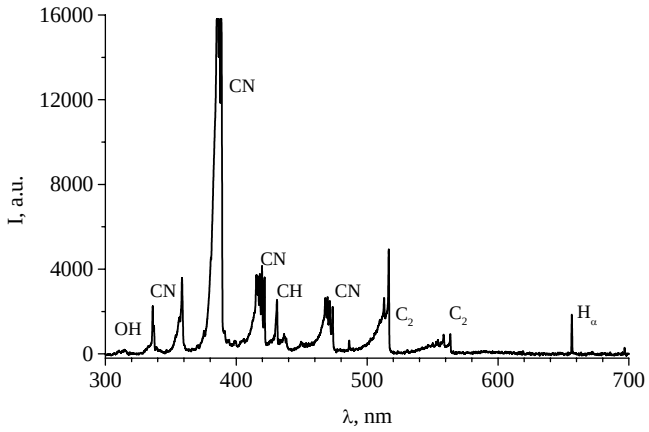

Fig. 1.91. Plasma radiation review spectrum of MW torch in propane-air mixture flow.

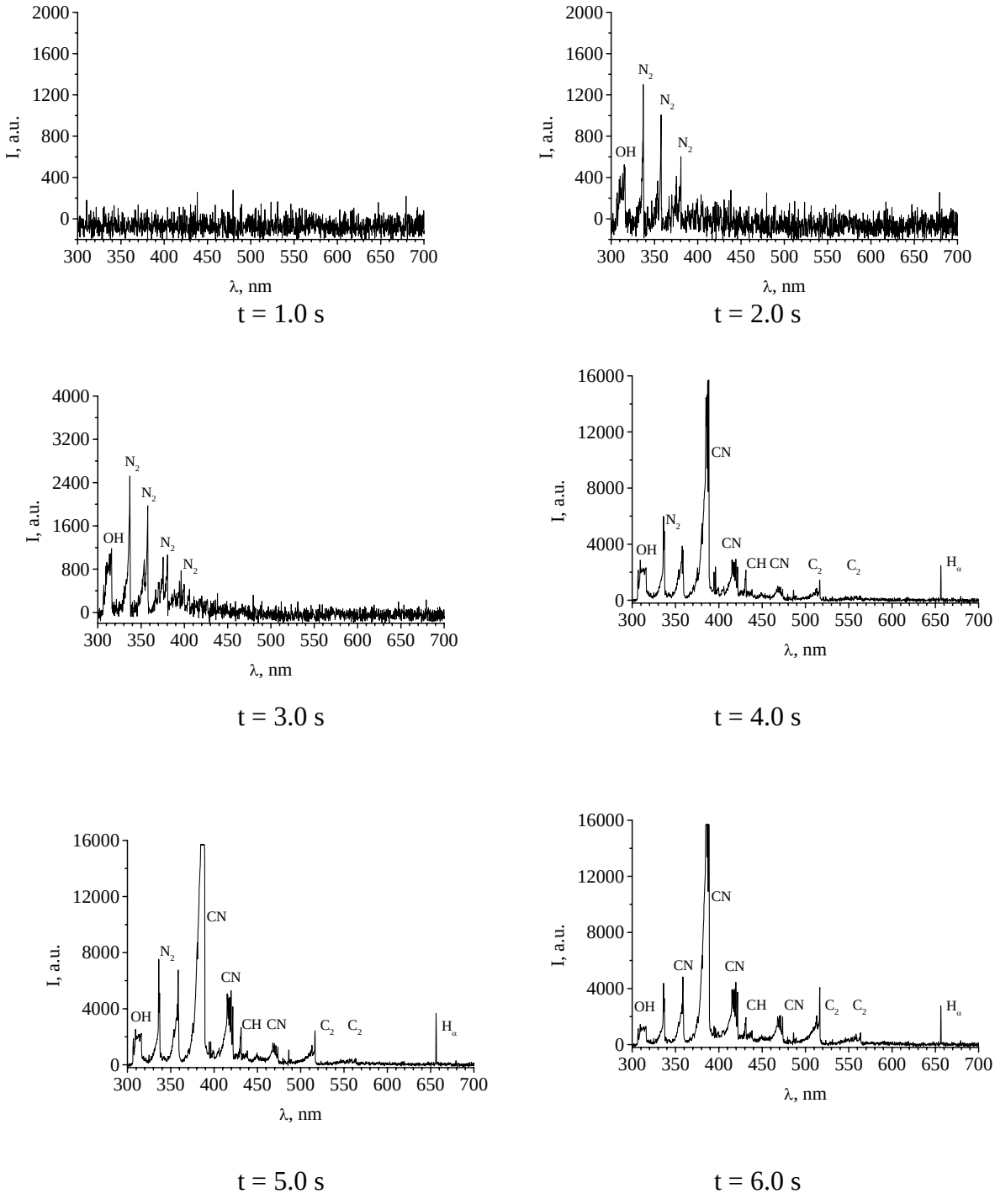

Fig. 1.92. Propane-air mixture flow inflammation process with a help of quasi stationary surface MW discharge initiated by metallic-dielectric target when the discharge is created in the stagnant zone behind a step in the aerodynamic channel.

In Fig.1.92 one can see the inflammation process of propane-air mixture flow with a help of quasi-stationary surface MW discharge created in the stagnant zone behind the step in the aerodynamic channel. Weak bands of nitrogen second positive system and OH hydroxyl band are observed in MW discharge radiation spectrum in airflow during the first stage of the process. General appearance is changed at propane injection to airflow. One can see that strong Cyan bands,

Swan bands of molecular carbon and CH band appear in the spectrum. Line of Balmer hydrogen series is also observed in the spectrum.

Gas temperature in airflow was measured by resolved rotational structure of the band (0,2) of nitrogen second positive system. Average over space gas temperature was about 1000 K in conditions of the experiment. The temperature was measured by relative intensities of Cyan bands I(1,1)/I(0,0) with quanta wavelengths $\lambda_{(1,1)}$=387,1 nm and $\lambda_{(0,0)}$=388,3 nm at propane inflammation in the area of surface MW discharge existence. The temperature obtained by this way in different time moments of the surface MW discharge existence lies in the range 2800-3400 K.

We have to note that now radiation was detected from the main supersonic flow at propane-air mixture flow inflammation in the stagnant zone of the aerodynamic channel with a help of MW torch discharge and surface MW discharge, and one can see from the discharge appearance that propane combustion takes place only in the stagnant zone in the vicinity of MW discharge. For combustion process optimization it is necessary to undertake following experimental investigations.

References to item 1.

1. Vinogradov,V.A., Shikhman,Yu.M., Albegov,R.V., Vedeshkin,G.K..“ Research of Methane Burning in High Speed Subsonic Airflow at Different Fuel Injection Schemes”, Presented at XVIth ISABE, Cleveland, Ohio, USA, August 31–September 5, AIAA Paper 2003-1152, 2003.

2. Vinogradov,V.A., Shikhman,Yu.M., Albegov,R.V., Vedeshkin,G.K..“ Experimental Research of Pre-Injected Methane Combustion in High Speed Airflow”, Presented at AIAA 12th International Space & Hypersonic Systems & Technologies Conference, Norfolk, USA, Dec.15-19, AIAA Paper 2003-6940, 2003.

3. V.Chernikov, A.Ershov, V.Shibkov, B.Timofeev, I..Timofeev, V.Vinogradov “Gas discharge in supersonic flows of air-propane mixtures”. Presented at 2 nd AIAA Plasmadynamics and Lasers Conference and 4 th Weakly Ionized Gases Workshop, 11-44 June 2001, Anaheim, CA, USA, AIAA 2001-2948.

4. A.Ershov, N.Ardelyan, V.Buchkov, V.Chernikov, V.Shibkov, O.Surkont, I. Timofeev. Transversal electric discharge sustention in supersonic air and propane-air flow”. 41 ST AIAA Aerospace Science Meeting and Exhibit, 6-9 January 2003, Reno, Nevada, AIAA-2003-0872.

5. Ershov A.P., Surkont O.S., Timofeev I.B., Shibkov V.M., Chernikov V.A. Transversal electrical discharges in transversal airflows. A Mechanisms of propagation and instabilities of the discharge. Teplofizika Vysokhih Temperatur. 2004. V.42. №4, P.516-522 (in Russian)

6. Ershov A.P., Surkont O.S., Timofeev I.B., Shibkov V.M., Chernikov V.A. Transversal electrical discharges in transversal airflows. Spatial-temporary structure and Ampere-Volt discharge characteristics. Teplofizika Vysokhih Temperatur. 2004. V.42. №5. 669-675 . (in Russian)

7. Vinogradov, V.A., Alexandrov, A.F. Timofeev,I.B., Esakov,I.I “The Effects of Plasma Formations on Ignition and Combustion.” Presented at Aerospace Sciences Conference, Jan. 5-8, Reno, USA, AIAA Paper 2004-1356, 2004

8. Chernikov A.V., Chernikov V.A., Chuvashev S.N., Ershov A.P., Shibkov V.M., TimofeevB.I, Timofeev I. B. “Crossed supersonic jets of a plasma and a dense gas”. The 2 nd Workshop on Magneto-plasma-aerodynamics in aerospace applications, 5-7 April 2000, Moscow, IHT of RAS, p.215-220.

9. A.F.Alexandrov, V.A.Chernikov, S.N.Chuvashev, A.P.Ershov, V.M.Shibkov, I.B. Timofeev. “Long-Lived Plasma Formations in Air”. 9 th International Space Planes and Hypersonic Systems and Technologies Conference, 1-4 November 1999, Norfolk, Virginia, USA, AIAA-99-4977.

10. S.I.Gritsinin, I.A.Kossyi, N.I.Malykh, M.A.Misakyan, S.M.Temchin and Yu.B.Bark. “Plasma Coaxial Discharge as a New Type of the Microwave Surface Discharge”. – XIV Int. Symposium on Plasma Chemistry, 1999, Prague, Symposium Proceedings, v. II, pp. 675-680.

11. G.M.Batanov, S.I.Gritsinin and I.A.Kossyi “Non-self-sustained microwave discharge and the concept of a microwave air jet engine”, J. Phys. D: Appl. Phys., v. 35, (2002), No 20, pp. 2687-2692.

12.G.M.Batanov, N.K.Berezhetskaya, I.A.Kossyi, A.N.Magunov and V.P.Silakov “Interaction of High-Power Microwave Beams with Metal-Dielectric Media”, European Physical Journal 11.

13. Strokin, V.N., Grachev, V.A. “Possible schemes of flameholding in hydrogen fueled scramjet combustors”. International Aerospace Congress, Moscow, v.1, 1997, pp. 630-633

14. Vinogradov, V.A., Chernikov, V.A., Timofeev, I.B., Kolesnikov, E.B. “Preliminary study of different plasma discharges at M=2 air flow”, Presented at Aerospace Sciences Conference, Jan. 8-11, Reno, USA, AIAA Paper 2005-988, 2004.

15. Calvin Morrison, Hsin-Yuan Lyu and Raymond Edelman “Fuel Sensitivity Studies Based on a Design System for High Speed Airbreathing Combustors”, Presented at XIIIrd ISABE, AIAA Paper 99-7235, 1999.

2. Numerical modeling of fuel/air ignition in the test channel by electrical discharge

2.1. Modeling of flow in the test channel

2.1.1. Gas-phase model

Basic assumptions

1. The gas is considered as an ideal one-temperature reacting mixture of perfect neutral gases,
2. Navier-Stokes approximation is employed to calculate molecular viscous fluxes.
3. Turbulent mean flow is described by the Favre averaged [1] pressure *p*, velocity vector $\vec{u}$, mole fractions of species X_i, $i = 1,\ldots,\nu$, and temperature *T*.
4. Correlations of temperature and chemical composition fluctuations are neglected ,
5. The Boussinesq approximation for the turbulent fluxes and Wilcox two-equations $k-\omega$ model [2] for calculation of turbulent transport coefficients are used.
6. Effect of electrical discharge on gas flow is modeled by a local heat supply.

State equation. The gas state equation is given by

$$p = \rho R_u T / M .$$

Here ρ is density, R_u is a universal gas constant, and M is an average molecular weight of the mixture that is expressed through molecular weights of species M_i as

$$M = \sum_{i=1}^{\nu} M_i X_i .$$

Thermodynamic properties. Molar enthalpy h_i and heat c_{pi} of species *i* are determined through partition function $Q_i(p,T)$:

$$h_i(T) = h_i^0 + R_u T^2 \frac{\partial \ln(Q_i V_m)}{\partial T}, \quad c_{pi}(T) = \frac{\partial h_i}{\partial T},$$

where h_i^0 is a formation heat of species *i* and $V_m = R_u T / p$ is a mole volume.

In considered gas-phase model an evaluation of thermodynamic functions is based on the following approximation of c_{pi} dependence from temperature

$$c_{pi}(T) = \frac{a_{-2,i}}{T^2} + \sum_{k=0}^{5} a_{k,i} T^k \quad \text{for } T_{1,i} \le T \le T_{2,i},$$

$$c_{pi}(T) = c_{pi}(T_{1,i}) \quad \text{for } T_{1,i} \ge T$$

$$c_{pi}(T) = c_{pi}(T_{2,i}) \quad \text{for } T_{2,i} \le T$$

where coefficients $a_{k,i}$ are determined by an interpolation known tabular data in a range of temperatures $T_{1,i} \le T \le T_{2,i}$. The approximating formulas for $h_i(T)$ and $Q_i(p,T)$ are determined with a successive integration expressions for $c_{p,i}(T)$ on temperature with use as constants integration of tabular values of h_i and $Q_i(p,T)$ at some fixed temperature $T = T^*$.

Elementary chemical reactions in gas phase. A molar rate of an elementary gas phase chemical reaction *j*

$$\sum_i \nu_{ji}[A_j] \Leftrightarrow \sum_i \nu'_{ji}[A_j],$$

where ν_{ji}, ν'_{ji} are stochiometric coefficients and $[A_i]$ is a symbol of chemical species *i* is expressed as

$$\bar{\omega}_j = k_j^f \prod_{i=1}^{\nu} (\rho\gamma_i)^{\nu_{ji}} - k_j^r \prod_{i=1}^{\nu} (\rho\gamma_i)^{\nu'_{ji}},$$

where k_j^f and k_j^r are forward and reverse rate constants of this reaction, γ_i is mass-mole fraction of *i*-th species defined as $\gamma_i = X_i / M$.

A molar production rate of species *i* per unit volume due to all chemical reactions is

$$\dot{\omega}_i = \sum_j (\nu'_{ji} - \nu_{ji}) \bar{\omega}_j .$$

Forward rate constants of reactions are approximated by the generalized Arrhenius formula

$$k_j^f = a_j T_j^{b_j} \exp(-E_j / T).$$

The reverse rate constants k_j^r are defined from detailed equilibrium condition

$$k_j^f / k_j^r = \prod_{i=1}^{\nu} (Q_i \exp(-h_i^0 / R_u T))^{(\nu'_{ji} - \nu_{ji})} .$$

Global chemical reactions in gas-phase

The global reactions is used in two-step chemical mechanism (quasi-global mechanism). Reactions of this type describe the fuel oxidation to CO and H_2

$$Fuel + n_1 O_2 \Rightarrow n_2 CO + n_3 H_2 .$$

The global reaction is often a convenient way of approximating the effects of the many elementary reactions which actually occur. Its rate represents an appropriate average of all of the individual reaction rates involved. The rate expression of the global reaction is given by

$$k_{global} = A T^n p^m \exp(-E_a / R_u T)[Fuel]^a [O_2]^b$$

Reaction rate parameters are varied in order to provide the best agreement between computed and experimentally observed flame speeds in selected mixtures of fuel and oxidizer [3].

Molecular transport properties. The molar diffusion fluxes $\vec{K}_{M,i}$ are determined from the Stefan-Maxwell relations [4] that are given by

$$\sum_{j=1}^{\nu} \bar{M} d_{ij} (\gamma_i \vec{K}_{M,j} - \gamma_j \vec{K}_{M,i}) = \frac{\partial \gamma_i M}{\partial \vec{r}}, \quad i = 1, 2, ..., \nu - 1$$

$$\sum_{j=1}^{\nu} \vec{K}_{M,j} M_j = 0,$$

where $d_{ij} = M / \rho \mathrm{D}_{ij}$, D_{ij} is a binary diffusion coefficient.

Molecular stress tensor $\hat{\tau}_M = (\vec{\tau}_{M,x}, \vec{\tau}_{M,y})^T$ (momentum fluxes tensor with reversed sign) is given by

$$\hat{\tau}_M = 2\mu_M \hat{\varepsilon}, \qquad \hat{\varepsilon} = \frac{1}{2}\left[\left(\frac{\partial \vec{u}}{\partial \vec{r}} \right) + \left(\frac{\partial \vec{u}}{\partial \vec{r}} \right)^T - \frac{2}{3} \left(\frac{\partial}{\partial \vec{r}} \cdot \vec{u} \right) \hat{I} \right]$$

where $\hat{\varepsilon}$ is tensor of deformation rates, $\hat{I}$ is unit tensor, μ_M is molecular viscosity.

The molecular heat flux $\vec{q}_M$ is given by following expression

$$\vec{q}_M = -\lambda_M \frac{\partial T}{\partial \vec{r}} + \sum_{i=1}^{\nu} \vec{K}_{M,i} h_i \,,$$

where λ_M is molecular thermal conductivity, $h_i(T)$ is molar enthalpy of species *i*. For calculation of molecular viscosity and thermal conductivity the approximate formulas Wilke-Wassiljewa type [5] are used

$$\mu_M = \sum_{i=1}^{\nu} M_i \gamma_i Sc_i D_i \,, \quad \lambda_M = \sum_{i=1}^{\nu} \gamma_i \left[c_{pi} + 2.5 R_u (1.5 Sc_i - 1) \right] D_i \,.$$

Here $Sc_i(T) = \mu_i / \rho_i \mathsf{D}_{ii}$ is Schmidt number of species *i* calculated on molecular viscosity μ_i, density ρ_i and a self-diffusion coefficient D_{ii} of this species in a pure form, D_i is coefficient defined by expression

$$D_i = \frac{1}{\sum_{j=1}^{\nu} \gamma_j d_{ij}} .$$

Functions $d_{ij}(T)$ and $Sc_i(T)$ are determined by formulas

$$d_{ij}(T) = 3.12 \cdot 10^5 \frac{\overline{\Omega}_{ij}^{(1.1)}(T) \sqrt{2 M_i M_j}}{\sqrt{T (M_i + M_j)}}, \qquad Sc_i(T) = \frac{5 \overline{\Omega}_{ii}^{(1.1)}(T)}{6 \overline{\Omega}_{ii}^{(2.2)}(T)} \,,$$

$[d_{ij}] = \sec \cdot m / kmole, \quad [\Omega] = \text{Å}^2,$

where $\overline{\Omega}_{ii}^{(1.1)}(T)$ and $\overline{\Omega}_{ii}^{(2.2)}(T)$ are collision integrals of diffusion and viscous types accordingly. The values of collision integrals are calculated through the potential of particles interaction at collision. In the present statement the simple interpolation dependence for calculation of collision integrals $\overline{\Omega}_{ii}^{(1.1)}(T)$ is used

$$\overline{\Omega}_{ii}^{(1.1)}(T) = (a_{ij} + b_{ij} \ln T)^2$$

Coefficients a_{ij} and b_{ij} are calculated on specified values of the collision integrals for $T_1 = 300K$ and $T_2 = 3000K$. Quantities of $\overline{\Omega}_{ii}^{(1.1)}(T_k)$ are determined on the Lennard-Jones potential. Values of potential parameters for identical particles pairs are taken from literature. Parameters of interaction potentials for the different particles are determined on combinatorial rules [4]. At an evaluation of the Schmidt number $Sc_i(T)$ for all components it is assumed to be $\overline{\Omega}_{ii}^{(2.2)}(T) = 1.1 \overline{\Omega}_{ii}^{(1.1)}(T)$.

Turbulent transport model

Turbulent (Reynolds) stress tensor $\hat{\tau}_T$, turbulent heat flux $\vec{q}_T$, and turbulent diffusion fluxes $\vec{K}_{T,i}$ are expressed as

$$\hat{\tau}_T = \mu_T \hat{\varepsilon}, \quad \vec{q}_T = -\lambda_T \frac{\partial T}{\partial \vec{r}} + \sum_{i=1}^{\nu} \vec{K}_{T,i} h_i, \; \vec{K}_{T,i} = -\rho D_T \frac{\partial \gamma_i}{\partial \vec{r}}$$

Eddy viscosity μ_T, turbulent thermal conductivity λ_T and turbulent diffusion coefficient D_T are determined through turbulent mixing energy k and specific dissipation rate ω

$$\mu_T = \rho \frac{k}{\omega}, \quad \lambda_T = \frac{\mu_T c_p}{\mathrm{Pr}_T}, \; \rho D_T = \frac{\mu_T}{Sc_T}$$

The values of turbulent energy k and specific dissipation rate ω are defined from two differential equations [2]:

$$\frac{\partial \rho k}{\partial t} + \frac{\partial}{\partial \vec{r}} \cdot \left(\rho \vec{u} k - (\mu + \sigma_T^* \mu_T) \frac{\partial k}{\partial \vec{r}} \right) = b_k,$$

$$\frac{\partial \rho \omega}{\partial t} + \frac{\partial}{\partial \vec{r}} \cdot \left(\rho \vec{u} \omega - (\mu + \sigma_T \mu_T) \frac{\partial \omega}{\partial \vec{r}} \right) = b_\omega,$$

where

$$b_k = \mu_T \varepsilon_{ij} \frac{\partial u_i}{\partial x_j} - \beta_T^* \rho \omega k, \quad b_\omega = \gamma_T \rho \varepsilon_{ij} \frac{\partial u_i}{\partial x_j} - \beta_T \rho \omega^2,$$

$$\beta_T^* = 0.09, \; \gamma_T = 0.56, \; \beta_T = 0.075, \; \sigma_T = 0.5, \; \sigma_T^* = 0.5.$$

It is assumed that turbulent Prandtl and Schmidt numbers are $\mathrm{Pr}_T = 1$, $Sc_T = 1$.

2.1.2. Governing equations and numerical method

Governing equations. The integral form of two-dimensional governing equations in the Cartesian coordinates (*x*,*y*) for above gas-phase model is written as

$$\frac{d}{dt} \int_S \mathbf{U} dS + \int_{\delta S} \vec{n} \cdot \vec{\mathbf{F}} dl = \int_S \mathbf{\Omega} dS,$$

where S is a fixed control domain in a plane (x, y), δS is a boundary of domain , $\vec{n} = (n_x, n_y)$ is an unit outward normal to δS, $\mathbf{U}$ is a set of conserved variables per unit volume, $\vec{\mathbf{F}} = \vec{\mathbf{F}}^{inv} + \vec{\mathbf{F}}^{vis}$ represents a sum of the inviscid and viscous fluxes of $\mathbf{U}$ through the domain boundary and $\mathbf{\Omega}$ consists of the source terms. For considered gas-phase model these vectors are given by

$$\mathbf{U} = \{\rho\gamma_1, \ldots, \rho\gamma_\nu, \rho u, \rho v, \rho e_0, \rho k, \rho\omega\}^{\mathrm{T}};$$

$$\vec{\mathbf{F}} = \begin{Bmatrix} \rho\vec{u}\gamma_1 \\ \vdots \\ \rho\vec{u}\gamma_\nu \\ \rho\vec{u}u + p\vec{n}n_x \\ \rho\vec{u}v + p\vec{n}n_y \\ \rho\vec{u}h_0 \\ \rho\vec{u}k \\ \rho\vec{u}\omega \end{Bmatrix} + \begin{Bmatrix} \vec{K}_1 \\ \vdots \\ \vec{K}_\nu \\ -\vec{\tau}_x \\ -\vec{\tau}_y \\ \vec{q}_h - u\vec{\tau}_x - v\vec{\tau}_y \\ \vec{q}_k \\ \vec{q}_\omega \end{Bmatrix};$$

$$\mathbf{\Omega} = \{\dot{\omega}_1, \ldots, \dot{\omega}_\nu, 0, 0, b_h, b_k, b_\omega\}^{\mathrm{T}}.$$

Here u, v are the components of velocity vector $\vec{u}$, $e_0 = e + 0.5(\vec{u} \cdot \vec{u})$ is a total energy per unit mass, $h_0 = e_0 + p/\rho$ is a total enthalpy, b_h is heat source power,

$$\vec{\tau}_x = (\tau_{xx}, \tau_{xy}),\ \ \vec{\tau}_y = (\tau_{yx}, \tau_{yy}),\ \ \hat{\tau} = \hat{\tau}_M + \hat{\tau}_T = 2(\mu_M + \mu_T)\hat{\varepsilon},$$

$$\vec{q}_h = \vec{q}_M + \vec{q}_T,\quad \vec{K}_i = \vec{K}_{M,i} + \vec{K}_{T,i},$$

$$\vec{q}_k = -(\mu + \sigma_T^* \mu_T)\frac{\partial k}{\partial \vec{r}},\quad \vec{q}_\omega = -(\mu + \sigma_T \mu_T)\frac{\partial \omega}{\partial \vec{r}}.$$

Numerical method. The governing equations are solved on the multiblocks structured mesh through a finite volume approach. At this approach the finite difference equations system consists of numerical analogs of the conservation equations for the quadrilateral cells covering the computation domain and the difference approximation of the boundary conditions. This method yields an approximate solution $\mathbf{Z} = \{pX_1, ..., pX_\nu, u, v, T, k, \omega\}$ in a center of each cell and in a center of each cell side lying on the wall. The cells are built by intersection of the two discrete curve sets. The inviscid fluxes $\mathbf{F}_G^{inv}$ through cell sides are calculated from result of the exact Riemann problem solution $\mathbf{Z}_G = \Re(\mathbf{Z}_G^L, \mathbf{Z}_G^R)$ where $\Re$ is the Riemann problem solver. The left and right interfacial values $\mathbf{Z}_G^L$ and $\mathbf{Z}_G^R$ are defined by the limited one-dimensional extrapolation of $\mathbf{Z}$ from the cell-centers to the cell sides. The numerical viscous fluxes $\mathbf{F}_G^{vis}$ through cell sides are evaluated using the central and one-sided difference formulas of the second order accuracy. For time-marching integrating of governing equations the implicit Runge-Kutta scheme of second order accuracy is used. On every time step the flowfield parameters are computed due Gauss-Seidel line relaxation numerical technique.

2.1.3. Channel model geometry.

Calculations have been performed for planar case of the channel geometry. Numerical model of the channel involves nozzle length of 50 mm, insulator length of 292 mm and combustor length of 400 mm. Height of nozzle throat is 148 mm, height of insulator is 250 mm, and height of combustor is 400 mm. Between lower surfaces of insulator and combustor is backward step height of 150 mm. Contour of nozzle is approximated by polynomial of a third degree. Rated value of Mach number on the nozzle exit is $M = 2$ (without boundary layer effect). All calculations were performed at air total pressure $p_{tot} = 2$ atm and total temperature $T_{tot} = 600\ K$.

2.2. Parametric calculations of propane/air mixture ignition by the heat deposition.

2.2.1. Schemes of propane injection and heat deposition into channel.

Propane is injected to air supersonic flow in normal direction from injector width of L_{inj}=5.5 mm placed on the lower surface of insulator at begin of this duct. Center of the injector are located on distances of 6 mm from the insulator origin. Propane injection is carried out with the total mass rate $G_{inj} = L_{inj}\,(\rho v)_{inj}$. Injection intensity is specified by parameter $b_{inj} = (\rho v)_{inj}/(\rho u)*$, where $(\rho u)*$ is an air mass flux in the nozzle throat. Present calculations were performed for propane injection intensity $b_{inj} = 0.05$. Temperature of injected propane is 600 *K*. Values of turbulent parameters of injected gas correspond to laminar flow (small turbulence energy and large energy dissipation).

Two schemes of heat deposition in channel have been considered. These schemes are shown on Fig. 2.1.

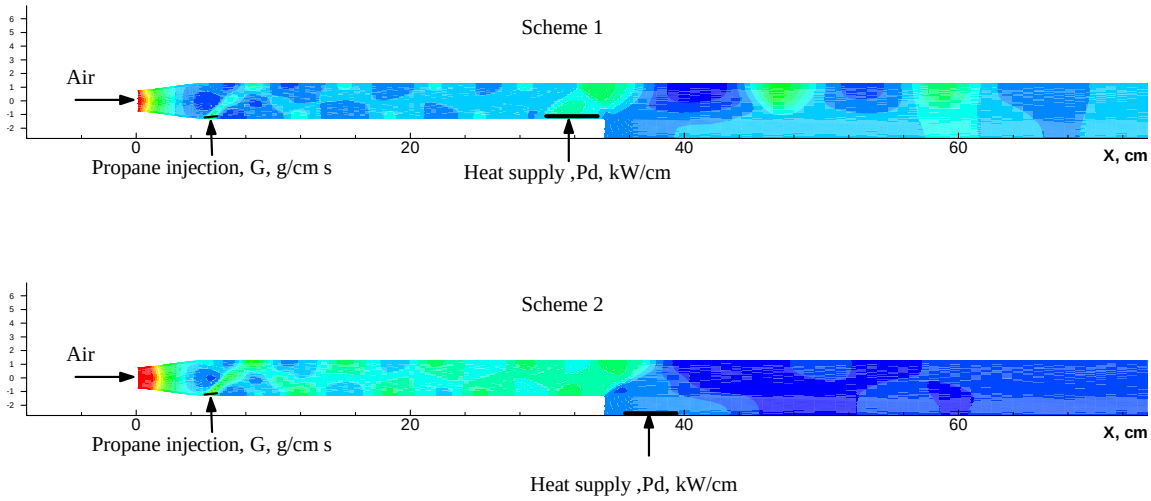

Fig.2.1. Considered schemes of propane injection and surface heat deposition in channel

In the first scheme heat is supplied with steady total power P_d uniformly distributed into near wall region of specified location and configuration. It is considered two configurations of the heat source:

1) rectangular $x_{qs} \le x \le x_{qf}$, $y_{qs} \le y \le y_{qf}$;
2) triangular $x_{qs} \le x \le x_{qf}$, $y_{qs} \le y \le y_{qs} + (y_{qf} - y_{qs})(x - x_{qs})/(x_{qf} - x_{qs})$,

where *x*,*y* is Cartesian coordinates with an origin located in the nozzle throat center and *x*-axes directed along channel. Heat source was located near end of the insulator (close to step). Considered parameters of the heat source are listed in Table 2.1. In the second scheme heat is supplied into rectangular region $x_{qs} \le x \le x_{qf}$, $y_{qs} \le y \le y_{qf}$ placed after step. Considered parameters of the heat source are listed in Table 2.4.

2.2.2. Models of chemical kinetics.

Three thermally equilibrium gas-phase models varying in chemical composition and chemical kinetics are used in calculations:

- model 1 with frozen chemical reactions involving three species (C_3H_8 ,O_2, N_2),
- model 2 with quasi-global chemical mechanism involving 12 species, one global reaction and 20 elementary chemical reactions taken from described in model 3 detailed chemical mechanism (see Appendix),

- model 3 with detailed chemical mechanism involving 28 species (C_3H_8 ,O, H, O_2, N_2, H_2, CO, OH, H_2O, HO_2, H_2O_2, HCO, CO_2, CH, CH_2, CH_3, CH_4, C_2H, C_2H_2, C_2H_3, C_2H_4, C_2H_5, C_2H_6, C_3H_5, C_3H_6, i-C_3H_7, n-C_3H_7, CH_2O) and 70 elementary chemical reactions taken in the main from [6] and listed in Tables of Appendix.

Only rate constants of recombination reactions were used in calculations. If in the reference source it was listed rate constants of dissociation reaction so rate constant of recombination reactions is calculated through equilibrium constant of this reaction and it is approximated by Arrhenius formula. These approximations are indicated in Table by symbol "*".

Cooled, fully non-catalytic model of gas-wall thermal and chemical interactions was used in calculations. All computations are performed for $T_w = 600\ K$.

2.2.3. Analysis of steady state propane/air mixture ignition for scheme 1 of propane injection and heat deposition.

Considered cases of calculations are listed in Table 2.1.

Table 2.1

Case	Heat deposition power P_d , kW/cm	Heat deposition region					Chemical mechanism
		Conf.	x_{qs}, cm	x_{qf}, cm	y_{qs}, cm	y_{qf}, cm	
1	3.0	Rect.	29	34	-1.25	-1.05	frozen
2	3.0	Rect.	29	34	-1.25	-1.05	detailed
3	3.5	Rect.	29	34	-1.25	-1.05	frozen
4	3.5	Rect.	29	34	-1.25	-1.05	detailed
5	4.0	Rect.	29	34	-1.25	-1.05	frozen
6	4.0	Rect.	29	34	-1.25	-1.05	detailed
7	4.0	Trian.	29	34	-1.25	-1.05	frozen
8	4.0	Trian.	29	34	-1.25	-1.05	detailed
9	4.0	Rect.	29	34	-1.25	-0.75	frozen
10	4.0	Rect.	29	34	-1.25	-0.75	detailed
11	4.0	Rect.	28	33	-1.25	-1.05	frozen
12	4.0	Rect.	28	33	-1.25	-1.05	detailed
13	4.0	Rect.	29	34	-1.25	-1.05	quasi-global

Cases 1, 2. Figs. 2.2-2.3 present some data predicted for uniform heat deposition of total power 3.0 kW/cm in rectangular region 29<x<34 cm, -1.25 < y< -1.05 cm before back step. Distribution of propane and oxygen mole fractions across channel before heating region is given on Fig. 2.2. Analysis presented on Fig. 2.2 data shows what gas in this section is a rich air-fuel mixture. Similar conditions have place for all considered cases of scheme 1.

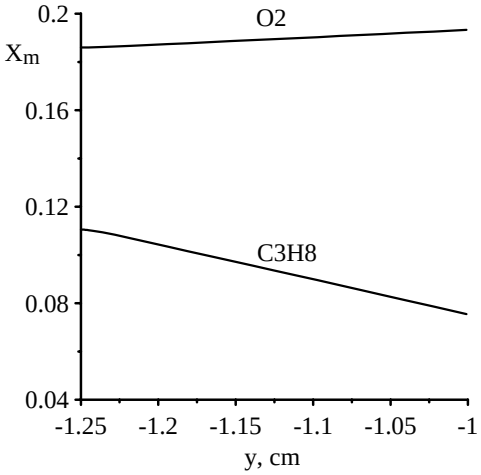

Fig. 2.2. Distributions of propane and oxygen mole fractions across channel for x = 29 cm

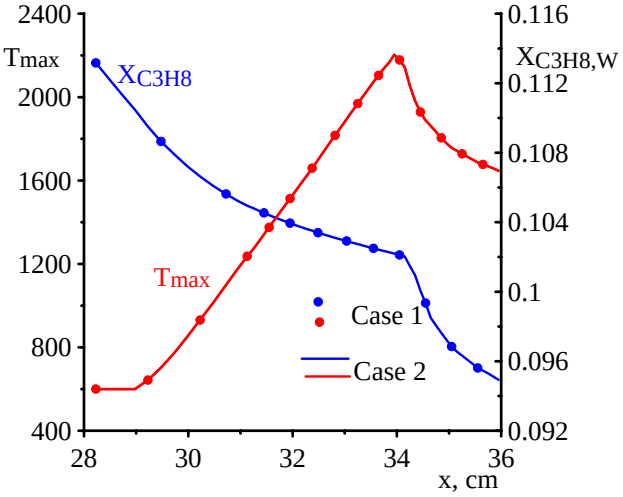

Fig. 2.3. Distributions of $T_{\max}$ and $X_{C3H8,W}$ in the heating region

Distributions along heating region maximal across channel gas temperature $T_{\max}$ and propane mole fraction $X_{C3H8,W}$ on lower wall are given on Fig. 2.3. For these conditions in the end of heating region is formed local peak of gas temperature with value of 2200 K. After step value of $T_{\max}$ rapidly decreases to ~800 K. It is seen that distributions of gas temperature and propane mole fraction coincide with 'frozen' indicated by circles. Ignition of propane/air mixture for this case is not predicted.

Cases 3, 4. Configuration and location of the heating region are same as for cases 1, 2 but the heat deposition power increased to 3.5 kW/cm. Distributions along heating region $T_{\max}$ and $X_{C3H8,W}$ for this case are given on Fig. 2.4.

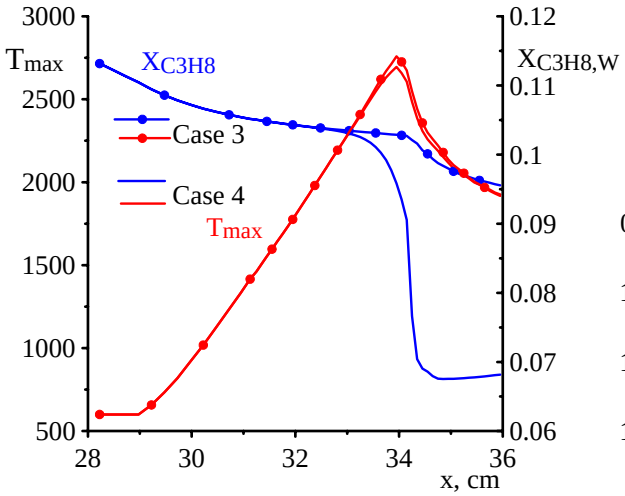

Fig. 2.4 Distributions of $T_{\max}$ and $X_{C3H8,W}$ in the heating region

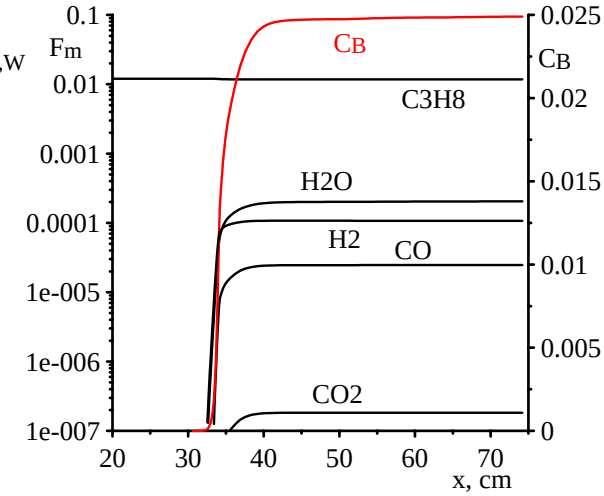

Fig. 2.5. Distributions along channel mole fractions F_m and parameter C_B

Fig.2.5 shows distributions of mole fractions F_m of some components in the total mole flux in channel and distribution of combustion completeness C_B assigned by

$$F_m = \frac{G_m / M_m}{\sum_i G_m / M_m}, \qquad C_B(x) = 1 - G_{fuel}(x) / G_{inj},$$

where $G_m(x)$ is mass flux of species m through considered section of channel. For non-reacting gas model $C_B(x)$ =0. It is seen that in this case gas temperature for frozen chemical model in the end of the heating region reaches 2750 K but further $T_{\max}$ rapidly decreases because of the heating finish and gas after step expansion. In these conditions process of burning is started but through the gas cooling one is finished not achieved stage of heat generation. Therefore distribution of gas temperature practically is not changed in comparison with model of frozen chemical reactions. Completeness of combustion C_B reaches after step of 0.025 and further is not changed.

Cases 5, 6. Configuration and location of the heating region are same as for cases 1, 2 but the heat deposition power is increased to 4.0 kW/cm. Distributions along heating region $T_{\max}$ (x) and $X_{C3H8,W}$ (x) for this case are given on Fig. 2.6. Fig. 2.7 shows distributions of $T_{\max}$ along combustor. For this heating power gas temperature for frozen chemical model in the end of the heating region reaches ~3500 K. As it is seen from Fig. 2.6, where distribution of $X_{C3H8,W}$ (x) are given, for considered conditions fuel/air mixture in the heating region fully burns off. Ignition is started at $T_{\max} \approx$ 2000 K. Combustion front has thickness of ~1 cm and one is placed near end of the heating region. Since fuel mixture in flow before ignition is rich combustion products content great fractions H2, CO and H2O (see Fig. 2.8). In combustor H2, CO partially burn out to CO2

and H2O due to inflow of oxygen from outer stream (Fig. 2.8, b). As a result of combustion heat generation peak of gas temperature increases on ~500 K (to 4000 K) and in combustor T_{max} increases on ~1000 K.

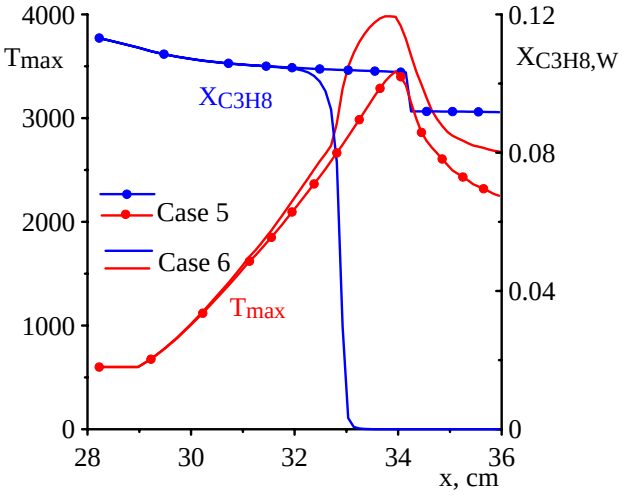

Fig. 2.6. Distributions of T_{max} and $X_{C3H8,W}$ propane mole fraction in heating region

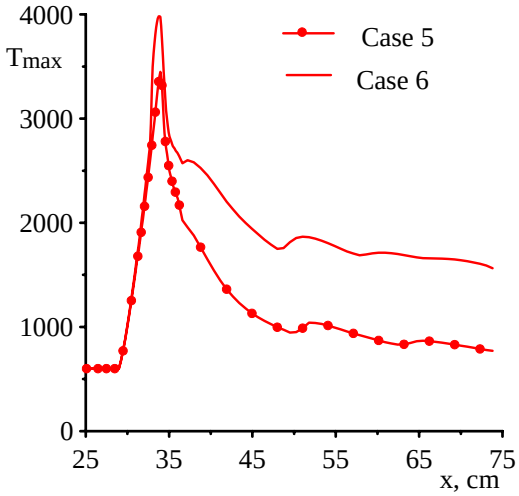

Fig.2.7. Distribution of T_{max} along channel

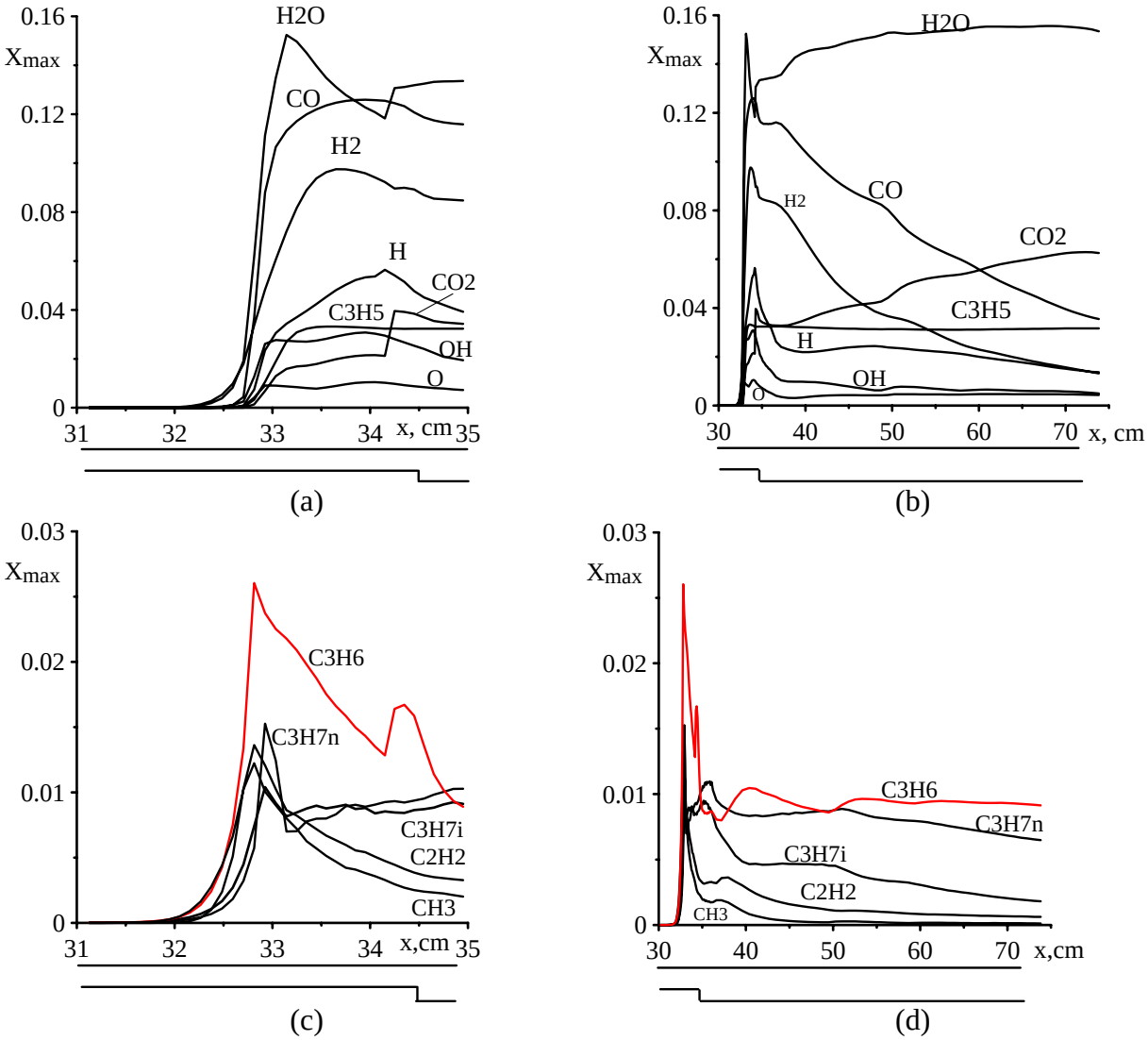

Fig. 2.8. Distributions of maximal across channel values of mole fractions species along heating region (a, c) and along combustor (b, d).

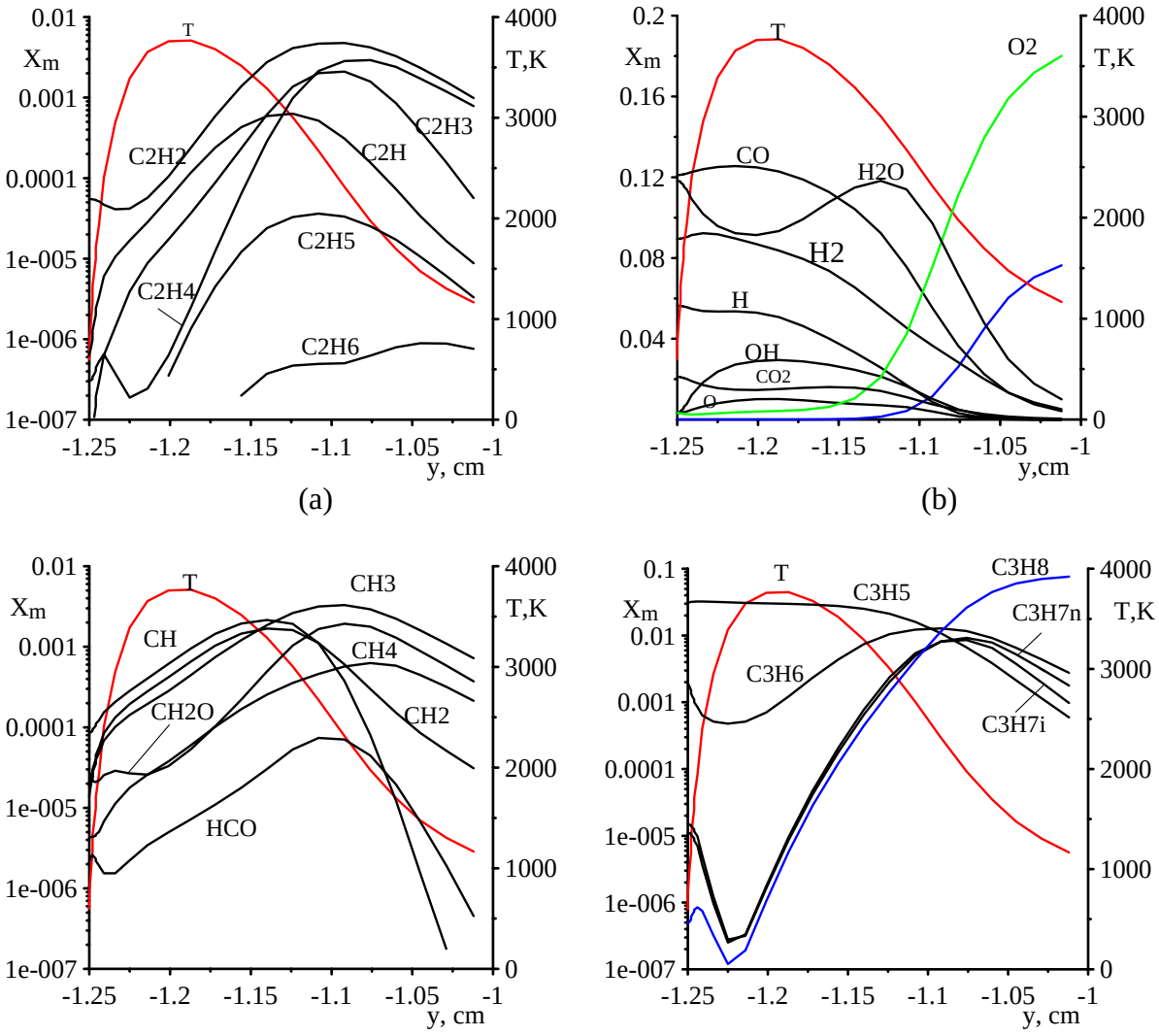

Fig. 2.9. Distributions of gas temperature and species mole fractions across channel section x= 34.15 cm

Variations of the gas temperature and chemical composition along channel are presented on Figs. 2.9 – 2.11. Fig. 2.9 shows distribution of above parameters in the end of insulator directly before back step (x = 34.15 cm). Distributions of temperature and species mole fractions across stagnation region after step (x= 36.05 cm) are given on Fig. 2.10. At last Fig. 2.11 shows the thermochemical structure of flow near combustor outlet (x= 70.02 cm).

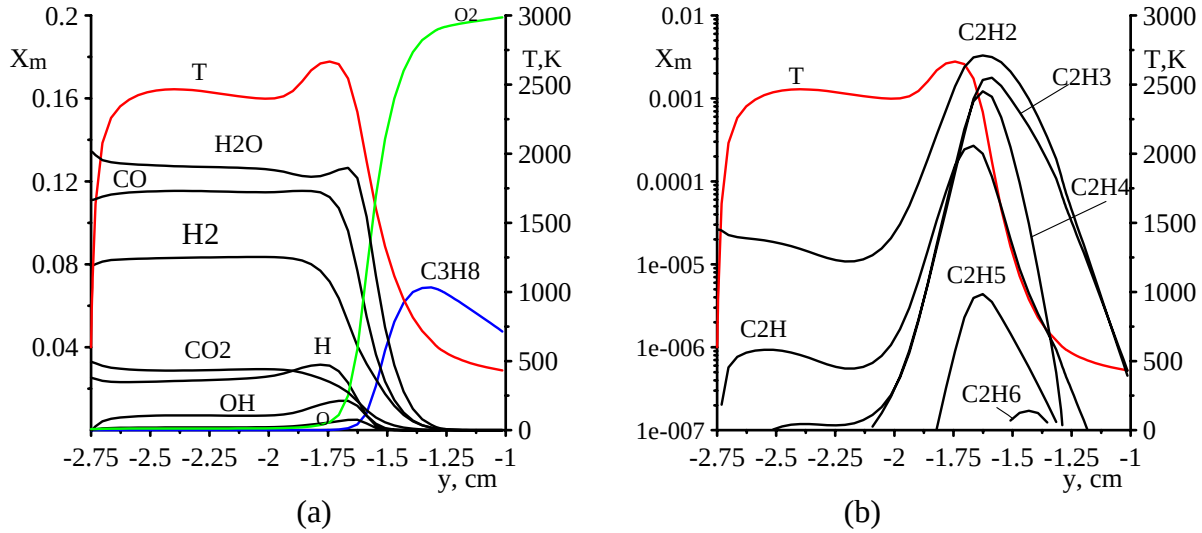

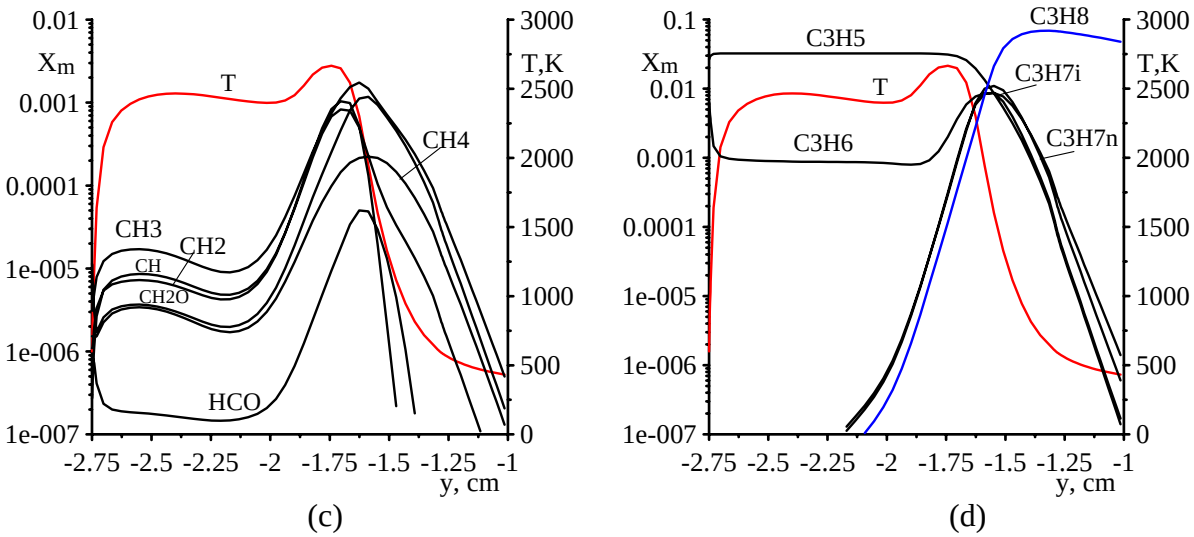

Fig. 2.10. Distributions of gas temperature and species mole fractions for section x= 36.05 cm

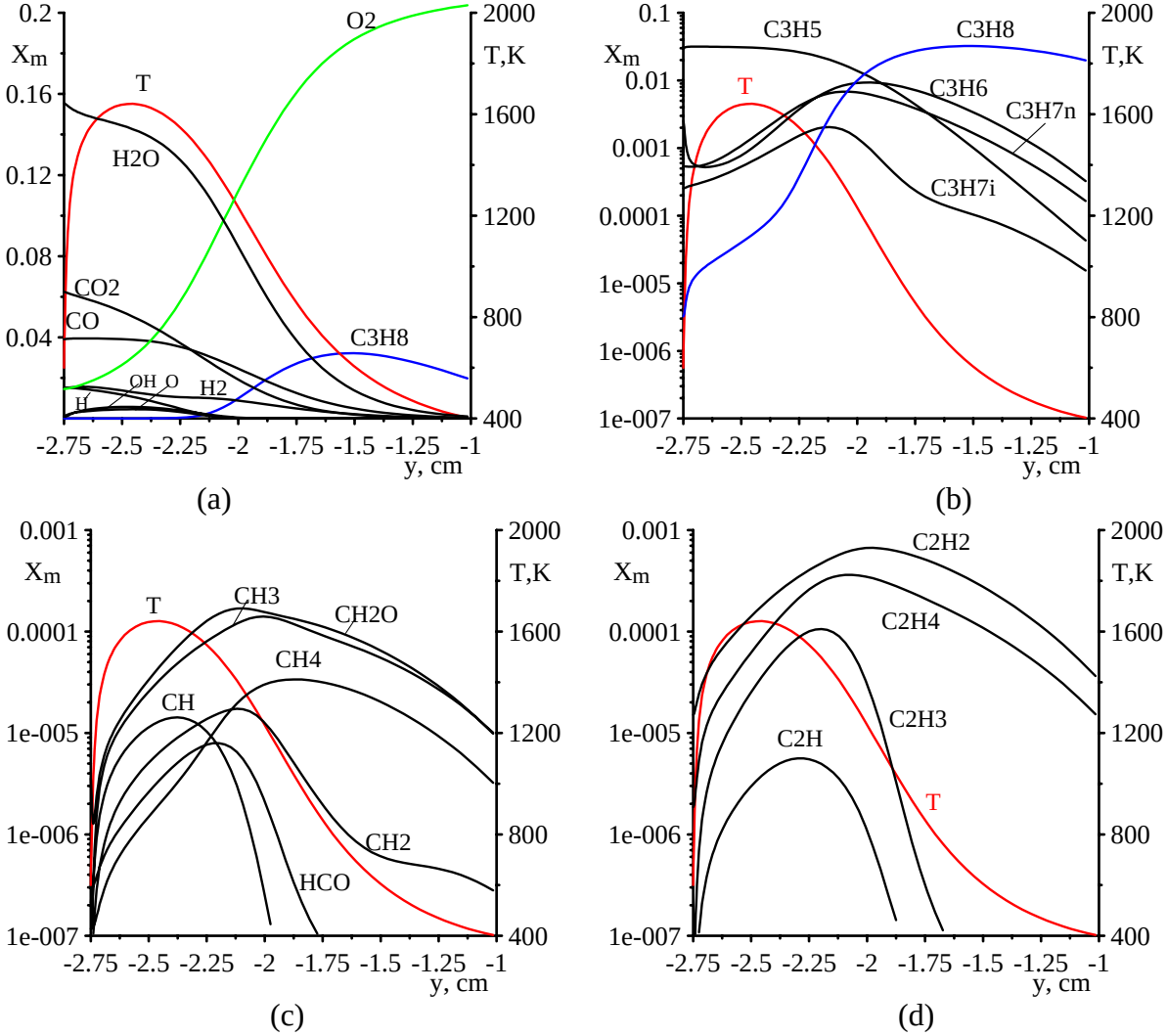

Fig. 2.11. Distributions of gas temperature and species mole fractions for section x=70.02 cm

Fig. 2.12 shows distributions of mole fractions of some components F_m in total mole flux in channel and distribution of combustion completeness C_B. It should be noted that value of C_B rises to the end of channel that is explained both above mentioned afterburning of CO and H2

and burning of propane/air mixture receiving from outer stream. To the end of combustor the burning completeness reaches of ~0.42.

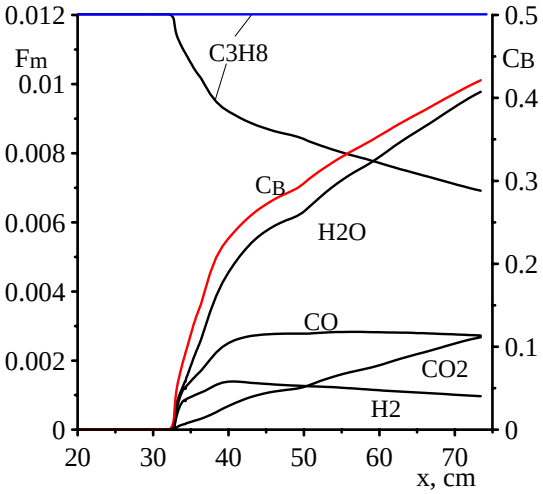

Fig. 2.12. Distributions of mole fractions F_m and combustion completeness C_B along channel for case calculation 6.

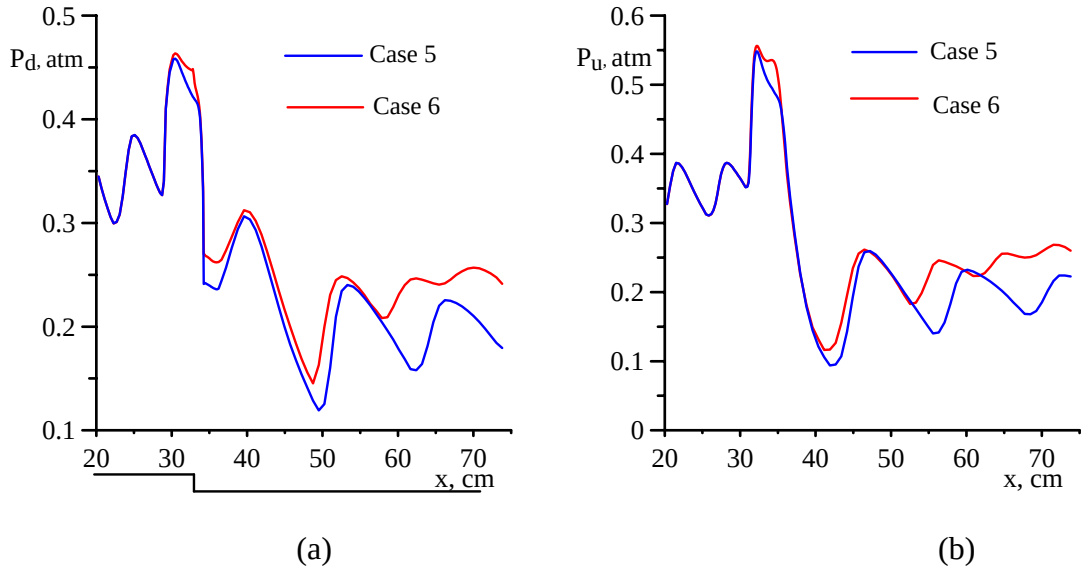

Fig. 2.13. Distributions of lower (a) and upper (b) walls pressure for cases 5 and 6.

Fig. 2.13 demonstrates effect of burning on distribution of pressure on lower (a) and upper (b) walls of the channel. It is seen that combustion has a marked effect on pressure distribution but one does not change a global structure of flow in channel.

Some results of calculations for this case are presented also on Figs. A.2.1-A.2.3 (see Illustrations).

Case 7, 8. In these cases heat source has triangular form and total power 4.0 kW/cm. Figs.2.14 – 2.15 show ignition data for these conditions. For comparison the similar data are given also for case 6. Changing heat source form leads to moving of ignition front on ~1 cm downstream. Peak of $T_{\max}$ increases on 500 K. Ignition starts also at $T_{\max} \approx 2000$ K. Afterburning and rise of C_B are saved. Value of C_B to combustor outlet is near 0.43.

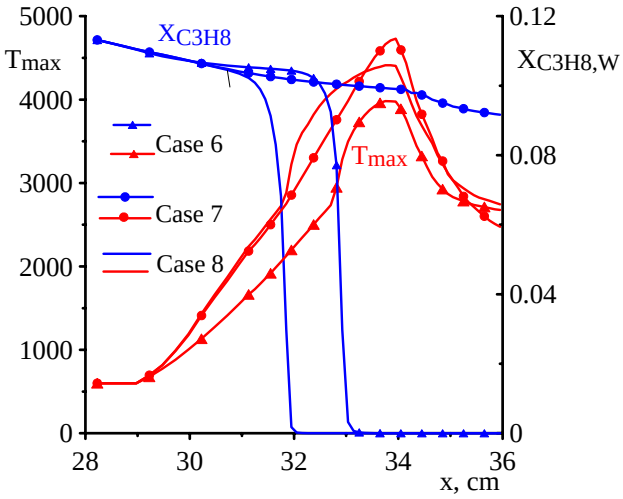

Fig. 2.14. Distributions of $T_{\max}$ and $X_{C3H8,W}$ in the heating region

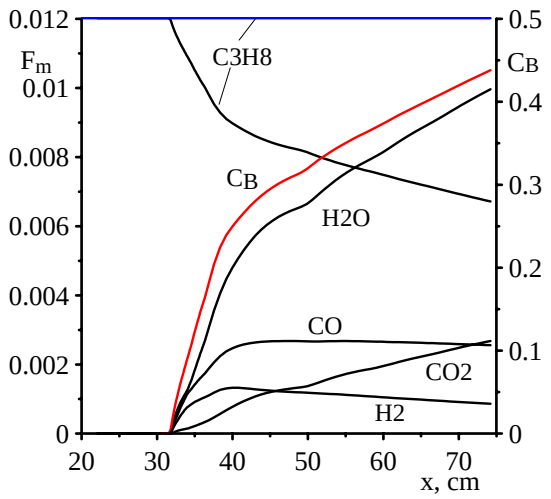

Fig.2.15. Distributions along channel mole fractions F_m and C_B

Case 9, 10. Location of the heating region is same as for cases 1, 2 but its height is increased to 0.5 cm. Heat deposition power is 4.0 kW/cm. Peak of $T_{\max}$ for frozen chemical model is near 1250 K and as it is seen from Figs.2.16, 2.17 the ignition of propane/air mixture for these conditions does not occurs.

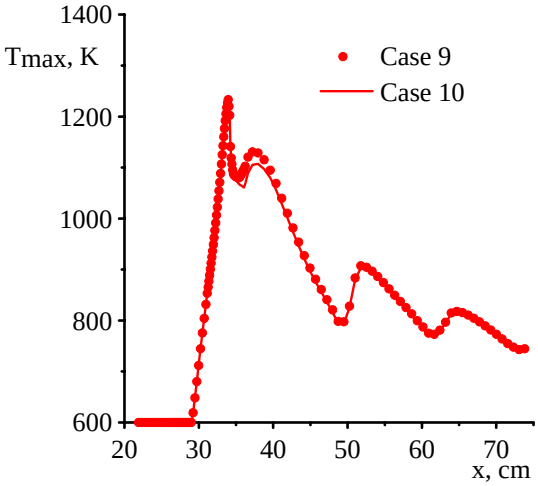

Fig. 2.16. Distribution of $T_{\max}$ along channel

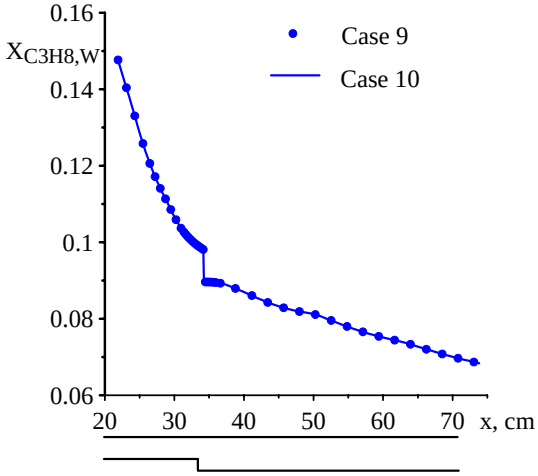

Fig.2.17. Distribution of $X_{C3H8,W}$ along channel

Case 11, 12. For these cases heat deposition region is rectangular: 28<x<33 cm, -1.25<y<-1.05 cm, heat power is 4.0 kW/cm. Heating region for these cases is moved upwind on 1 cm. For insulator of constant height steady state solution for case 12 does not establish. Therefore calculations have been performed for weakly expanding configuration of insulator. In computations the slope tangent of upper wall insulator was equal 0.01. Comparison of Figures 2.18, 2.19 with Figures 2.6, 2.12 shows that predicted for these cases results are similar to results obtained for case 5, 6.

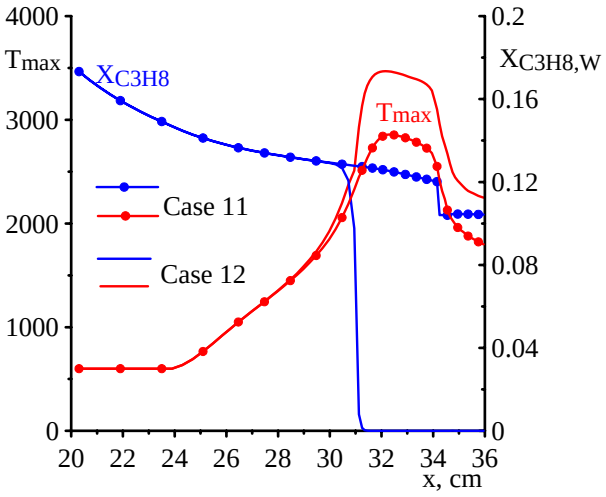

Fig. 2.18. Distributions of $T_{\max}$ and $X_{C3H8,W}$ in heating region for case 12

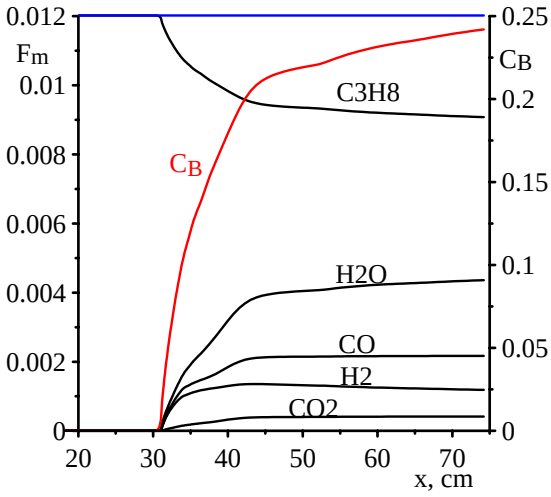

Fig.2.19. Distributions along channel mole fractions F_m and C_B for case 12.

Case 13. In this case it is used parameters of heating same as for case 6 and quasi-global chemical kinetic models with E_{qgl} = 30 and 40 kcal/mol. Effect of the chemical mechanism variation for these conditions is demonstrated by Figs.2.20, 2.21. It is seen that quasi-global model gives significantly more slow evolution of the ignition process. Ignition is started at lower gas temperature (near 1200 K) and is not finished to peak of $T_{\max}$ (~ 4000 K). Predicted by both quasi-global models results have not large distinction. Peak values of combustion completeness C_B are lower then value of C_B predicted by calculations using detailed chemical mechanism.

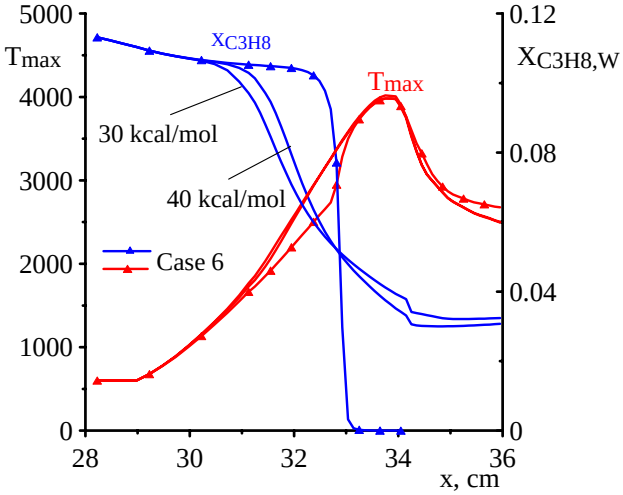

Fig. 2.20. Distributions of $T_{\max}$ and $X_{C3H8,W}$ in the heating region for case 13

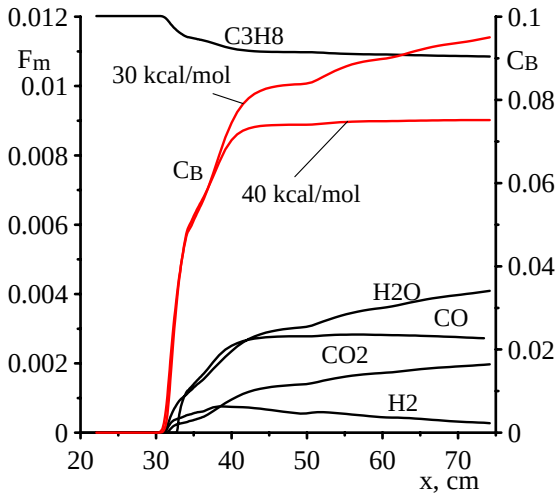

Fig. 2.21. Distributions along channel mole fractions F_m and combustion completeness C_B for case 13

2.2.4. Analysis of unsteady ignition of propane/air mixture for scheme 1 of propane injection and heat deposition.

Analysis of unsteady propane/air ignition and burning is performed for case 6 of heat source power, configuration and location. It is supposed that heat deposition is started by a jump at time t =0. Predicted time variation of maximal across duct temperature $T_{\max}$ and mole fractions of

some species are presented on Figs. 2.22 – 2.23. Indicated data are shown for 5 sections of the insulator and 7 sections of the combustor listed in Tables 2.2, 2.3.

Table 2.2. Coordinates of insulator sections.

N	1	2	3	4	5
x, cm	28.48	30.95	32.05	33.14	34.15

Table 2.3. Coordinates of combustor sections.

N	6	7	8	9	10	11	12
x, cm	35.15	36.23	43.42	51.02	58.62	66.22	73.82

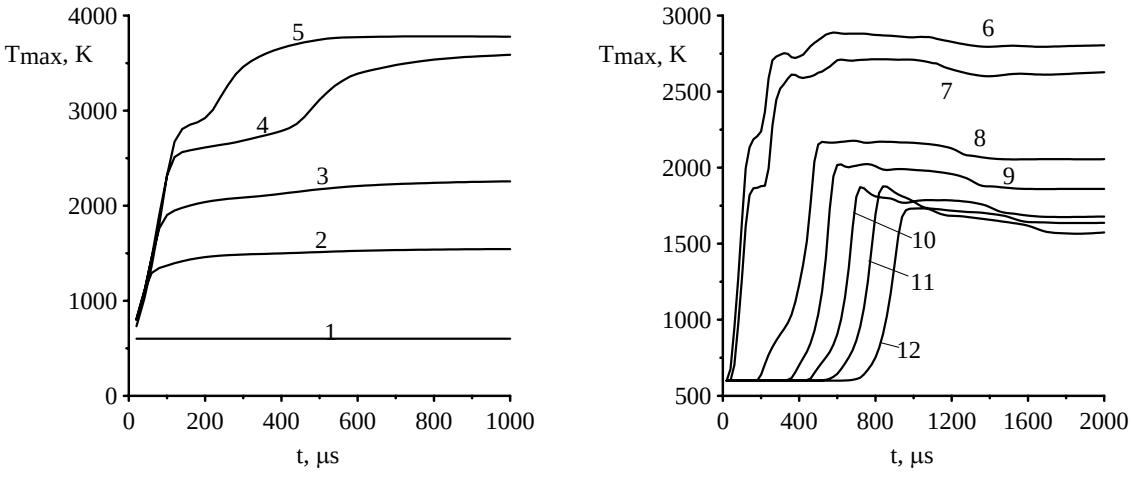

(a) (b)

Fig. 2.22. Time variation of maximal temperature $T_{\max}$ in the different sections of the channel.

Fig. 2.22 shows time distribution of $T_{\max}$. Section 1 is located outside of the heat deposition region and here temperature does not change. For sections 2 - 3 profile of temperature consists of initial part of fast gas heating and following slow exit on steady value. For section 4 and 5 time profile consists of the heating part, relatively short part of slow increasing, part of speedy increasing connected with fuel mixture ignition and asymptotic exit to steady value. Time length of gas heating for section 5 is near 120 μs that corresponds to averaged velocity in the heating region about 430 m/s. Time length of exit to steady solution is near 1000 μs. Ignition in section 5 occurs before then in section 4 because of lower temperature and more long induction period in this section.

Time profile of $T_{\max}$ for combustor sections also has frontal part and following slowly changing 'wake'. Front of gas heating moves coupled with the combustor flow at averaged velocity near 600 m/s. Amplitude of the front decreases from section to section because of heat transfer to cooled walls of the channel. Time of the frontal passage through section 12 is near 900 μs. Time length of flow establishing in whole channel is ~2000 μs.

Figs. 2.23 – 2.26 show time profiles of maximal across duct values of mole fractions of the propane combustion products CO, H2, CO2, H2O. It is seen that ignition in section 5 is started at t =100 μs, whereas in section 4 one is began on 200 μs after. Front of combustion products moves coupled with combustor flow. Diffusion of oxygen from outside stream causes afterburning of CO and H2 with forming of final combustion products CO2 and H2O.

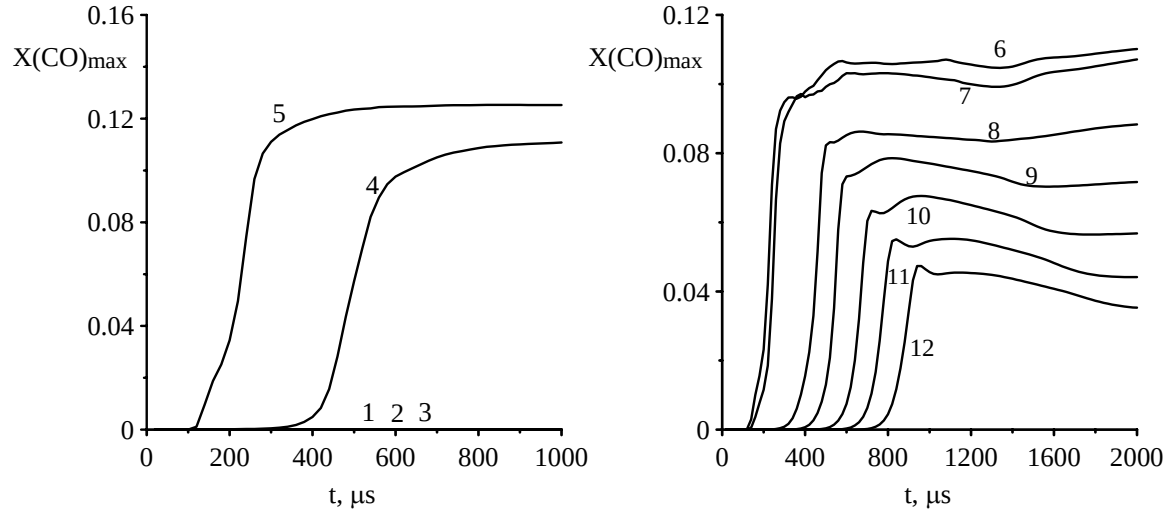

Fig. 2.23. Time profiles of maximal across duct value of CO mole fraction for specified sections

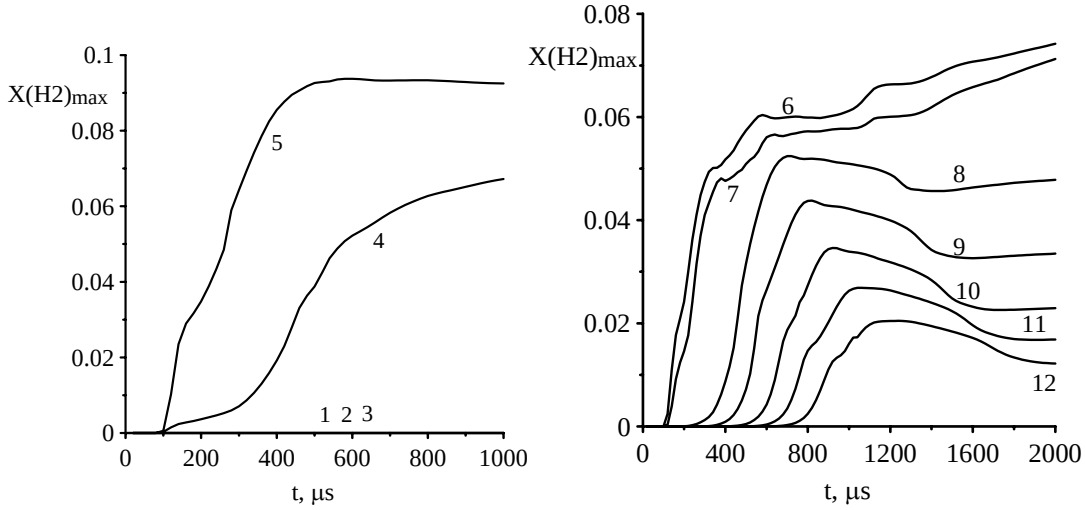

Fig. 2.24. Time profiles of maximal across duct value of H2 mole fraction for specified sections

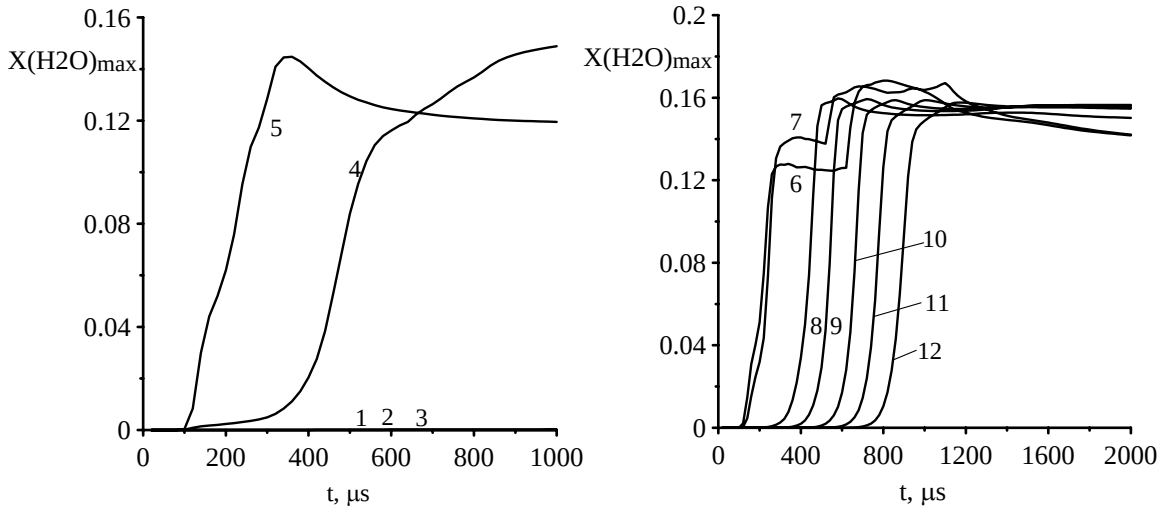

Fig. 2.25. Time profiles of maximal across duct value of H2O mole fraction for specified sections

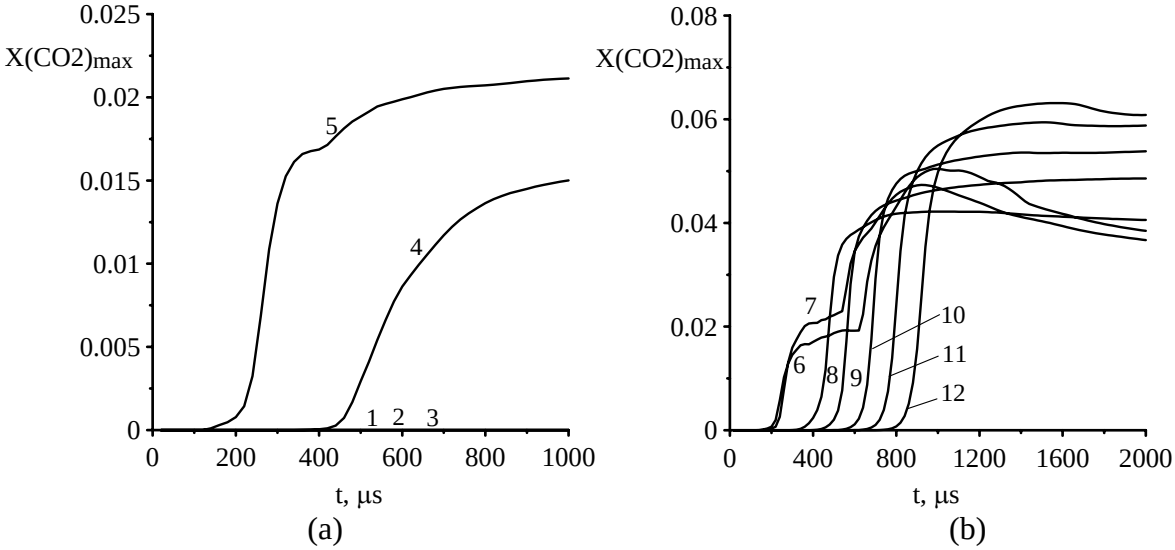

(a) (b)

Fig. 2.26. Time profiles of maximal across duct value of CO2 mole fraction for specified sections

Figs.2.27 – 2.29 present similar data for radicals H, O, CH4. Fronts of some species profiles and peak of CH4 profiles can be used for spectroscopic diagnostic of locations, speed of propagation and intensity of combustion in channel.

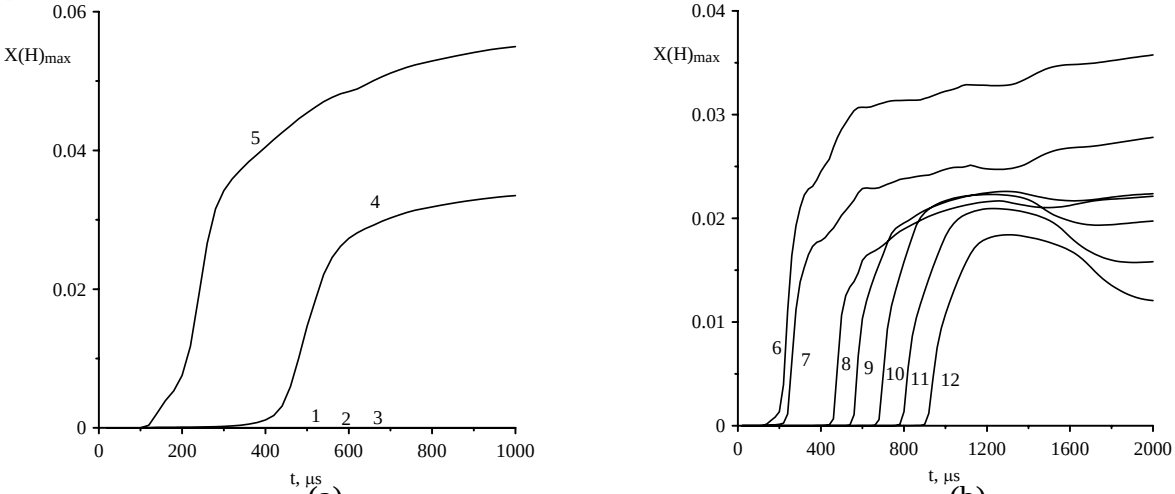

(a) (b)

Fig. 2.27. Time profiles of maximal across duct value of H mole fraction for specified sections

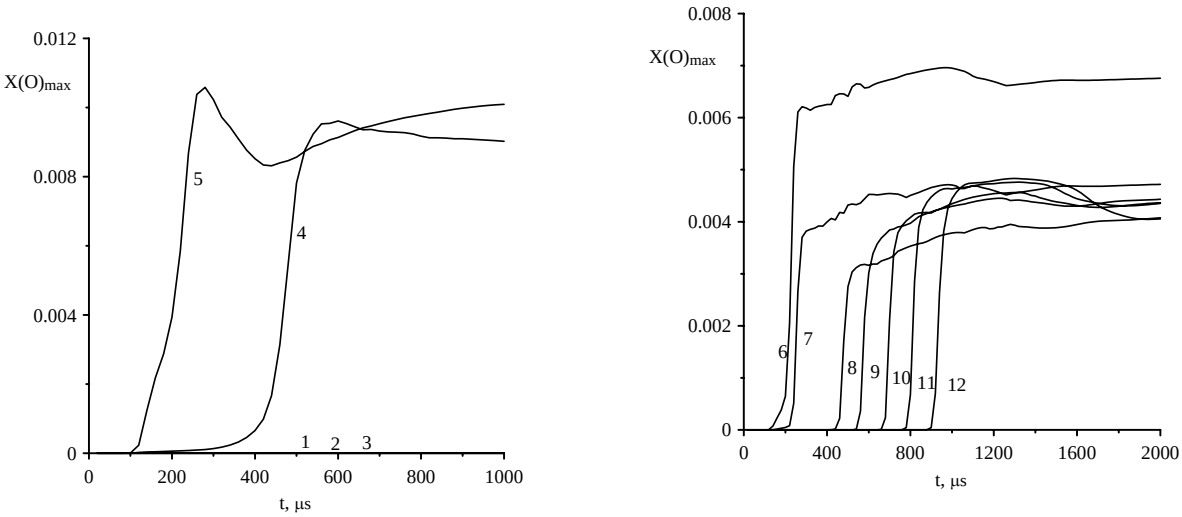

(a) (b)

Fig. 2.28. Time profiles of maximal across duct value of O mole fraction for specified sections

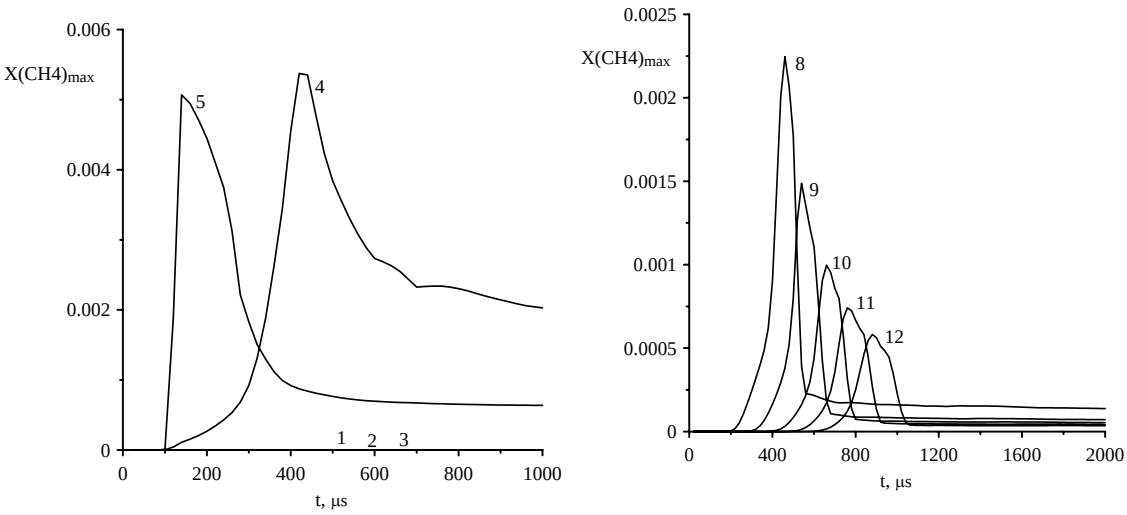

(a) (b)

Fig. 2.29. Time profiles of maximal across duct value of CH4 mole fraction for specified sections

As illustration on Figs. A.2.6-A.2.11 (see Illustrations) the time dynamics of gas temperature and combustion products mole fractions contours in the heat deposition region (indicated by red line) are presented.

For considered conditions the heat source is not only igniter but and a flame holder. After stopping of the heat deposition combustion is finished. Figs. 2.30-2.31 show time variation of T_{max} and $X(CO)_{max}$, $X(H2)_{max}$ and $X(H2O)_{max}$ for some sections of the channel from steady state regime with gas heating to steady state regime without heating. It is supposed that heat deposition is finished by a jump at time t =0. It is seen that after stopping of the heat deposition burning of propane/air mixture is finished as in the insulator so in the combustor but relaxation time for combustor sections is greater than for insulator sections.

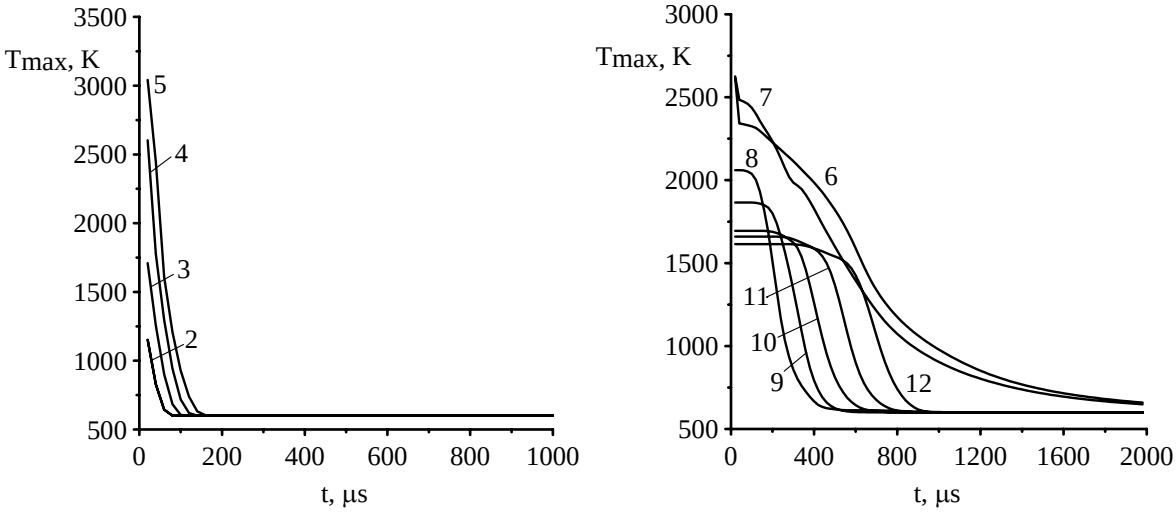

(a) (b)

Fig.2.30. Time variation of maximal temperature T_{max} in the different sections of the combustor after stopping of heat deposition.

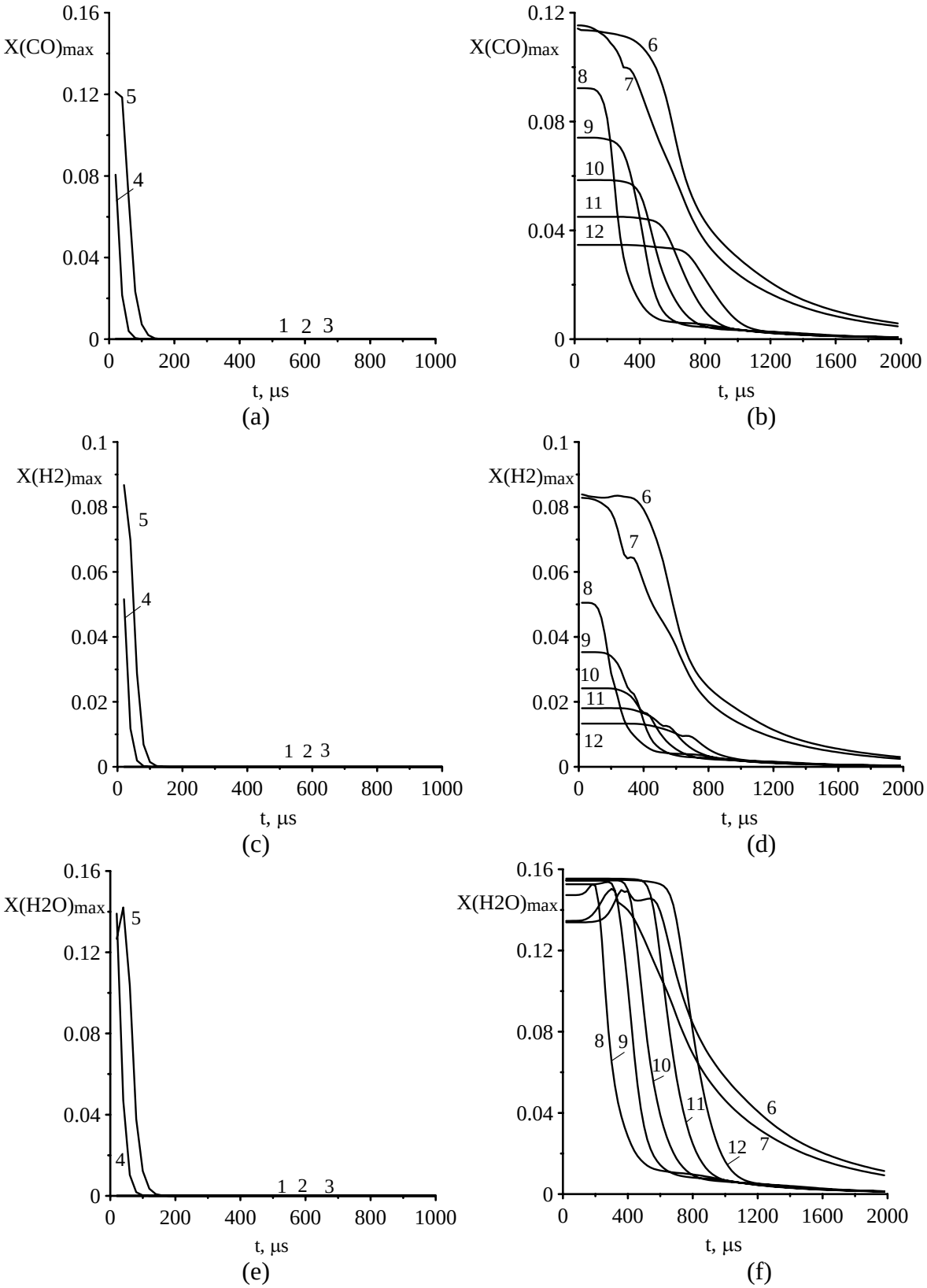

Fig.2.31. Time variation of peak mole fraction of CO (a,b), H2(c,d) and H2O (e,f) in the different sections of combustor after stopping of the heat deposition

2.2.5. Analysis of steady state propane/air mixture ignition for scheme 2 of heat deposition.

This item contains analysis of steady state propane/air mixture ignition and burning in the supersonic channel for cases when heat source modeling electrical discharge is placed into separated region after the back step of the channel. Heat is supplied with steady total power P_d uniformly distributed into rectangular region $x_{qs} < x < x_{qf}$, $y_{qs} < y < y_{qf}$ located near lower wall of combustor, near surface of the back step or inside of separated region after step. Calculations have been performed for frozen and detailed chemical mechanisms. All considered cases of calculations are listed in Table 2.4.

Table 2.4. Cases of calculations.

Case	x_{qs}, cm	x_{qf}, cm	y_{qs}, cm	y_{qf}, cm	P_d, kW/cm	T_{max}, K
1	36	38	-2.75	-2.55	0.5	2497
2	36	38	-2.75	-2.55	1.0	6280
3	35	37	-2.75	-2.55	0.5	4480
4	35	37	-2.75	-2.55	1.0	9480
5	37	39	-2.75	-2.55	0.5	1820
6	37	39	-2.75	-2.55	1.	4030
7	34.2	34.7	-2.7	-1.3	0.5	5408
8	34.2	34.7	-2.7	-1.3	0.75	9850
9	36	38	-2.3	-2.1	0.5	2237
10	36	38	-2.3	-2.1	1.0	7026

Fig. 2.32 shows the pressure contours and streamlines in the separated region after step predicted for case without heat supply. It is seen that stagnation point on x-line is located at x ≈ 38.8 cm so length of the separated region is near 4.6 cm. Center of a separated vortex is located at x ≈ 36cm, y ≈ -2.1 cm. Pressure level in the separated region is 0.15 – 0.20 atm.

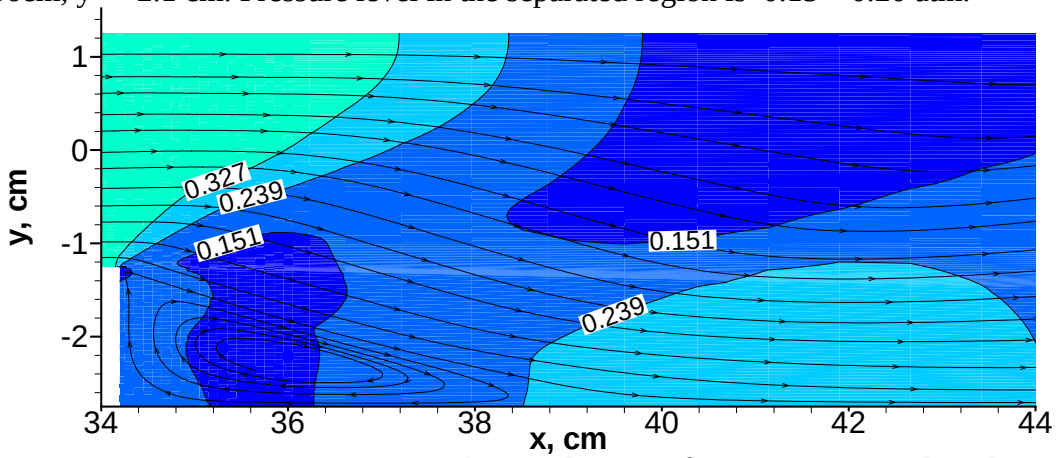

Fig.2.32. Pressure (atm) contours and streamlines in after step region without heat supply

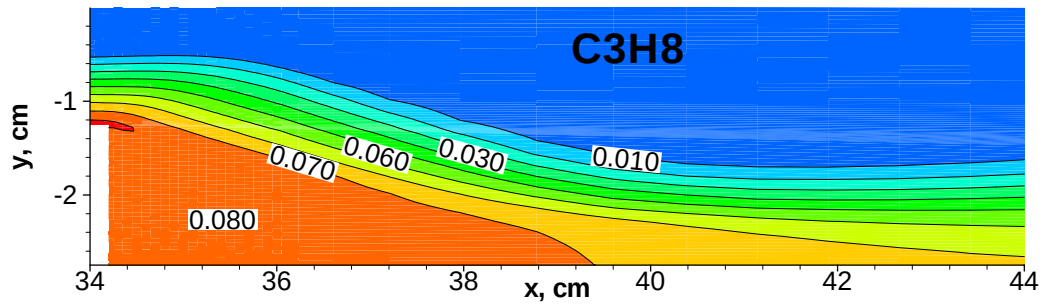

Fig.2.33. C_3H_8 mole fraction contours in after step region without heat supply

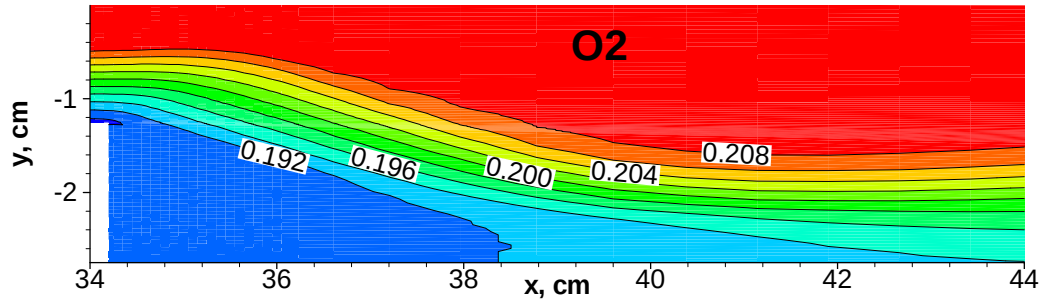

Fig.2.34. O_2 mole fraction contours in after step region without heat supply

Figs. 2.33 – 2.34 present contours of propane and oxygen mole fraction for the same conditions. It is seen from these Figures that in separated region rich fuel mixture is formed. Table 2.4 contains local peaks of temperature predicted for considered cases using chemically frozen model. Table data show that heat supply even relatively small power (~1 kW/cm) into separated region leads to a local increasing of temperature sufficient by estimations for propane/air mixture ignition. These estimations are justified by results of calculations for chemically nonequilibrium models. Below it is given short analysis of results obtained for listed in Table 2.1 heat sources location and power.

Cases 1, 2. In these cases heat is supplied near lower wall of combustor into rectangular region with length of 2 cm, height of 0.2 cm and x-coordinate of centre equal to 37 cm. Fig. 2.35 .shows temperature contours for P_d=0.5 kW/cm (a) and P_d=1.0 kW/cm (b). On this Figure and on the next similar Figures region of heat deposition is indicated by a black frame. For both cases fuel mixture in separated region is ignited. Peaks temperature for these cases are reached near left (down stream) end of the heating region and amount 3723 and 4574 K accordingly. For comparison, peak values of temperature predicted for chemically frozen gas phase model are 2427 and 6280 K. Higher temperature for frozen model in case 2 is explained by partial dissociation of some mixture components in the peak temperature region.

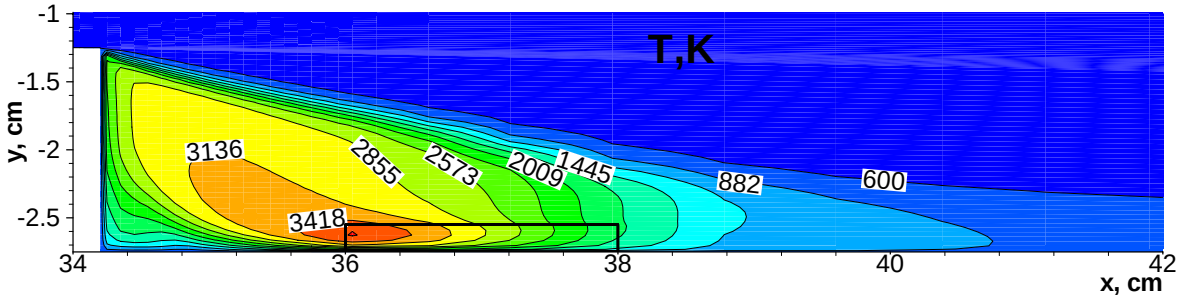

(a)

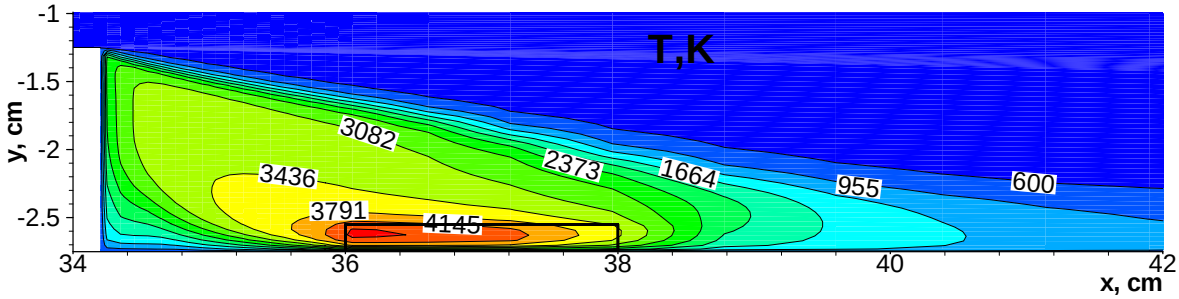

(b)

Fig.2.35. Gas temperature contours in after step region for case 1 (a) and case 2 (b).

Fig. 2.36 presents distributions of propane mole fraction in after step region predicted for cases 1 and 2.

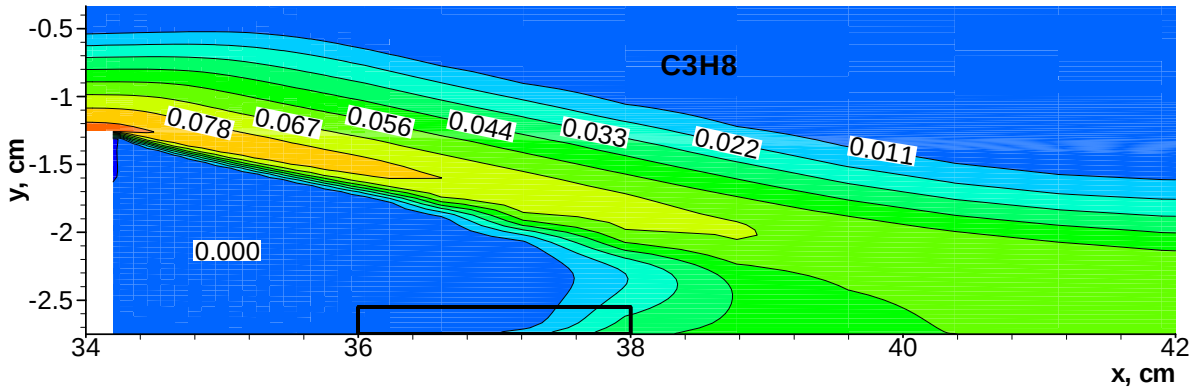

(a)

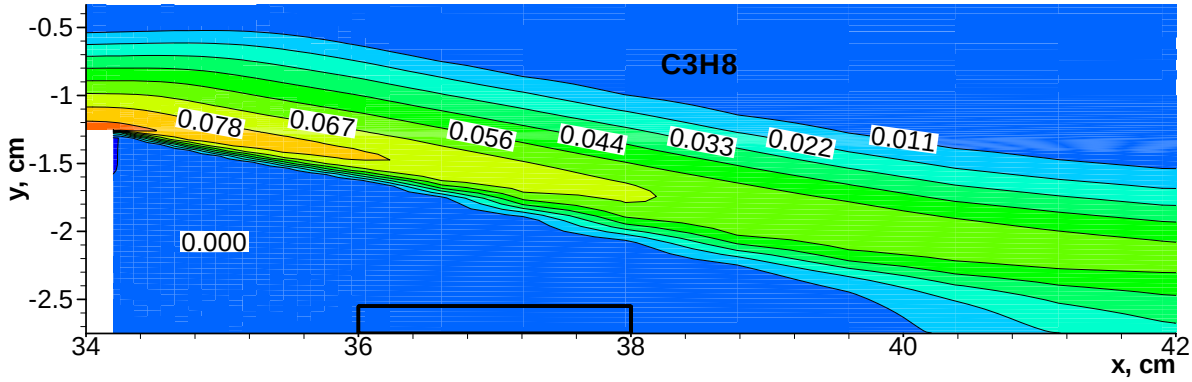

(b)

Fig.2.36. Propane mole fraction in after step region for case 1 (a) and case 2(b)

Fig. 2.37 presents distributions of combustion products CO (a),CO2 (b), H2 (c), H2O (d), H(e) and (O) mole fractions in after step region predicted for Pd=1kW/cm (case 2)

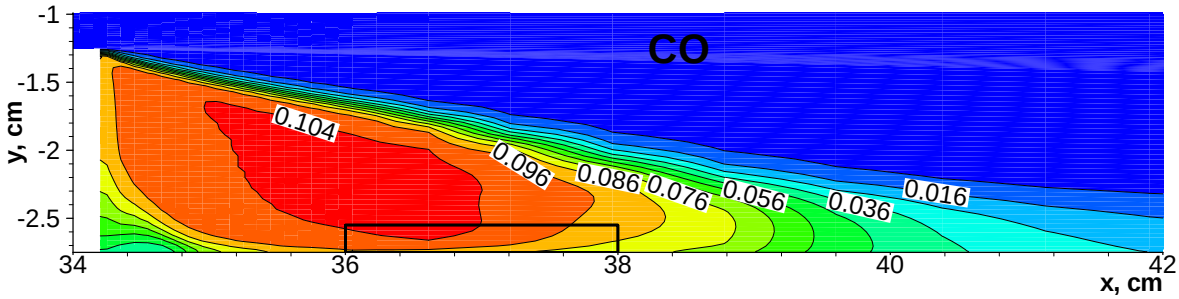

(a)

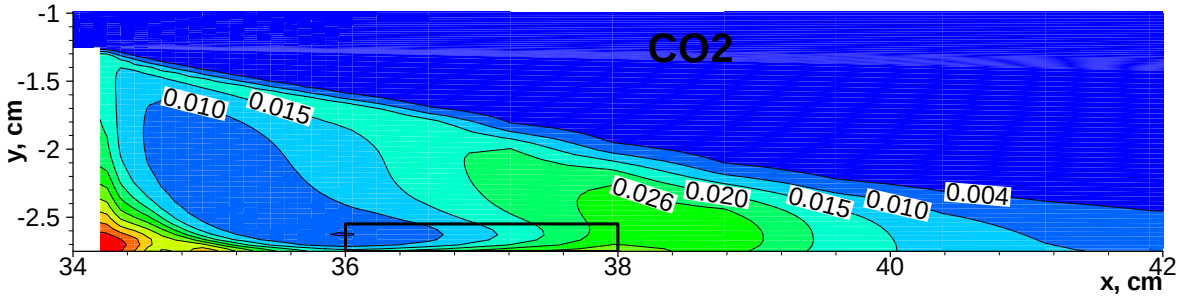

(b)

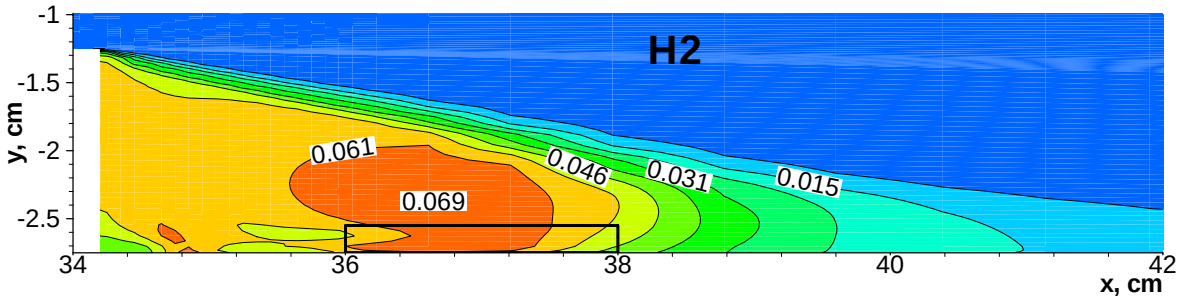

(c)

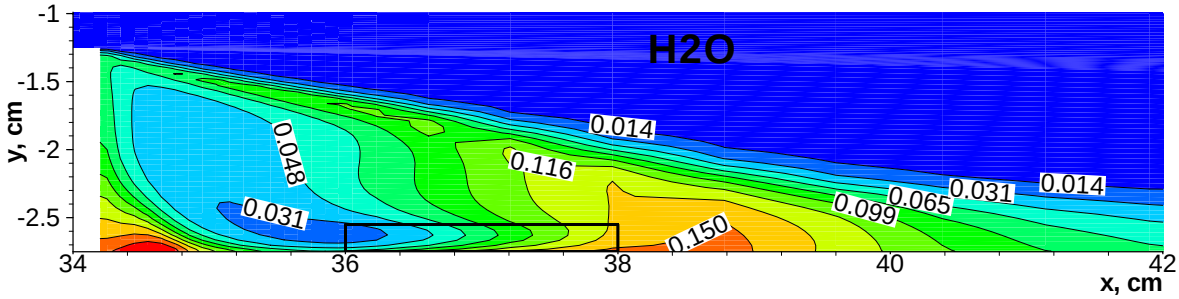

(d)

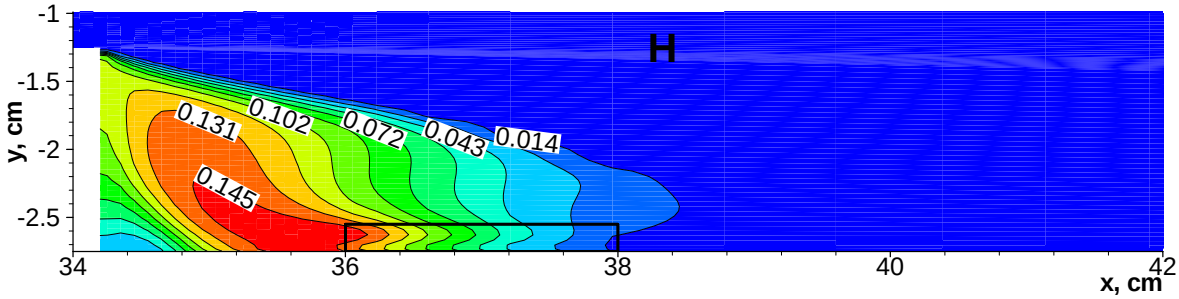

(e)

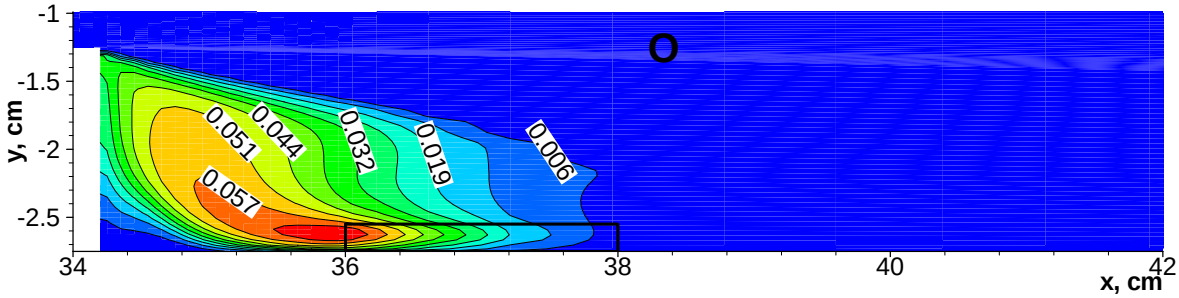

(f)

Fig.2.37. Contours of species mole fraction in after step region for case 2.

Analysis of presented data shows that zone of intensive combustion is formed in a mixing layer located near discriminating stream-line. Fuel mixture diffuses across this layer from internal flow and partially burns off. Unreacted components of fuel mixture and products of combustion are transported down stream into both separated region and boundary layer forming on lower wall of combustor after stream attachment. In separated region propane fully burns out. Separated region is filled up by final and intermediate combustion products. In the temperature peak region some species partially dissociate. In the attached boundary layer also there is after-burning of molecular species but rate of these processes is small.

Fig. 2.38 shows distribution along combustor of mole fractions F_i of total mole flux through duct for combustion products and distribution of burning completeness C_B. It is seen that

propane burns off mainly in separated region. There is also some afterburning in the boundary layer. Value of burning completeness C_B increases with increase of heating power. At the combustor outlet value of C_B increases from 0.06 for P_d = 0.5 kW/cm to 0.12 for P_d =1 kW/cm.

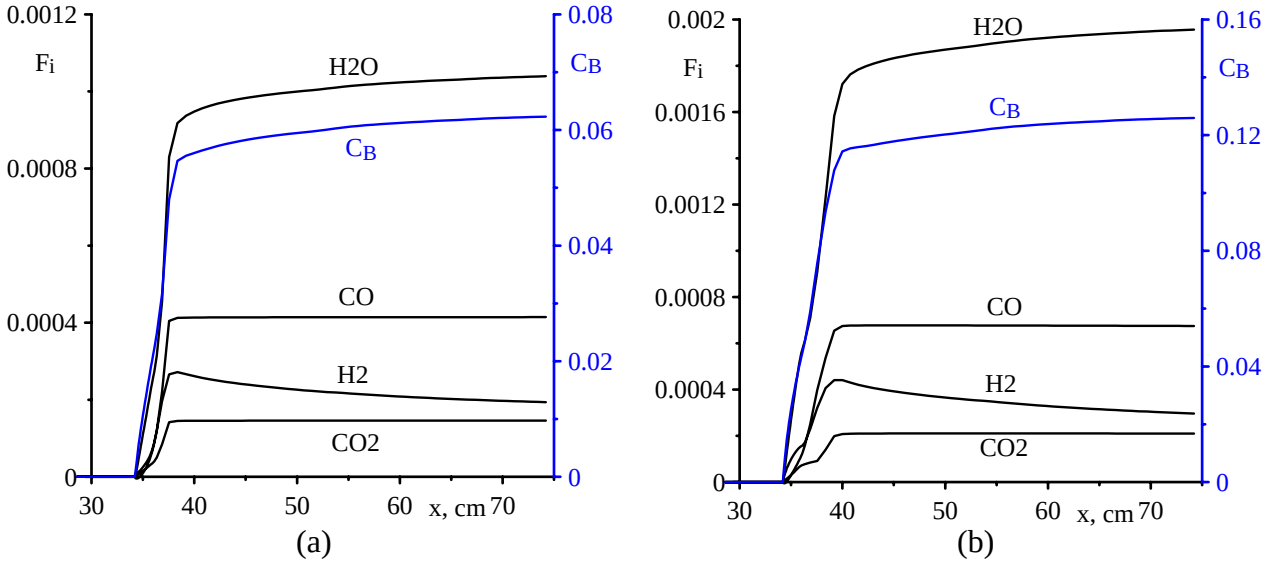

Fig.2.38. Distributions along channel of flux mole fraction F_i and burning completeness C_B for case 1 (a) and case 2 (b)

Cases 3,4. In these cases heat source is moved on 1 cm to the left relatively cases 1, 2. Fig. 2.39 shows temperature contours for P_d =0.5 kW/cm (a) and P_d =1.0 kW/cm (b) and Fig. 2.40 shows propane mole fraction contours for the same heat deposition powers. These Figures show that for both cases fuel mixture in separated region is ignited. Peaks temperature for these cases are also reached near left (down stream) end of the heating region and amount 4128 and 6131 K accordingly. Peak values of temperature predicted for chemically frozen gas phase model are 4480 and 9480 K.

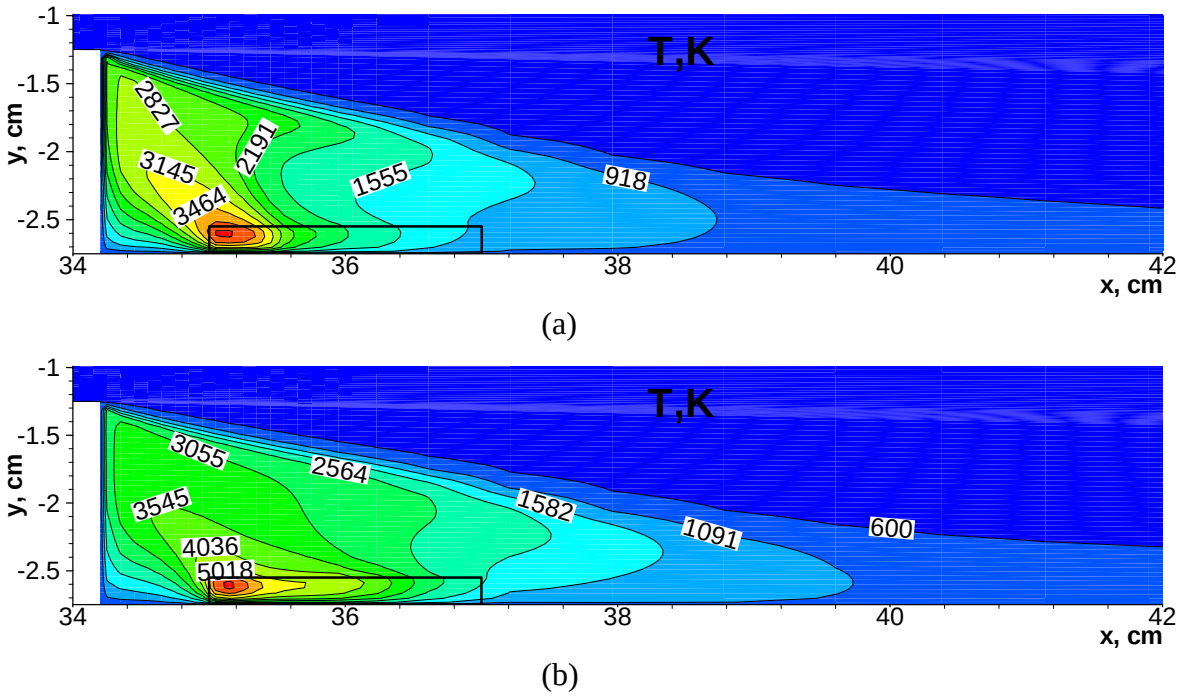

Fig.2.39. Temperature contours in after step region for P_d =0.5 kW/cm (a) and P_d =1.0 kW/cm

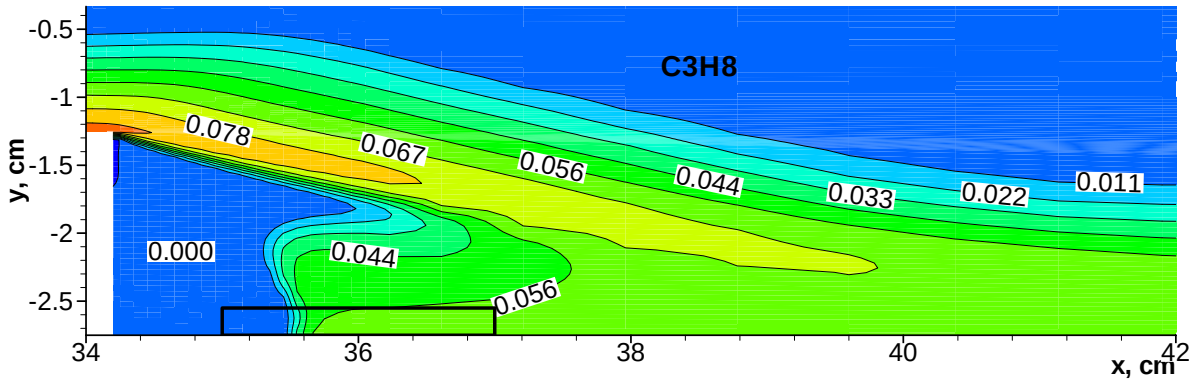

(a)

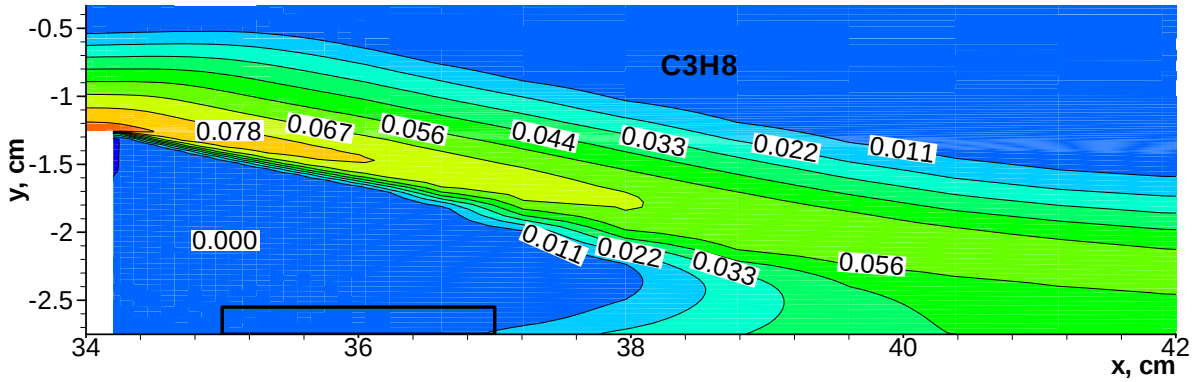

(b)

Fig.2.40. Propane mole fraction contours in after step region for P_d =0.5 kW/cm (a) and P_d =1.0 kW/cm (b)

Fig. 2.41 shows distributions along combustor of the total flux mole fractions F_i and burning completeness C_B. Behavior of these curves is similar to presented on Fig. 2.38 but level of the burning completeness some below.

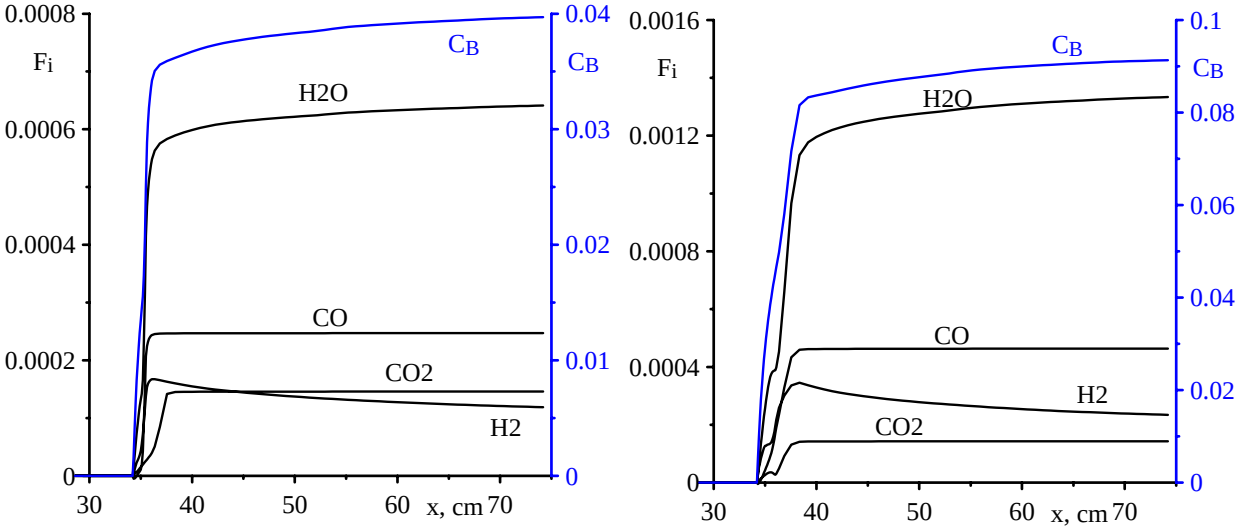

Fig.2.41. Distributions along channel of flux mole fraction F_i and burning completeness C_B for case 3 (a) and case 4(b).

Cases 5, 6. In these cases heat source is moved on 1 cm to the right relatively cases 1, 2. Fig. 2.42 shows temperature contours for P_d =0.5 kW/cm (a) and P_d =1.0 kW/cm (b) and Fig. 2.43 shows propane mole fraction contours for the same heat deposition powers. Fig. 2.43,a demonstrates that for this heat source location fuel mixture in separated region at P_d =0.5 kW/cm is not ignite. Predicted peak temperature in the separated region is 1820 K for both frozen and nonequilibrium chemical models. At P_d =1.0 kW/cm (case 6) mixture is ignited. Peak temperature for chemically frozen model is 4030 K while for reacting model one is 4365K. Propane mole fraction distribution in separated region for this case is similar to it for case 2 (compare Fig.2.36,b and Fig.2.43,b)

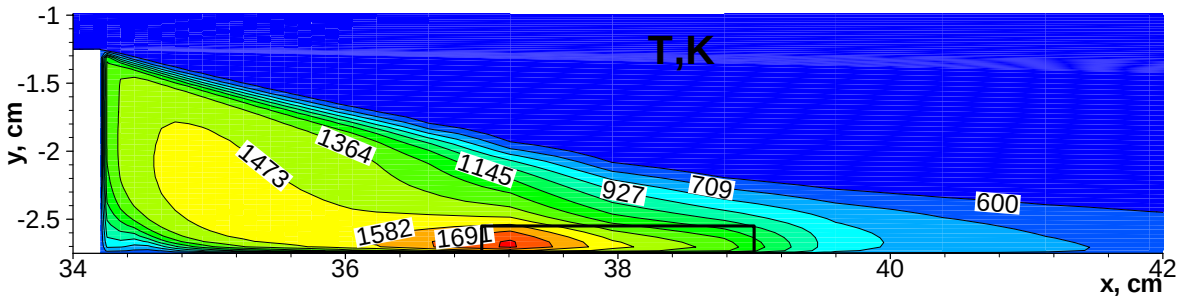

(a)

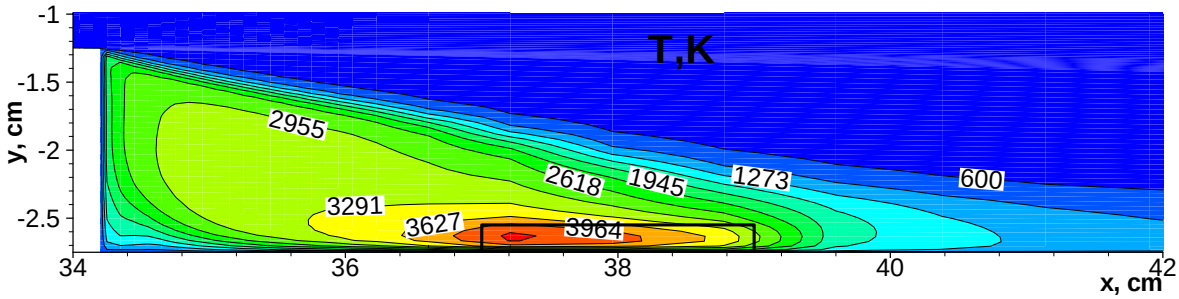

(b)

Fig.2.42. Temperature contours in after step region for case 5 (a) and case 6 (b)

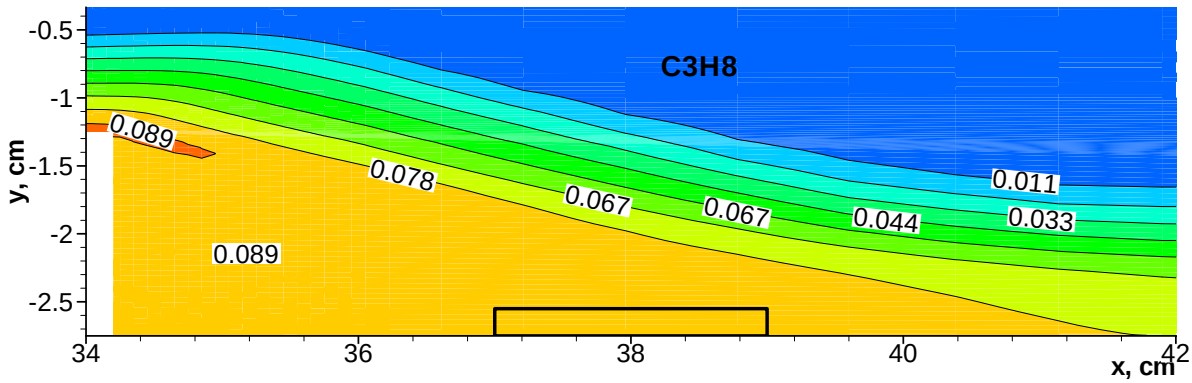

(a)

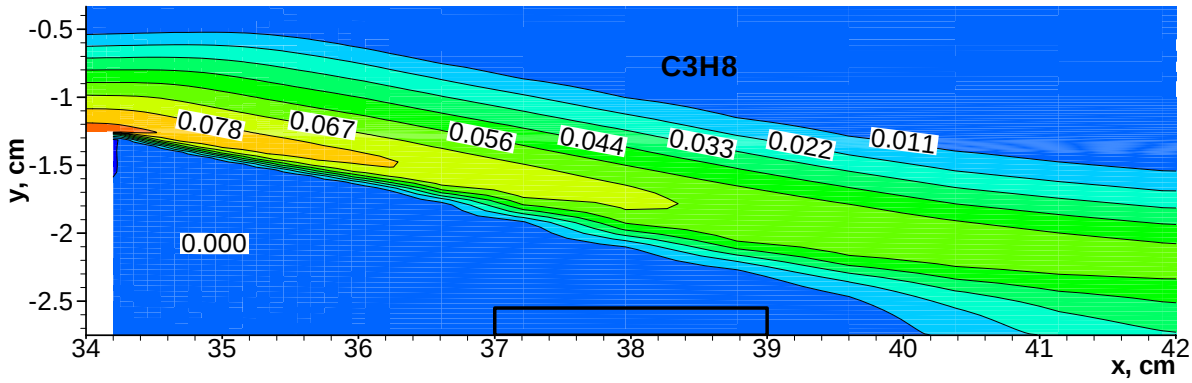

(b)

Fig.2.43. Propane mole fraction contours in after step region for case 5 (a) and case 6 (b)

Burning completeness for case 6 also is closed to it for case 2 (Fig. 2.44). Value of C_B at combustor outlet is near 0.12.

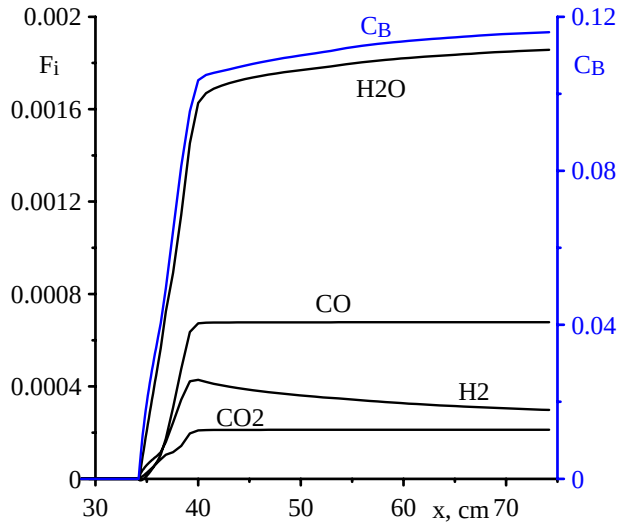

Fig.2.44. Flux mole fraction F_i and burning completeness C_B distributions along channel for case 6.

Cases 7, 8. In these cases heat source is placed near step surface. Rectangular heat deposition region has width of 0.5 cm, length of 1.4 cm and a center coordinates x=34.75 cm, y=-2.0cm. For case 7 heating power is 0.5 kW/cm, while for case 8 P_d = 0.75 kW/cm. For grater heating power steady state solution was not found. Fig. 2.45 presents temperature contours for P_d =0.5 kW/cm (a) and P_d =0.75 kW/cm (b). Fig. 2.46 shows propane mole fraction contours for the same heat deposition powers. For both cases fuel mixture in separated region is ignited. Peaks temperature for these cases are reached near upper end of the heating region and amount 4129 and 6118 K accordingly. Peak values of temperature predicted for chemically frozen gas phase model are 5408 and 9850 K.

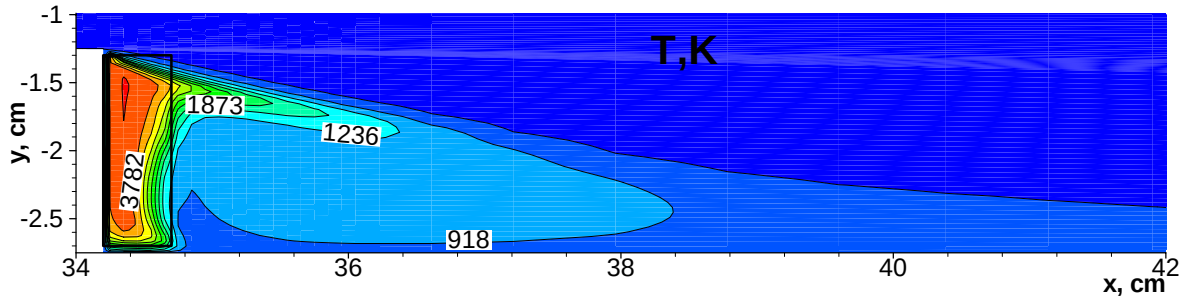

(a)

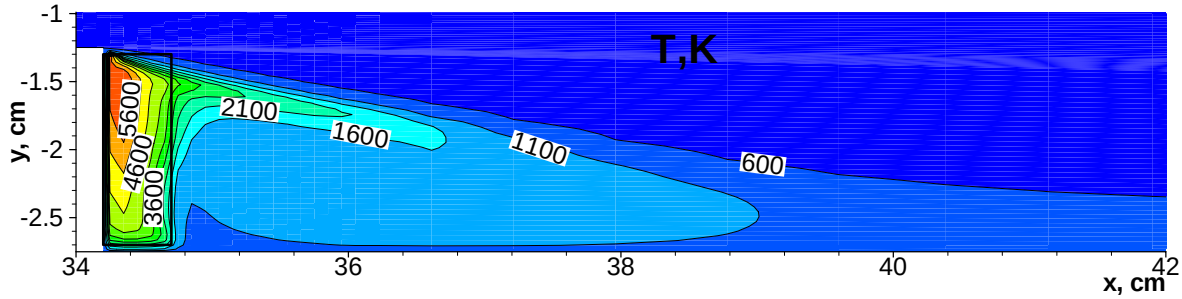

(b)

Fig. 2.45. Temperature contours in after step region for case 7 (a) and case 8 (b)

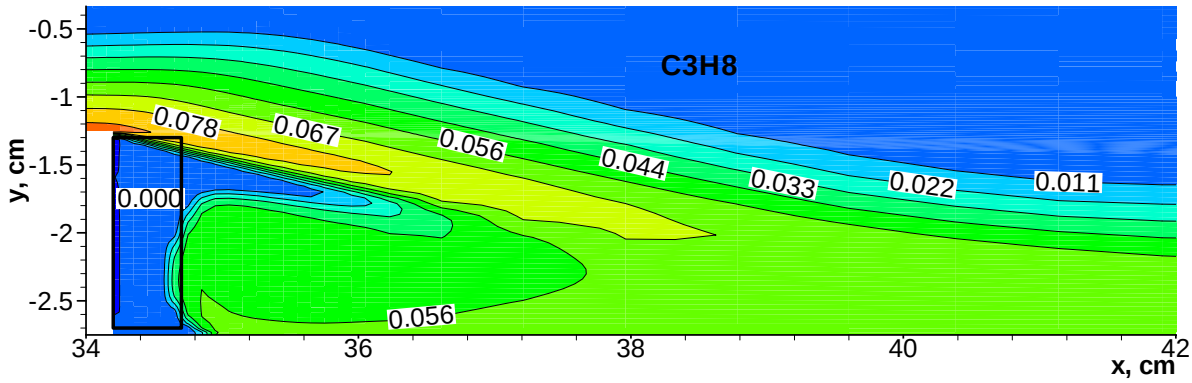

(a)

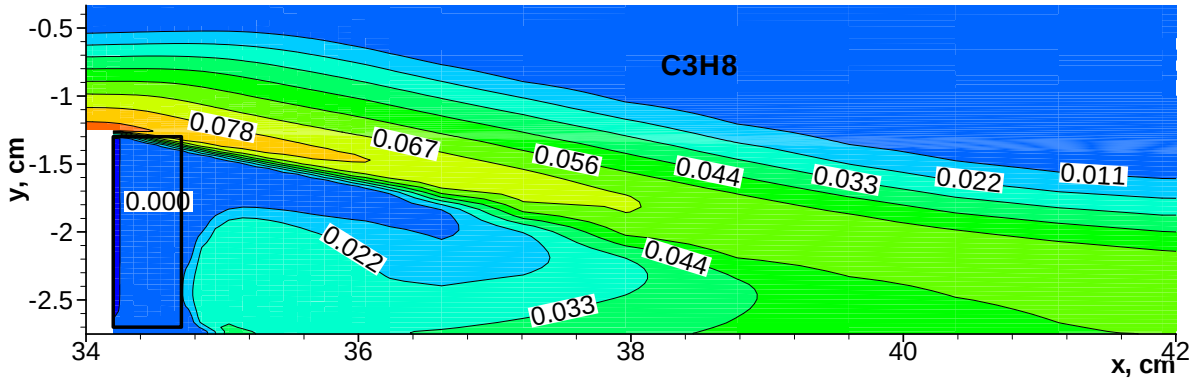

(b)

Fig. 2.46. Propane mole fraction in after step region for case 7 (a) and case 8 (b)

Fig. 2.47 shows distributions along channel of the total flux mole fraction F_i and burning completeness C_B for case 7 (a) and case 8 (b). It is seen that value of C_B in these cases does not exceed 0.08.

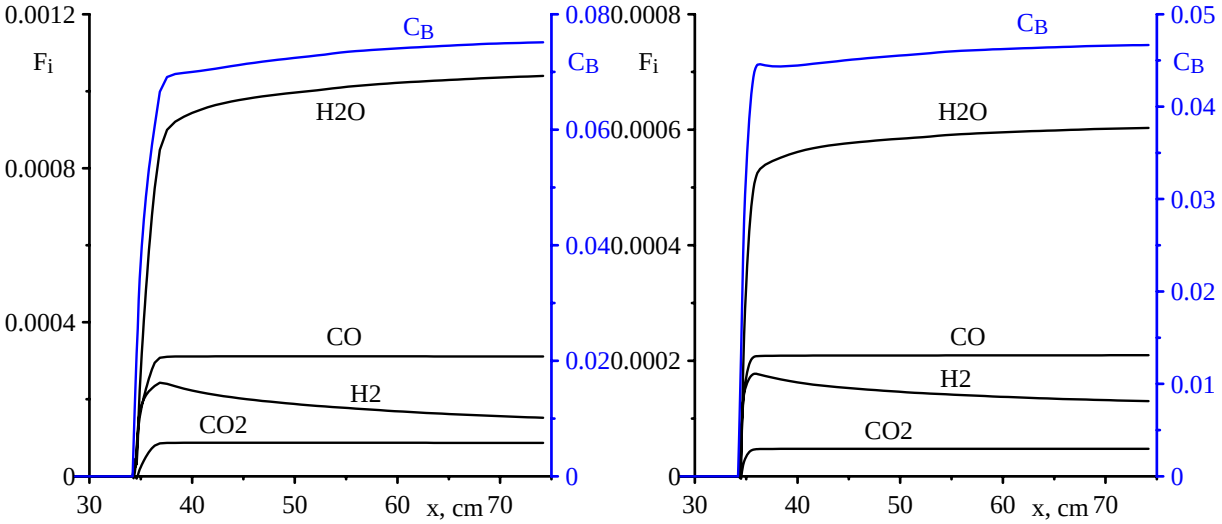

Fig.2.47. Distributions along channel of flux mole fraction F_i and burning completeness C_B for case 7 (a) and case 8 (b).

Cases 9, 10. In these cases heat source is placed in center of the separated region. This location of heat source simulates volumetric electrical discharges. Rectangular heat deposition region has length (along x-coordinates) of 2 cm, height of 0.2 cm and coordinates of center x=37 cm, y = -2.2 cm. Fig. 2.48 shows temperature contours for P_d =0.5 kW/cm (a) and P_d =1.0 kW/cm (b). Propane mole fraction contours is shown on Fig. 2.49 for the same heat deposition powers. It is seen that ignition of the fuel mixture in separated region is occurred only for P_d =1.0 kW/cm (case 10). Peaks temperature for both cases are reached near left end of the heating region and amount 2247 and 5052 K accordingly. Peak values of temperature predicted for chemically frozen gas phase model are 2237 and 7026 K. Some results of calculations for this case are presented also on Figs. A.2.4-A.2.5 (see Illustrations)

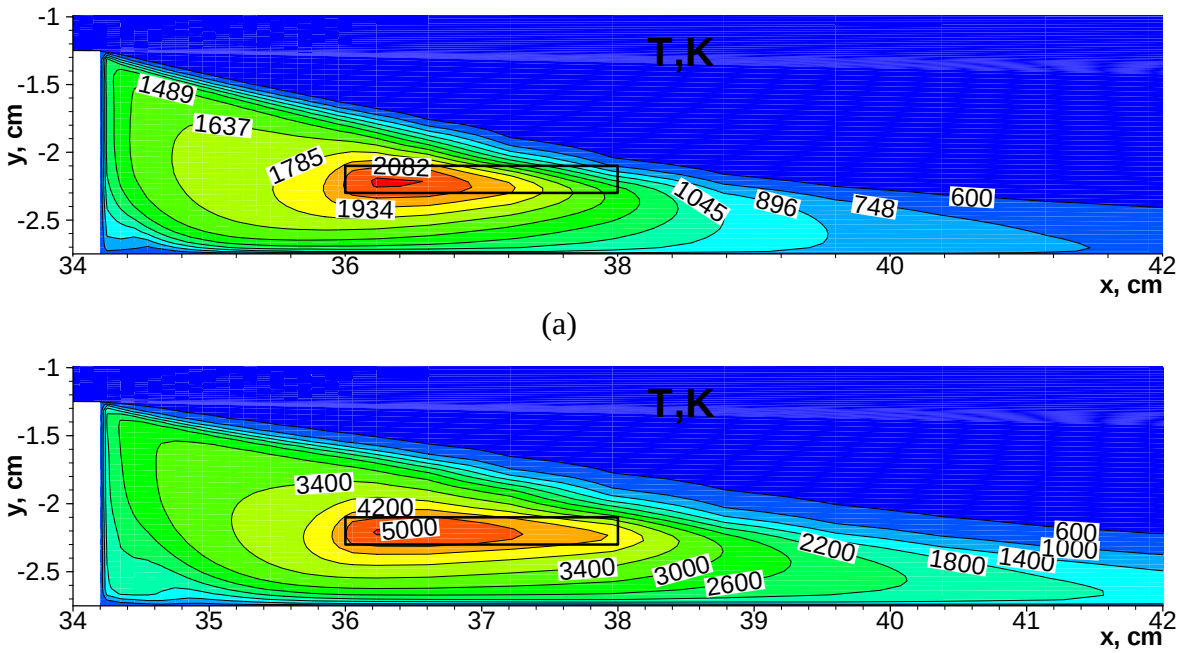

(b)

Fig. 2.48. Temperature contours in after step region for case 9 (a) and case 10 (b)

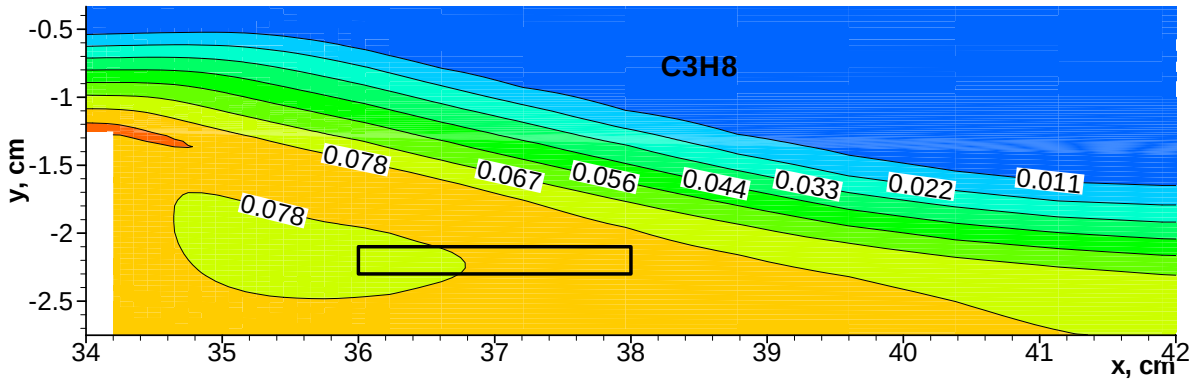

(a

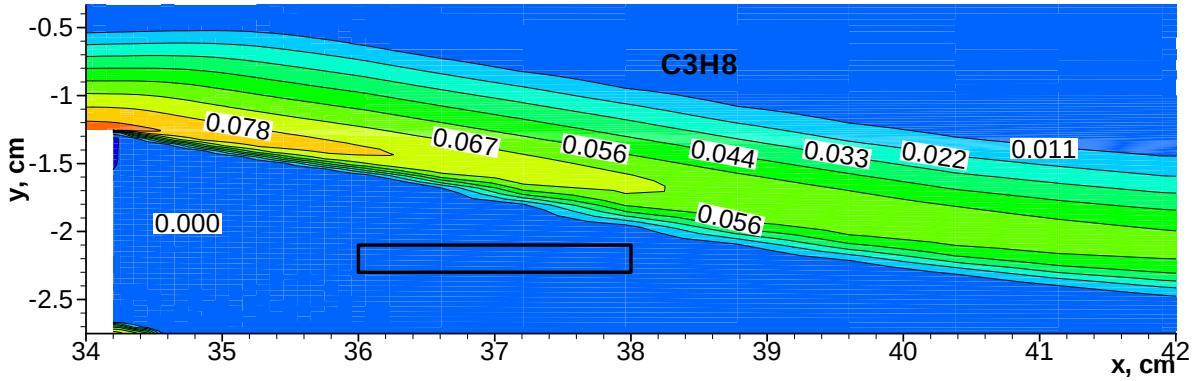

(b)

Fig.2.49. Propane mole fractions in after step region for case 9 (a) and case 10 (b)

Distributions along combustor of the total flux mole fractions F_i and burning completeness C_B predicted for case 10 is shown on Fig. 2.50. Presented data show that in this case the most burning completeness is reached relatively other considered cases. For this case value of C_B at the combustor outlet is near 0.2.

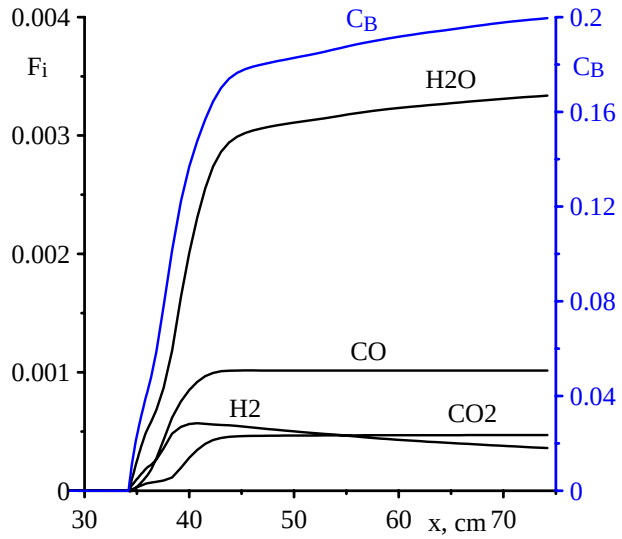

Fig 2.50. Distributions along channel of the total flux mole fraction F_i and burning completeness C_B for case 10.

2.2.6. Analysis of unsteady ignition of propane/air mixture for scheme 2 of propane injection and heat deposition.

Computations of unsteady propane/air ignition and burning is performed for case 10 of the heat source power, configuration and location. It is supposed that heat deposition is started by a jump at time t =0. Predicted time variation of maximal across duct temperature T_{max} and mole fractions of CO are presented on Fig. 2.51. Indicated data are shown for 7 sections of the combustor listed in Tables 2.3. Section 6 is located at once after step, section 7 cuts left part of the heating region. Other sections is located after separated region.

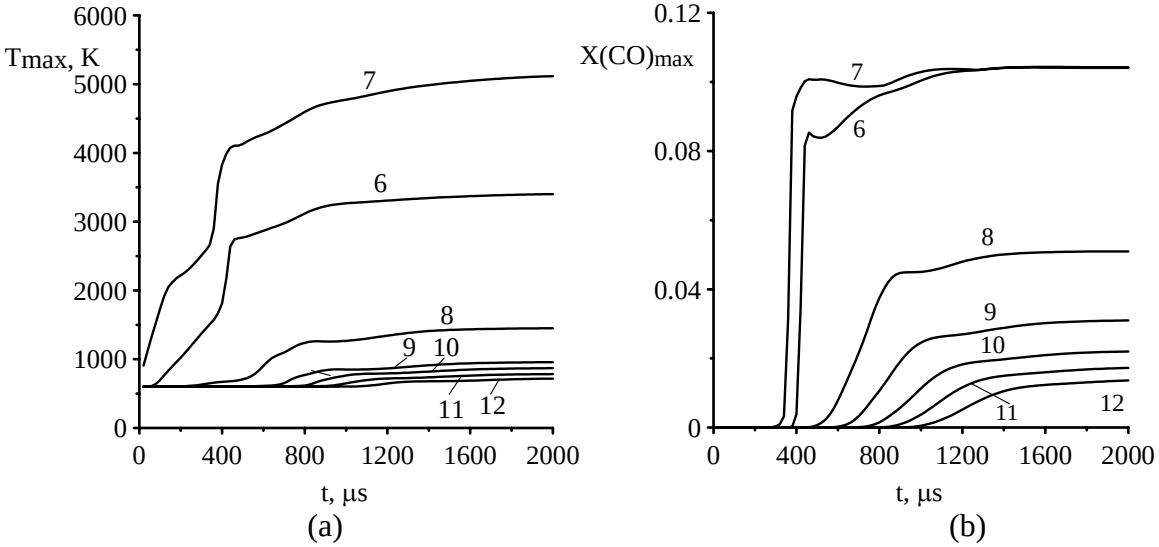

Fig.2.51. Time variation of maximal temperature T_{max} (a) and peak of mole fraction CO (b) in the different sections of the combustor after starting of heat deposition.

Analysis of presented data shows that for considered conditions ignition of propane/air mixture occurs from ~350 μs after the heat deposition start in the peak temperature region when peak temperature reaches ~ 2500 K. Time length of gas heating for section 7 is near 200 μs Time of exit to steady state regime in whole combustor is near 2000 μs. Process of fuel mixture ignition and flow establishment in after step region is illustrated by Figs. A.2.12-A.2.20 located in Illustrations.

Fig. 2.52 shows similar time variation data after heat deposition stopping. Presented data show that as for scheme 1 after heating shut-down burning in combustor is finished. Relaxation time for separated region is near 2000 μs.

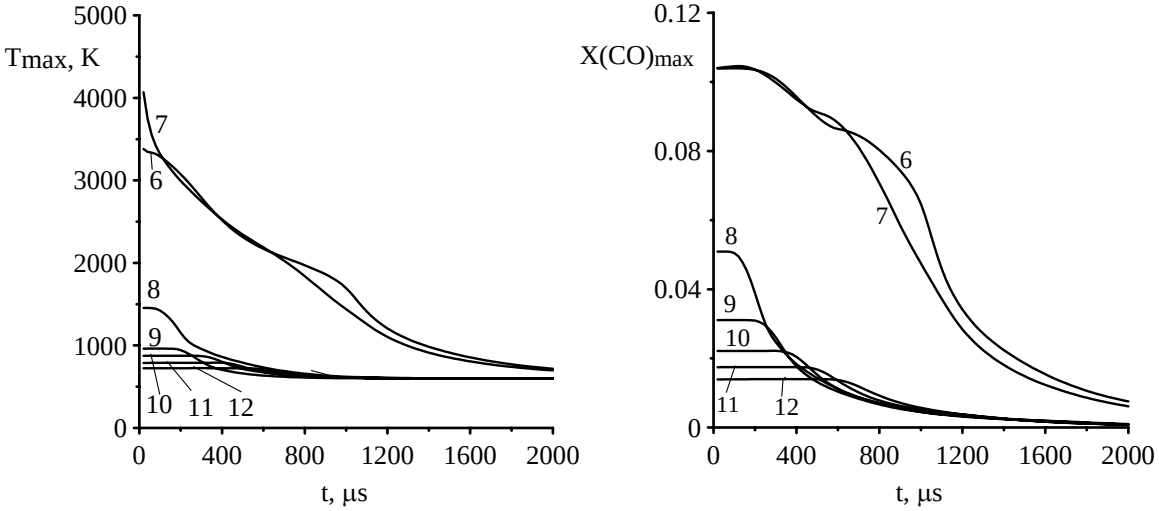

Fig.2.52. Time variation of maximal temperature T_{max} (a) and peak of mole fraction CO (b) in the different sections of the combustor after stopping of heat deposition.

2.3. Numerical analysis of steady state kerosene/air mixture ignition and burning in supersonic channel by heat deposition modeling electrical discharge

2.3.1.One-formula surrogate model of kerosene

Common hydrocarbon fuel as kerosene is derived from petroleum and one is complex mixture of many components. Exact composition of this mixture and its properties vary from batch to batch. For example, it is reported [9] that kerosene consists of 10 hydrocarbons containing 10-16 carbon atoms per molecule. It is obvious that using all 10 kerosene species would be highly inefficient in the complex calculations. One of way for kerosene model simplification is based on using of surrogate models. The surrogate fuel model composed of a neat compound or several neat components of the fuel while important thermochemical properties such as the heat of combustion are retained. For example, one formula models $C_{10}H_{19}$ [9] and $C_{12}H_{23}$ [9] were used to represent kerosene. The simplistic nature of those one-formula fuel models makes them easy to use but those simple formulas present some problems when used in calculations [8]. Other than one-formula fuel model approach is multiple–formula models [11]. However, this approach often creates extra chemical species, thereby slowing down the computation.

In the present report one-formula kerosene model $C_{12}H_{24}$ proposed in Ref [8] is employed to study kerosene/air ignition and combustion holding in the supersonic test channel by heat deposition that is simulated surface and volumetric electrical discharges. Because only one parent fuel is involved there is computational efficiency. In addition, although this model takes the form of one-formula surrogate fuel, kinetically one is modeled as mixture of 41.7% paraffin and 58.7% naphthene, matching approximately the reported paraffin/ naphthene, split of 41/36. In fact $C_{12}H_{24}$ does not represent a certain molecule, but rather a mixture of many neat components that have the same averaged thermochemical parameters as that of the reported kerosene.

The three thermodynamics functions of heat capacity C_p, enthalpy H and entropy S of $C_{12}H_{24}$ are calculated using fourth-order polynomial heat capacity form:

$$C_p / R_u = a_1 + a_2 T + a_3 T^2 + a_4 T^3 + a_5 T^5,$$

$$H / R_u T = a_1 + (a_2/2)T + (a_3/3)T^2 + (a_4/4)T^3 + (a_5/5)T^4 + (a_6/T),$$

$$S / R_u = a_1 \ln T + a_2 T + (a_3/2)T^2 + (a_4/3)T^3 + (a_5/4)T^4 + a_7,$$

where T is gas temperature, R_u is universal gas constant. Coefficients $a_1 - a_7$ are taken from Ref. 8, and listed in Table 2.5 for two temperature intervals.

Table 2.5. Thermodynamic coefficients for $C_{12}H_{24}$

Coefficient	1000 – 5000 K	300- 1000 K
a_1	0.36440206E+02	0.39508691E+01
a_2	0.54614801E-01	0.10207987E+00
a_3	-0.16091151E-04	0.13124466E-04
a_4	0.21478497E-08	-0.76649284E-07
a_5	-0.10131180E-12	0.34503763E-10
a_6	-0.63890109E+05	-0.52093574E+05
a_7	-0.15798973E+03	0.21980951E=02

Quasi-global kinetics model [8] includes two global reactions and 12 elementary reactions between species – *O, H, OH, H_2, O_2, CO, CO_2* .(see Appendix). Used in the present calculations chemical mechanism does not contain soot formation and oxidation reactions. So considered gas-phase model contains 11 species : $C_{12}H_{24}$ (as paraffin), $C_{12}H_{24}$ (as naphthene), O, H, OH, O_2, H_2, H_2O, CO, CO_2, N_2.

2.3.2. Kerosene injection, and heat source parameters.

Calculations have been performed for numerical model of the supersonic channel described above. Gaseous kerosene (the same as propane) is injected to air supersonic flow in normal direction from injector width of L_{inj} =5.5 mm placed on the lower surface of insulator at begin of this duct. Center of the injector are located on distances of 6 mm from the insulator origin. Kerosene injection is carried out with the total mass rate $G_{inj} = L_{inj}\,(\rho v)_{inj}$. Injection intensity is specified by parameter $b_{inj} = (\rho v)_{inj} / (\rho u)*$, where $(\rho u)*$ is an air mass flux in the nozzle throat. Present report contains some results of flowfield calculations fulfilled for kerosene injection intensity $b_{inj} = 0.05$. Temperature of injected kerosene is 600 *K*.

Heat is supplied with steady total power P_d uniformly distributed in rectangular region $x_{st} \le x \le x_{fin}, y_{st} \le y \le y_{fin}$ Two schemes of heat deposition in channel modeling electrical discharge have been considered. In the first scheme heat source was located near lower insulator surface close to step. In the second scheme heat source was located into after step flow separated region: near combustor wall and in the separated region center. All considered cases of calculations are listed in Table 2.6

Table 2.6. Cases of calculations.

Case	x_{st}, cm	x_{fin}, cm	y_{st}, cm	y_{fin}, cm	P_d, kW
1	29	34	-1.25	-1.05	3.5
2	29	34	-1.25	-1.05	4.0
3	36	38	-2.75	-2.55	0.5
4	36	38	-2.75	-2.55	1.0
5	36	38	-2.30	-2.10	0.5
6	36	38	-2.30	-2.10	1.0

2.3.3. Analysis of computations results for scheme 1.

Case 1. Some data about ignition and burning of kerosene/air mixture in supersonic channel with back step predicted for scheme 1 are shown on Figs. 2.53 - 2.59. Fig.2.53 demonstrates distributions of maximal across channel temperature $T_{\max}(x)$ and wall kerosene mole fractions along heat deposition region for P_d =3.5 kW/cm. It is seen that for considered conditions ignition is started from global step at x= ≈ 32 cm when $T_{\max}$ reaches value near of 1750 K. Intensity of ignition and burning is defined by naphthene kerosene fraction. On this step CO and H_2 are produced in equal fractions. At x= ≈ 32.7 cm is started second step defined by detailed chemical mechanism. On this step occurs partially afterburning of CO and H_2 with formation of intermediate (O, H, OH) and final products (CO_2, H_2O) of combustion.

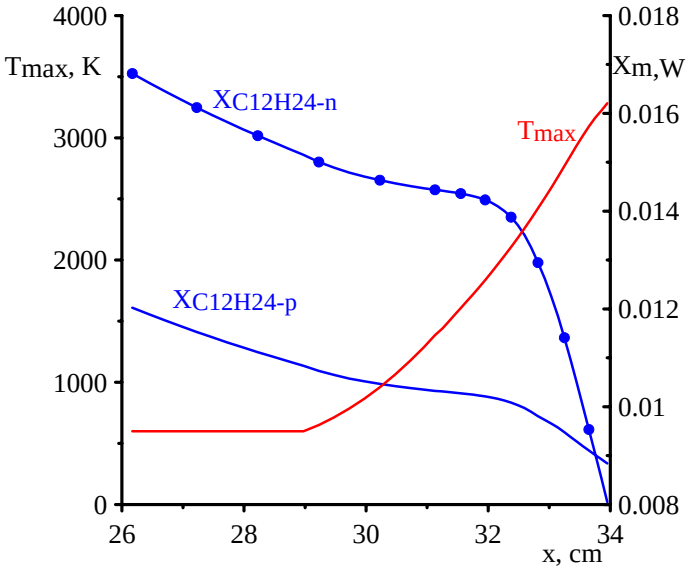

Fig.2.53. Distributions of $T_{max}(x)$ and wall kerosene fractions along heat deposition region for P_d =3.5 kW/cm

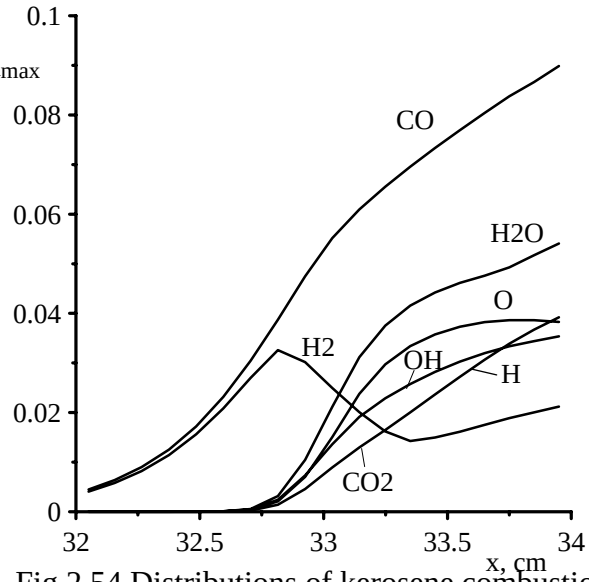

Fig.2.54.Distributions of kerosene combustion intermediate and final products along heat deposition region for P_d =3.5 kW/cm

Fig. 2.55 shows distributions of the gas temperature and composition in cross-section x=34.15 cm at once after heating region end.

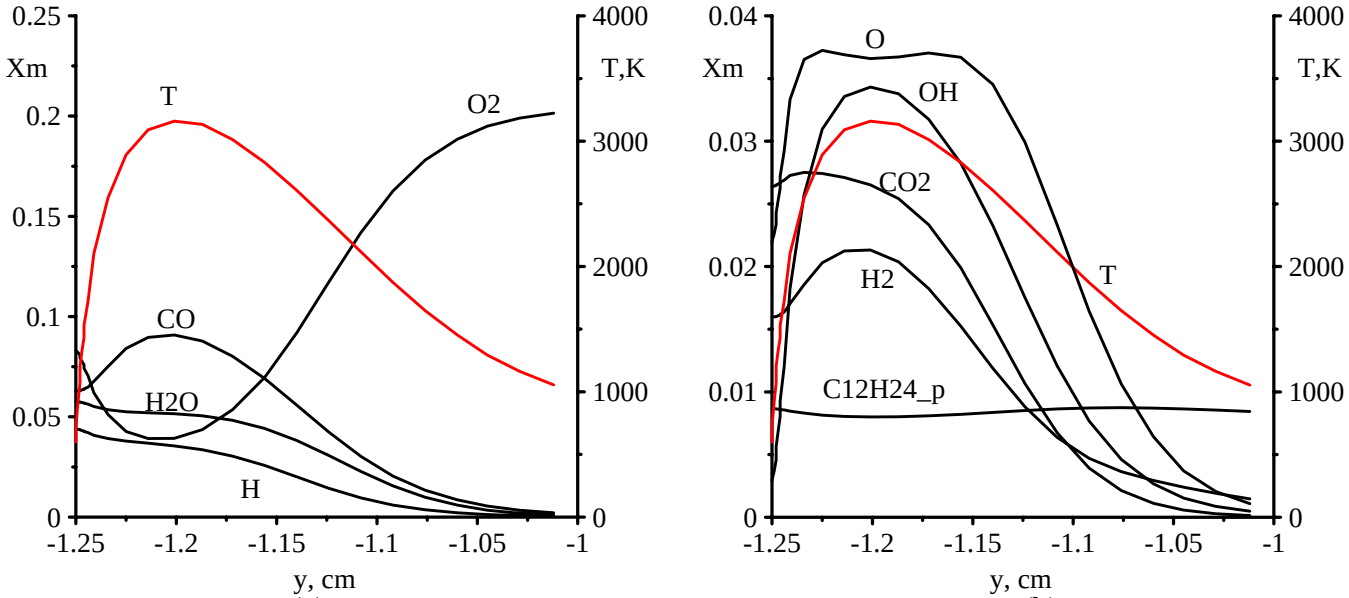

Fig.2.55. Distributions of the gas temperature and composition in cross-section x=34.15 cm for P_d =3.5 kW/cm

Fig. 2.56 shows distributions of mole fractions F_m of some components in the total mole flux in channel and distribution of combustion completeness C_B It is seen that in near after step region occurs some afterburning of mixture. Completeness of combustion C_B reaches after step of 0.035 and further is not changed.

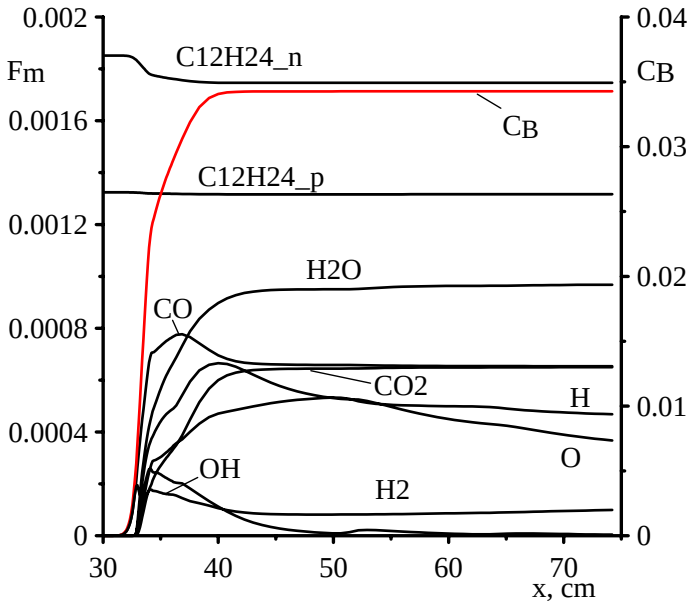

Fig.2.56. Distributions of mole fractions F_m of some components in the total mole flux in channel and distribution of combustion completeness C_B along channel for P_d =3.5 kW/cm.

Case 2. Some calculation data received for P_d =4.0 kW/cm are shown on Figs 2.57 -2.59. Comparison of presented results shows that for this heating power process of ignition occurs similarly to described above for P_d =3.5 kW/cm but location of ignition starting is moved upstream to x= ≈ 31.5 cm. Values of T_{max} in the ignition starting section for both considered cases are near of 1750 K.

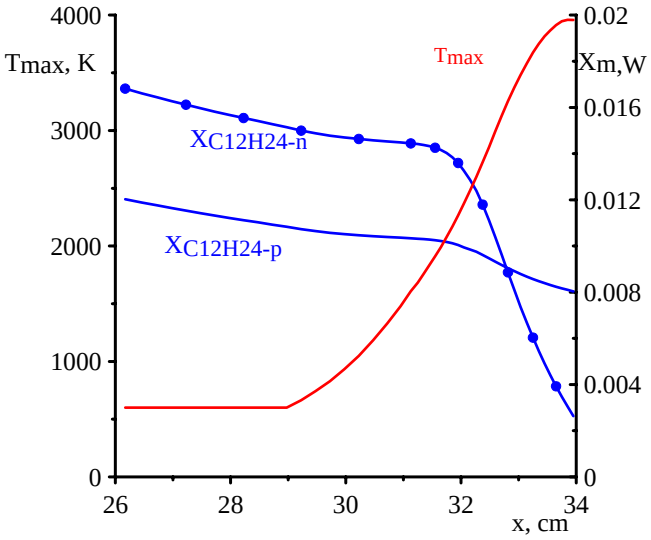

Fig.2.57. Distributions of $T_{max}(x)$ and wall kerosene fractions along heat deposition region for P_d =4.0 kW/cm

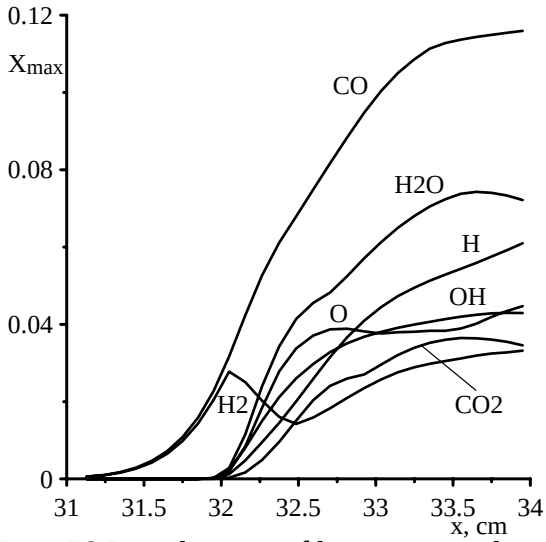

Fig.2.58.Distributions of kerosene combustion intermediate and final products along heat deposition region for P_d =4.0 kW/cm

It is not changed also the behavior of chemical processes in after step region (Fig. 2.57). Peak value of the combustion completeness C_B increases to 0.046 and further is not changed.

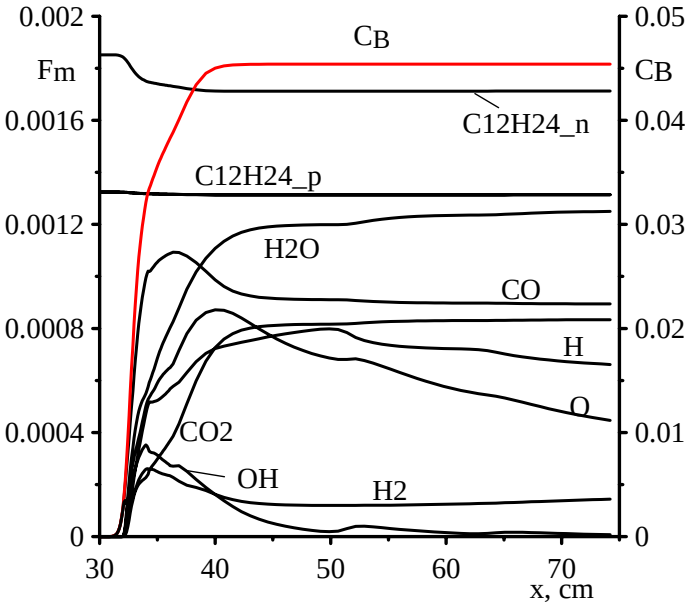

Fig.2.59. Distributions of mole fractions F_m of some components in the total mole flux in channel and distribution of combustion completeness C_B along channel for P_d =4.0 kW/cm.

2.3.4. Analysis of computations results for scheme 2

Cases 3,4. In these cases heat is supplied near lower wall of combustor into rectangular region with length of 2 cm, height of 0.2 cm and x-coordinate of centre equal to 37 cm. Fig. 2.60 .shows temperature contours for P_d=0.5 kW/cm (a) and P_d=1.0 kW/cm (b). On this Figure and on the next similar Figures region of heat deposition is indicated by a black frame. For both cases fuel mixture in separated region is ignited. Peaks temperature for these cases are reached near left (down stream) end of the heating region and amount 3240 and 4400 K accordingly.

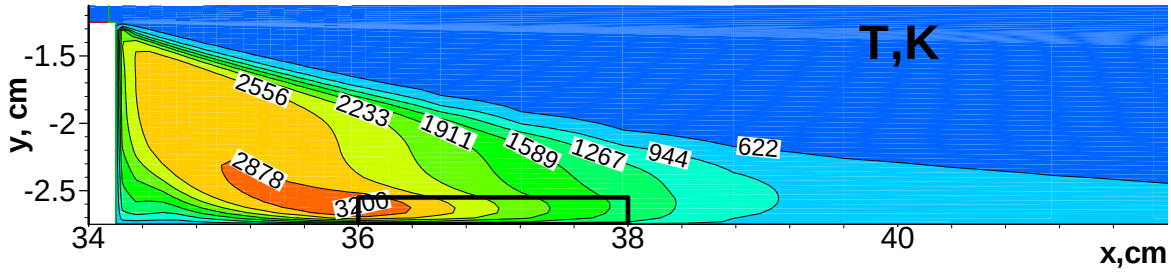

(a)

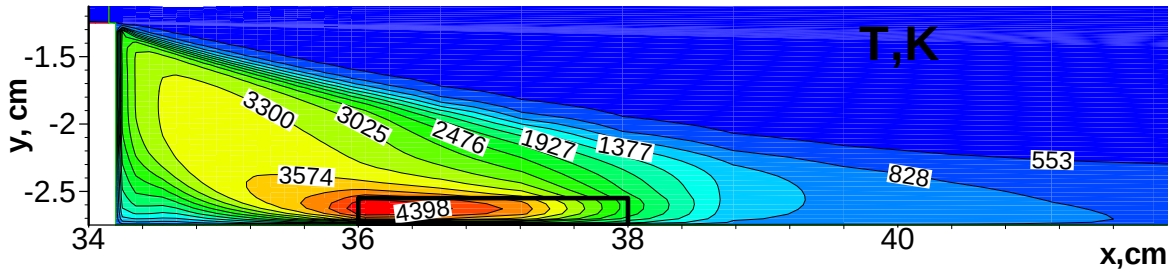

(b)

Fig. 2.60. Temperature contours in near after step region for case 3 (a) and case 4 (b).

Figs. 2.61-2.63 present contours of paraffin (C12H24_p), naphthene (C12H24_n) and oxygen mole fractions in after step region predicted for cases 3 and 4.

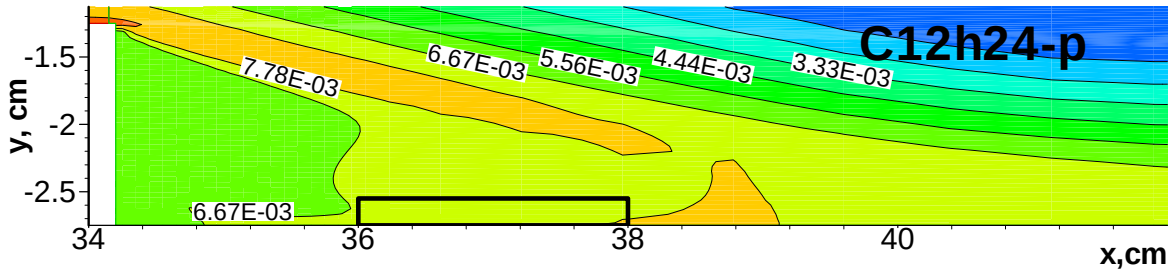

(a)

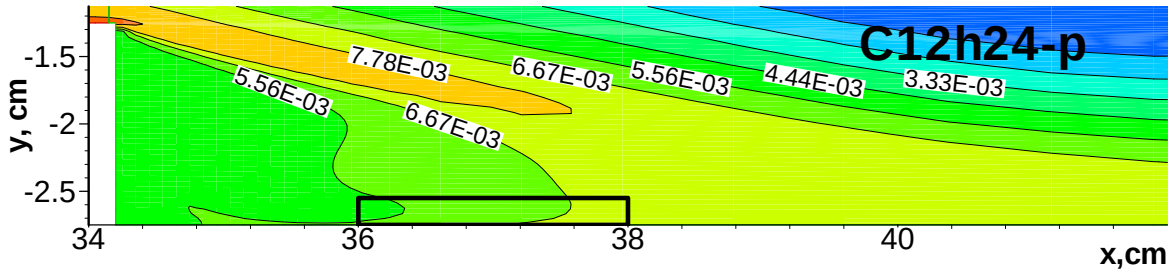

(b)

Fig. 2.61. Contours of paraffin (C12H24_p) mole fraction in after step region predicted for cases 3(a) and 4 (b).

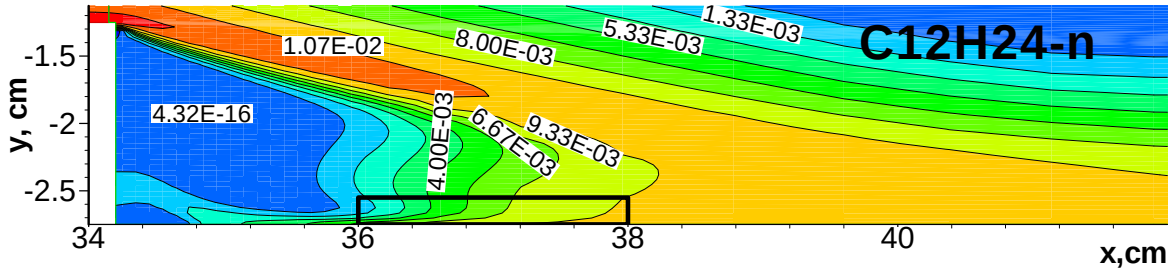

(a)

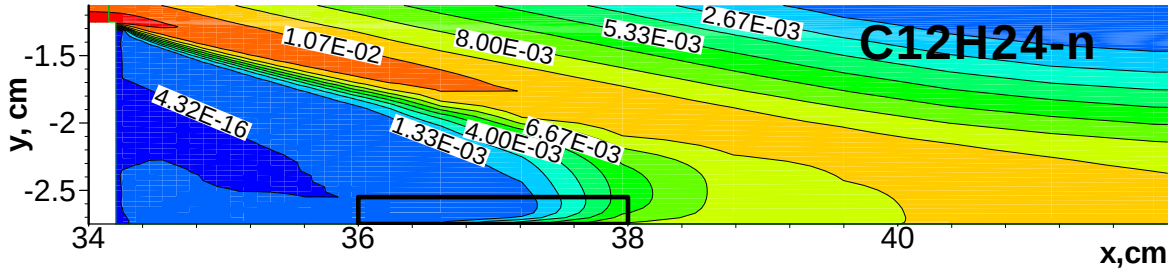

(b)

Fig.2.62. Contours of naphthene (C12H24_n) mole fraction in after step region predicted for cases 3 (a) and 4 (b).

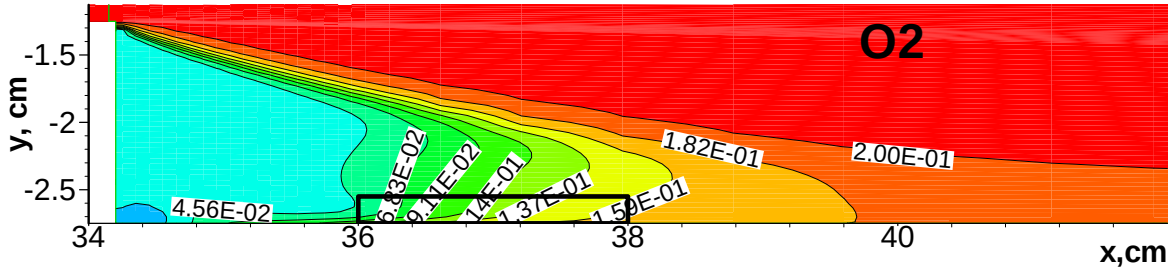

(a)

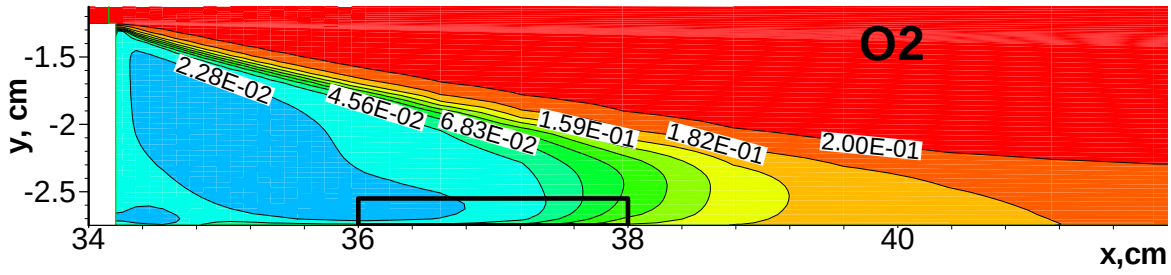

(b)

Fig.2.63. Contours of O2 mole fraction in after step region predicted for cases 3 (a) and 4 (b).

Analysis of predicted data shows that the same as for propane ignition zone of intensive combustion is formed in a mixing layer located near discriminating stream-line. Fuel mixture diffuses across this layer from internal flow and partially burns off. Unreacted components of fuel mixture and products of combustion are transported down stream into both separated region and boundary layer forming on lower wall of combustor after stream attachment. In separated region only naphthene kerosene fraction fully burns out. Paraffin fraction practically does not burn even for P_d=1.0 kW/cm. Separated region is filled up by final and intermediate combustion products. In the temperature peak region some species partially dissociate. In the attached boundary layer also there is after-burning of molecular species but rate of these processes is small.

Fig. 2.64 shows distribution along combustor of mole fractions F_m for combustion products and distribution of burning completeness C_B. It is seen that kerosene burns off mainly in separated region. There is also some afterburning in the boundary layer. Value of burning completeness C_B increases with increasing of the heating power. At the combustor outlet value of C_B increases from 0.011 for P_d = 0.5 kW/cm to 0.014 for P_d =1.0 kW/cm.

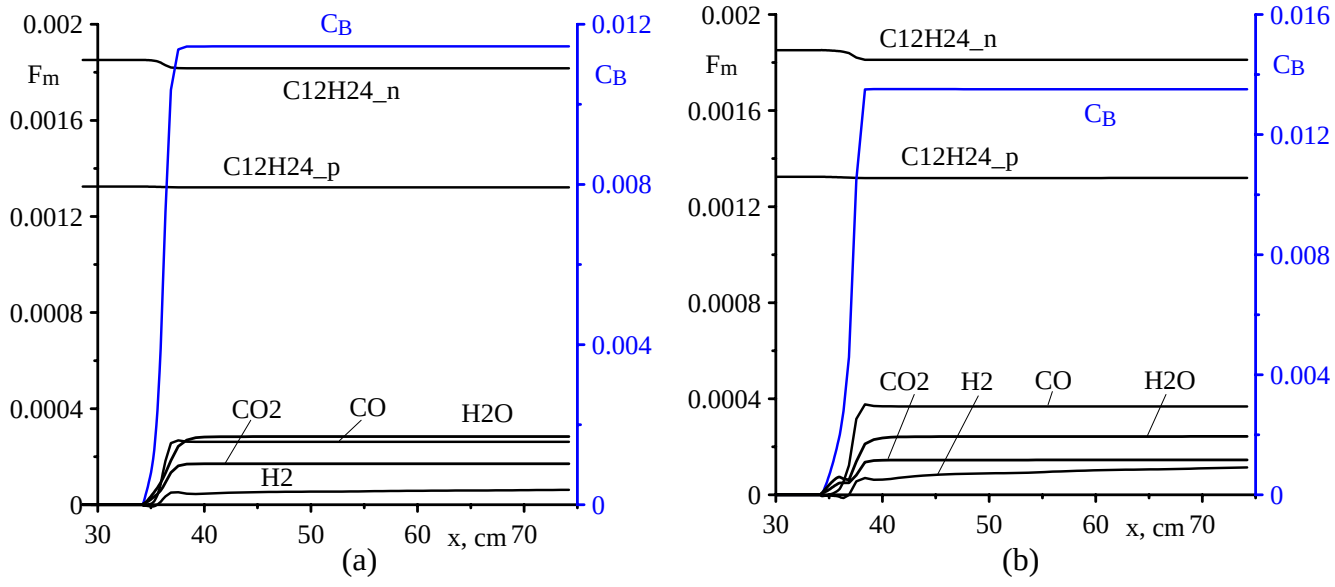

Fig.2.64. Distributions along channel of flux mole fraction F_m and burning completeness C_B for case 3 (a) and case 4 (b)

Cases 5, 6. In these cases heat source is placed in center of the separated region. This location of heat source simulates volumetric electrical discharges. Rectangular heat deposition region has length (along x-coordinates) of 2 cm, height of 0.2 cm and coordinates of center x=37 cm, y=-2.2 cm. Fig. 2.65 shows temperature contours for P_d =0.5 kW/cm (a) and P_d =1.0 kW/cm (b).

Kerosene and O_2 mole fraction contours are shown on Fig. 2.66-2.68 for the same heat deposition powers. It is seen that ignition of the fuel mixture in separated region is occurred both for P_d =0.5 kW/cm and P_d =1.0 kW/cm. Peaks temperature for both cases are reached near left end of the heating region and amount 3100 and 5000 K accordingly.

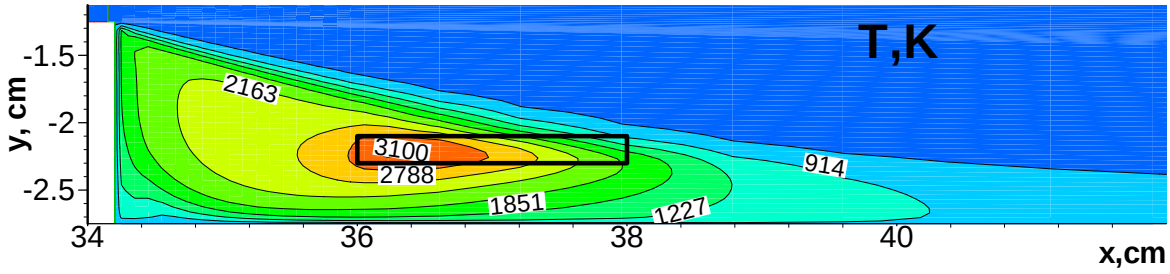

(a)

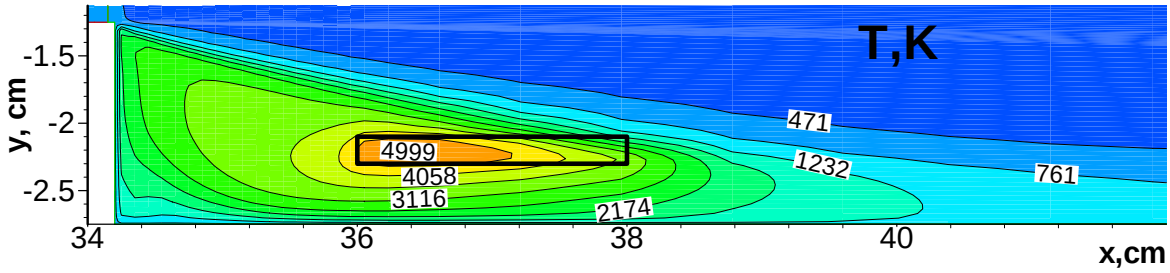

(b)

Fig. 2.65. Temperature contours in near after step region for case 5 (a) and case 6 (b).

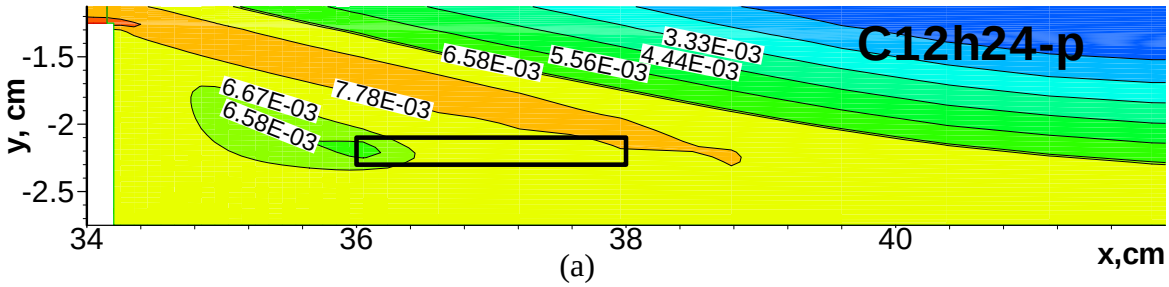

(a)

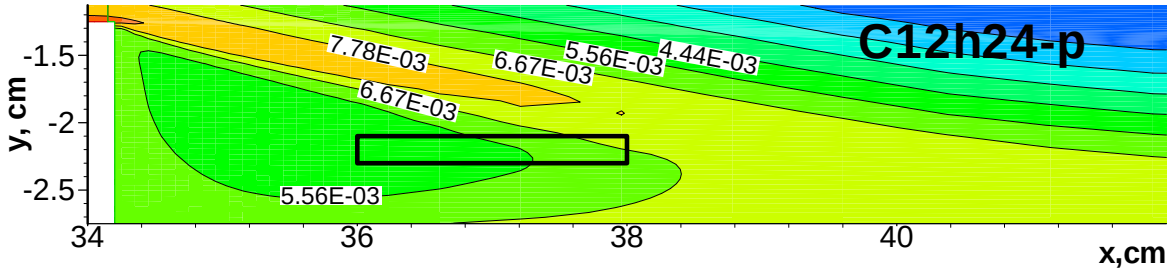

(b)

Fig..2.66. Contours of paraffin (C12H24_p) mole fraction in after step region predicted for cases 5(a) and 6 (b).

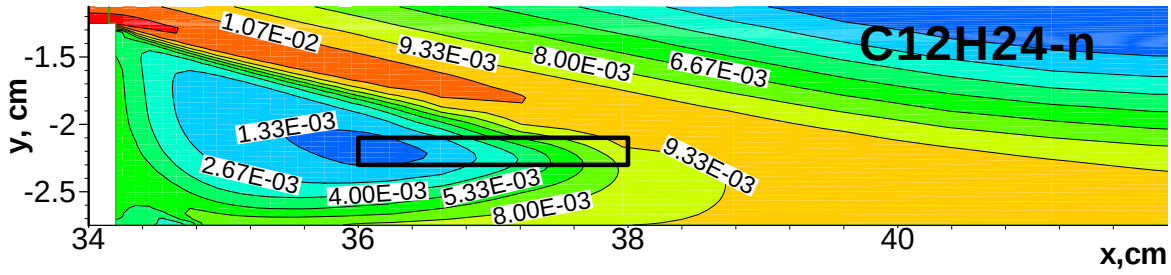

(a)

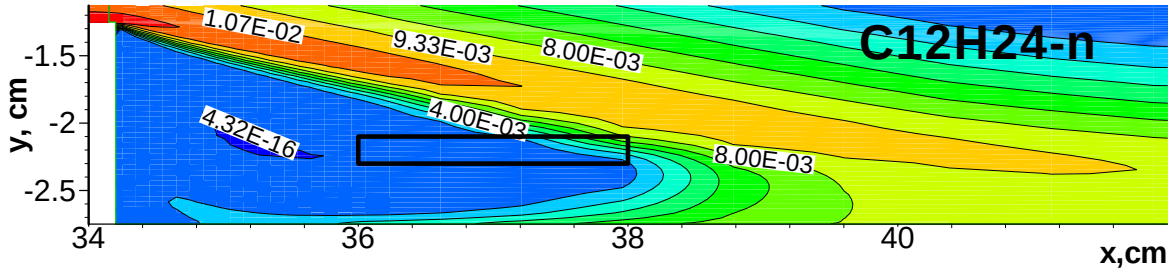

Fig.2.67. Contours of naphthene (C12H24_n) mole fraction in after step region predicted for cases 5 (a) and 6 (b).

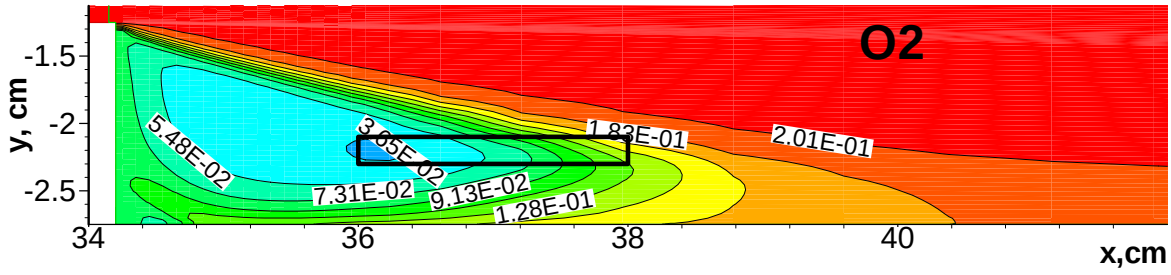

(a)

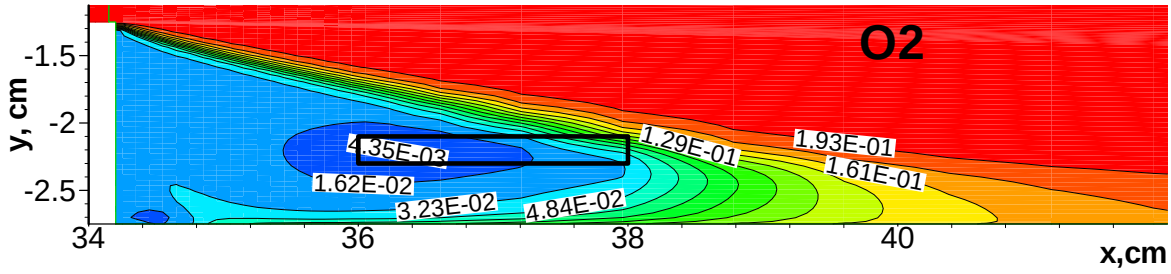

(b)

Fig.2.68. Contours of O2 mole fraction in after step region predicted for cases 5 (a) and 6 (b).

Fig. 2.69 shows distribution along combustor of mole fractions F_m of total mole flux through duct for combustion products and distribution of burning completeness C_B.It is seen that kerosene burns off mainly in separated region. There is also some afterburning in the boundary layer. Value of burning completeness C_B increases with increasing of the heating power. At the combustor outlet value of C_B increases from 0.011 for P_d = 0.5 kW/cm to 0.016 for P_d =1kW/cm.

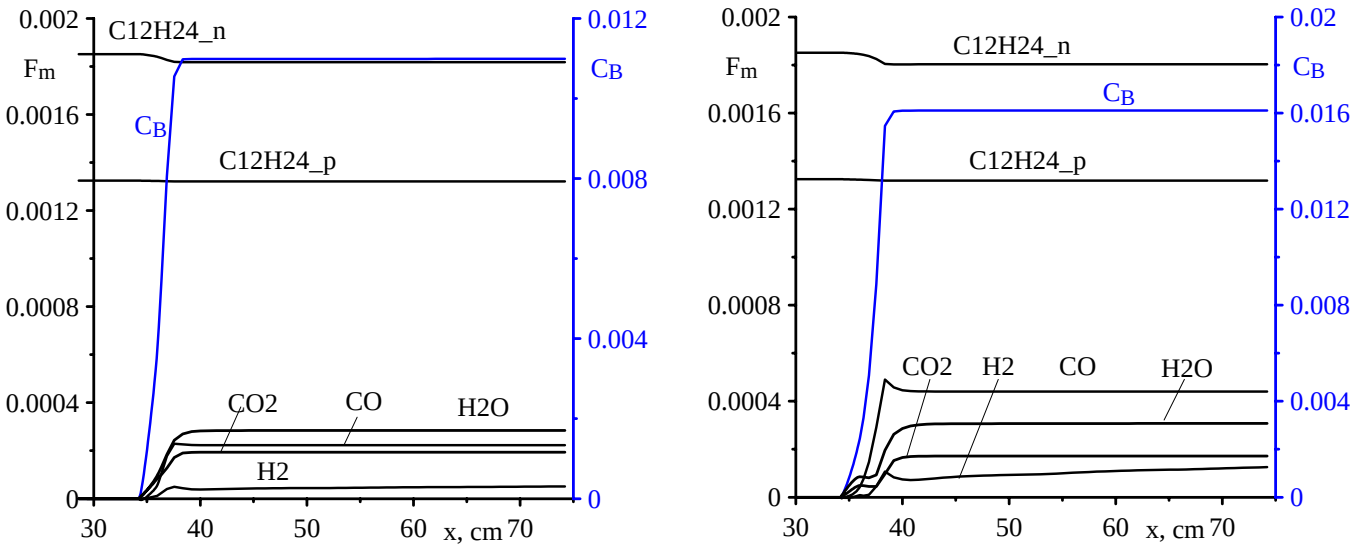

(a) (b)

Fig.2.69. Distributions along channel of flux mole fraction F_m and burning completeness C_B for case 5 (a) and case 6 (b)

Results and Conclusions

Developed, manufactured and mounted in MSU laboratory the supersonic stand including the following systems: high pressure air system, gaseous fuel delivery system, Cowper air and fuel heater, aerodynamic duct insuring supersonic air flow, model channel imitating direct flow combustion chamber and exhaust system of gas delivery to pressure chamber. Model chamber consists of two section of constant cross section: the isolator of length L=0.25 mm and the section of Lc=0.4-0.8 m, where the main combustion is supposed and with sudden widening by 1.6 times. A fuel can be delivered through two sections of sprayers at the inlet of the isolator and at its outlet, it can be also delivered directly to the zone of combustion stabilization behind the step. The supersonic flow with M=2 was created by profiled axisymmetrical and rectangular nozzles, and the channel sections behind the reverse were of rectangular cross section 25×40 mm^2 with optical windows for video observation.

Diagnostic complex for collection and analysis of information on the stand functioning and working process in investigated combustion chamber was created. It includes: pressure tenzosensors, Chromel-Alumel thermocouples, spectrograph, video camera, etc.

Undertaken stand calibration tests and measurements of full and static pressure allowed to determine flow parameters at the outlet from the supersonic nozzle and in the cross section of the outlet from the isolator at P_t=0.07-0.3 MPa and T_t= 290 K (M=2±.0.02).

Experimental investigations of plasma generators are made in above represented conditions at their location in the widening part of the combustion chamber behind the step. In particular we undertook investigations with the following plasma generators: longitudinally-transversal constant current discharge of power N=1.5 -2.0 kW, magneto-plasma generator, microwave torch discharge N=0.8-0.9kW and spark plugs.

Obtained results allow to conclude:

- all investigated discharge generators were functioning in investigated conditions without digression from rated conditions;
- fuel combustion was observed only in the area side to the discharge and only during discharge existence at gaseous propane delivery with mass flow rates corresponding to the fuel excess coefficient $\phi = 0.7 – 1.8$. Combustion in the region behind the step was not stabilized in spite of delivered power, so the fuel mixture combustion stopped with discharge shut down.

Experiments with longitudinally transversal discharge showed that inflammation of propane-air mixture takes place with the highest probability (of 60% - 80%) at values $\phi = 1 \pm 0.2$. The flame propagated to the step in the channel in the case of lower electrodes position, but the combustion was not stabilized. We did not manage to stabilize the combustion even at location of additional wedge in the channel that created a cavity, it was because of low static temperature of airflow.

MPC investigations showed that thermal pulse initiated by the discharge lead to fuel mixture inflammation in the whole channel volume and to intense short time throttling of the flow, but the combustion also was not stabilized at the discharge shut down, it stopped by reasons indicated earlier.

Tests with microwave torch discharge demonstrated fuel mixture inflammation in the zone behind the step and its combustion during discharge functioning, but mixture combustion stopped with MW discharge shut down as it was in cases with other discharge types.

The mixture combustion after the inflammation was observed over the whole discharge length in near wall layer at realization of MW surface discharge, it can be caused by chain of processes in MW discharge. The mixture combustion stopped at MW generator shut down analogous to the case of MW torch discharge.

Spectroscopic measurements validated observed propane-air mixture inflammation and its combustion in the discharge region with temperature level T=2400-2800 ^{0}K.

Analysis of all obtained results show necessity of continuation of investigations on initiation and stabilization of hydrocarbon-air mixtures with a help of plasma generators with prior application of preliminary air and fuel heating up to temperatures T=800-900 ^{0} K.

New effective numerical models and codes have been developed to provide researches under the Project Task 4. For description of turbulent flows Favre averaged Navier-Stokes equations and $k-\omega$ turbulence model is used. Global, quasi-global and detailed chemical mechanisms is employed for simulation of chemical processes in gas mixture On the first stage of investigations the heat source model of gas discharge was employed for description of discharge effect on gas flow. Thermochemical models for fuel mixture hydrogen/air, propane/air and kerosene/air were developed to provide researches under Project.

Developed numerical technique have been employed to research steady state and unsteady propane/air and kerosene/air mixture heating and ignition in a planar model of test channel with back step on lower surface for two schemes of fuel injection and heat deposition. Considered schemes simulate ignition of fuel/air mixture by the surface or volumetric gas discharges.

The main attention was given to numerical researches of propane/air mixture ignition and combustion stabilization in supersonic channel by electrical discharge for experiments condition. Two chemical models were used for calculation. Reduced model involves 12 species, one global reactions and 20 elementary reactions. Full model involves 28 species and 70 elementary chemical reactions. For estimate of gas heating rate calculations for non-reacting gas model were performed also.

Parametric calculations of steady state propane/air mixture flow in the channel were performed for each from schemes. Propane mixture ignition and combustion stabilization by the heat supply is demonstrated. Effect of chemical model, and heat source power, configurations and location on ignition and burning processes in channel were analyzed.

It is shown that for first scheme of the heat deposition when heat source is located before step ignition occurs for heating power $P_d \geq 4$ kW/cm. Combustion completeness C_B on the channel outlet for this scheme reaches of 0.43. For heat deposition after step ignition occurs already at power P_d =0.5 kW/cm. Value of C_B in considered cases reaches of 0.2 for this scheme. There is essential difference of results obtained for scheme 1 using reduced and detailed chemical mechanisms. Predicted by reduced model value of combustion completeness is near 0.01.

Unsteady processes at the heat deposition turning on and turning of were studied. It was shown that after heating shut down combustion in channel is finished. Estimates of inductive and relaxation time were obtained.

Similar investigations of the steady state flows for gaseous kerosene injection in supersonic channel were performed also. One-formula kerosene model $C_{12}H_{24}$ and quasi-global chemical model including 11 species, 2 global and 12 elementary reactions was employed in computations.

The parametric calculations of the channel flow were performed for the same mass injection rate as for propane case. Effects of the heat source power and location on the kerosene/air mixture ignition and burning effectiveness is analyzed.
It is shown that for heat deposition before step with power P_d =3.5 kW/cm and higher mixture is ignited. For heat deposition after step ignition occurs already for power P_d =0.5 kW/cm. Value of burning completeness in considered cases does not exceed of 0.045 for first scheme and 0.016 for second scheme heat deposition.

Results of the fulfilled numerical investigations can be used for planning and interpretation of experiments on created experimental facility.

Developed numerical models and codes are basis for elaboration of more realistic thermo-physical and geometry models and corresponding codes.

References to Item 2

1. Favre, A., “Equations des gas turbulents compressibles”, Journal de Mecanique, **4**, 1965.

2. Coakley, T.J. “Development of Turbulence Models for Aerodynamic Applications,” AIAA Paper 97-2009, 1997

3.Westbrook, C.K., Dryer, F.L. Simplified Reaction Mechanisms for the Oxidation of Fuels in Flames. Combustion Science and Technology, 1981, Vol.27, pp.31-43

4. Hirschfelder J.O., Curtiss C.F., and Bird R.B., Molecular Theory of Gases and Liquids. John Wiley, New York, 1954.

5. Reid, R.C., Prausnitz, J.M., and Sherwood, T.K., The Properties of Gases and Liquids, McGraw-Hill Book Company, New York, 1977

6.Katta, V.R., Roquemore, W.M. Simulation of Unsteady Flows in an Axisymmetric Research Combustor Using Detailed-Chemical Kinetics. AIAA/ASME/SAE/ASEE Joint Propulsion Conference & Exhibit, 34th, Cleveland, OH, July 13-15, 1998

7.Warnatz, J., Maas, U., Dibble, R.W. *Combustion. Physical and Chemical Fundamentals, Modeling and Simulations, Experiments, Pollutant Formation.* Springer, 2001

8. Ten-See Wang, “Thermophysics Characterization of Kerosene Combustion’. J. of Thermophysics and Heat Transfer, Vol.15, N0.2, 2001.

9. Amsden, A.A., “KIVA-III: A KIVA Program with Block Structure Mesh for Complex Geometry,” Rept.LA-12503-MS, Los Alamos National Lab., Los Alamos, NM, March 1993

10. Harsha, P.T., Edelman, R.B., and Farmer, R.C. “Fundamental Combustion Technology for Ramjet Applications - Technology Reiew”, CPIA Publ.363, Vol.2, Chemical Propulsion Information Agency, Laurel, MD, Sept.1982

11. Farmer, R.C., and Anderson, P.G., “Soot Formation in Rocket Propulsion System,” Rept. SECA-FR-95-12, SECA, Inc., Huntsville, AL, 1995

12. Edelman, R.B., and Harsha, P.T., ”Laminar and Turbulent Gas Dynamics in Combustors – Current Status,” *Progress in Energy and Combustion Science* ,Vol.4, No.1, 1978, pp.1-62

13. Wang, T.S., Farmer, R.C., and Edelman, R.B., “Turbulent Combustion Kinetics for Complex Hydrocarbon Fuels,” AIAA Paper 88-0733, 1988

Appendix

.Propane combustion kinetics

Quasi-global reaction mechanism [3]

Global reaction: $C_3H_8 + 1.5O_2 \Rightarrow 3CO + 4H_2$,
reaction rate: $\omega = A\exp(-E_{qgl}/R_uT)[C_3H_8]^{\alpha}[O_2]^{\beta}$ mol/cm^{3}s , [] – mole fraction, mol/cm^3
A=1.5×10^{12}, E_{qgl} =30 and 40 kcal/mol, α = 0.1, β =1.65

Elementary dissociation-recombination reactions (model 2)
Reverse rate constant $k_r = AT^n \exp(-E/T)$, cm^6/mol^2 s

Reaction	A	n	E, K	Source
O2 + M ⇔ O + O + M	2.5e14	0.	-1500.	3*
H2O + M ⇔ OH + H + M	1.4e15	0.	-7000.	3*
H2 + M ⇔ H + H + M	6.0e13	0.	-4000.	3*
OH + M ⇔ O + H + M	1.0e16	0.	0.	3*
CO2 + M ⇔ CO + O + M	5.9e15	0.	2063.	3
HO2 + M ⇔ H + O2 + M	1.5e15	0.	-500.	3
H2O2 + M ⇔ OH + OH + M	1.7e15	0.	-1800.	3*

Detailed reaction mechanism [6,7]
Elementary dissociation-recombination reactions
Reverse rate constant $k_r = AT^n \exp(-E/T)$, cm^6/mol^2 s

Reaction	A	n	E, K	Source	Mod. 2
O2 + M* ⇔ O + O + M*	2.9e17	-1.	0.	7	+
H2O + M* ⇔ OH + H + M*	2.2e22	-2.	0.	7	+
H2 + M* ⇔ H + H + M*	1.8e18	-1.	0.	7	+
OH + M ⇔ O + H + M	1.0e16	0.	0.	6*	+
CO2 + M* ⇔ CO + O + M*	7.1e13	0.	-2285.	7	+
HO2 + M* ⇔ H + O2 + M*	2.3e18	-0.8	0.	7	+
H2O2 + M* ⇔ OH + OH + M*	3.3e22	-2.0	0.	7	+
HCO + M ⇔ CO + H + M	1.1e15	0.	0.	6*	
CH4 + M ⇔ CH3 + H + M	6.0e16	-1.0	0.	6	
CH2O + M ⇔ HCO + H + M	4.0e15	0.	0.	6*	
C2H4 + M ⇔ C2H2 + H2 + M	8.0e15	0.	18000.	6*	
C2H5 + M ⇔ C2H4 + H + M	4.2e13	0.	0.	6*	
C2H6 + M ⇔ CH3 + CH3 + M	3.6e13	0.	0.	6	
C3H6 + M ⇔ C2H3 + CH3 + M	4.5e10	0.	0.	6*	
C3H7I + M ⇔ C2H4 + CH3 + M	2.0e11	0.	8000.	6*	
C3H7N + M ⇔ C2H4 + CH3 + M	3.0e11	0.	5000	6*	
C3H7N + M ⇔ C3H6 + H + M	2.0e14	0.	1500	6*	
C3H8 + M ⇔ CH3 + C2H5 + M	1.4e08	0.8	0.	6*	
C3H8 + M ⇔ C3H7n + H + M	3.6e13	0.	0.	6	
C3H8 + M ⇔ C3H7i + H + M	2.4e13	0.	0.	6	

M – catalytic activity of all species relatively indicated in table is equal to 1.0.
M* - – catalytic activity of H2O is 6.5, O2 – 0.4, N2 - 0.4, CO – 0.75, CO2 – 1.5, CH4 – 3 , all other species – 1.0 relatively indicated in Table [7]

Elementary exchange reactions

Reverse rate constants $k_r = AT^n \exp(-E/T)$, $cm^3/mol\,s$

Reaction	A	n	E, K	Model 2
OH + O = H + O2	2.00e14	0.	8455.	+
OH + H = O + H2	5.06e04	2.67	3160.	+
H2O + H = H2 + OH	1.00e08	1.60	1661.	+
O + H2O = OH + OH	1.50e09	1.14	50.	+
OH + OH = HO2 + H	1.50e14	0.0	503.	+
H2 + O2 = HO2 + H	2.50e13	0.0	348.	+
H2O + O2 = HO2 + OH	6.00e13	0.0	0.	+
H2O + O = HO2 + H	3.00e13	0.0	866.	+
OH + O2 = HO2 + O	1.80e13	0.0	-204.	+
H2O2 + O2 = HO2 + HO2	2.50e11	0.0	-624.	+
H2O + OH = H2O2 + H	1.00e13	0.0	1802.	+
H2O + HO2 = H2O2 + OH	5.40e12	0.0	503.	+
CO2 + H = CO + OH	4.40e06	1.5	-372.	+
HCO + O = CH + O2	3.00e13	0.0	0.	
HCO + CO = CO2 + CH	3.40e12	0.0	348.	
CO + H2 = HCO + H	2.00e14	0.0	0.	
CO + H2O = HCO + OH	1.00e14	0.0	0.	
CO + HO2 = HCO + O2	3.00e12	0.0	0.	
CH + H2 = CH2 + H	8.40e09	1.5	169.	
HCO + H2 = CH2O + H	2.50e13	0.0	2008.	
HCO + OH = CH2O + O	3.50e13	0.0	2008.	
HCO + H2O = CH2O + OH	3.00e13	0.0	604.	
CH2 + H2 = CH3 + H	1.80e14	0.0	7574.	
CH2O + H = CH3 + O	7.00e13	0.0	0.	
CH2O + OH = CH3 + O2	3.40e11	0.0	4499.	
CH3 + H2 = CH4 + H	2.20e04	3.0	4399.	
CH3 + OH = CH4 + O	1.20e07	2.1	3835.	
CH3 + H2O = CH4 + OH	1.60e06	2.1	1238.	
C2H2 + H = C2H + H2	1.10e13	0.0	1443.	
CH2 + CO = C2H2 + O	4.10e08	1.5	854.	
C2H + H2O = C2H2 + OH	1.10e13	0.0	3522.	
C2H2 + H2 = C2H3 + H	3.00e13	0.0	0.	
C2H2 + HO2 = C2H3 + O2	5.40e11	0.0	0.	
C2H3 + H2 = C2H4 + H	1.50e14	0.0	5133.	
C2H3 + H2O = C2H4 + OH	3.00e13	0.0	1515.	
CH3 + CH3 = C2H5 + H	3.00e13	0.0	0.	
C2H4 + HO2 = C2H5 + O2	2.00e12	0.0	2513.	
C2H5 + H2 = C2H6 + H	5.40e02	3.5	2621.	
C2H5 + OH = C2H6 + O	3.00e07	2.0	2573.	
C2H5 + H2O = C2H6 + OH	6.30e06	2.0	325.	
C3H5 + H2 = C3H6 + H	5.00e12	0.0	765.	
C3H6 + HO2 = C3H7I + O2	1.00e12	0.0	2513.	
C3H7n + H2 = C3H8 + H	1.30e14	0.0	4881.	

C3H7i	+	H2	=	C3H8	+	H	1.00e14	0.0	4196.	
C3H7n	+	OH	=	C3H8	+	O	3.00e13	0.0	2897.	
C3H7i	+	OH	=	C3H8	+	O	2.60e13	0.0	2248.	
C3H7n	+	H2O	=	C3H8	+	OH	3.70e12	0.0	829.	
C3H7i	+	H2O	=	C3H8	+	OH	2.80e12	0.0	433.	
C3H8	+	O2	=	C3H7n	+	HO2	5.50e05	1.5	0.	
C3H8	+	O2	=	C3H7i	+	HO2	2.60e09	0.5	0.	

Kerosene quasi-global combustion kinetics mechanism

Rate constants of reactions in form $k_f = AT^B \exp(-E/R_uT)$, mole, cm, s, atm

Reaction	A	B	E/R_u, K	Form	Ref.
Paraffin global step					
$C_{12}H_{24}+6O_2 \rightarrow 12CO+12H_2$	3.888E4	1	1.220E4	$p^{0.3}[C_{12}H_{24}]^{0.5}[O_2]$	[8]
Naphthene global step					
$C_{12}H_{24}+6O_2 \rightarrow 12CO+12H_2$	2.312E7	1	1.965E4	$p^{0.3}[C_{12}H_{24}]^{0.5}[O_2]$	[8]
Elementary reactions dissociation-recombination					
$M+O+O \Leftrightarrow O_2+M$	2.550E18	-1.0	0.	Mass action law	[12,13]
$M+H+H \Leftrightarrow H_2+M$	5.000E18	0.0	0.	Mass action law	[12,13]
$M+H+O \Leftrightarrow OH+M$	1.000E16	0.0	0.	Mass action law	[12,13]
$M+H+OH \Leftrightarrow H_2O+M$	8.400E21	-2.0	0.	Mass action law	[12,13]
$M+CO+O \Leftrightarrow CO_2+M$	6.000E13	0.0	0.	Mass action law	[12,13]
Elementary exchange reactions					
$H_2+O_2 \Leftrightarrow OH+OH$	1.700E13	0	24070	Mass action law	[12,13]
$OH+H_2 \Leftrightarrow H_2O+H$	2.190E13	0	25900	Mass action law	[12,13]
$OH+OH \Leftrightarrow H_2O+O$	6.023E12	0	550	Mass action law	[12,13]
$O+H_2 \Leftrightarrow H+OH$	1.800E10	1.0	4480	Mass action law	[12,13]
$H+O_2 \Leftrightarrow O+OH$	1.220E17	-0.91	8369	Mass action law	[12,13]
$CO+OH \Leftrightarrow H+CO_2$	4.000E12	1.0	4030	Mass action law	[12,13]
$CO+O2 \Leftrightarrow O+CO_2$	3.000E12	1.0	25000	Mass action law	[12,13]

Here p is pressure in atm, [ ] is mole fraction of species.

Illustrations

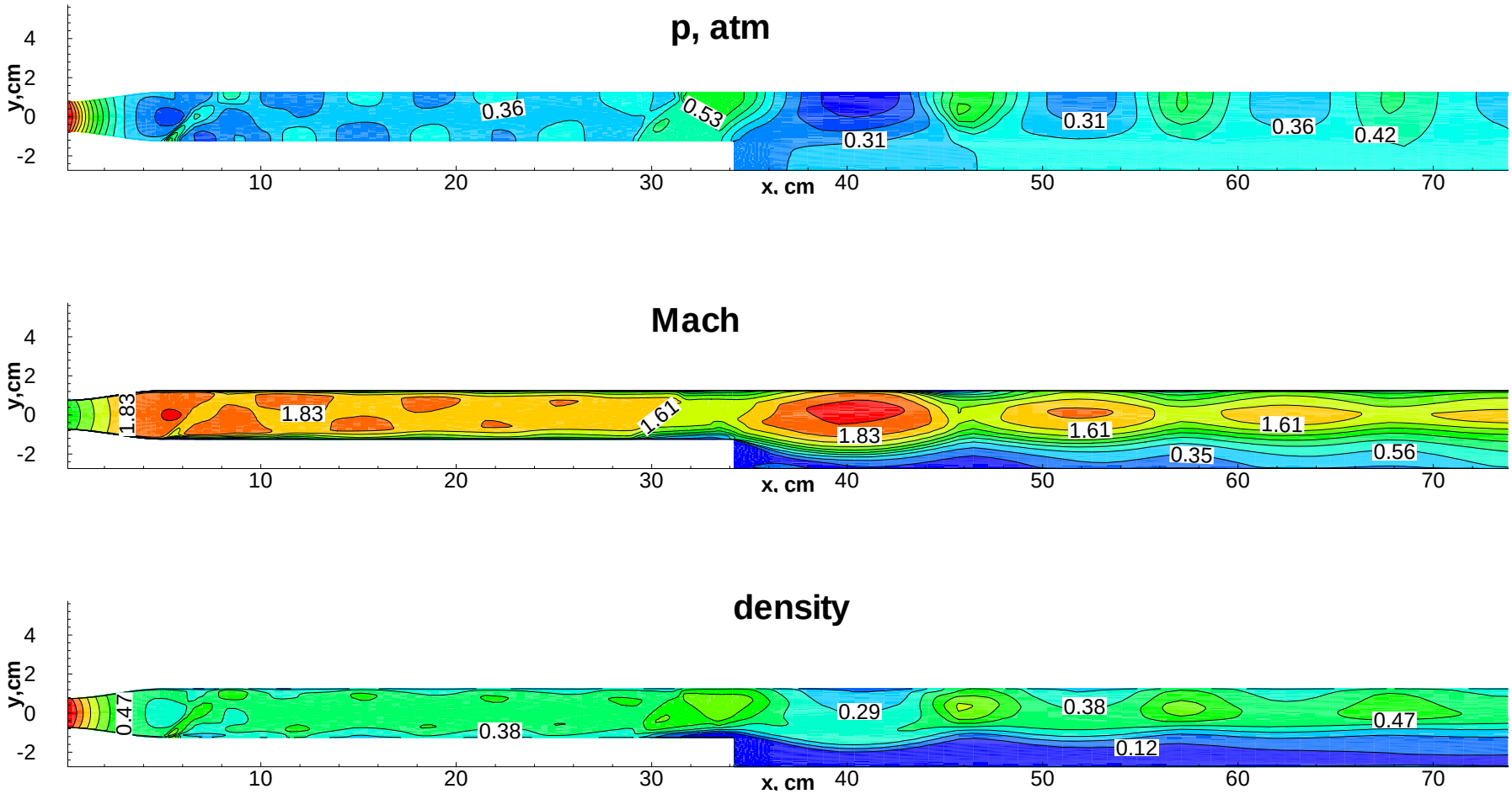

Fig.A.2.1. Distributions of pressure p , atm , Much number M and density ρ related to critical value of density $\rho*$
Scheme 1, case of calculations 6.

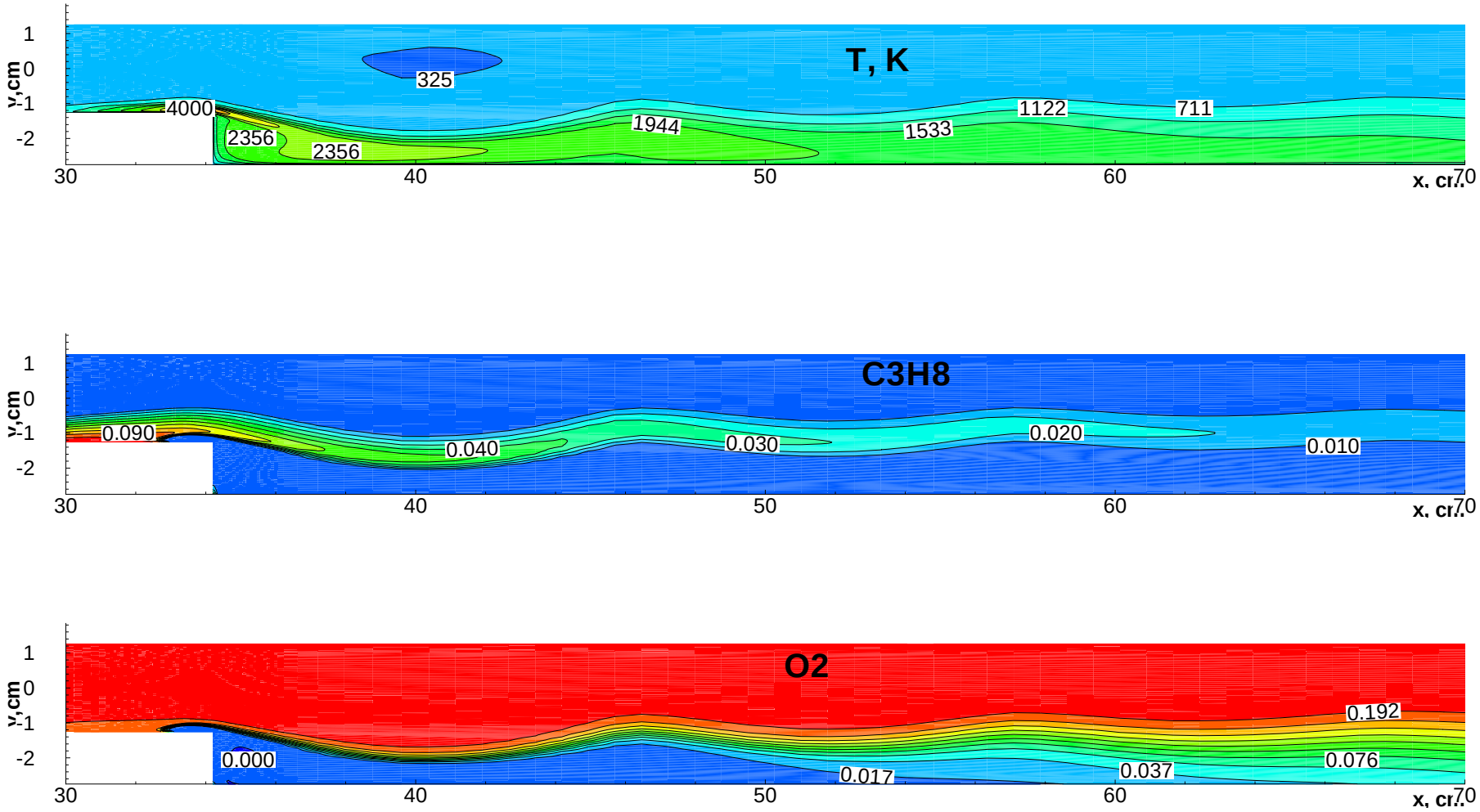

Fig.A.2.2. Distributions of temperature $T\,K$, mole fractions of C_3H_8 and O_2.
Scheme 1, case of calculations 6.

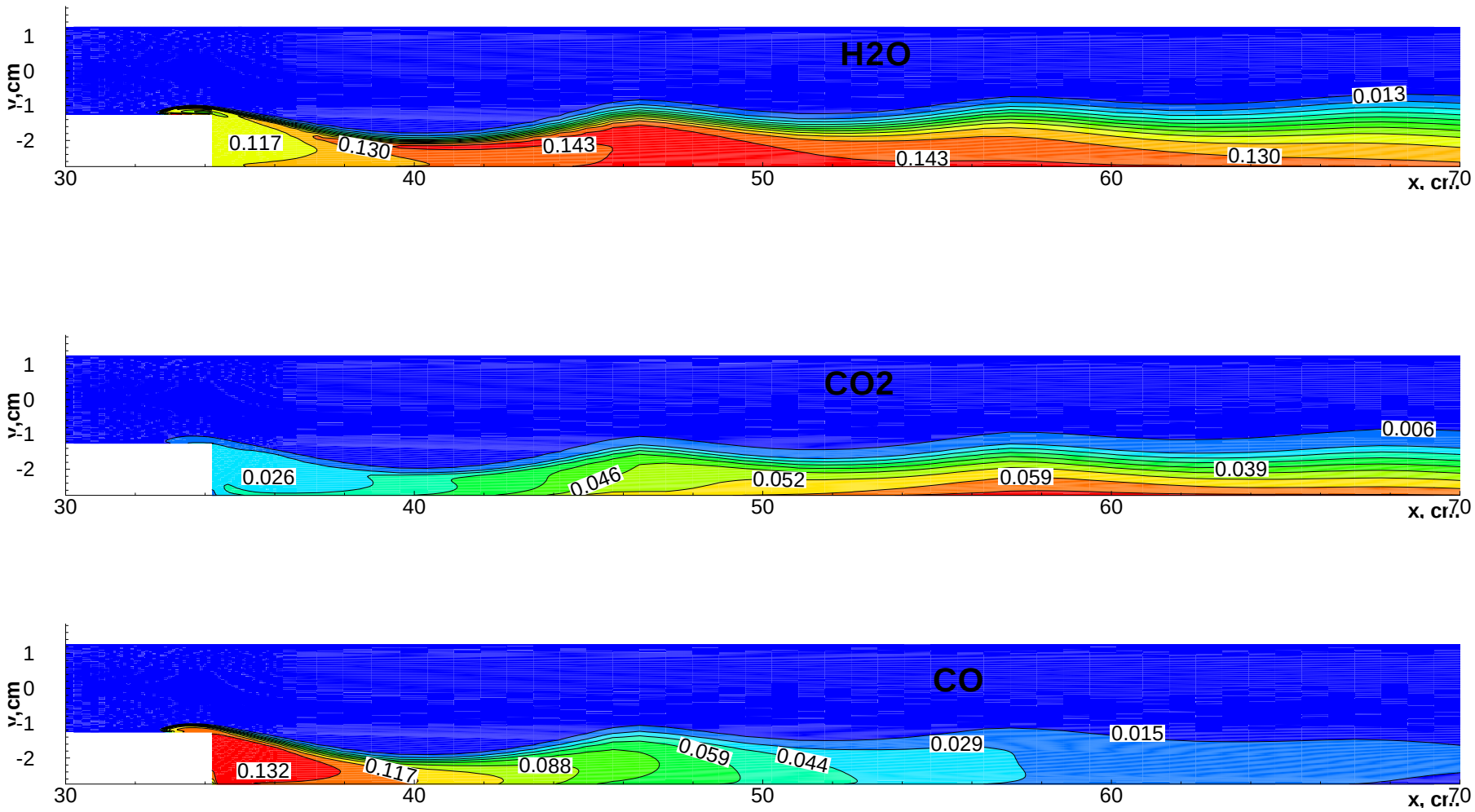

Fig. A.2.3. Distributions of mole fractions of H_2O , CO_2 and CO .
Scheme 1, case of calculations 6.

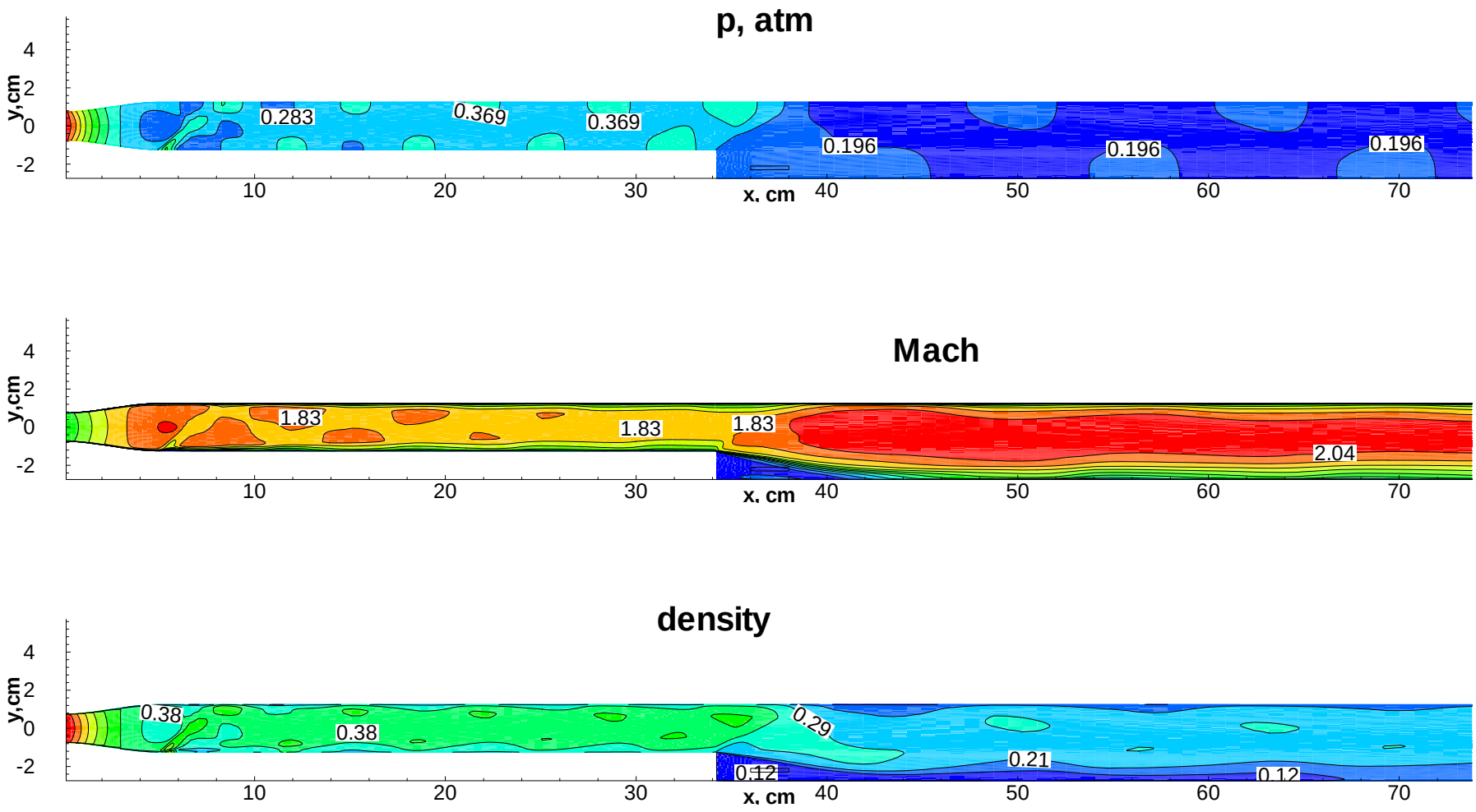

Fig.A.2.4. Distributions of pressure p , atm , Much number M and density ρ related to critical value of density $\rho*$ Scheme 2, case of calculations 10.

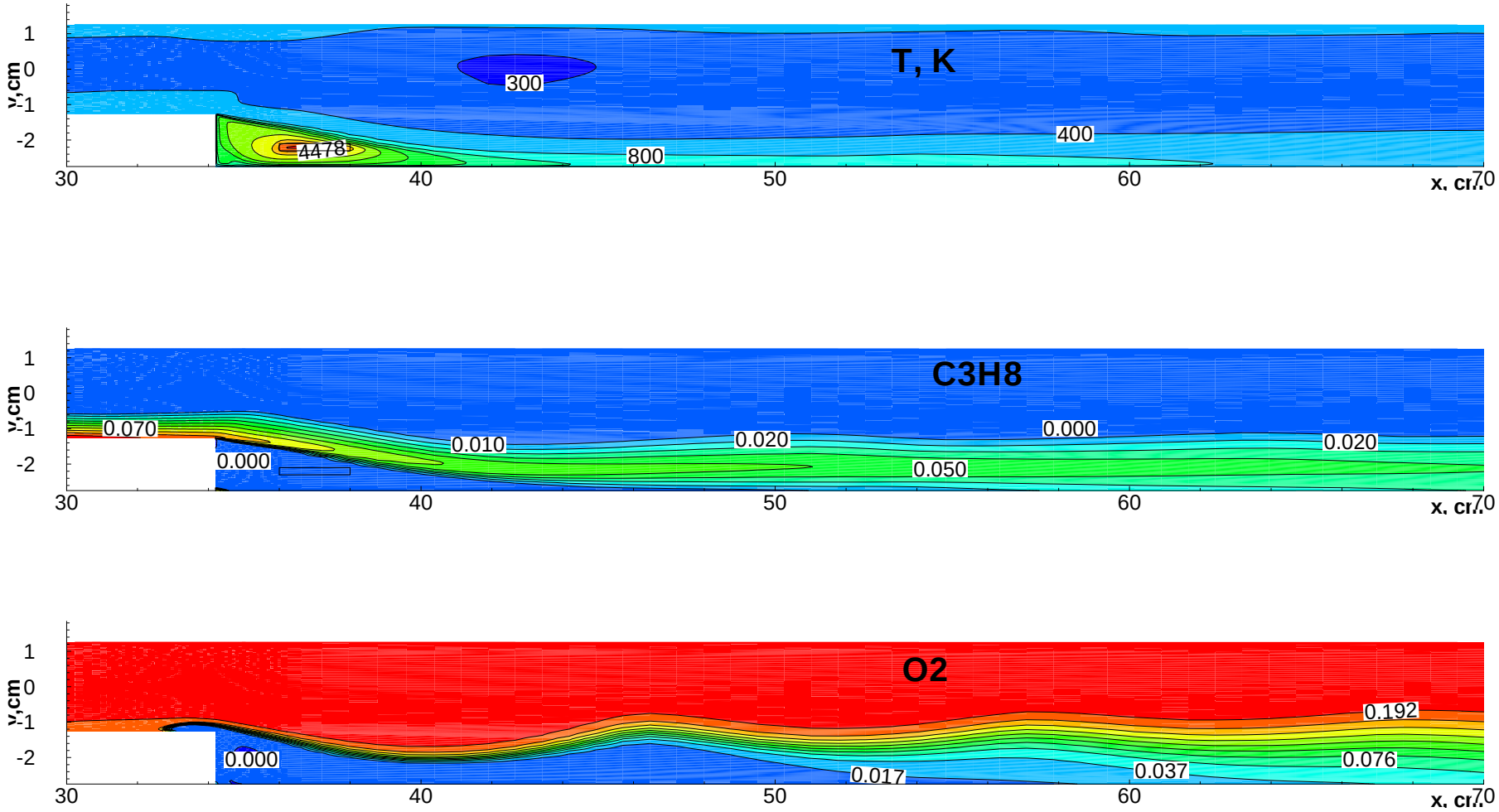

Fig.A.2.5. Distributions of temperature $T\,K$ and mole fractions of C_3H_8 and O_2 .
Scheme 2, case of calculations 10.

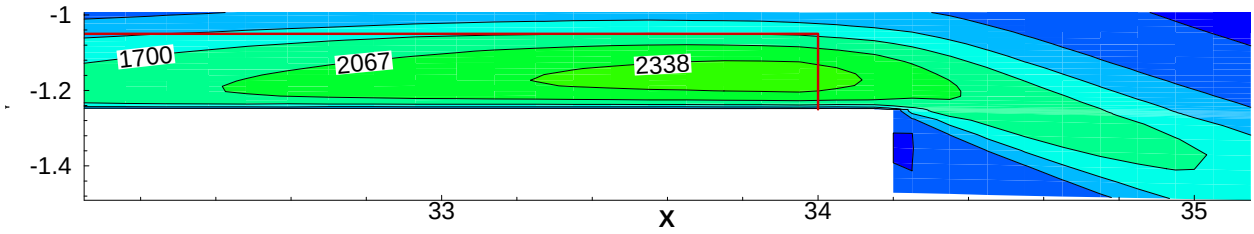

t =100 μs

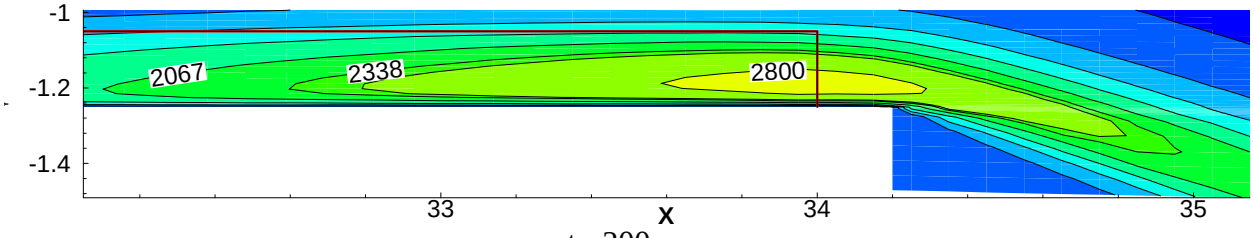

t =200 μs

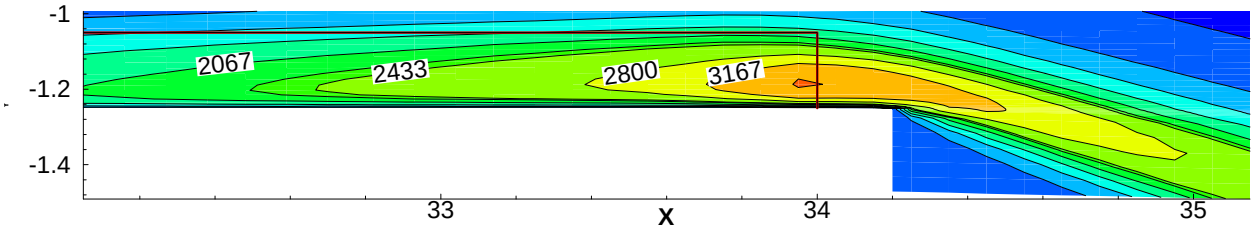

t =300 μs

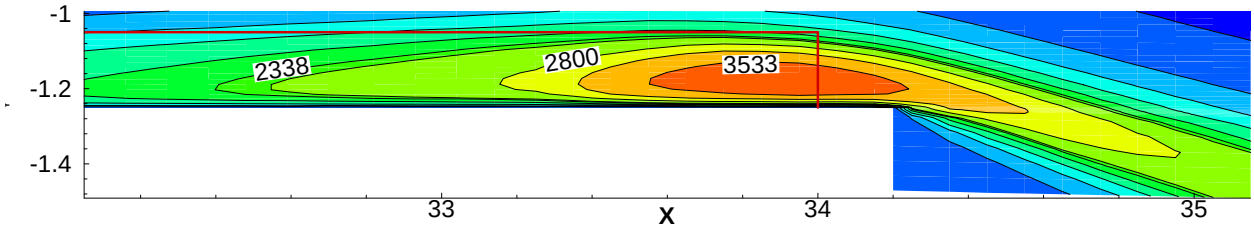

t =400 μs

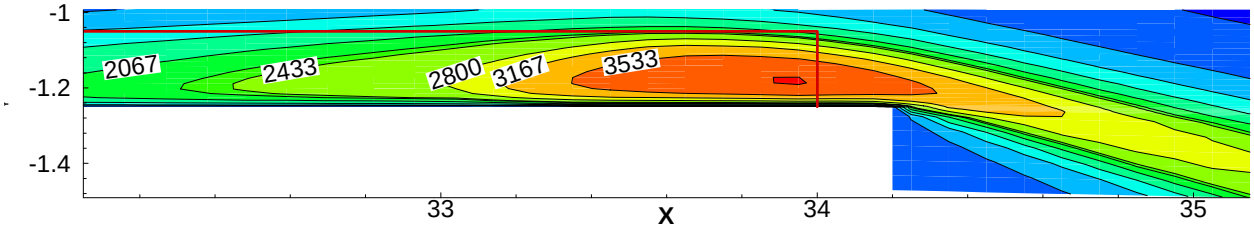

t =500 μs

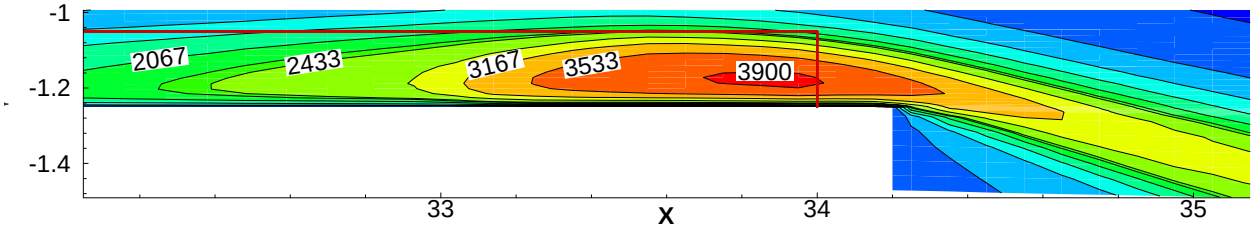

t =600 μs

Fig. A.2.6.Time dynamics of gas temperature contours in the heat deposition region Scheme 1, case of calculations 6.

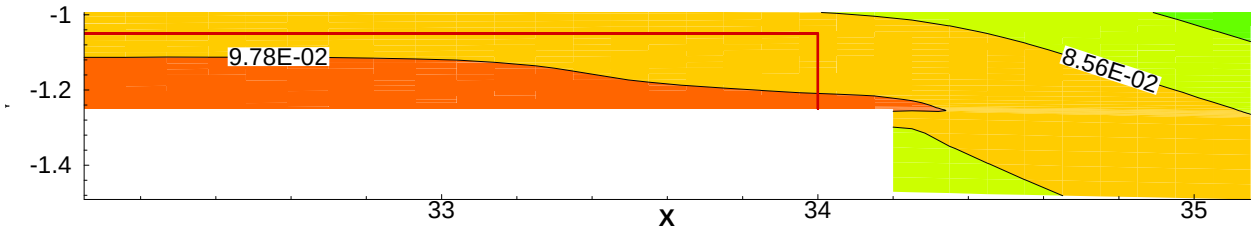

t =100 μs

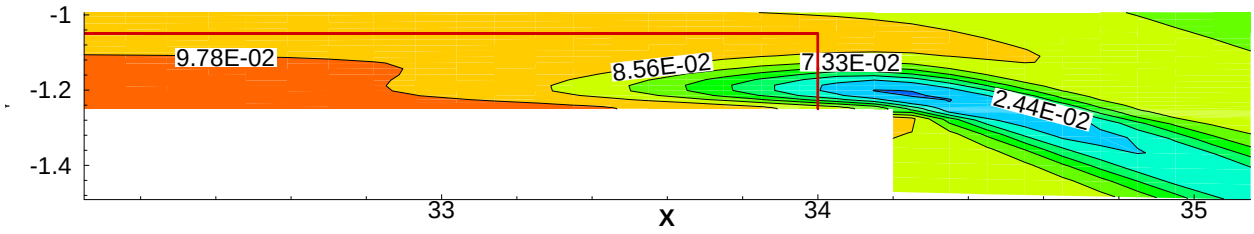

t =200 μs

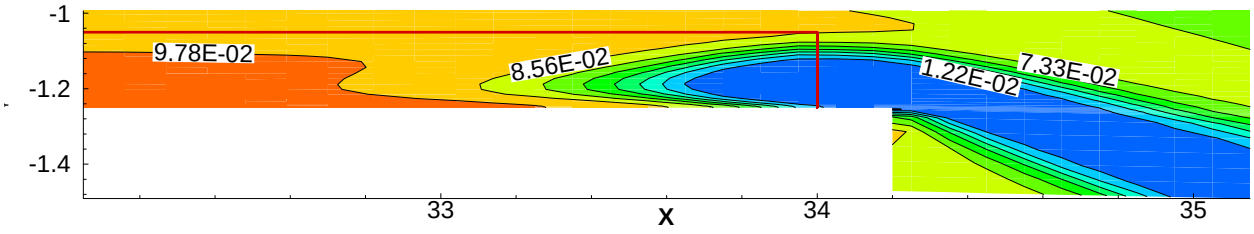

t =300 μs

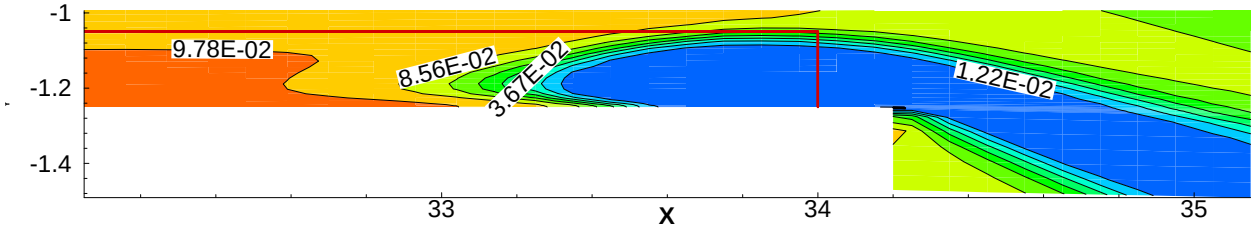

t =400 μs

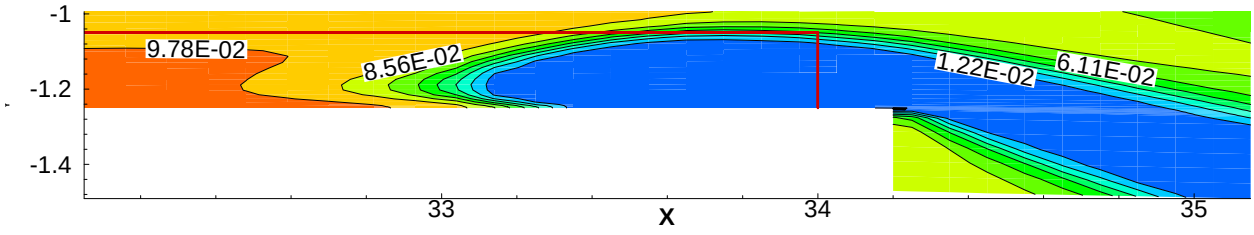

t =500 μs

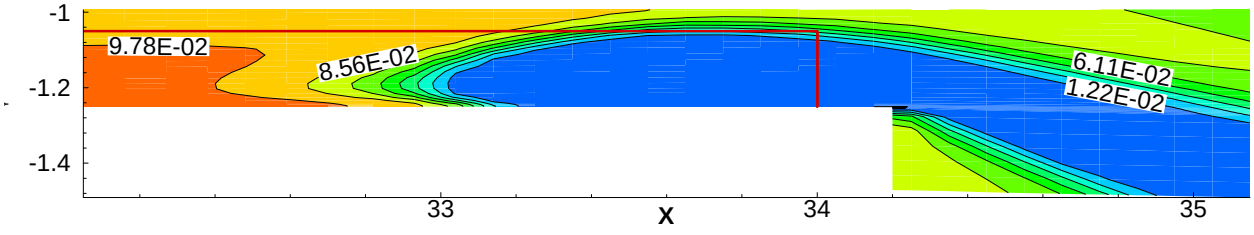

t =600 μs

Fig. A.2.7.Time dynamics of propane mole fraction contours in the heat deposition region Scheme 1, case of calculations 6.

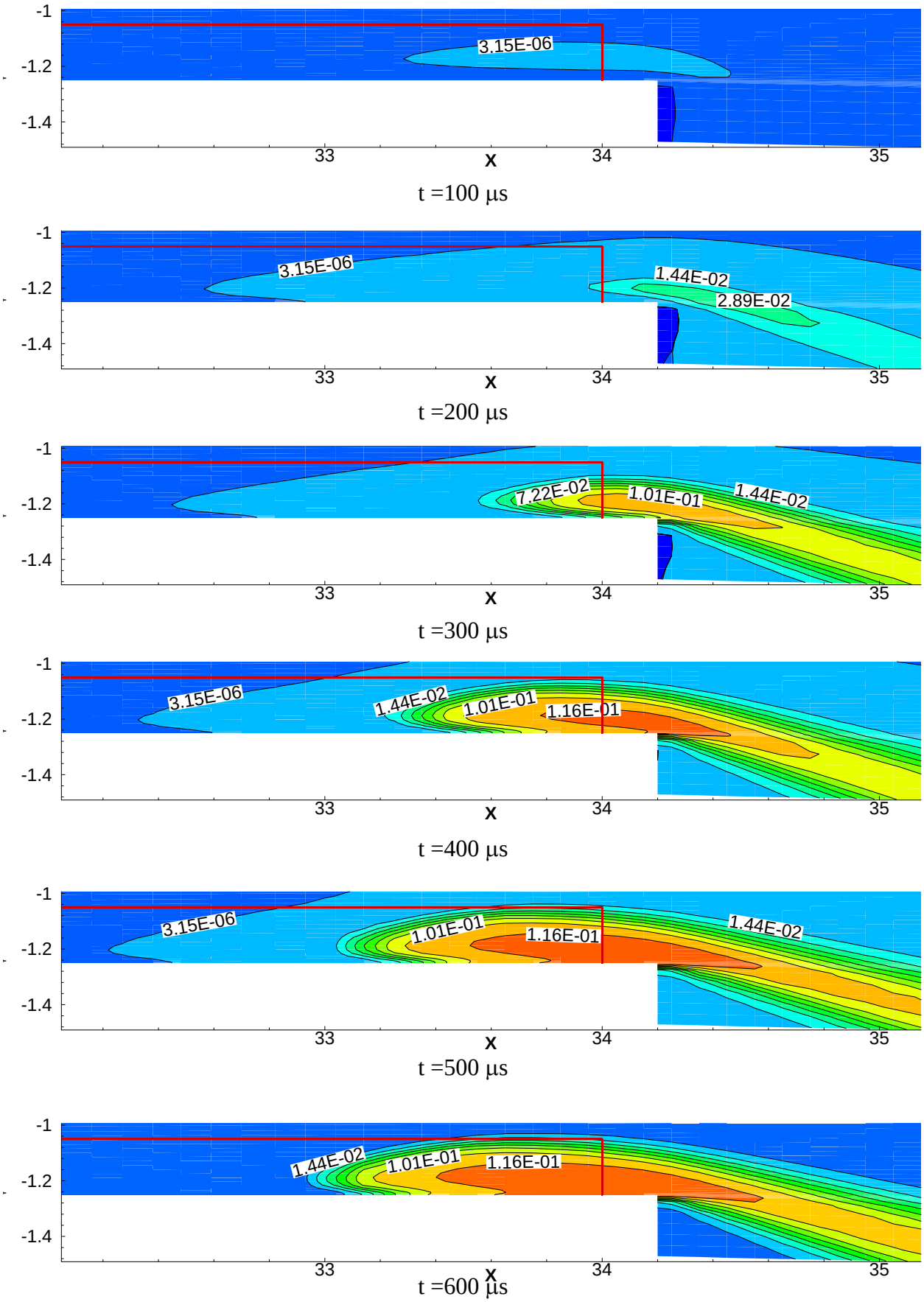

Fig. A.2.8.Time dynamics of CO mole fraction contours in the heat deposition region Scheme 1, case of calculations 6.

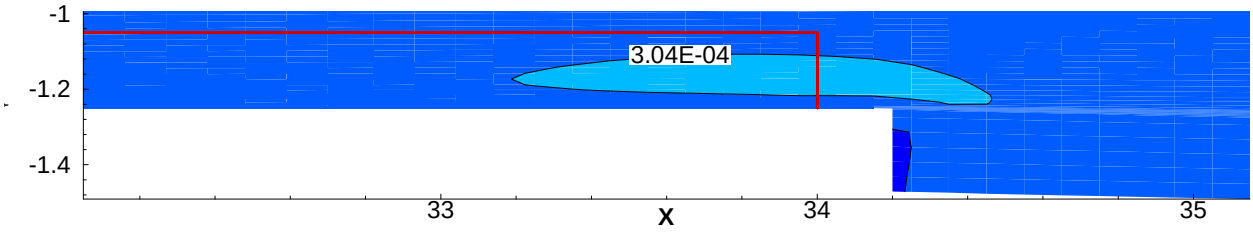

t =100 μs

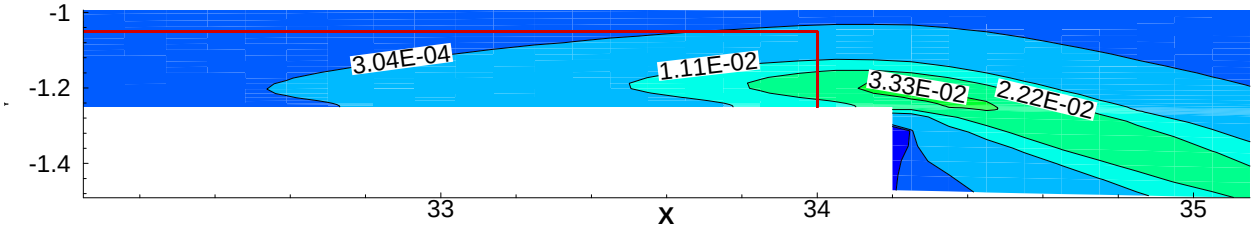

t =200 μs

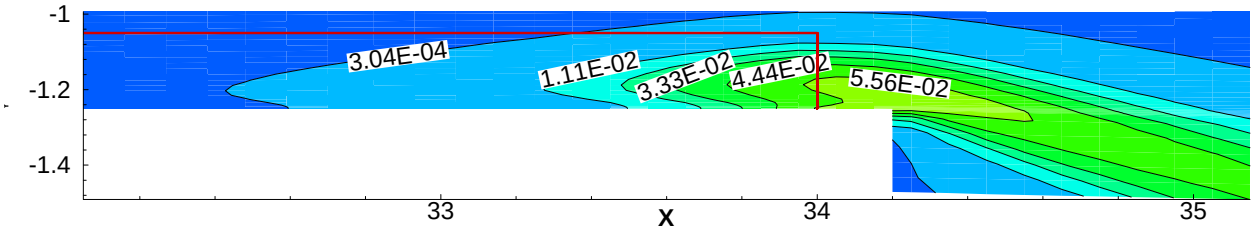

t =300 μs

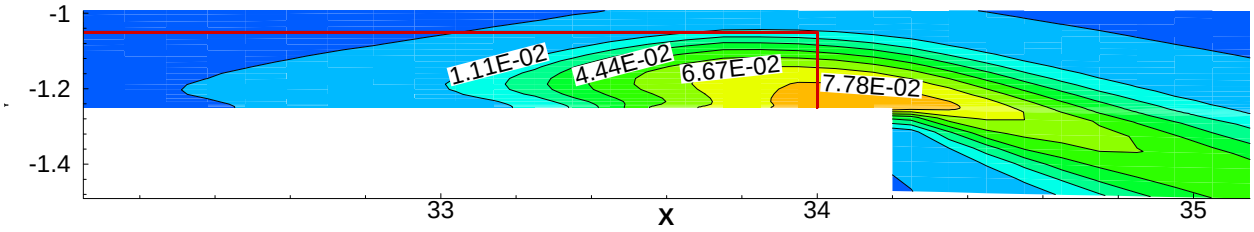

t =400 μs

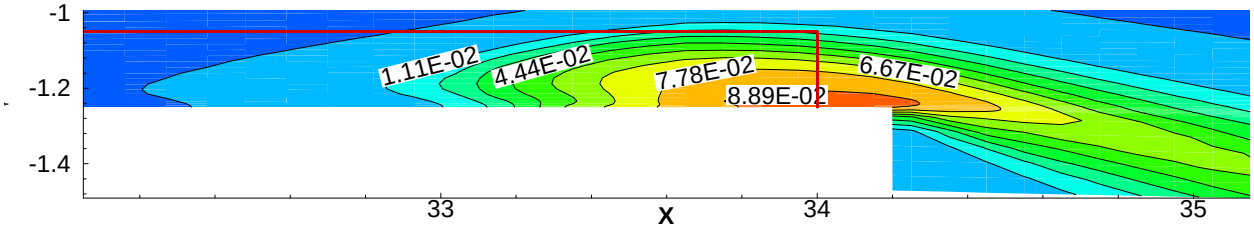

t =500 μs

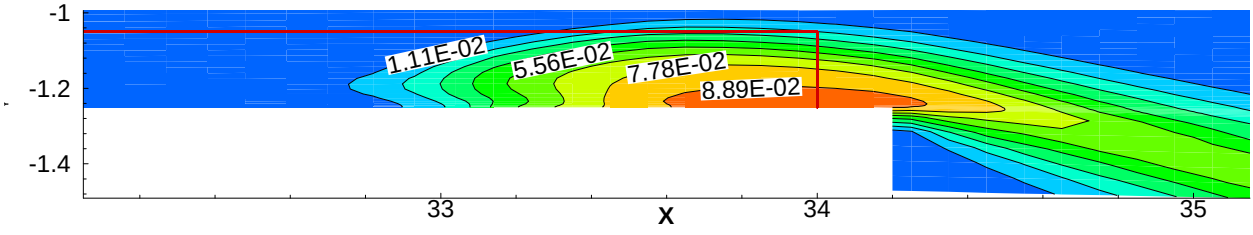

t =600 μs

Fig. A.2.9.Time dynamics of H2 mole fraction contours in the heat deposition region Scheme 1, case of calculations 6.

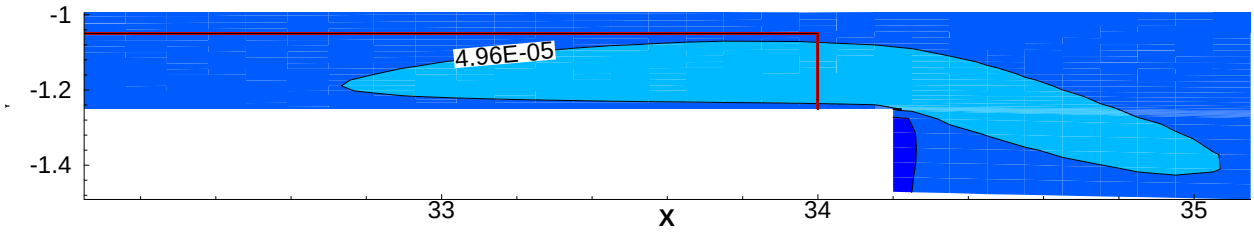

t =100 μs

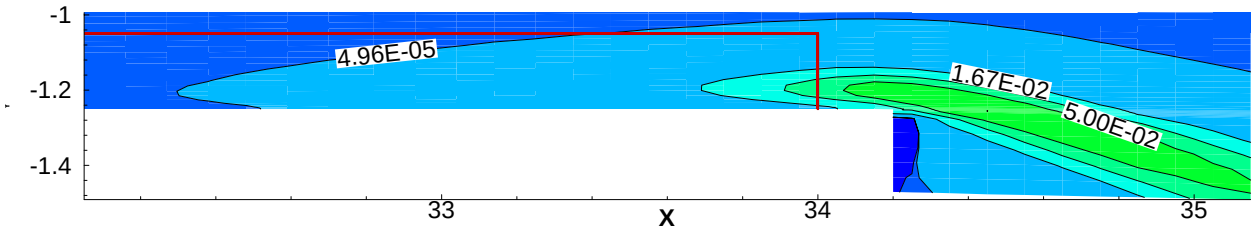

t =200 μs

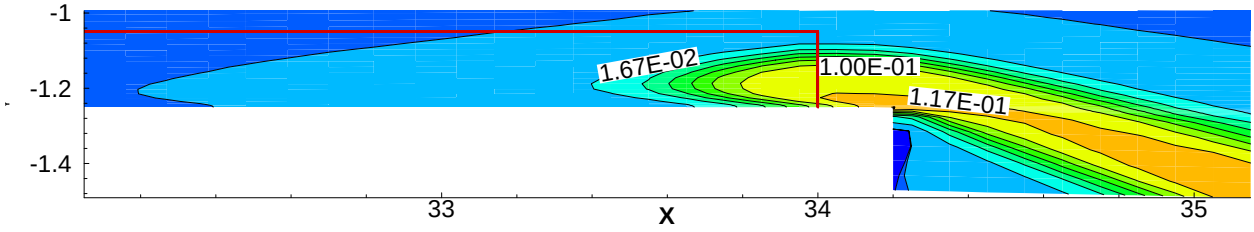

t =300 μs

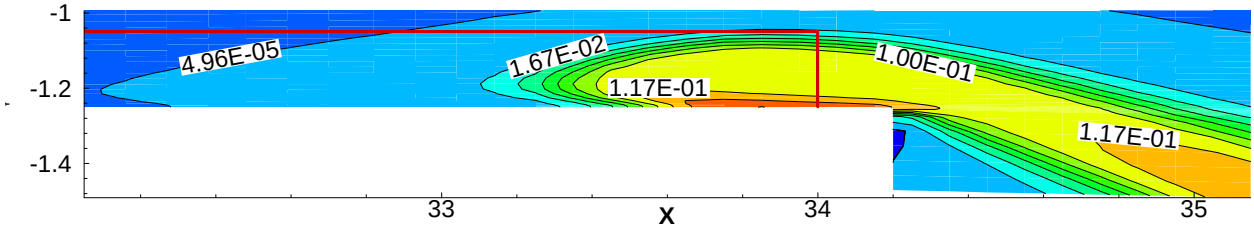

t =400 μs

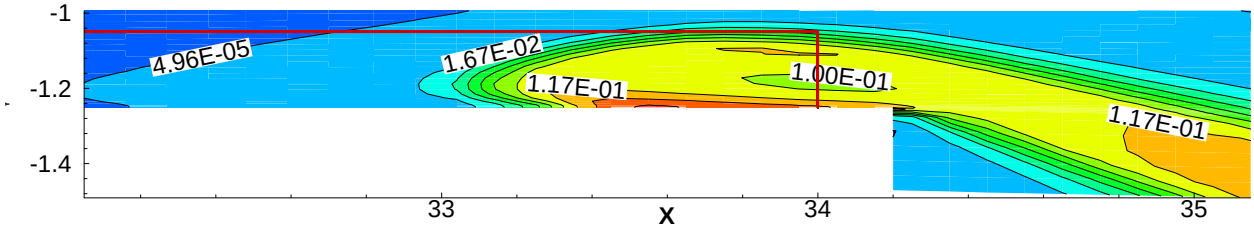

t =500 μs

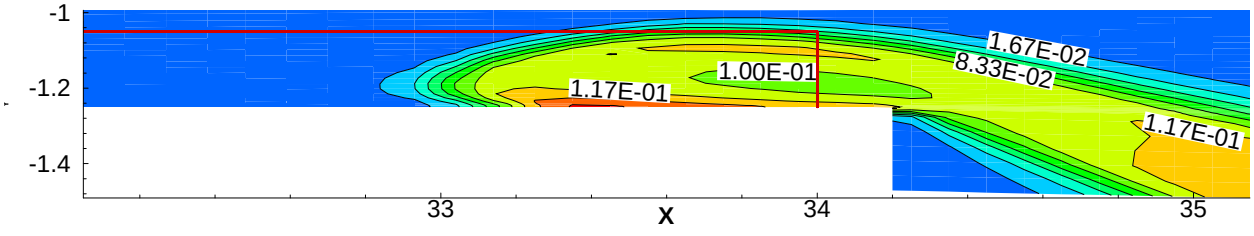

t =600 μs

Fig. A.2.10. Time dynamics of H2O mole fraction contours in the heat deposition region Scheme 1, case of calculations 6.

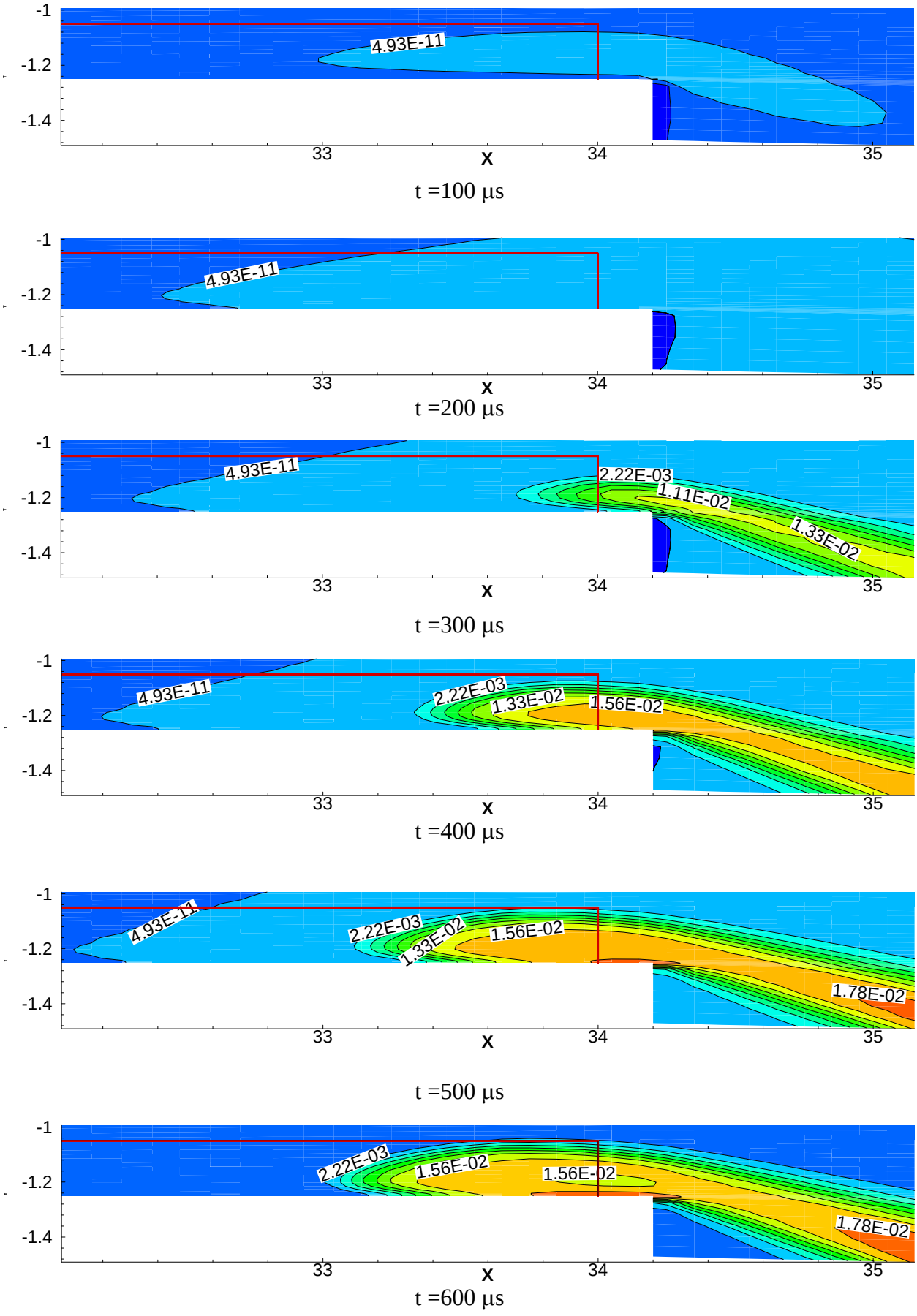

Fig. A.2.11.Time dynamics of CO2 mole fraction contours in the heat deposition region Scheme 1, case of calculations 6.

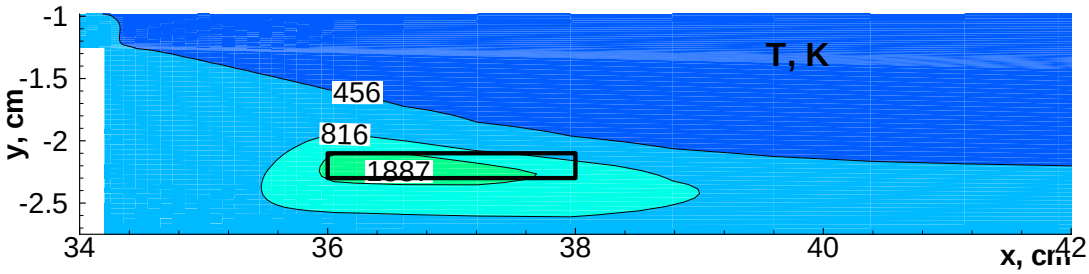

t = 200 μs

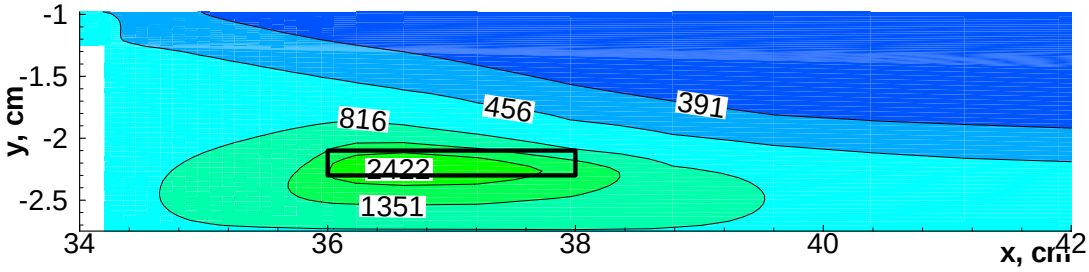

t = 400 μs

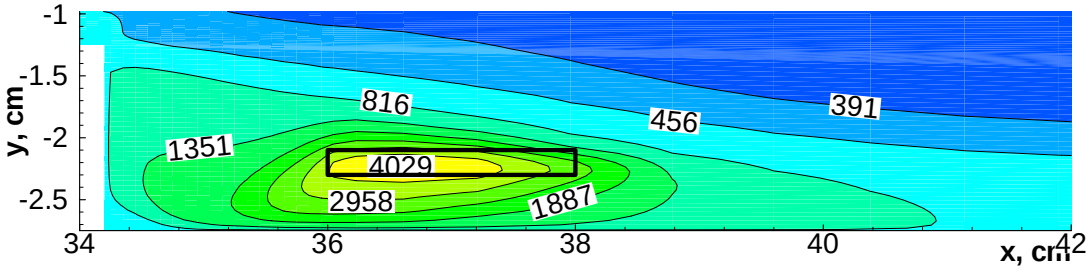

t = 600 μs

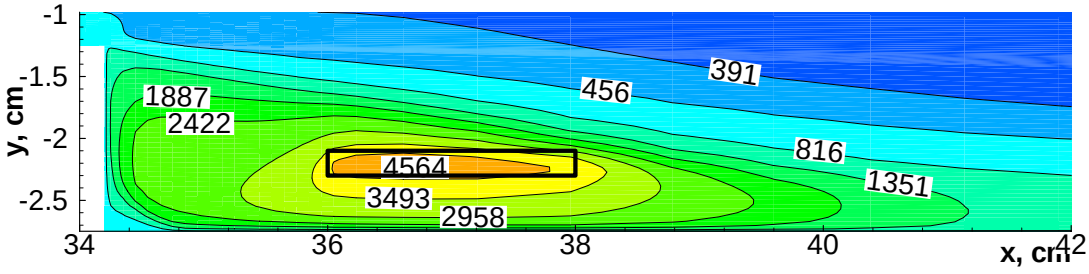

t = 800 μs

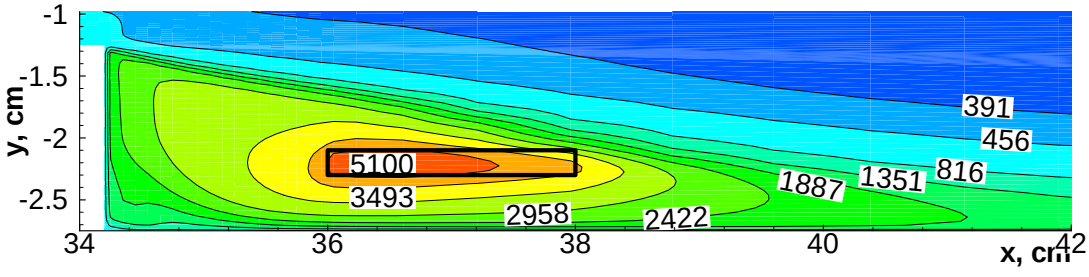

t = 1600 μs

Fig. A.2.12.Time dynamics of temperature contours in the after step region Scheme 2, case of calculations 10.

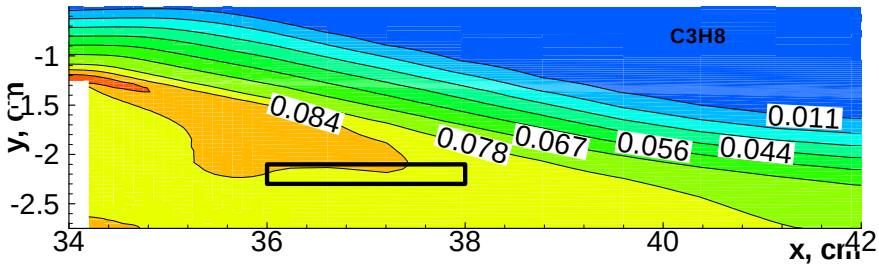

t = 200 μs

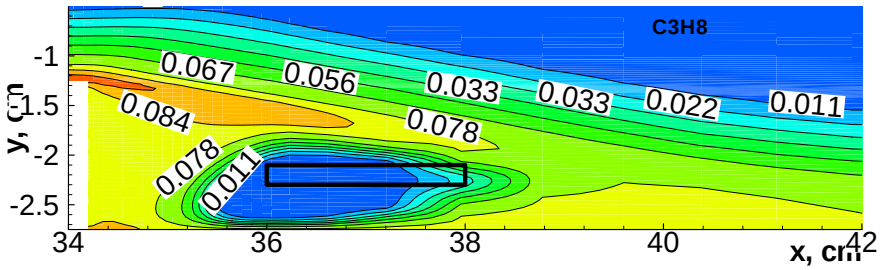

t = 400 μs

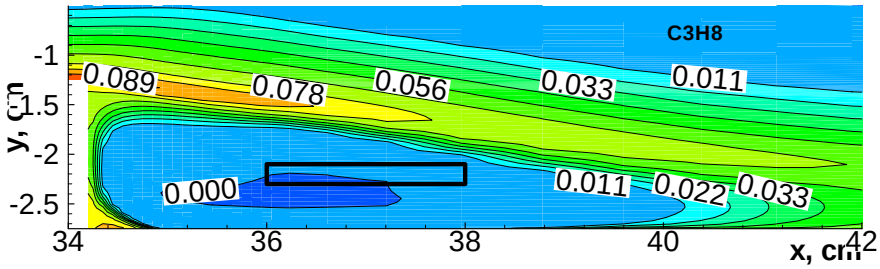

t = 600 μs

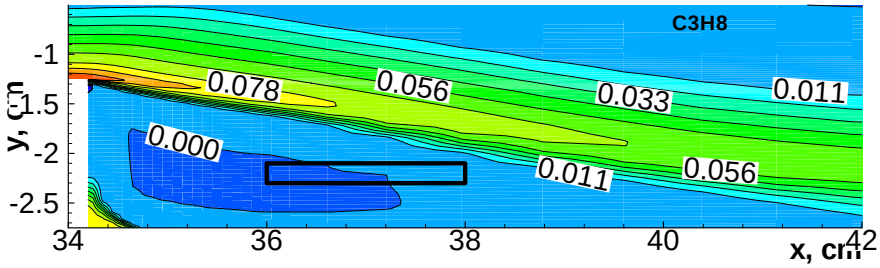

t = 800 μs

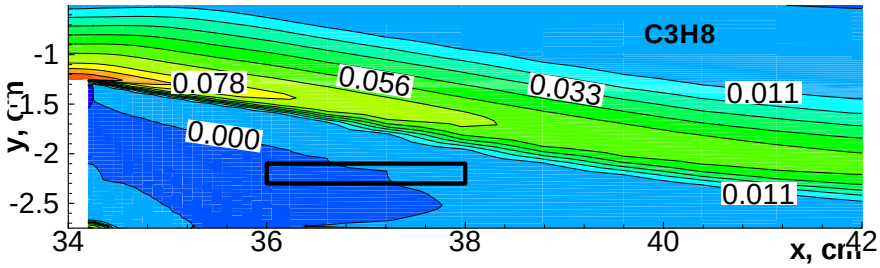

t = 1600 μs

Fig. A.2.13.Time dynamics of propane mole fraction contours in the after step region Scheme 2, case of calculations 10.

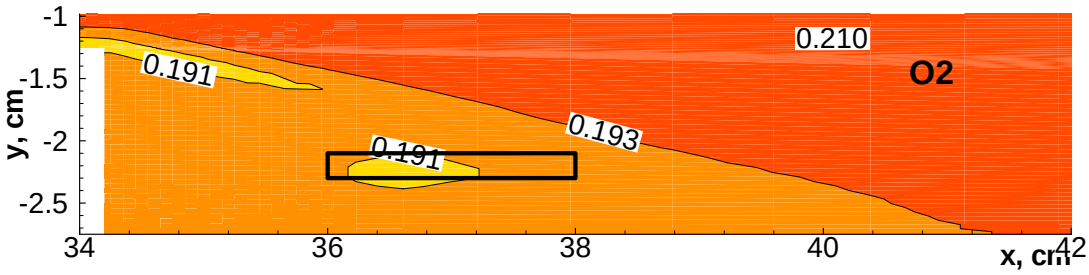

t = 200 μs

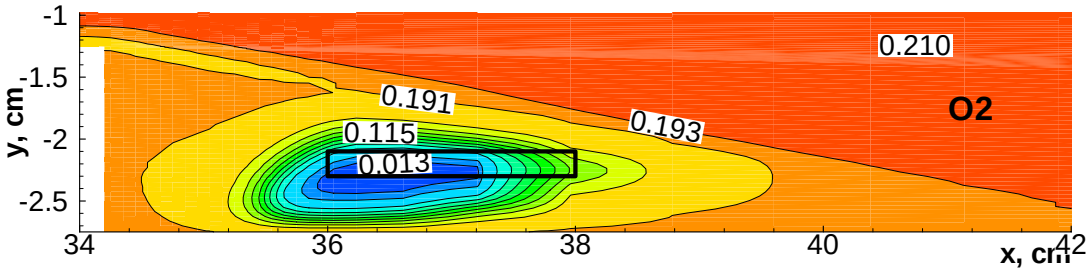

t = 400 μs

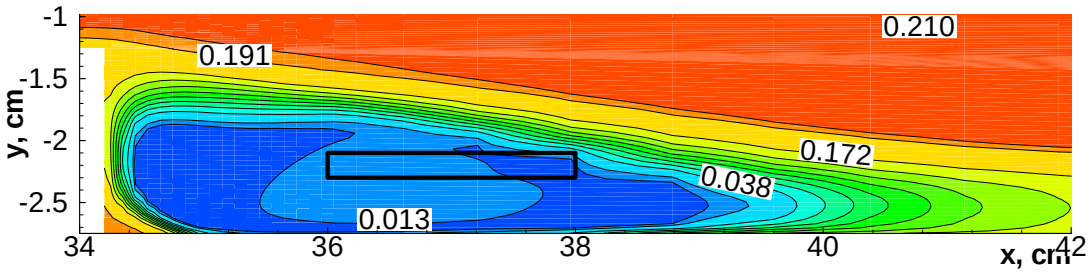

t = 600 μs

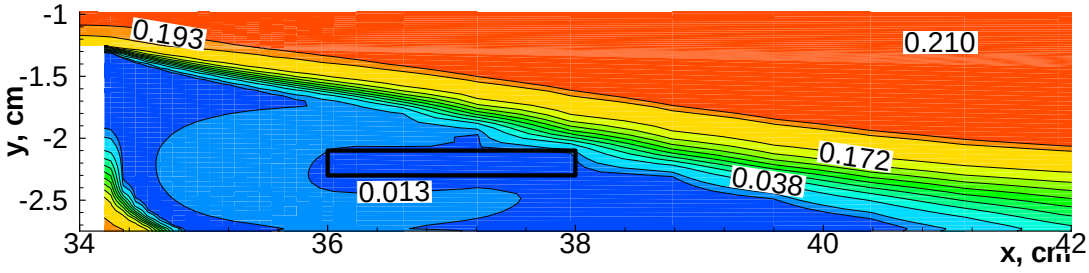

t = 800 μs

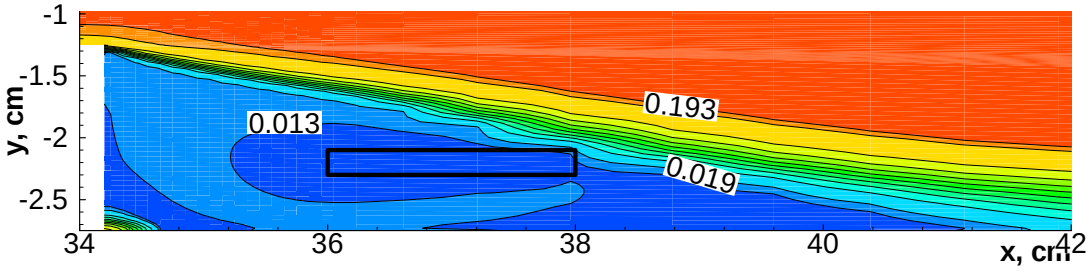

t = 1600 μs

Fig. A.2.14.Time dynamics of O_2 mole fraction contours in the after step region Scheme 2, case of calculations 10.

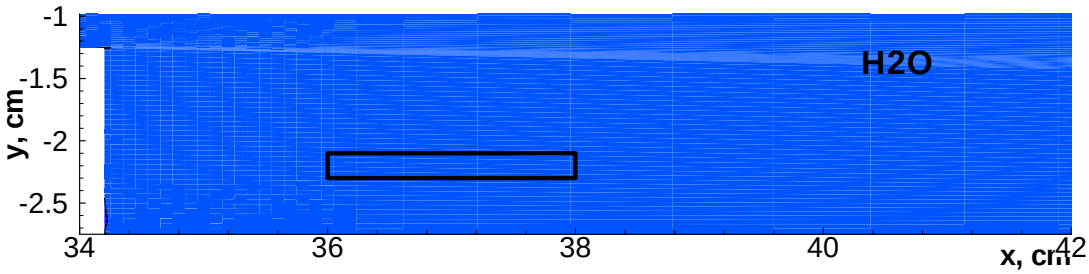

t = 200 μs

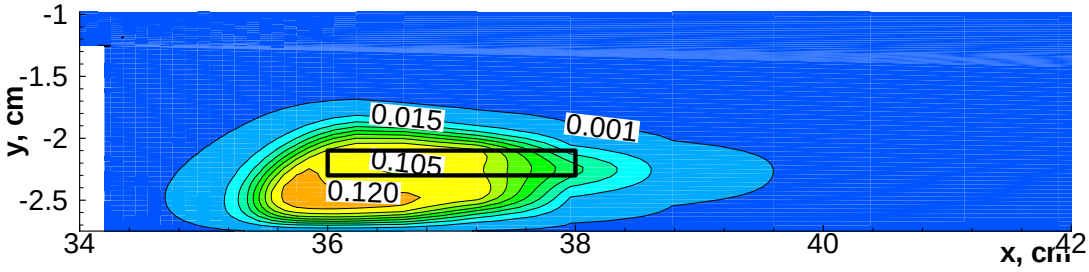

t = 400 μs

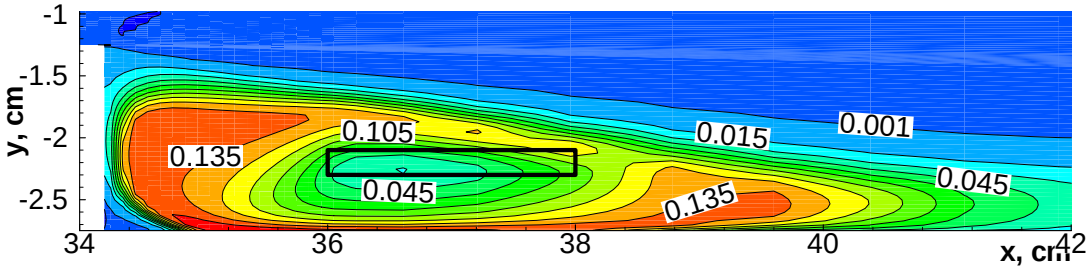

t = 600 μs

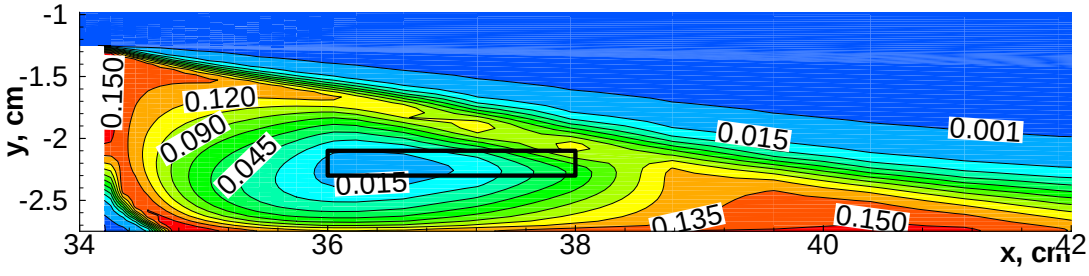

t = 800 μs

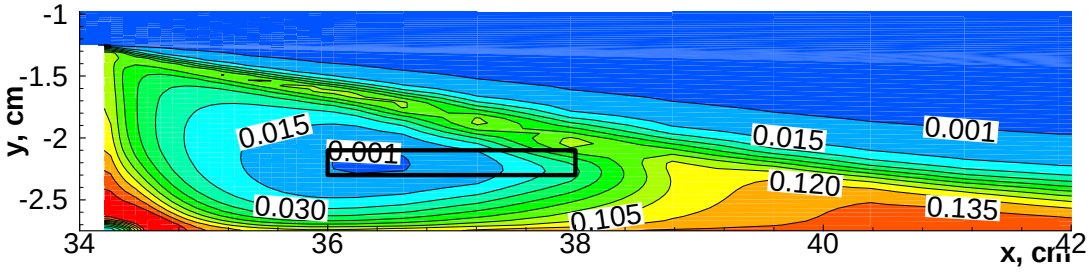

t = 1600 μs

Fig. A.2.15.Time dynamics of H_2O mole fraction contours in the after step region Scheme 2, case of calculations 10.

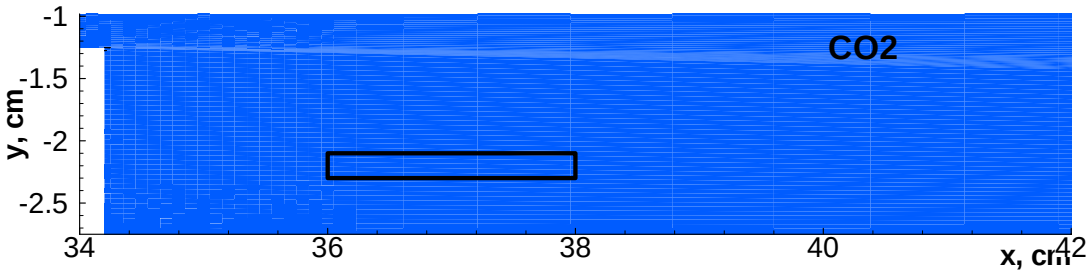

t = 200 μs

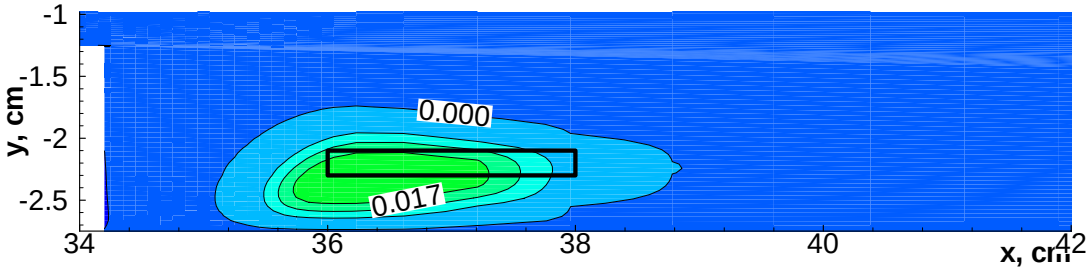

t = 400 μs

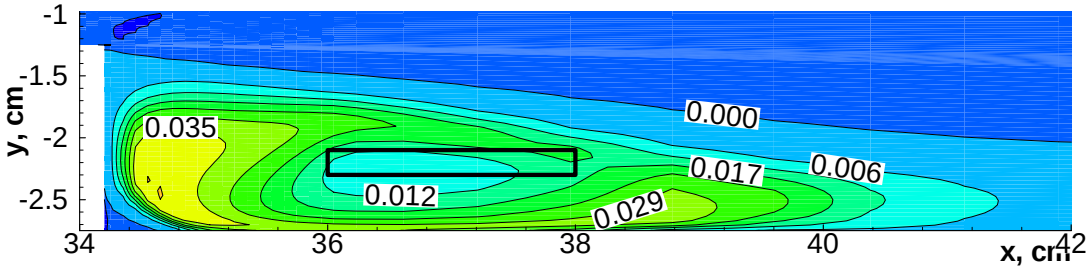

t = 600 μs

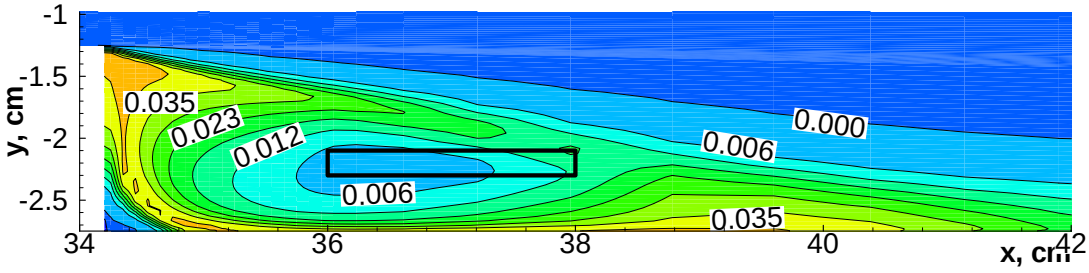

t = 800 μs

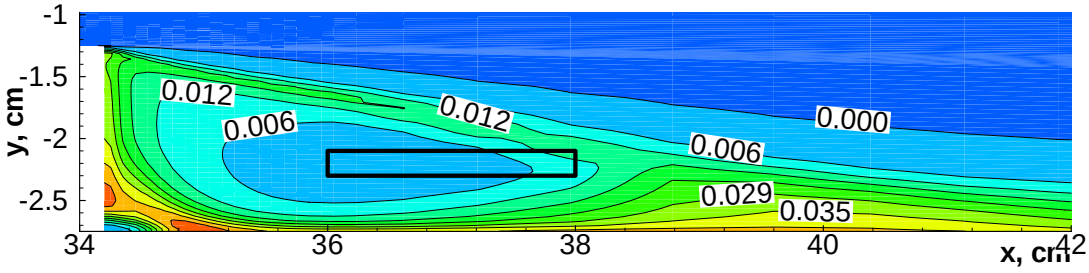

t = 1600 μs

Fig. A.2.16.Time dynamics of CO_2 mole fraction contours in the after step region Scheme 2, case of calculations 10.

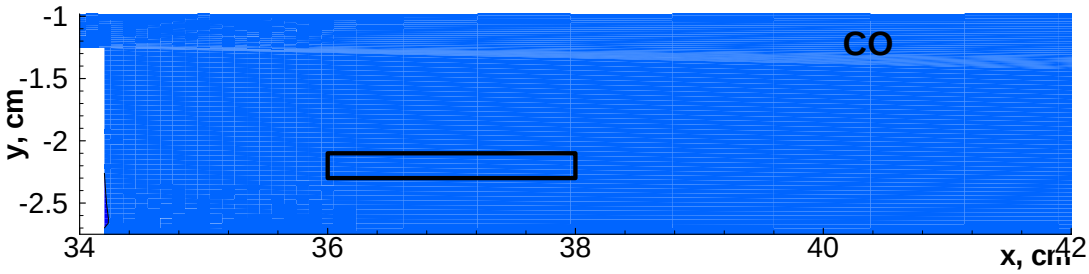

t = 200 μs

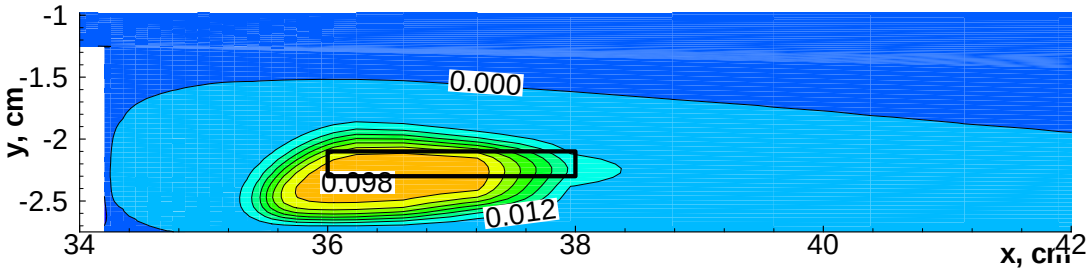

t = 400 μs

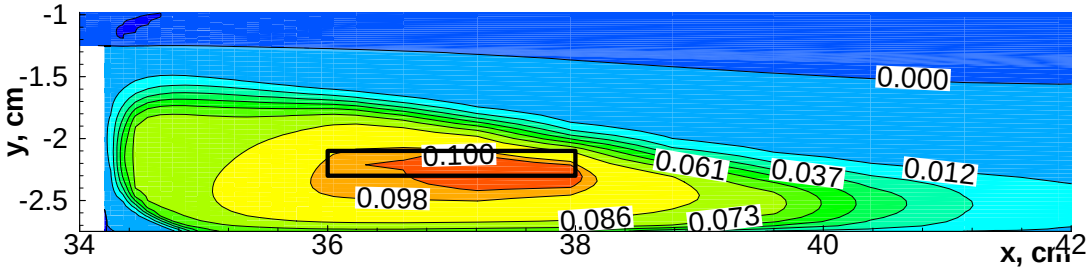

t = 600 μs

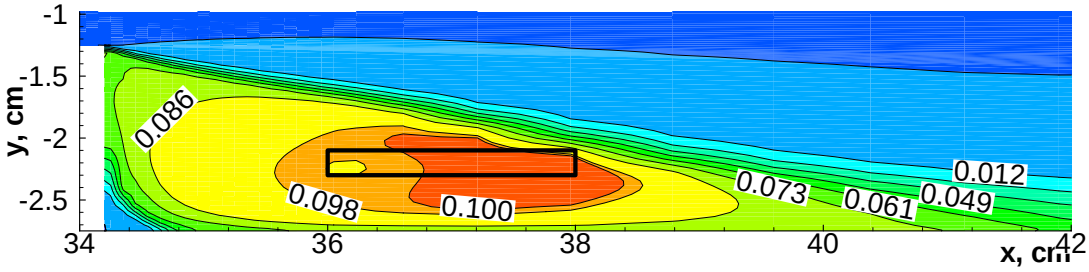

t = 800 μs

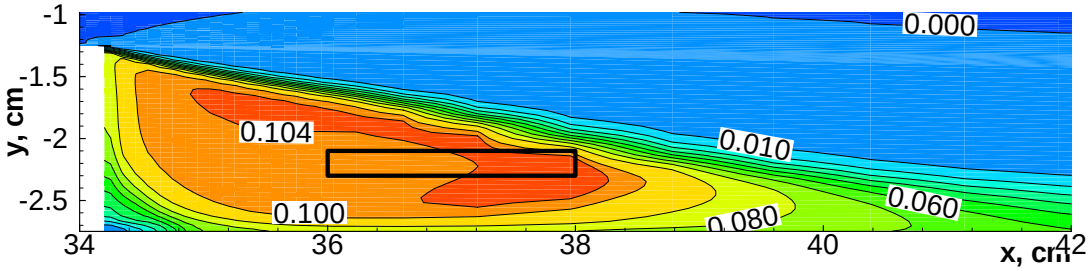

t = 1600 μs

Fig. A.2.17.Time dynamics of CO mole fraction contours in the after step region Scheme 2, case of calculations 10.

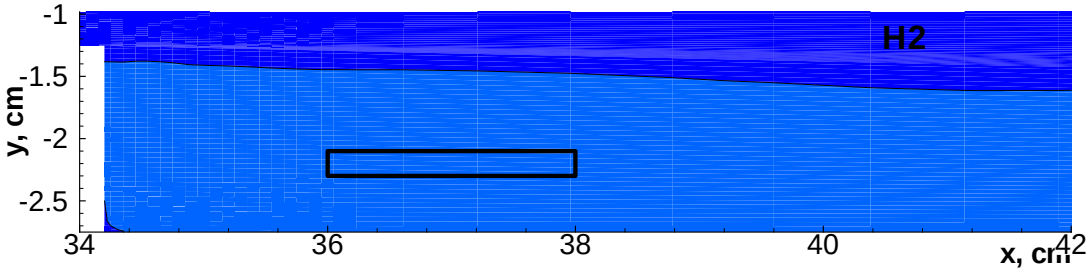

t = 200 μs

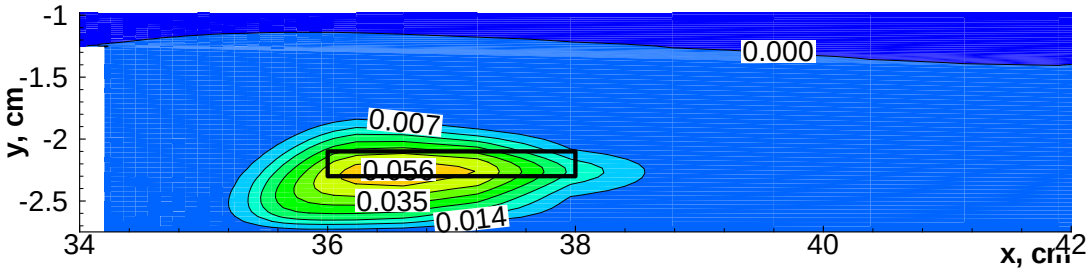

t = 400 μs

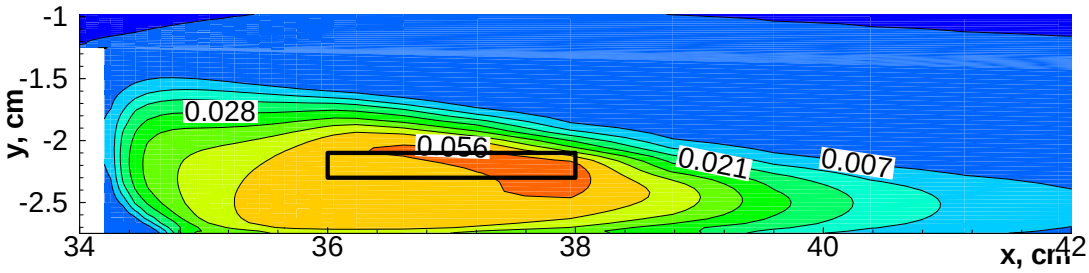

t = 600 μs

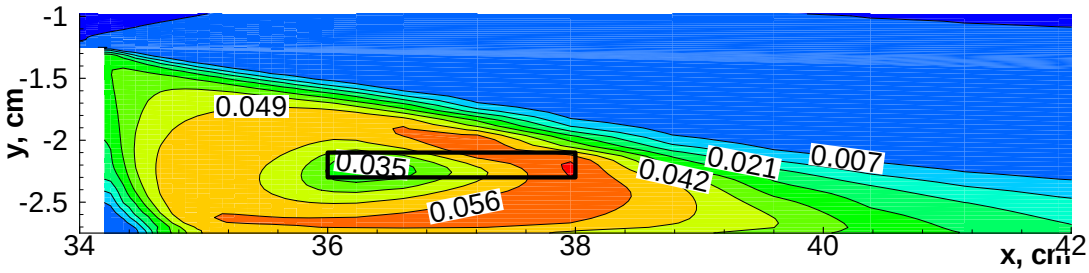

t = 800 μs

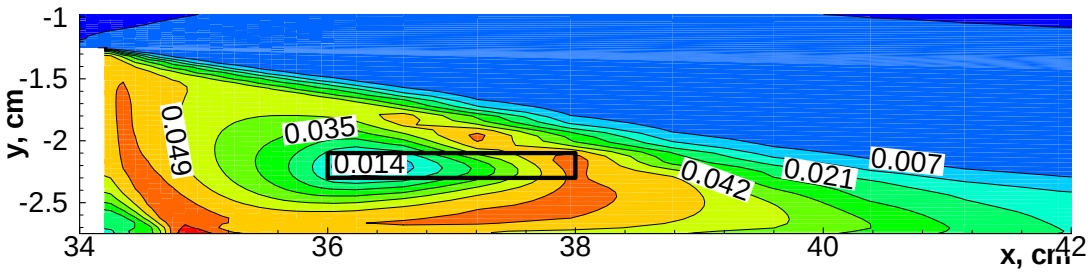

t = 1600 μs

Fig. A.2.18.Time dynamics of H_2 mole fraction contours in the after step region Scheme 2, case of calculations 10.

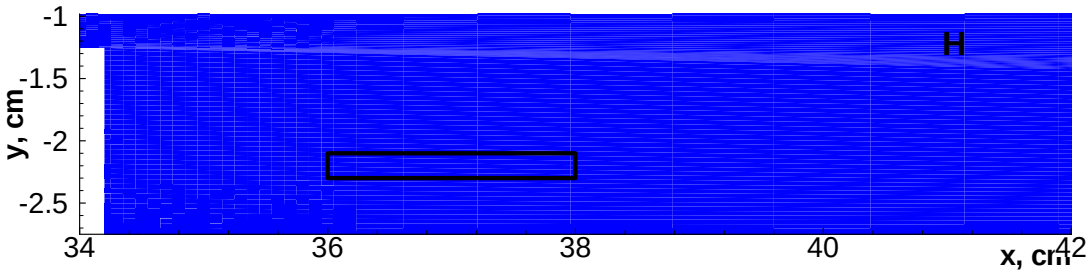

t = 200 μs

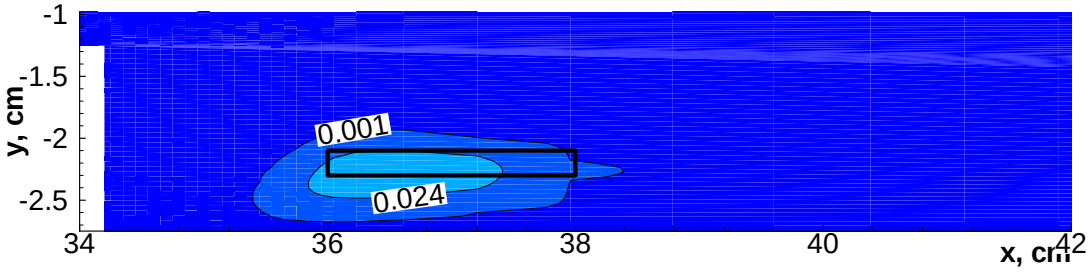

t = 400 μs

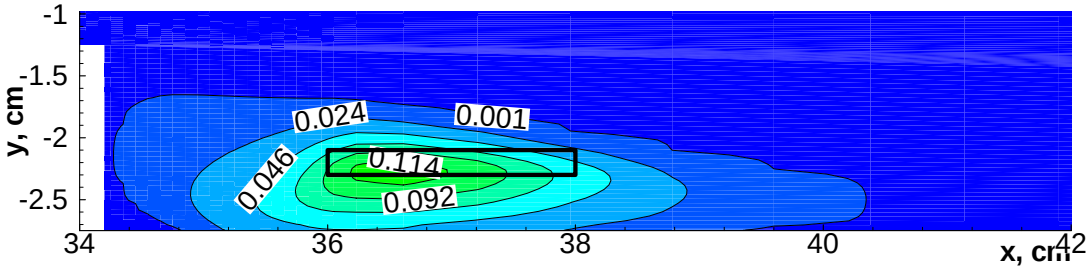

t = 600 μs

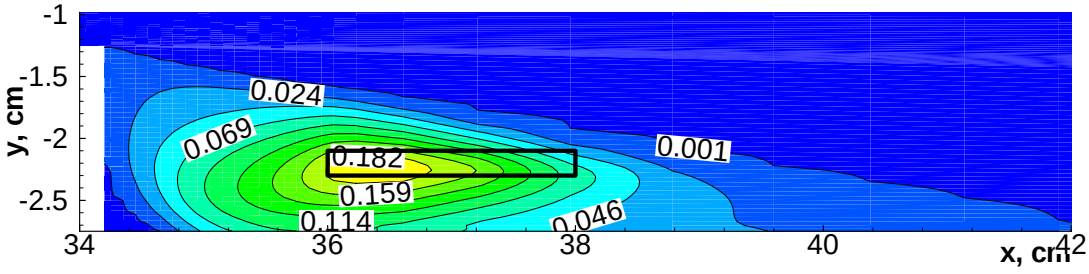

t = 800 μs

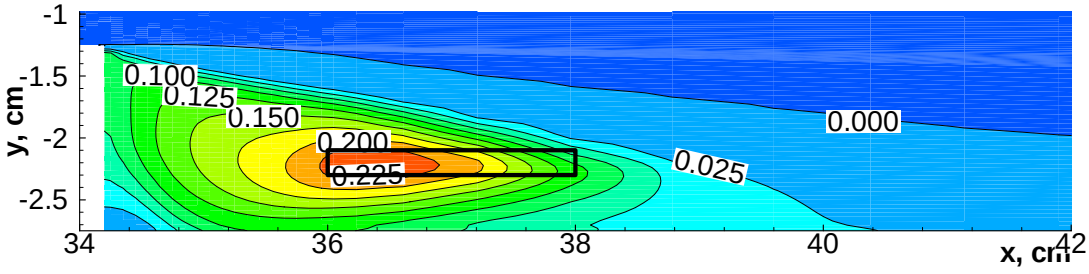

t = 1600 μs

Fig. A.2.19.Time dynamics of H mole fraction contours in the after step region Scheme 2, case of calculations 10.

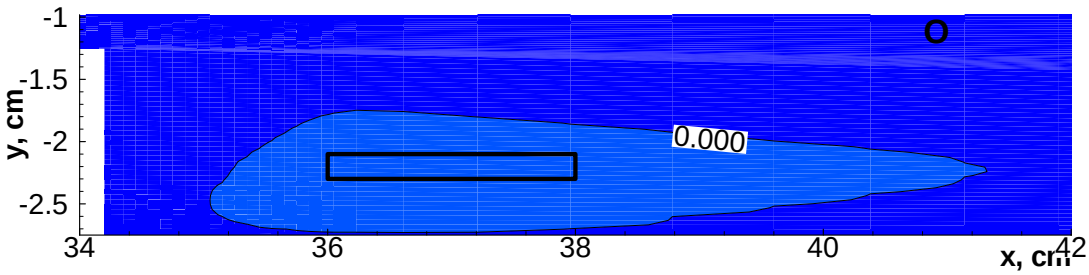

t = 200 μs

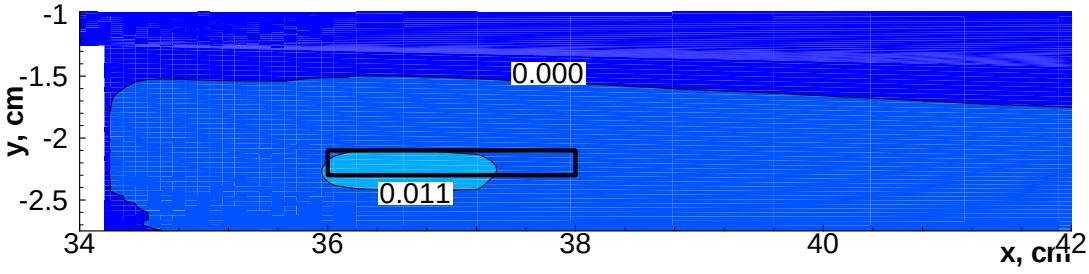

t = 400 μs

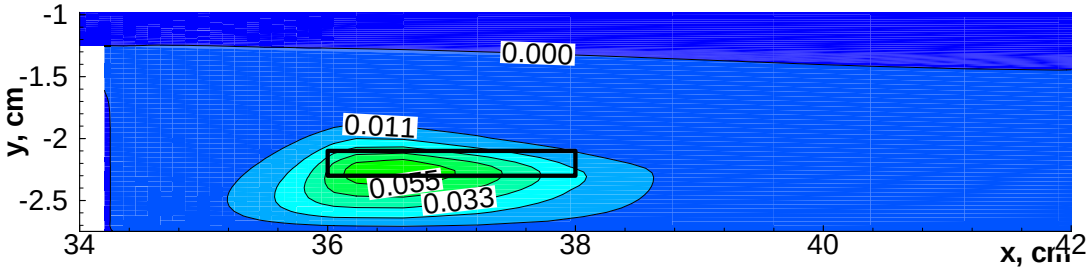

t = 600μs

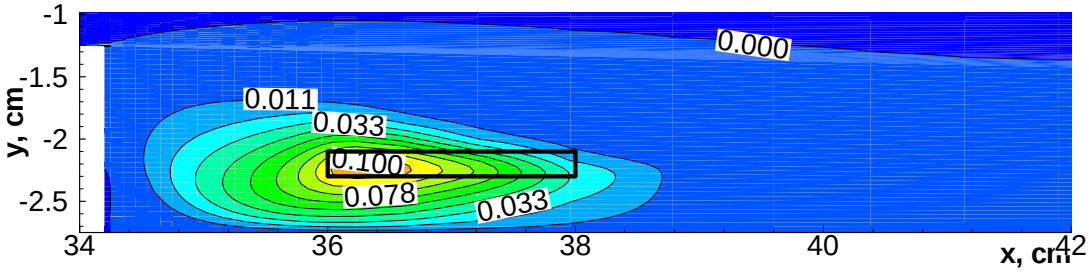

t = 800 μs

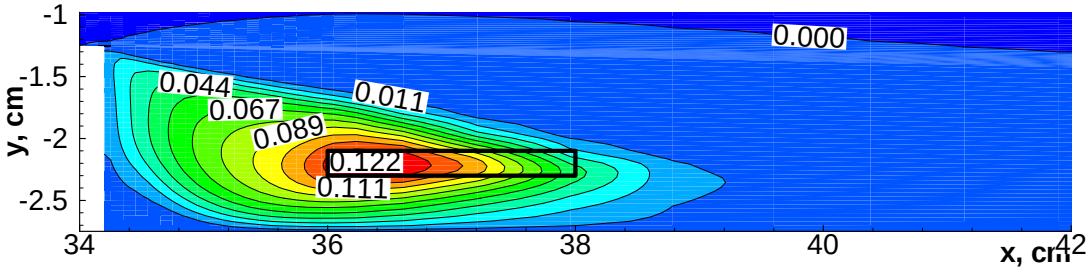

t = 1600 μs

Fig. A.2.20.Time dynamics of O mole fraction contours in the after step region Scheme 2, case of calculations 10.